

Immobilization of Functionalized Triphenylphosphine Ligands and their Complexes for Application in Catalysis

Dissertation zur Erlangung

des Doktorgrades der Naturwissenschaften (Dr. rer. nat.)

genehmigt vom Fachbereich Chemie

der Technischen Universität Kaiserslautern

(D 385)

Vorgelegt von

Lei Wang

Betreuer der Arbeit: Prof. Dr. W. R. Thiel

Tag der wissenschaftlichen Aussprache: 17.02.2011

Kaiserslautern 2011

Vom Fachbereich Chemie der Technischen universität Kaiserslautern

17.02. 2011 als Dissertation angenommen.

Dekan:	Prof. Dr. W. E. Trommer
Vorsitzender er Prüfungskommission:	Prof. Dr. H. Sitzmann
1. Berichterstatter:	Prof. Dr. W. R. Thiel
2. Berichterstatter:	Prof. Dr. S. Ernst

Die vorliegende Arbeit wurde im Fachbereich Chemie Technischen Universität Kaiserslautern im Arbeitskreis von Prof. Dr. W. R. Thiel in der Zeit von November 2007 bis Januar 2011 angefertigt.

To my parents and Daniel

Abbreviations

AAS	atomic absorption spectrometry
a.u	Arbitrary Units
BET	Brunauer-Emmet-Teller
BJH	Barrett-Joyner-Halenda
BTEB	1,4-bis(triethoxysilyl)benzene
CMC	critical micelle concentration
CP MAS	Cross Polarization Magic Angle Spinning
CTAB	Cetyltrimethylammonium bromide
dppe	bis(diphenylphosphino)ethane
EtOH	Ethanol
EtOAc	Ethylacetate
FT-IR	Fourier Transform Infrared Spectroscopy
GC	Gas Chromatography
ICP	Inductive Coupled Plasma
LCT	Liquid Crystal Template
MCM	Mobil Crystalline Material
Me	Methyl
NMR	Nuclear Magnetic Resonance

MNPs	magnetic nanoparticles
OTAB	Octadecyltrimethylammonium bromide
PMO	Periodic Mesoporous Organosilica
PSD	pore size distribution
SBA	Santa Barbara Amorphous
SEM	Scanning Electron Microscopy
SMNP	silica coated magnetic nanoparticles
TEM	Transmission Electron Microscopy
TEOS	Tetraethyl Orthosilicate
TOF	turnover frequency
TON	turnover number
TG-DTG	Thermogravimetric and Differential Thermogravimetric analysis
THF	Tetrahydrofuran
TPP	triphenylphosphine
XRD	X-ray diffraction

Table of Contents

Chapter 1. Introduction	1
1.1 Immobilized catalysts	1
1.2 Synthesis of support materials	2
1.2.1 Periodic mesoporous silicas	3
1.2.2 Periodic mesoporous organosilicas	6
1.2.3 Silica coated magnetic nanoparticles	7
1.3 Covalent immobilization	8
1.3.1 Post-grafting method	9
1.3.2 Co-condensation method	11
1.3.3 Periodic mesoporous organosilicas (PMOs)	11
1.4 Non-covalent immobilization: electrostatic interactions	12
1.5 Catalytic application of immobilized catalysts	13
1.5.1 Suzuki reaction	14
1.5.2 Hydrogenation	16
1.5.3 Hydroformylation	17
1.5.4 Other reactions	18
1.6 Motivation	19
Chapter 2. Covalent Immobilization of Triphenylphosphine Complexes	20
2.1 Immobilization of a Palladium Complex by the Post Grafting Method	20
2.1.1 Introduction	20
2.1.2 Results and discussion	24
2.2 Immobilization of a Rhodium Complex by the Post Grafting Method	44
2.2.1 Introduction	44
2.2.2 Results and discussion	45
2.3 Immobilization of a Ruthenium Complex by the Post Grafting Method	69
2.3.1 Introduction	69
2.3.2 Results and discussion	70
2.4 Immobilization of a Palladium Complex by Co-condensation Method	82

2.4.1 Introduction.....	82
2.4.2 Results and discussion	83
Chapter 3. Non-covalent Immobilization of a Triphenylphosphine Ligand.....	99
3.1 Introduction.....	99
3.2 Results and discussion	100
3.2.1 Synthesis	100
3.2.2 Characterization	104
3.2.3 Catalysis.....	123
3.2.4 Extended research	129
Chapter 4. Imidazolium Salt Incorporated in a Mesoporous Framework.....	135
4.1 Introduction.....	135
4.2 Results and discussion	137
4.2.1 Synthesis	137
4.2.2 Characterization	139
4.2.3 Catalysis.....	151
4.2.4 Conclusion	154
Chapter 5. Conclusion	156
Chapter 6. Experimental Section.....	161
Regarding to Chapter 2.1	161
Regarding to Chapter 2.2	163
Regarding to Chapter 2.3	165
Regarding to Chapter 2.4	166
Regarding to Chapter 3	166
Regarding to Chapter 4	169
References.....	171
Eidesstattliche Erklärung.....	185
Acknowledgements	187

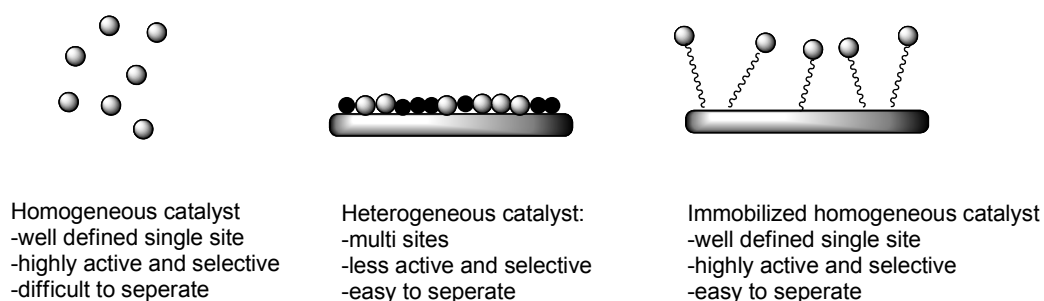
Chapter 1. Introduction

1.1 Immobilized catalysts: A bridge between homogeneous and heterogeneous catalysis

Catalysts play an important role in chemical industry since the use of catalysts can effectively decrease the activation energy of difficult chemical transformations. Traditionally, catalysis is divided into two main fields: homogenous and heterogeneous catalysis. The essential distinction between these two kinds of catalysis is whether the catalysts are present in the same phase as the substrate. Homogeneous catalysts based on molecular species usually contain a single site which can be well defined and characterized by spectroscopy. Because of advanced synthesis and characterization techniques, these catalysts can be designed to be highly active and selective for a desired reaction. However, since homogeneous catalysts are present in the same phase as the substrate, this causes difficulties in the product separation process, such as generation of large volumes of waste, consumption of energy and decomposition of expensive catalysts. In contrast to homogeneous catalysts, heterogeneous catalysts provide numerous opportunities for recovering and reusing. However, possessing multi active sites, heterogeneous catalysts tend to be less active and selective than homogeneous catalysts due to the complicated chemical environment of the active centers. Furthermore, the design of effective heterogeneous catalysts is limited by the rare understanding of active centers caused by less advanced characterization techniques.

Due to the limitations of traditional homogeneous and heterogeneous catalysts, much effort has been donated to bridge the gap between homogeneous and heterogeneous catalysis.^[1-4] Among all the concepts, immobilization of homogeneous catalysts on solid supports allows simple separation and thus reuse of expensive noble metal catalysts. Due to the obvious benefits in terms of environmental and economic aspects,

this method has widely been studied during the last two decades (Scheme 1. 1) [2, 5-7]. The term “interphase” has been introduced for this new concept of heterogeneous catalysis, which is defined as a region within a material in which a stationary and mobile component penetrate each other on a molecular level.^[8-9] The stationary phase is composed of an inert matrix, a flexible spacer and an active center, whereas the mobile phase consists of a solvent or a gaseous, liquid or dissolved reactant. In an ideal interphase the reactive center is uniform, well-defined and highly mobile. It is able to simulate homogeneous reaction conditions and can be easily recovered and reused as heterogeneous catalysts.



Scheme 1. 1 Comparison of homogeneous, heterogeneous and immobilized catalysts.

1.2 Synthesis of support materials

The solid supports play a key role for the performance of immobilized catalysts. Two main factors should be considered for choosing a material as a support: First, the material should exhibit a highly thermal and chemical stability during the reaction process. Second, the structure of the material should have a reasonably high surface area and a large pore size, allowing the creation of well dispersed and easily accessible active sites on the surface. Inorganic matrixes have potential advantages compared to organic polymer supports due to their enhanced thermal and mechanical stability.

Zeolites are the most widely used catalysts in industry. These crystalline hydrated aluminosilicates contain a periodic arrangement of micropores and feature a narrow pore size distribution. They have been successfully applied for oil refining, petrochemistry and organic synthesis.^[4] The reason for their success in catalysis is related to

several specific properties, such as high surface area and adsorption capacity, tailored active sites, resistance towards heat, steam and chemicals, simple operation and recyclability.

Despite these catalytically desirable properties of zeolites, they are not suitable supports due to the small size of their channels (less than 1 nm) and cavities (typically < 1.5 nm), which result in difficulties for the reactants to access the active sites, besides, blockage of pores after immobilization of organic functionalities.^[10] Two rational approaches can overcome diffusion limitation: One way is to increase the pore diameter to a mesoporous scale. Compared to the dimensions of the zeolite micropores (< 2 nm), mesopores (2-50 nm) permit faster migration of guest molecules in the host frameworks. Another way is to keep the size of the support particles as small as possible. Due to the high external surface areas of non-porous nanoparticles a high loading of catalytically active sites is guaranteed and diffusion will no longer limit the kinetics.

1.2.1 Periodic mesoporous silicas

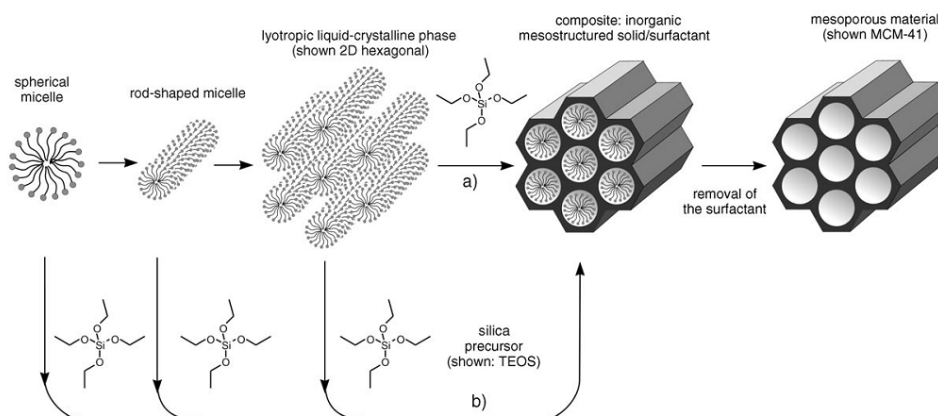
The so-called M41S periodic mesoporous silicas were discovered in the early 1990s by scientists at Mobil Oil Company, in part as a response for the need of extending the applications of zeolites.^[11-12] These new materials break past the pore size constraint (< 2 nm) of microporous zeolites, which allows the fixation of large active complexes, reduces diffusional restriction of reactants and enables reactions involving bulky molecules to take place. They have extremely high surface areas as well as long-range ordered pores, which is beneficial for catalytic activity.

Liquid crystal templating mechanism

The M41S materials established a new approach in materials synthesis, which uses long carbon chain molecules (such as cetyltrimethylammonium salts) as the structure directing agent instead of the conventional single small amine molecules.^[13-15]

1. Introduction

Following this synthesis concept, various types of M41S and related mesoporous materials have been synthesized, including ordered two-dimensional hexagonal (2D, $p6mm$) ordered three-dimensional hexagonal $P6_3/mmc$, 3D cubic, bicontinuous cubic, disordered and other structures.^[13]



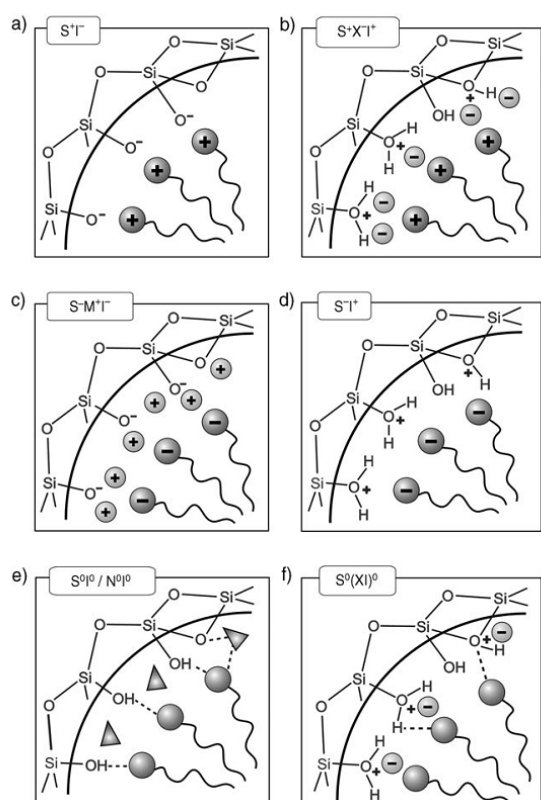
Scheme 1. 2 Possible mechanistic pathways for the formation of MCM-41: (a) liquid crystal initiated and (b) silicate anion initiated. [source^[2]]

Beck et al. proposed a liquid crystal templating (LCT) mechanism to explain the formation of mesoporous materials as shown in Scheme 1. 2.^[2, 16] They proposed that the structure is defined by the organization of surfactant molecules into liquid crystals which serve as templates. In other word, the first step in the synthesis would be the formation of micellar rods by aggregated surfactants, which in the second step will produce hexagonally arrayed rods, followed by incorporation of silicate anions around the rodlike structures (mechanism **a**). However, it is now known that mechanism **a** is not correct because the surfactant concentrations used in some conditions of the synthesis of MCM-41 were far below the critical micelle concentration (CMC) required for hexagonal LC formation.^[13, 17] Considering that the liquid crystal structures formed in surfactant solutions are highly sensitive to the overall characteristics of the solution, the authors also proposed the second mechanistic pathway (Scheme 1. 2 b): The silicate anions mediated, in some manners, the ordering of the surfactants into a hexagonal arrangement.^[16] Beck et al. postulated as a

cooperative self-assembly of the ammonium surfactant and the silicate precursor species below the CMC.

A generalized liquid crystal templating mechanism: Electrostatic interaction

A fundamental mechanism of LCT is based on an electrostatic interaction between the surfactant head group S and the silica source I, which was proposed by Huo et al. as



Scheme 1. 3 Various electrostatic interaction.

[source^[2]]

shown in Scheme. 1. 3.^[18] Cationic surfactants S^+ are used for the structuring of negatively charged inorganic species I^- (S^+I^-). On the other hand, anionic surfactants S^- are employed for structuring cationic inorganic species I^+ (S^-I^+). It is also possible to combine surfactants and ionic inorganic species with identical charge, but then the formation of the mesostructure is mediated by the countercharged ions ($S^+X^-I^+$ and $S^-M^+I^-$ (X^- = counteranions, and M^+ = metal cations)).^[19] The electrostatic

interaction mechanism can be divided into two synthesis routes: the basic route (S^+I^-) and the acidic route ($S^+X^-I^+$). LCT mechanism **b** outlined in Scheme 1. 2 involving anionic silicate species and cationic quaternary ammonium surfactants, could be categorized as the S^+I^- pathway. For example, three well defined mesostructures MCM-41, MCM-48 and MCM-50 of the M41S family belong to the basic route.

One of the most important mesoporous materials synthesized through the acidic route ($S^0H^+X^-I^+$) with [triblock copolymer of poly(ethyleneoxide)poly(propyleneoxide)-

poly(ethyleneoxide)] as surfactant is SBA-15.^[1, 4-5] It is a 2D hexagonal mesoporous silica material first created by Zhao and Stucky in 1998 and exhibits a wall thickness of 3-7 nm and large pore sizes between 6 and 15 nm, improving the thermal and hydrothermal stability compared to MCM type and related silica materials.^[20] It is an ideal candidate for catalyst supports due to its high surface area for chemical modifications, thermal and structural stability, well defined and characterized nature, and chemical inertness to most reaction conditions.^[21]

1.2.2 Periodic mesoporous organosilicas

Although mesoporous silica materials are excellent support candidates, the hydrophilic properties due to the surface silanol groups sometimes are undesirable for organic transformations. In order to control the surface polarity, silylation (with trimethylsilyl or similar groups) of the hydroxyl groups is widely used. An alternative method is the synthesis of periodic mesoporous organosilicas (PMOs) through the surfactant-templated polycondensation of bridged organosilane precursors $(R'O)_3-Si-R-Si-(OR')_3$, where R is a bridging group, such as $-CH_2CH_2-$, $-CH=CH-$ or $-C_6H_4-$.^[22-24] These new materials possess a homogeneous distribution of organic groups in the channel walls and a high degree of order and uniformity of pores, which can enhance surface hydrophobicity and facilitate the diffusion and adsorption of organic molecules. Further research confirms that, depending on the catalytic reaction, the use of structurally well-defined and hydrophobic PMOs as supports can enhance activity and stability compared with hydrophilic mesoporous silica supports. As reported by W. R. Thiel et al., immobilized complexes of the type $(L-L)MoO(O_2)_2$ on phenylene-bridged mesoporous organosilicas show a 10-fold increase in catalytic activity and a high stability in liquid phase epoxidation reactions, with H_2O_2 as the oxidant, compared to the corresponding MCM-41 derived systems.^[25]

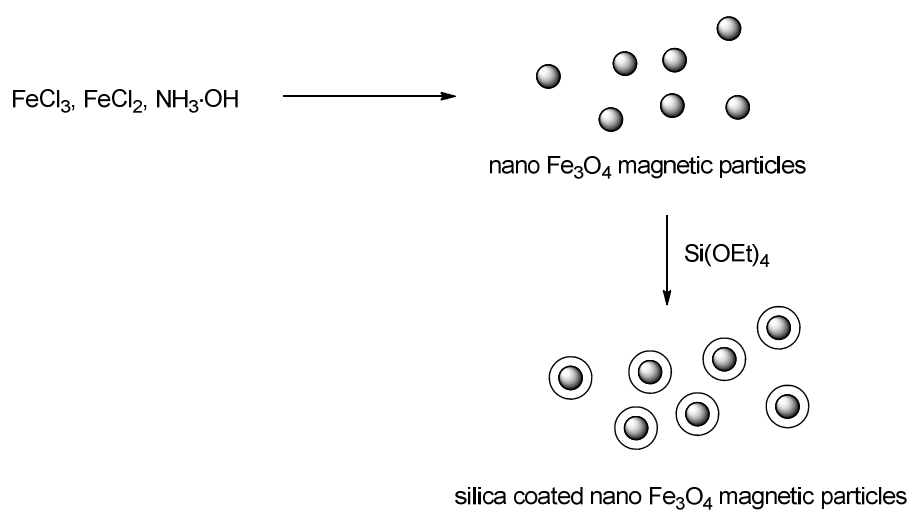
So far, there have been many reports on the preparation of PMOs with alkane, alkene, phenyl, and aromatic bridging functional groups. Furthermore, incorporation of

organometallic complexes into the walls of a PMO can turn the material into a heterogeneous catalyst,^[26-29] which will be discussed later.

1.2.3 Silica coated magnetic nanoparticles

Immobilizaion of a homogeneous catalyst on mesoporous silica support allows easy catalyst recovery as well as product separation by simple filtration. However, due to the diffusion of substrates and products through the pores of the support materials, a substantial decrease in activity of the immobilized catalyst is commonly observed compared to the homogeneous system. Nanoparticles have received increasing attention as an alternative support for catalysis due to the high external surface areas of non-porous nanoparticles, which guarantees that diffusion of reactants to the active sites will no longer limit the kinetics.^[30] However, these nanoparticles can be difficult to recover, which limits their application.

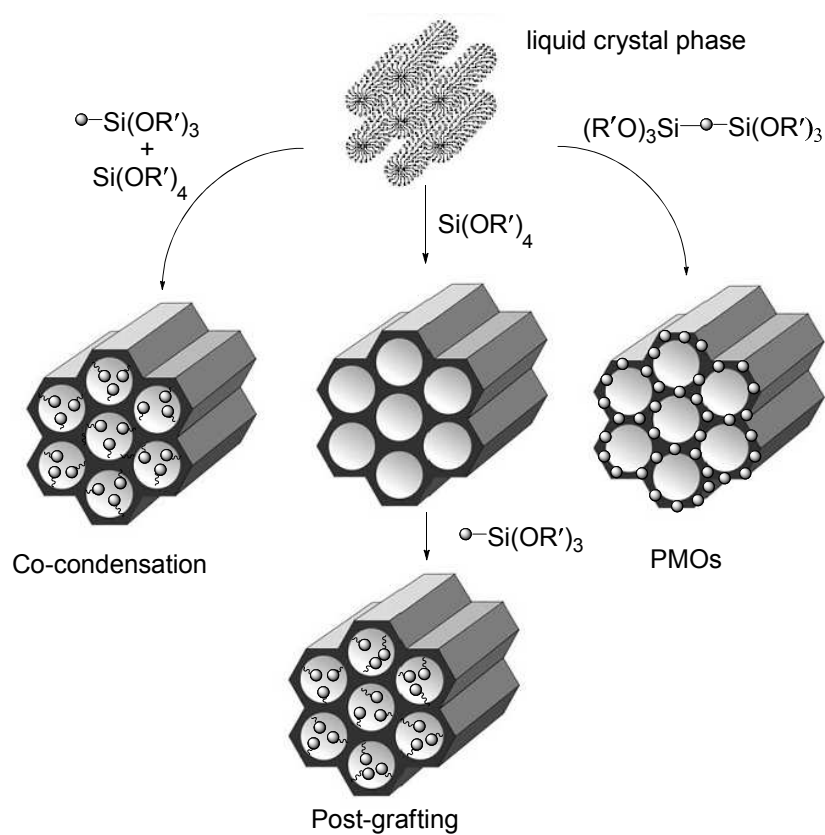
Coating magnetic nanoparticles with silica is becoming a promising and important approach in the development of magnetic nanoparticles for both fundamental studies and technology applications.^[25, 31-34] Because such materials can combine the unique magnetic properties (easily recycled by external magnetic field) with the possibility to further functionalize the surface. There are two main methods for the coating of magenetic nanoparticles with silica. One is acidic hydrolysis of silicate in aqueous solutions, another one, which is the most widely used method, is sol-gel process as shown in Scheme 1. 4. In this method, the silica phase (with silicon alkoxides as the source of silica matrix) is formed on colloidal magnetic nanoparticles in a basic alcohol/water mixture.^[35-36] The outer shell of silica not only protects the inner magnetite core from oxidation and aggregation but also provides sites for surface functionalization.



Scheme 1. 4 Procedure for synthesizing silica-coated magnetic nanoparticles.

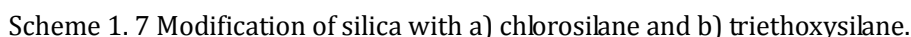
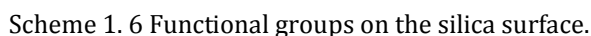
1.3 Covalent immobilization

Three pathways are available for the immobilization of organic species on porous silica material via covalent bonding as shown in Scheme 1. 5.



Scheme 1. 5 Three pathways for the immobilization of organic species.

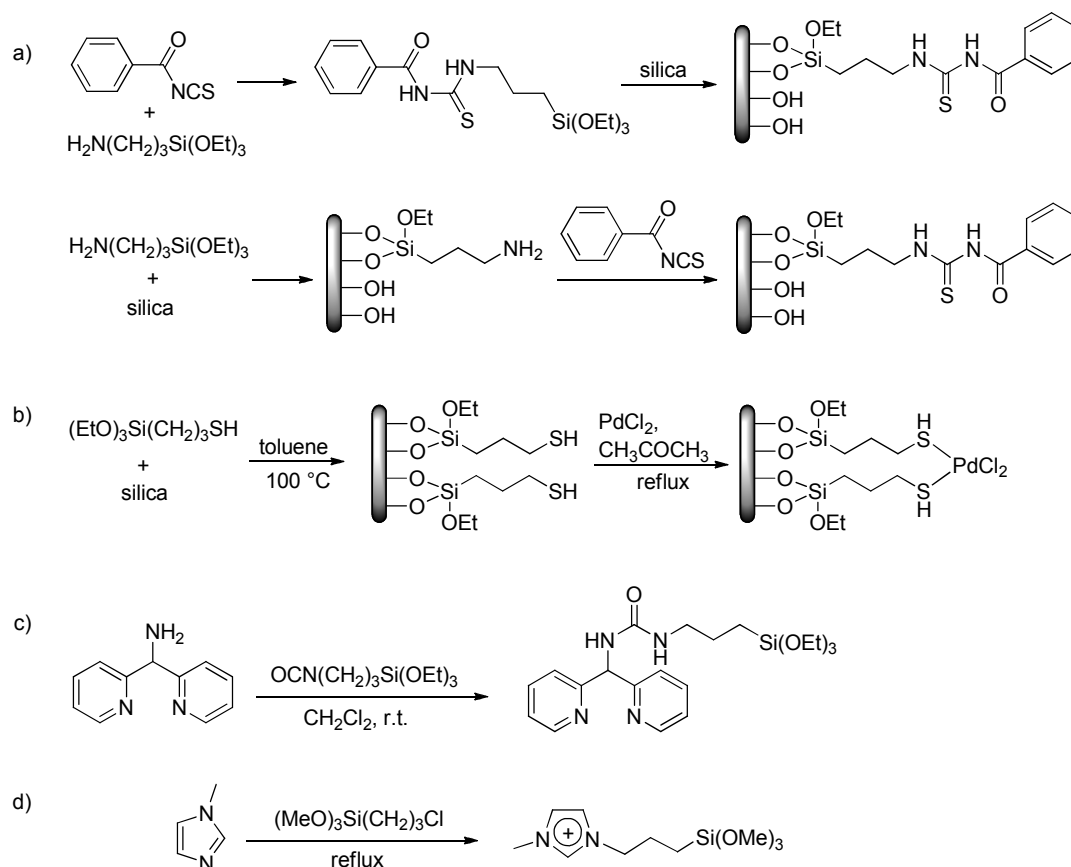
Post-grafting is the subsequent modification of the pore surface of a purely silica material. It is the most common route for the synthesis of heterogeneous catalysts. The silica surfaces consist of two types of groups, siloxane (Si-O-Si) and silanol (Si-OH) groups (Scheme 1. 6). Covalent immobilization of homogeneous catalysts on silica surfaces is based on the presence of silanol groups which can react with silylating reagents.^[3] The most widely used silylating agents are chlorosilanes and trialkoxysilanes. The reactions of these reagents with surface silanol groups are shown in Scheme 1. 7. The reaction of chlorosilane with the surface silanol groups liberates HCl, which may cause damage to the structure of the silica or have other undesired effects on the organic component (Scheme 1. 7, **a**). The usage of triethoxysilane as linker prevents this disadvantage (Scheme 1. 7, **b**).



9

1. Introduction

topropyltriethoxysilane (Scheme 1. 8, **b**),^[38] 3-isocyanatopropyltriethoxysilane (Scheme 1. 8, **c**),^[39] and 3-chloro-propyltrimethoxysilane (Scheme 1. 8, **d**).^[40] In general, there are two ways to immobilize an organic compound covalently on the surface of a solid support as shown in Scheme 1. 8, **a**: on one hand, the silane functionalized compound can be prepared prior to the grafting procedure, by this way, the functionalized compound can be purified and characterized before the grafting and the defined hybrid material can be obtained. On the other hand, the silane coupling agent can be grafted first followed by treatment of this hybrid material with an appropriate source of the active site.



Scheme 1. 8 Preparation of functionalized organic species.

Although a large number of different organic groups can be immobilized using this pathway, there are three main drawbacks with this method: (1) Limited surface silanols amount often leads to low loading of organic functionalities, resulting in the need for

relatively large amounts of catalyst. (2) Most of the organic moieties congregate near the entries of the mesopores and the exterior surfaces, which leads to inhomogeneous surface coverage.^[41] (3) The functional groups occupy the channel volume which reduces the free pore space and can lead to a total pore blocking.

1.3.2 Co-condensation method

Co-condensation is the simultaneous condensation of a silica precursor (typically a tetraalkoxy orthosilicate) with an organosilicate precursor (typically a terminal trialk-oxysilane) in the presence of surfactants. The most important impetus for this approach has come from the discovery of the M41S materials, which has allowed the predictable formation of very regular mesoporous materials with organosilicate precursors. This method has been reported to overcome the drawbacks of the post-grafting route and to enable a higher and more homogeneous distribution of organosilane functionalities.^[42-43] However, the mesostructure of the resulting materials often suffers from a certain degree of degradation.

1.3.3 Periodic mesoporous organosilicas (PMOs)

Synthesis of periodic mesoporous organosilicas (PMOs) is the third method to obtain immobilized catalysts as mentioned in 1.2.2. It is the incorporation of organic groups as bridging components directly and specifically into the pore walls by the use of bisilylated single-source organosilica precursors. In contrast to the hybrid materials which are obtained by post-grafting or co-condensation routes, the organic units in this case are incorporated in the framework of the silica matrix through two covalent bonds and thus are distributed homogeneously in the pore walls. These materials have large inner surface areas as well as a high thermal stability.

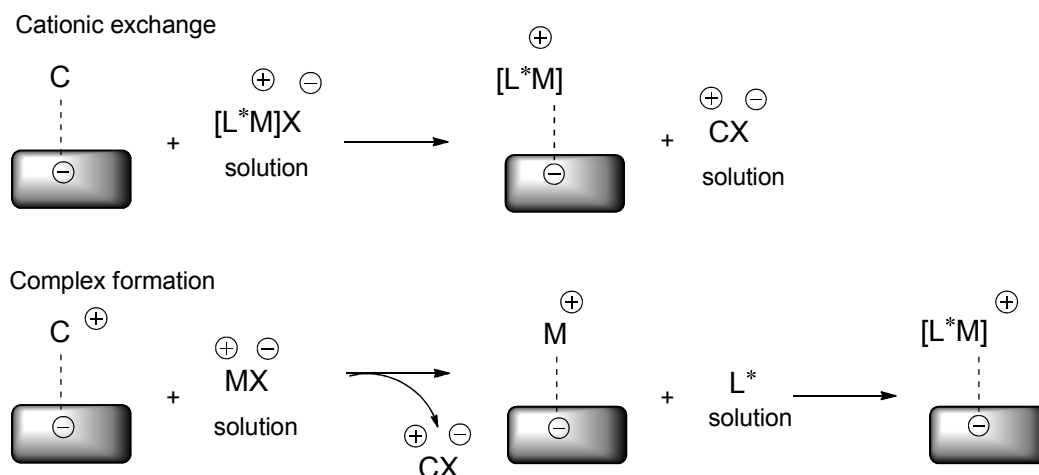
Although significant advances in the synthesis of PMOs have been made, not all alkoxy silane bridged precursors, especially those exhibiting large pore volumes, are able to self-assemble into well-ordered mesostructures by this method.

1.4 Non-covalent immobilization: electrostatic interactions

For the synthesis of immobilized catalysts, in most cases, covalent grafting of single-site catalysts is chosen. It can be achieved by functionalizing a ligand system with appropriate substituents that guarantee an irreversible tethering on the surface. However, non-covalent electrostatic anchoring of catalysts is an interesting alternative approach which is rather underestimated, since the Coulomb interactions between the catalytically active sites and the support are considered to be weaker compared to covalent interactions. In contrast, a non-covalent attachment increases the freedom of choice concerning the grafting methods, the supports, the catalytic centers, and the portfolio of the catalytic transformations. Furthermore it allows a larger mobility of the ligands on the surface which may be advantageous for stabilizing the catalyst.

Depending on the synthesis and the reaction conditions, electrostatically grafted catalysts have shown excellent activities, selectivities and stabilities, making them attractive for technical applications.^[44-46] Immobilization of cationic complexes through an electrostatic interaction is the process in which weakly coordinating anions (typically PF_6^- , BF_4^-) of cationic complexes are exchanged by the negative charged surface. These negative charges will then act as counterions for the cationic complexes (Scheme 1. 9). The formed salt by the compensation cation of the solid (C^+) and the counteranion of the complex (X^-) will be eliminated to the solution or will remain on the solid, depending on the solvent used in the exchange process. Two general methods can be used to immobilize the cationic complex: the direct cationic exchange of the complex preformed in solution and the formation of the complex on a pre-exchanged metal center (Scheme 1. 9). Both methods have advantages and disadvantages. The direct exchange, by far the most frequently employed method, allows a fully characterization of the complex before immobilization on the solid. But sometimes the unstable cationic complex can be destroyed. The addition of the ligand on the pre-exchanged metal center on the solid allows the formation of the complex with an excess of ligand, however, the metal salt in inaccessible sites has difficulties to form a

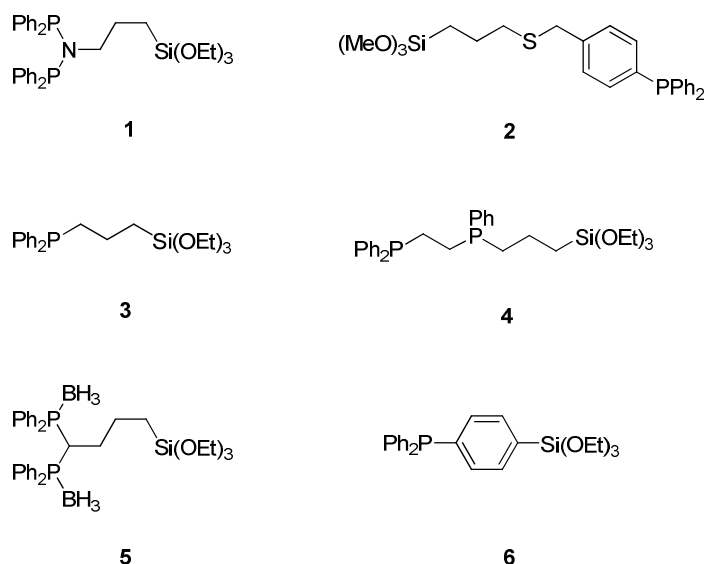
complex with the ligand. The solvent is very important for the ion exchange reaction. It must facilitate the ion mobility in order to achieve the best exchange ratio.



Scheme 1. 9 Two methods to immobilize cationic complexes through ion exchange.

1.5 Catalytic application of immobilized catalysts

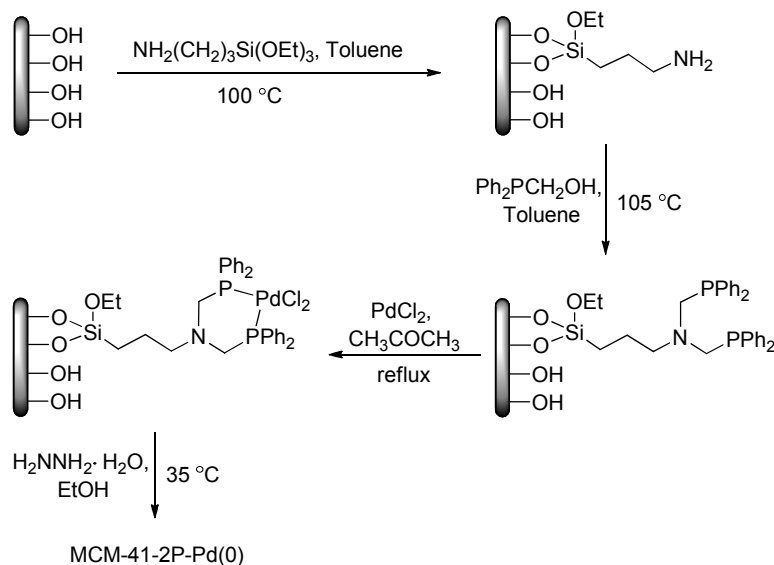
Mesoporous silica materials modified with various homogeneous catalysts can catalyze a wide range of reactions.^[5, 8] Triphenylphosphine (TPP) is one of the most important and widely used ligands for transition metal based homogeneous catalysts. $\text{Pd}(\text{PPh}_3)_4$ and other TPP palladium compounds are widely used for catalytic C-C coupling reactions such as Suzuki and Heck reactions,^[47] whereas Wilkinson's catalyst ($\text{RhCl}(\text{PPh}_3)_3$) was the first homogeneous catalyst that could efficiently catalyze the hydrogenation of alkenes.^[48] In order to immobilize TPP or related ligands and complexes on the mesoporous silica materials, much effort has been made to functionalize TPP with silylating agents. Ethoxysilane is the most popular silylating agent (Scheme 1. 10), which is commonly used for immobilization of metal complexes.^[49] Chlorosilanes are more reactive than alkoxy silanes, but this advantage with respect to surface binding makes them also unpleasant to handle.



Scheme 1. 10 Functionalized ligands for immobilization of metal complexes.

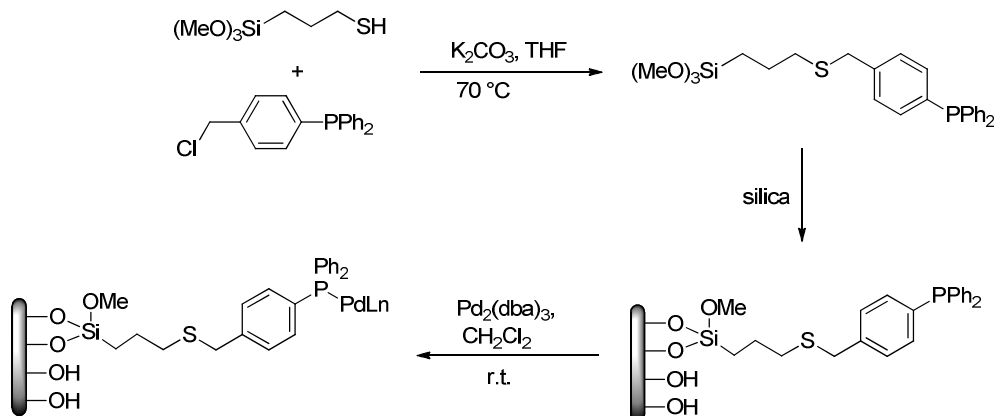
1.5.1 Suzuki reaction

The research for polymer-supported TPPs and their complexes has achieved great success during the last three decades.^[50-52] However, to the best of my knowledge, there are only a few articles about immobilization of TPP on silica materials and application for Suzuki reaction. Cai M. et al. have studied the immobilization of bidentated phosphine palladium (0) complex with ligand **1** (Scheme 1. 10).^[53] The synthesis started with the immobilization of aminopropyltriethoxysilane on MCM-41, followed by reacting the amine with diphenylphosphinomethanol. The phosphine ligand was reacted with palladium chloride which was reduced later with hydrazine hydrate (Scheme 1. 11). The authors tested different bases and solvents in order to optimize the reaction conditions. It turned out that anhydrous base K_2CO_3 and solvent dioxane are the best choices. With these optimized conditions, the catalyst not only showed excellent activity, but also reusability. Leaching tests were carried out to determine whether the reaction was truly heterogeneous. No further reaction occurs after the catalyst was filtrated, which suggests that the palladium remaining on the support is the real active center. The catalyst was further used for Heck reaction and also showed excellent performance.



Scheme 1. 11 MCM-41 supported bidenated phosphine palladium (0) complex by linker **1**.

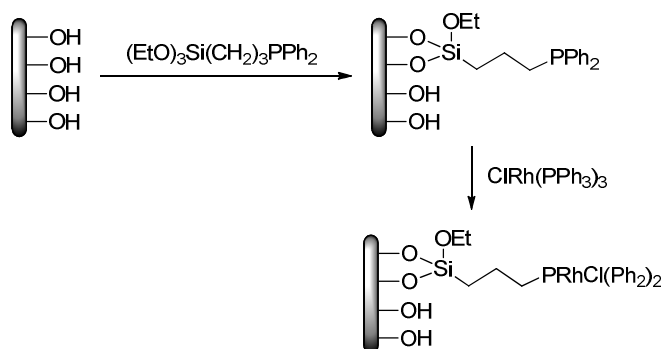
Bao et al. have recently reported the immobilization of ligand **2** (Scheme 1. 10) on SBA-15, followed by a ligand-exchange reaction with $\text{Pd}_2(\text{dba})_3$ (Scheme 1. 12). The obtained catalyst exhibited high activity in Suzuki reaction for various aryl bromides with arylboronic acids in supercritical carbon dioxide and could be reused at least seven times without loss of activity. The three phase test, which is a definitive test for the presence of catalytically active homogeneous metal species in the reaction solution, was carried out in their work. The test results clearly indicate the catalyst is very stable and almost all of the catalysis occurs due to the heterogeneous catalyst.



Scheme 1. 12 SBA-15 supported palladium complex by ligand **2**.

1.5.2 Hydrogenation

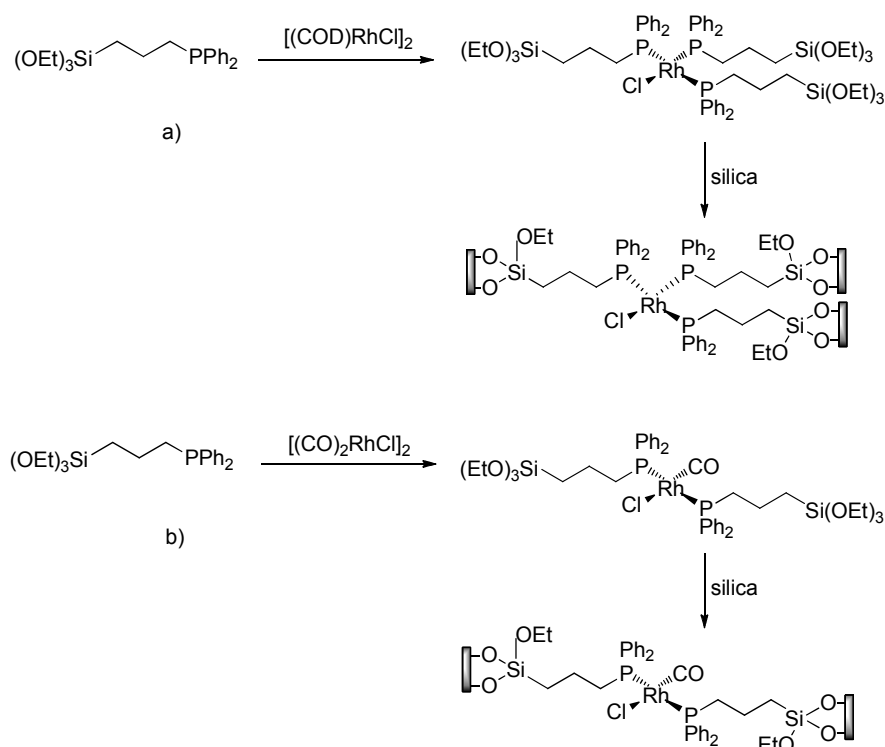
Wilkinson catalyst may be the most widely used homogeneous catalyst for olefin hydrogenation. Shyu S. et al. have immobilized a rhodium TPP complex on MCM-41, by first grafting ligand **3** (Scheme 1. 10) on silica, followed by treatment with $\text{ClRh}(\text{PPh}_3)_3$ (Scheme 1. 13).^[54] Catalytic hydrogenation of cyclohexene to cyclohexane was used to test the activity of this hybrid material. It was found out that this material gave a three times higher turnover frequency (TOF) than the homogeneous catalyst ($\text{Rh}(\text{PPh}_3)_3$). The catalyst needed an induction time at beginning of the reaction to achieve good activity



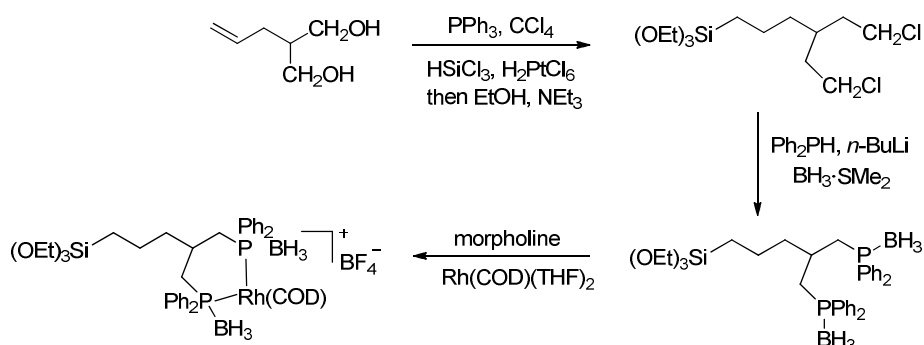
Scheme 1. 13 Immobilization of Wilkinson type catalyst by first grafting ligand.

The group of J. Blümel later also immobilized a Wilkinson-type catalyst on silica gel.^[55] Instead of grafting ligand **3** (Scheme 1. 10), the Wilkinson-type complex was first synthesized as shown in Scheme 1. 14, **a**. By this way, the rhodium complex can be well characterized before the immobilization and a well defined heterogeneous catalyst can be obtained. They also synthesized another catalyst by this method with $[(\text{CO})_2\text{RhCl}]_2$ as rhodium source (Scheme 1. 14, **b**). Further work, by the same group, a rhodium complex with dppe-type phosphine was immobilized on silica. Through adjusting the synthesis conditions such as the length of linker, the surface area of the support, they learned that even very small modifications can improve the efficiency, stability and lifetime of the immobilized catalyst.^[56-57] In order to minimize leaching, the group of C. Crudden has designed a bidentate phosphine (ligand **5**, Scheme 1. 10)

for immobilization of a rhodium complex as shown in Scheme 1. 15. The catalyst is highly active for olefin hydrogenation, however, it is extremely sensitive to the air.^[58]



Scheme 1. 14 Immobilization of Wilkinson type catalyst by first synthesizing complex (a) and immobilization of $\text{RhCl}(\text{CO})(\text{PPh}_3)_2$ type complex (b).

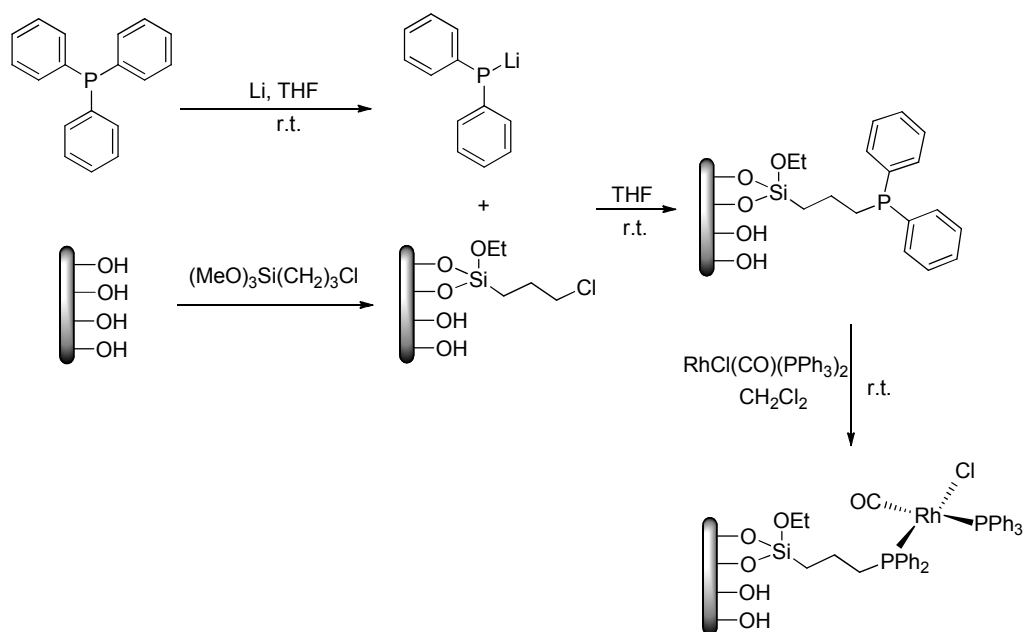


Scheme 1. 15 Immobilization of TPP type complex with ligand 5.

1.5.3 Hydroformylation

Hydroformylation is another important reaction which can be catalyzed by TPP rhodium complexes. The group of D. He used a multi-step procedure to immobilize a TPP type ligand as shown in Scheme 1. 16.^[59-61] Parent SBA-15 was first functiona-

lized by 3-chloropropyltrimethoxysilane via a post-grafting route. A diphenyl phosphino ligand was further reacted with the grafted 3-chloropropyltrimethoxysilane to yield an immobilized TPP type ligand. The obtained hybrid material was further treated with a rhodium source. The resulting catalyst showed a higher activity in shorter linear olefin hydroformylation and lower activity in the hydroformylation of inner and branched olefins. This strategy for immobilization of rhodium complex was also used by Kawi et al.^[62] The same catalyst was applied in olefin hydrogenation, which exhibited excellent activity, selectivity and reusability under mild conditions. They did not detect any rhodium species in the filtrate by Inductive Coupled Plasma Emission Spectrometer (ICP). These results indicate the immobilized phosphine ligand can effectively stabilize the rhodium centers.



Scheme 1. 16 Immobilization of $\text{RhCl(CO)(PPh}_3)_2$ type complex by first grafting ligand.

1.5.4 Other reactions

TPP type ligands are widely used in catalysis, except above mentioned reactions, they can be applied in many other reactions. The group of U. Schubert incorporated $\text{Rh(CO)Cl[PPh}_2\text{CH}_2\text{-CH}_2\text{Si(OEt)}_3]_2$ into the silica matrixes by a sol-gel process. The

heterogeneous catalyst exhibited higher stability and better catalytic properties than corresponding homogeneous catalyst in the hydrosilylation of 1-hexene.^[63] Kröcher et al. employed sol-gel process derived silica-anchored iridium, palladium, platinum, ruthenium and rhodium complexes (ligand **3**, Scheme 1. 10).^[64-65] The catalysts were tested for the solvent free synthesis of N, N-dimethylformamide (DMF) from carbon dioxide, hydrogen and dimethylamine. The ruthenium-containing hybrid material proved to be the most active catalyst for DMF synthesis, however, rhodium containing heterogeneous catalyst had only low activity and the rhodium complex decomposed under the reaction conditions.

1.6 Motivation

The main goal of this thesis was to synthesize mesoporous silica materials with immobilized triphenylphosphine complexes featuring high activity, selectivity and reusability in catalysis. The required work can be divided into the following tasks:

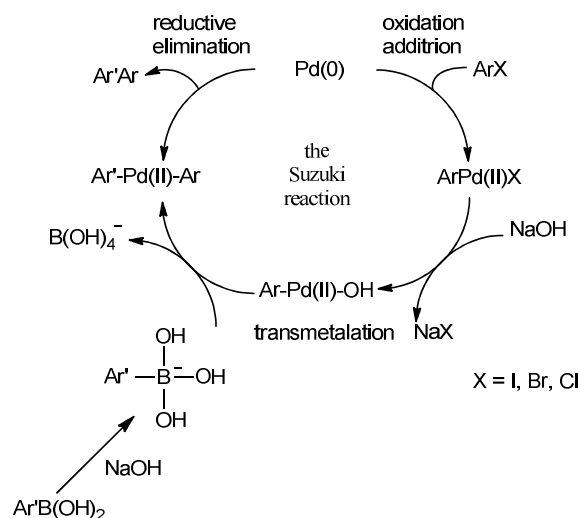
- (1) Synthesis of easily accessible functionalized TPP ligands.
- (2) Preparation of various transitional metal complexes with the obtained TPP ligands, which should have potential applications in organic transformations.
- (3) Immobilization of the resulting complexes on different supports with covalent and non-covalent strategies.
- (4) Studying of the immobilized catalysts in liquid phase reactions and investigation of their catalytic activity, selectivity and reusability. Based on the reaction results and the obtained characterization data, the influence of the transition metal, the linker, the support and the reaction conditions on the catalytic performance should be examined.

Chapter 2. Covalent Immobilization of Triphenylphosphine Complexes

2.1 Immobilization of a Palladium Complex by the Post Grafting Method

2.1.1 Introduction

The palladium(0) catalyzed Suzuki cross-coupling of aryl halides with arylboronic acids to form biaryls has emerged as an extremely powerful tool in organic synthesis.^[66-68] Since palladium(II) complexes are generally more stable than their palladium(0) counterparts, precatalysts in the palladium(II) oxidation state were usually employed in the Suzuki reaction. It is presumed that they are reduced in-situ to palladium(0). The whole catalytic cycle switches between palladium(0) and palladium(II) and involves three distinctive steps (Scheme 2. 1).



Scheme 2. 1 General mechanism for Suzuki reactions.

First, an aryl halide is oxidatively added to palladium(0) to form a palladium(II) intermediate. This is followed by a transmetalation reaction to produce a palladium(II) complex containing the two moieties to be coupled. For this step the boronic acid must be activated with base, which enhances the polarisation of the organic ligand and

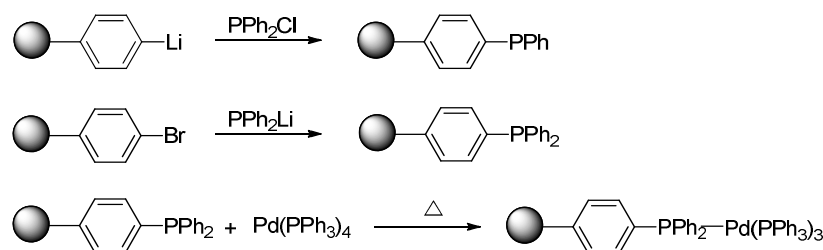
facilitates transmetallation.^[69] Several further roles have been proposed for the added base on the basis of experimental studies, though they have not been definitely established.^[70] The final step is the rapid reductive elimination of the product and the regeneration of the active palladium(0) catalyst.^[68, 70]

There are many homogeneous palladium complexes available for Suzuki reaction with N, O, P and S as donor ligands, palladacycles as well as *N*-Heterocyclic carbene containing precatalysts.^[71] Among them, triphenylphosphine complexes are most widely used for this reaction, mainly due to the simple handling of the derived complexes and the low price of the *P*-donor ligand. Depending on the substrate they show good activity and selectivity. Indeed, until now most coupling reactions rely on use of palladium triphenylphosphine complexes such as $\text{Pd}(\text{PPh}_3)_4$, $\text{PdCl}_2(\text{PPh}_3)_2$.^[72-73] The basic experimental conditions like the range of reactants, the effect of the temperature, the solvent and the Pd: P ratio are still being studied. In the past few years, great advances have been achieved in developing active and efficient catalysts by modifying traditional ligands and discovering new ones. Sterically demanding and electron-rich phosphines such as $\text{P}(t\text{-Bu})_3$, PCy_3 have shown high cross-coupling activities even with non-active aryl chlorides as reactants.^[74-75]

Although significant efforts have been achieved to develop homogeneous palladium catalysts, such systems are difficult to be separated and reused, which is of special disadvantage for large-scale preparations and industry applications. One way to generate active and stable heterogeneous catalysts is immobilization of homogeneous catalysts on solid materials.^[5, 71, 76]

Lots of efforts have been made to synthesize immobilized triphenylphosphine palladium complexes for application in coupling reactions during the last decades. By using halogenated and cross-linked polystyrene as the starting material, a series of polymers containing phosphines as functional groups have been prepared.^[76] These polymers then can act as ligands to bind catalytically active metal sites (Scheme 2. 2).

2. Covalent Immobilization of Triphenylphosphine Complexes

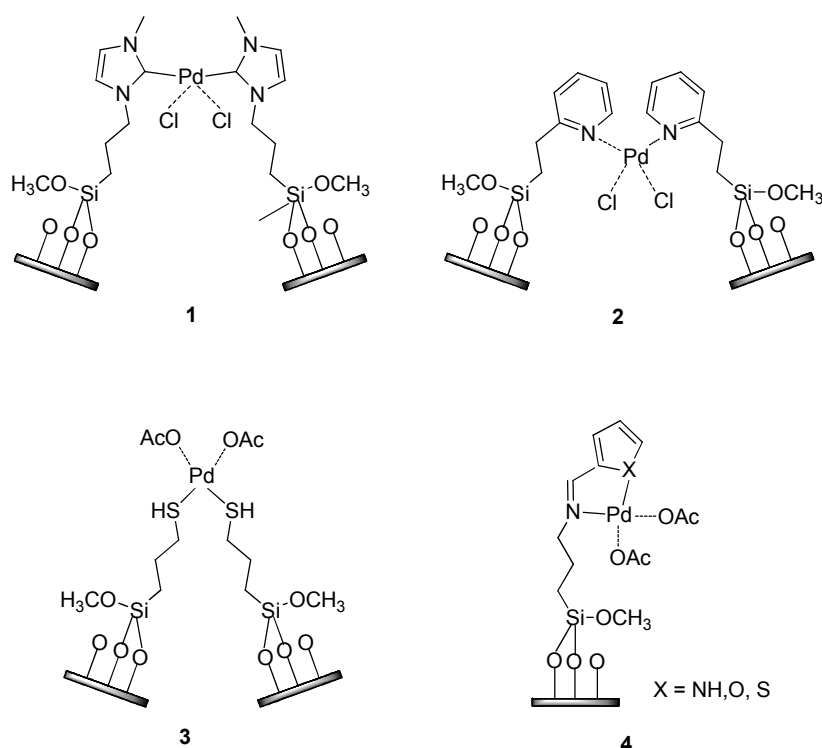


Scheme 2. 2 Synthesis of polymer supported palladium triphenylphosphine complex.

In an early report Trost et al. described the first polymer-supported palladium catalysts based on diphenylphosphanyl functionalized polystyrene.^[77] In the following years a variety of other polymer-supported palladium triphenylphosphine complexes were synthesized and used for coupling reactions.^[50-52, 78-79] These heterogeneous materials were reported as active, stable and reusable catalysts in Suzuki reactions. However, with the polymeric resins as the support, the state of palladium was unclear. Additionally, the solvent dependent swelling of these resins often is a drawback for applications in catalysis. On the other hand, silica materials have been widely used as supports for catalytically active sites. They exhibit - depending on the preparation procedure - excellent mechanical and chemical stability, extremely high surface areas and defined porous structures.

Different palladium complexes, bearing ligands such as carbenes, amines or thiols, have been immobilized on silica supports.^[80-82] In a detailed study Clark and Paul investigated the relationship between the chemical structure and the catalytic activity in the Suzuki coupling reaction for a wide variety of bidentate ligands grafted on silica including *N,N*-, *N,S*- and *N,O*-donating systems (Scheme 2. 3).^[83] They found that lowering the bond energy between the palladium center and the ligand results in an increase in reactivity. Grudden et al. reported that thiol modified mesoporous materials are remarkable scavengers for palladium, and the resulting palladium encapsulated materials catalyze Suzuki type coupling reactions with virtually no leaching of palladium.^[84] Corma et al. immobilized an oxime-carbapalladacycle complex on mercaptopropyl modified silica. This solid is an active and stable heterogeneous catalyst for the Suzuki coupling reaction of aryl bromides and chlorides in water.^[85] All

these successful examples prove that the immobilization of homogeneous single-site catalysts is an effective and promising method to combine the superior activities and selectivities of homogeneous with the simple recovery of heterogeneous catalysts. However, since the surface Si-OH groups of the silica support are the only reactive sites available for grafting of the catalyst and the degrees of freedom in the ligand synthesis are limited, only few triphenylphosphines have been covalently grafted on silica.^[54, 56, 86]



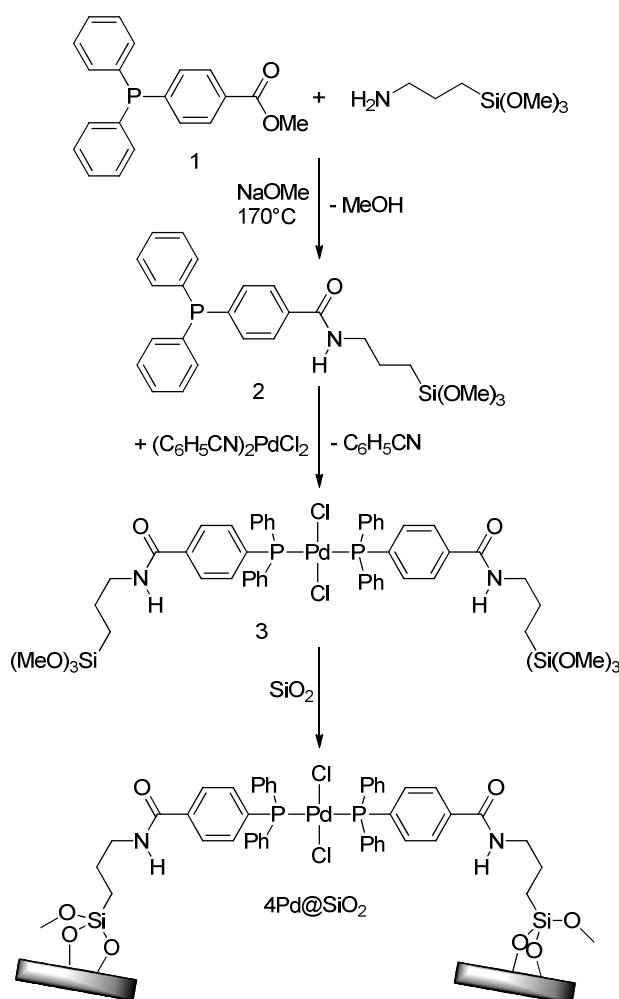
Scheme 2. 3 Immobilization of palladium complexes on silica.

One of my targets was to functionalize a triphenylphosphine ligand with a trimethoxysilane group which can further react with Si-OH units on the silica surface. In my approach the functionalized ligand was coordinated to $\text{PdCl}_2(\text{CNPh})_2$ to obtain a functionalized palladium complex which can be purified and characterized before grafting. The resulting functionalized palladium triphenylphosphine complex was then covalently bound to a mesoporous silica support. Furthermore, the catalytic properties of the palladium containing material were studied for the Suzuki cross-coupling between aryl halides and arylboronic acids.

2.1.2 Results and discussion

Synthesis

It should be mentioned at this point that the usage of diarylalkyl phosphines like $\text{Ph}_2\text{P}(\text{CH}_2)_3\text{Si}(\text{OEt})_3$ has already been reported for the synthesis of phosphine functionalized silica materials.^[54-55, 86-87] However, these ligands are much more sensitive towards oxidation than triarylphosphines. Additionally the steric demand of the alkyl chain is moderate and the linker between the phosphorous donor and the silicon based anchoring group is short, which might favor additional interactions between the framework walls and the active site. We therefore focused on immobilizing a triphenylphosphine based system onto silica via an alkyl chain linker attached to one of the aryl rings of the phosphine ligand. In general, there are two ways to immobilize a catalytically active complex covalently on the surface of a solid support, on one hand, the active complex can be prepared prior to the grafting procedure; On the other hand, the ligand system can be grafted first followed by treatment of this hybrid material with an appropriate source of the active site. For our palladium system we chose the first route, since it determines the molar ratio of palladium and phosphine to exactly 1:2, the palladium complex can be purified and spectroscopically characterized before starting the anchoring procedure and the two phosphines will be anchored in an ideal position for coordination to one palladium site on the surface. This prevents the generation of palladium centers coordinated to one or three phosphine molecules. Another advantage of this route is to avoid that phosphineoxide species are generated when the phosphine ligand is grafted on the silica surface, which are no longer able to bind palladium.^[86] The palladium triphenylphosphine functionalized hybrid silica was prepared as summarized in Scheme 2. 4 .

Scheme 2. 4 Synthesis of the heterogeneous palladium catalyst **4Pd@SiO₂**.

The compound 4-diphenylphosphinylbenzenecarboxylicacid methylester **1** was prepared following a procedure developed by my colleague Andreas Reis. Starting from **1**, the $-\text{Si(OR)}_3$ function required for the grafting was introduced by a solvent free NaOMe catalyzed thermal aminolysis with 3-trimethoxysilylpropylamine. This reaction is extremely sensitive to oxygen and H_2O , which can cause oxidation of phosphine and hydrolysis of the $-\text{Si(OR)}_3$ group. After the reaction the catalyst NaOMe must be removed by filtration with a Whatman filter, otherwise a trace of H_2O can cause considerable hydrolysis of the $-\text{Si(OR)}_3$ group, which leads to an insoluble palladium complex in the next step. For the synthesis of the palladium(II) complex **3**, ligand **2** was dissolved in CH_2Cl_2 and treated with half an equivalent of di(benzonitrile)dichloropalladium(II), giving the desired product good yields. In the end, the functionalized palladium complex was grafted onto silica which was a

commercially available mesoporous but not ordered silica gel (Aldrich, TLC standard grade). The obtained hybrid material must be extracted with CH_2Cl_2 in a Soxhlet apparatus for 24 h in order to remove all non-covalently grafted palladium complex.

Characterization

The oily product **2** was characterized by NMR spectroscopy. Figure 2. 1 shows three sets of signals at high field in the ^1H NMR spectrum (3.46, 1.74, 0.71 ppm), which are typical for the silicon functionalized propylene chain and a sharp singlet (3.57 ppm) for the $-\text{Si}(\text{OMe})_3$ group. A weak peak beside this resonance is caused by a little hydrolysis of the $-\text{Si}(\text{OMe})$ group, which also reduces the peak area of the $-\text{Si}(\text{OMe})_3$ group. One broad singlet at 6.51 ppm for the NH group and a quite complex pattern of resonances between 7.3 and 7.8 ppm for five magnetically inequivalent protons of the aryl rings, which are all coupling with the phosphorous atom are complexing the spectrum. The ^{13}C NMR spectrum (Figure 2. 2) shows signals for the aryl groups in the range from 126.8 to 141.8 ppm. Three resonances at 42.3, 22.7, 6.6 ppm can be correlated with the resonances of the propylene linker in the precursor **3** (42.4, 22.7 and 6.6 ppm). The resonance at 50.7 ppm can be assigned to the organosilica $-\text{Si}(\text{OCH}_3)_3$ group and a signal at 167.2 ppm can be assigned to the $\text{C}=\text{O}$ group of the linker. The resonance for the methyl group of compound **1** (around 52 ppm) disappears after the reaction, which is a powerful evidence for the successful aminolysis reaction between ester and amine groups. The ^{31}P NMR spectrum shows one sharp resonance at -4.10 ppm, typical for a triaryl substituted phosphorous atom (Figure 2. 3).

The ^1H NMR, ^{13}C NMR and ^{31}P NMR spectra of the palladium complex **3** are shown in Figure 2. 4, Figure 2. 5 and Figure 2. 6. The ^1H NMR, ^{13}C NMR data are in complete agreement with the spectroscopic features of the precursor ligand **2**. The ^{31}P NMR spectrum of complex **3** exhibits a peak around 24.4 ppm. Compared to the free ligand this resonance shifts about 28 ppm downfield, indicating coordination through the phosphorous atom.

2. Covalent Immobilization of Triphenylphosphine Complexes

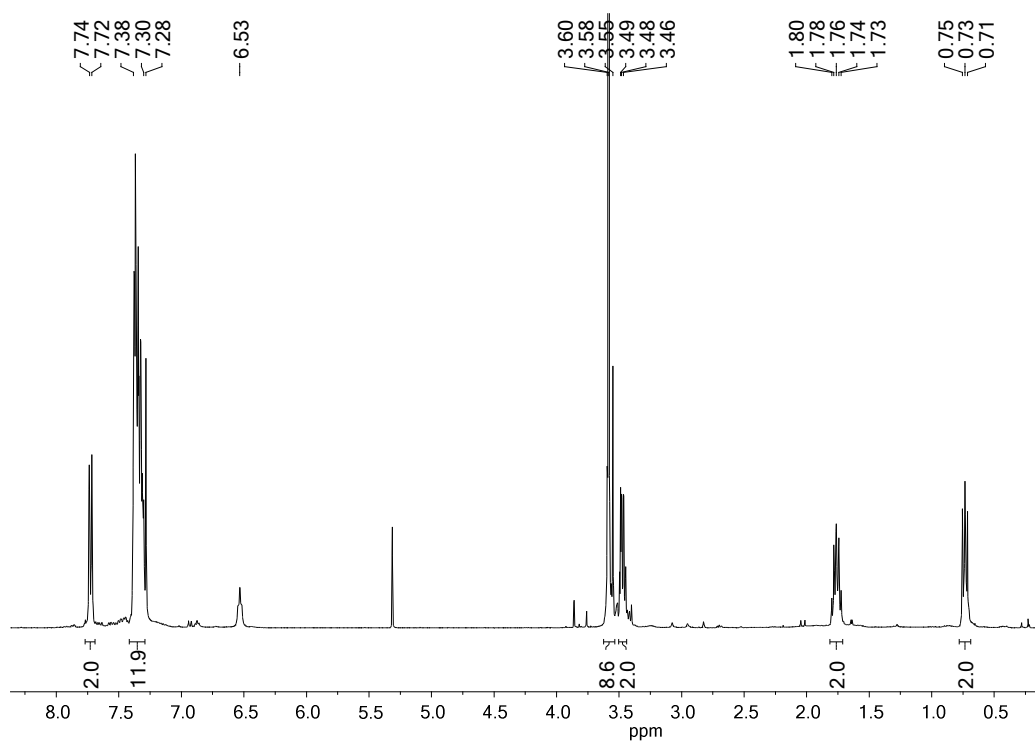


Figure 2. ¹H NMR spectrum of ligand **2** (400.13 MHz, 25 °C, CDCl₃).

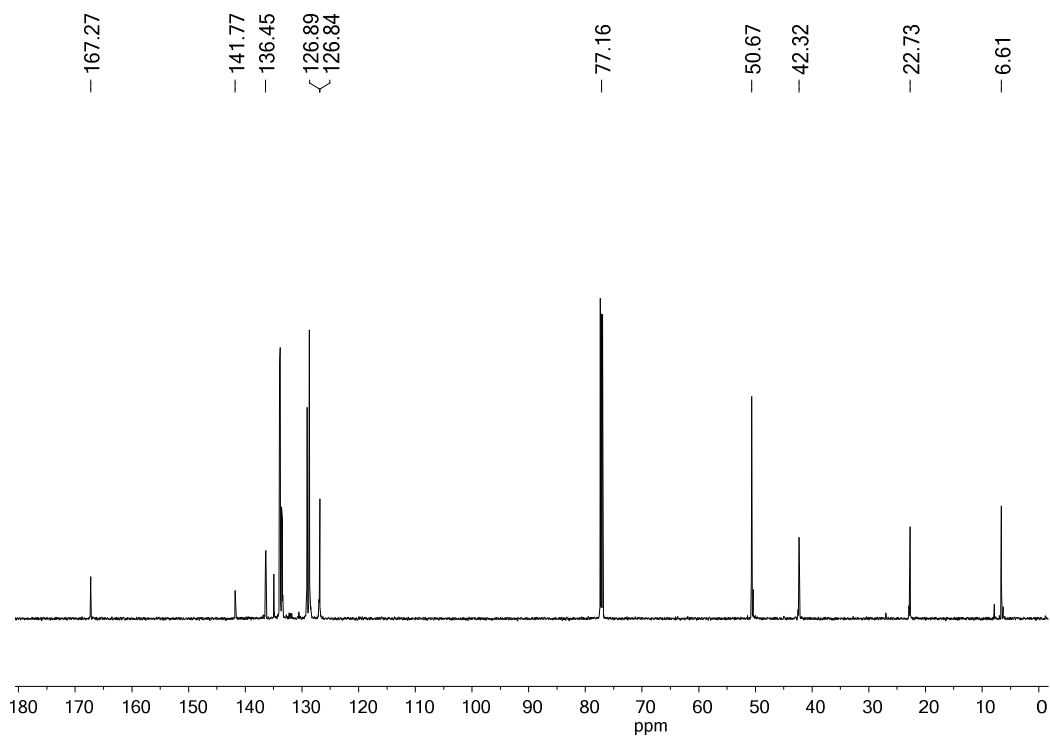


Figure 2. ¹³C NMR spectrum of ligand **2** (100.62 MHz, 25 °C, CDCl₃).

2. Covalent Immobilization of Triphenylphosphine Complexes

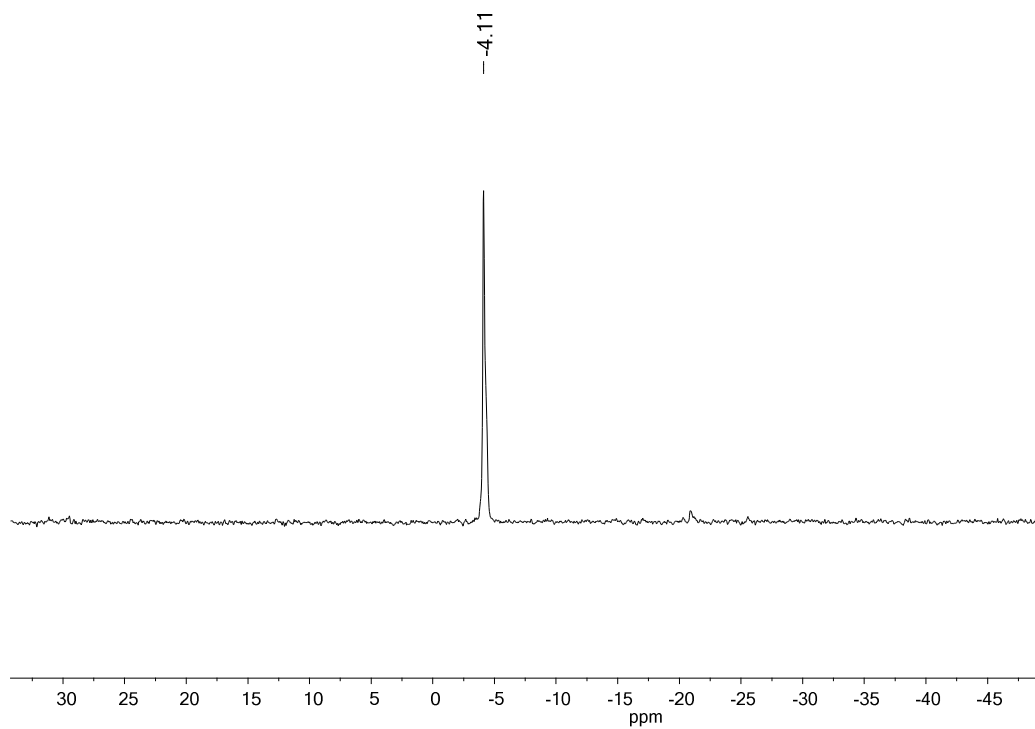


Figure 2. ^{31}P NMR spectrum of ligand **2**.

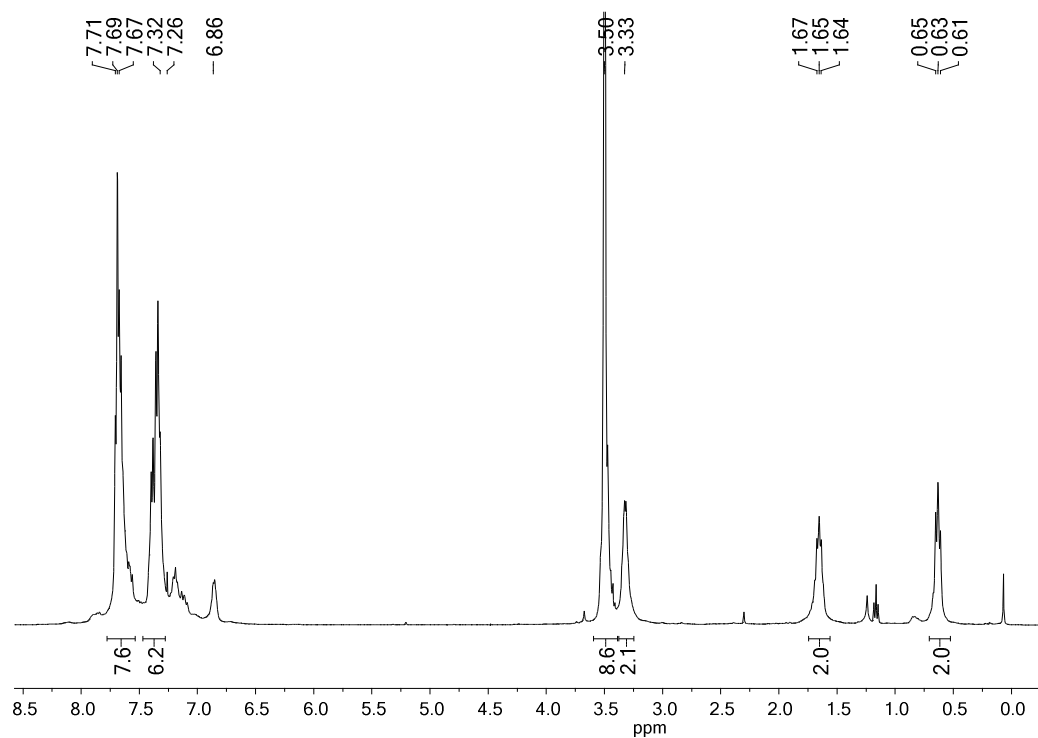


Figure 2. ^1H NMR spectrum of palladium complex **3** (400.13 MHz, 25 $^\circ\text{C}$, CDCl_3).

2. Covalent Immobilization of Triphenylphosphine Complexes

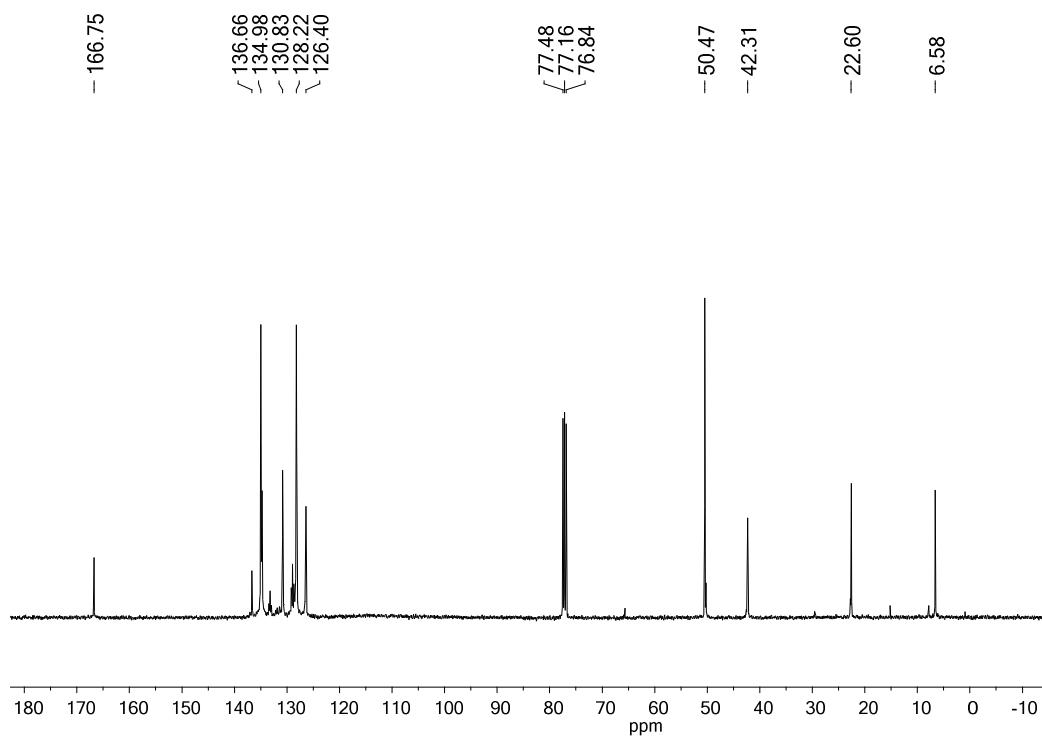


Figure 2. 5 ^{13}C NMR spectrum of palladium complex **3** (100.62 MHz, 25 $^{\circ}\text{C}$, CDCl_3).

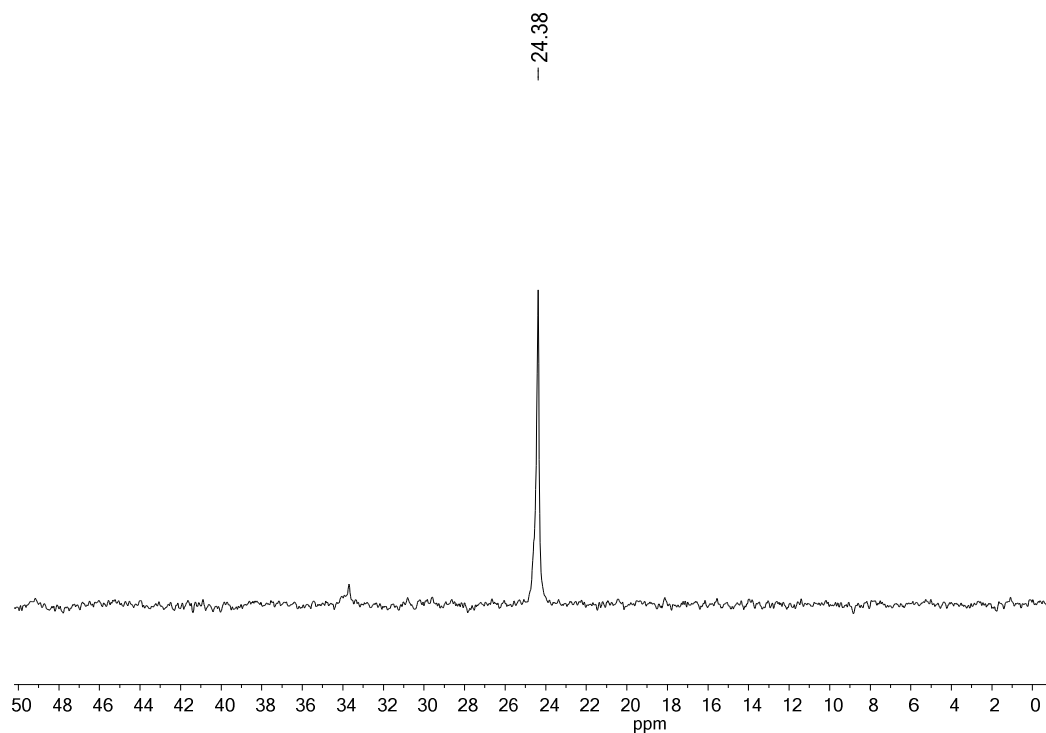
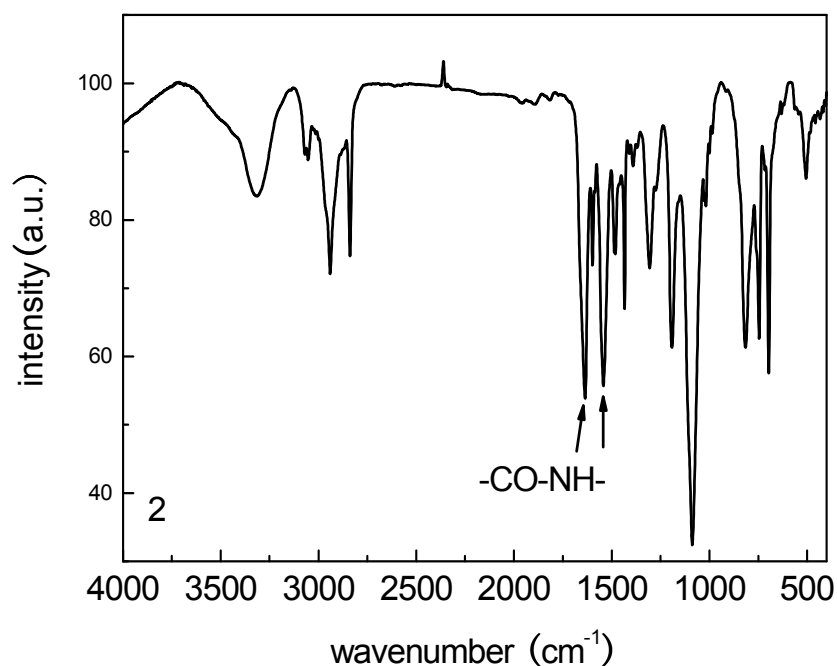


Figure 2. 6 ^{31}P NMR spectrum of palladium complex **3**.

The infrared spectral data of ligand **2** and palladium complex **3** are shown in Figure 2. 7. The sharp band of ligand **2** at 1636 cm^{-1} is assigned to the $\nu\text{ C=O}$ stretching vibration (amide I). The N-H bending vibration (amide II) is observed at 1541 cm^{-1} . In the IR spectrum of **3**, the amide I peak is slightly shifted to a higher frequency (1645 cm^{-1}) due to the electron withdraw by the Lewis acidic palladium(II), which is in agreement with the ^{31}P NMR spectra of ligand **2** and complex **3**. Both IR spectra show several bands around 3000 cm^{-1} , which are assigned to the C-H and N-H stretching vibrations.

A SEM micrograph of the hybrid material **4Pd@SiO₂** shows that the modified silica is built up from irregular blocks and these blocks have a smooth surface (Figure 2. 8). However, as the resolution limit of SEM is just 50 nm, a more detailed information about state of the grafted palladium species (fresh and used catalyst) cannot be obtained. Figure 2. 9 gives the EDX spectrum taken from the fresh catalyst **4Pd@SiO₂**, which confirms the presence of palladium on the mesoporous silica matrix.



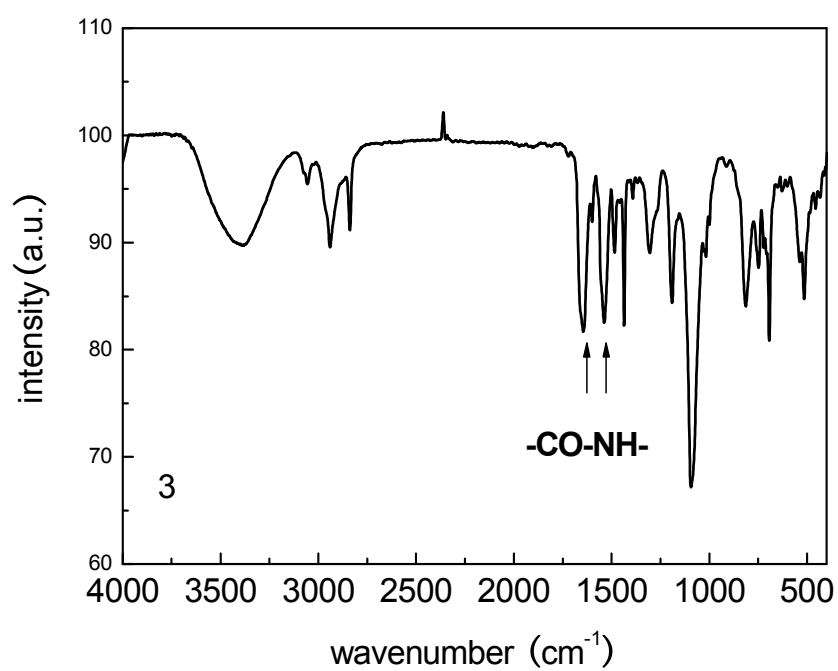


Figure 2. 7 FT-IR spectroscopy of ligand **2** and palladium complex **3**.

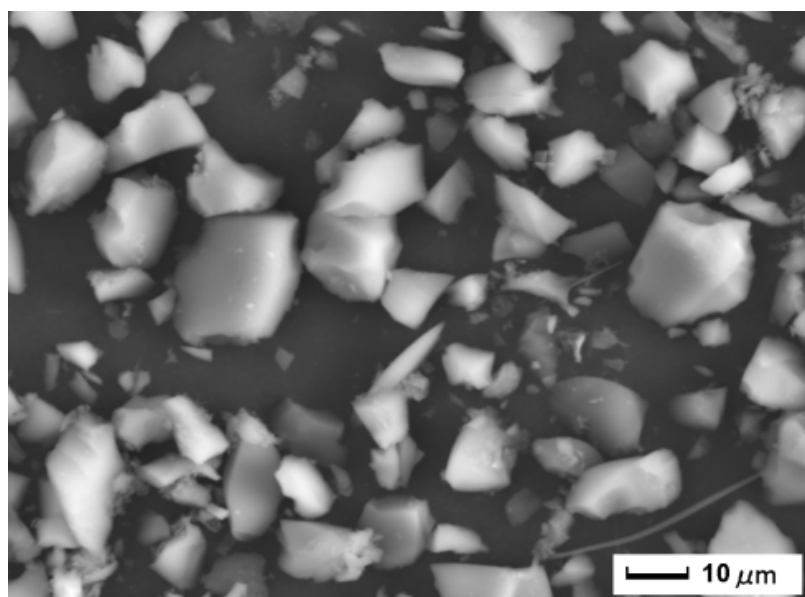


Figure 2. 8 SEM image of the freshly prepared catalyst **4Pd@SiO₂**.

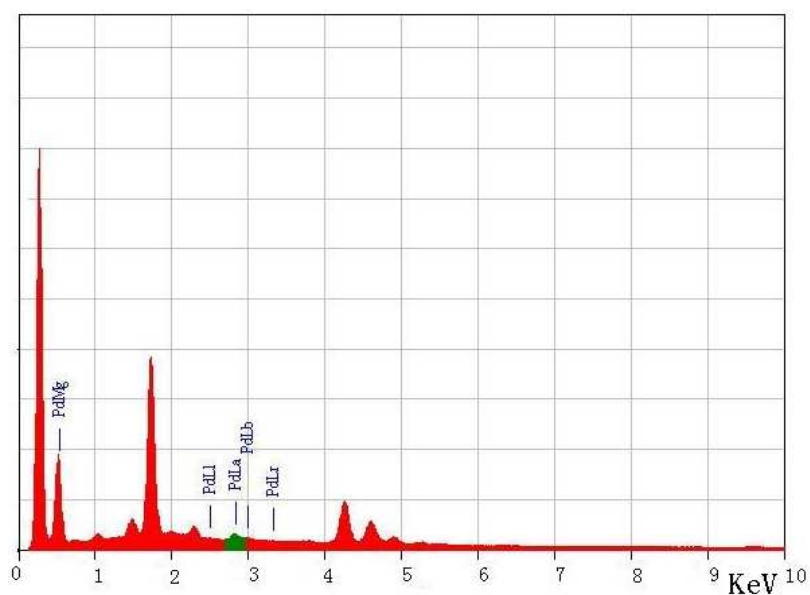


Figure 2. 9 EDX spectrum of the freshly prepared catalyst **4Pd@SiO₂**.

Nitrogen sorption was used to measure the changes of the pore structures as a result of the organic modification in the channels. The specific surface areas and the textural properties of the analysis of the nitrogen adsorption and desorption data exhibited a type IV isotherm with a hysteresis characteristic for mesoporous materials possessing pore diameters between 2 and 50 nm (Figure 2. 10, A).^[88] This indicates that the overall mesoporosity is maintained after the introduction of the palladium complex. The pore size distribution (PSD) was obtained by applying the BJH pore analysis according to the desorption branch of the nitrogen desorption isotherms (Figure 2. 10, B).

The measured data for the BET surface area, the total pore volume and the pore size of **4Pd@SiO₂** are 247 m²·g⁻¹, 0.43 cm³·g⁻¹ and 5.5 nm respectively. As expected, the surface area, the pore volume and pore size of the hybrid material are decreased compared to the neat silica support (500 m²·g⁻¹, 0.82 cm³·g⁻¹ and 6.0 nm) (Table 2. 1). These results indicate that the palladium complex was grafted in the pores of the support. The loading of the palladium complex (0.18 mmol·g⁻¹) was determined by measuring the nitrogen content of the material.

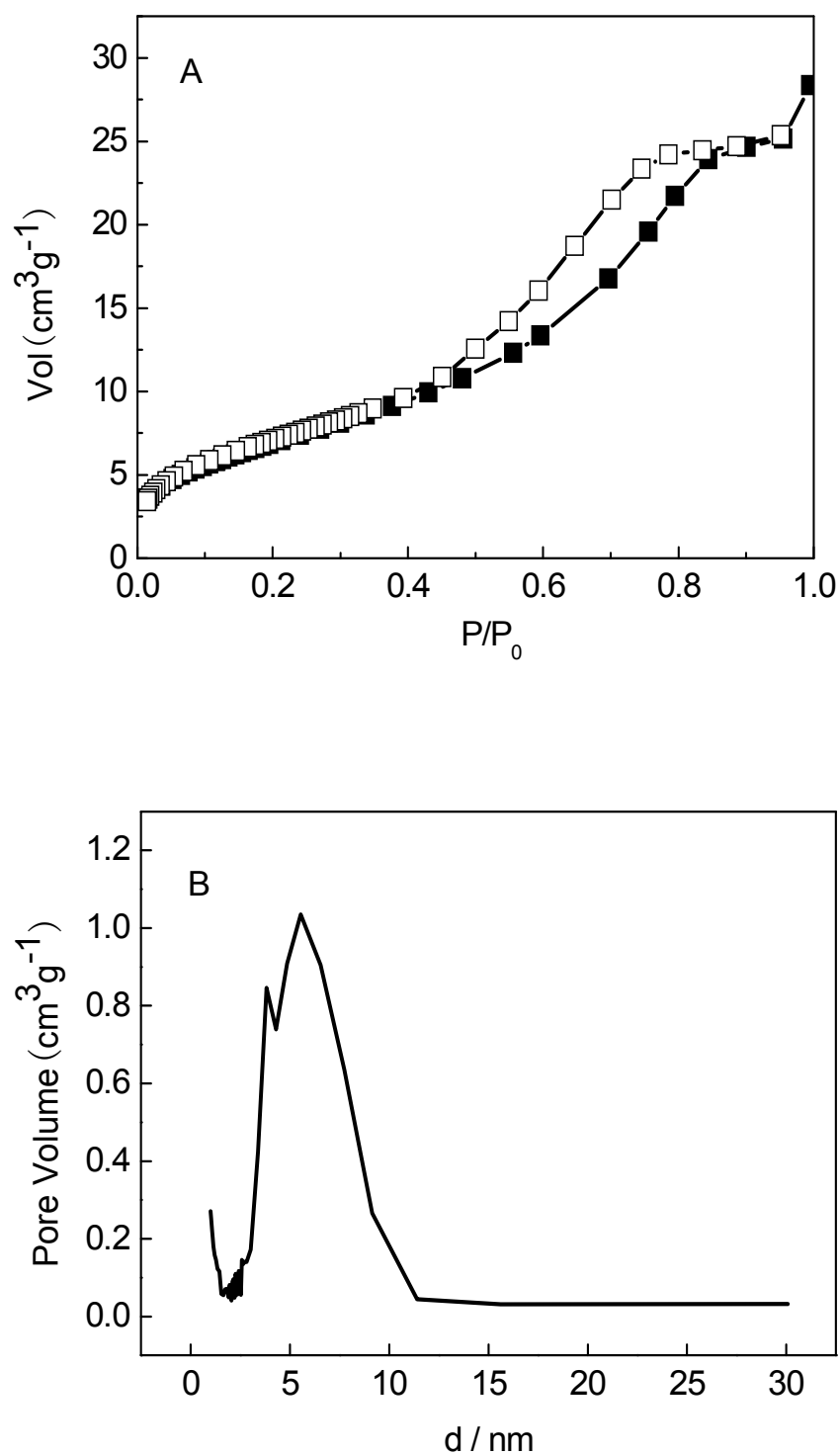


Figure 2. 10 (A) N_2 sorption isotherms at 77 K and (B) pore size distribution of 4Pd@SiO_2 ; adsorption points are marked by solid and desorption points by empty squares.

2. Covalent Immobilization of Triphenylphosphine Complexes

Table 2. 1 Characterization of the parent silica gel and the hybrid material **4Pd@SiO₂**.

material	S _{BET} [m ² g ⁻¹]	pore vol. [cm ³ g ⁻¹]	BJH pore diam. [nm]	chem. composition (wt. %)			Pd ^a [mmol g ⁻¹]
				C	H	N	
neat silica	500	0.75	6.0	-	-	-	-
4Pd@SiO₂	247	0.43	5.5	10.2	1.4	0.5	0.18

^aCalculated according to the nitrogen of the material.

The ²⁹Si CP-MAS NMR spectrum (Figure 2. 11) of the hybrid material **4Pd@SiO₂** gives direct evidence for the covalent incorporation of the phosphinepalladium(II) complex **3**. According to the literature, the signals at -110, -101, and -92 ppm correspond to the Si(OSi)₄(Q⁴), HOSi(OSi)₃(Q³), and (HO)₂Si(OSi)₂(Q²) sites of the inorganic silica framework.^[89] Covalent grafting of **3** on the silica surface makes the Q² signal of the neat silica almost disappear, which is due to the consumption of highly reactive geminal Si-OH groups during the condensation reaction.^[90] For the modified material **4Pd@SiO₂**, three additional broad and overlapping signals appear at -49, -58, and -67 ppm, which can be assigned to R-Si(RO)₂(OSi)(T¹), R-Si-(RO)(OSi)₂(T²), and R-Si(OSi)₃(T³) organosiloxane sites. Since the T¹ resonance is dominant over T² and T³, the covalent grafting of the silylated phosphine is mainly due to R-Si(RO)₂(OSi) sites.

The ¹³C CP-MAS NMR spectrum of **4Pd@SiO₂** (Figure 2. 12) shows signals for the aryl groups in the range from 145.1 to 120.1 ppm. Three resonances at 42.8, 22.7 and 9.0 ppm can be correlated with the resonances of the propylene linker in the precursor **3** (42.4, 22.7 and 6.6 ppm). A signal at 168.0 ppm can be assigned to the C=O group of the linker. It is found at an almost similar chemical shift as for **3**, which indicates, that the interaction between the amide group of the linker and the silica framework is only weak.^[91] The dominant resonance at 48.9 ppm can be assigned to organosilica C-SiOCH₃ groups, implying that the hydrolysis/condensation of **3** is not fully completed and residual methoxy groups are bound to the coupling group of the ligand as already mentioned in the discussion of the ²⁹Si CP-MAS NMR spectrum.

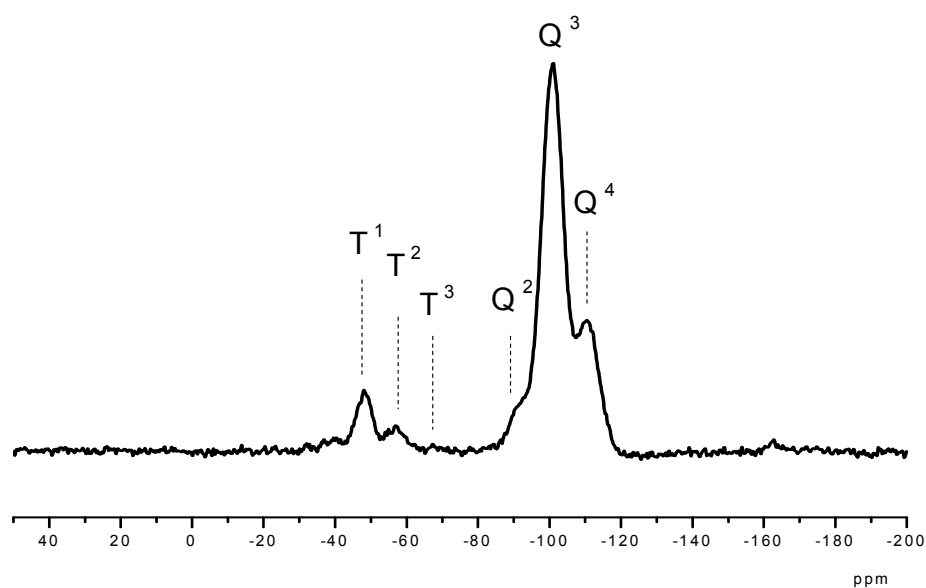


Figure 2. 11 ^{29}Si CP-MAS NMR spectrum of the hybrid material **4Pd@SiO₂**.

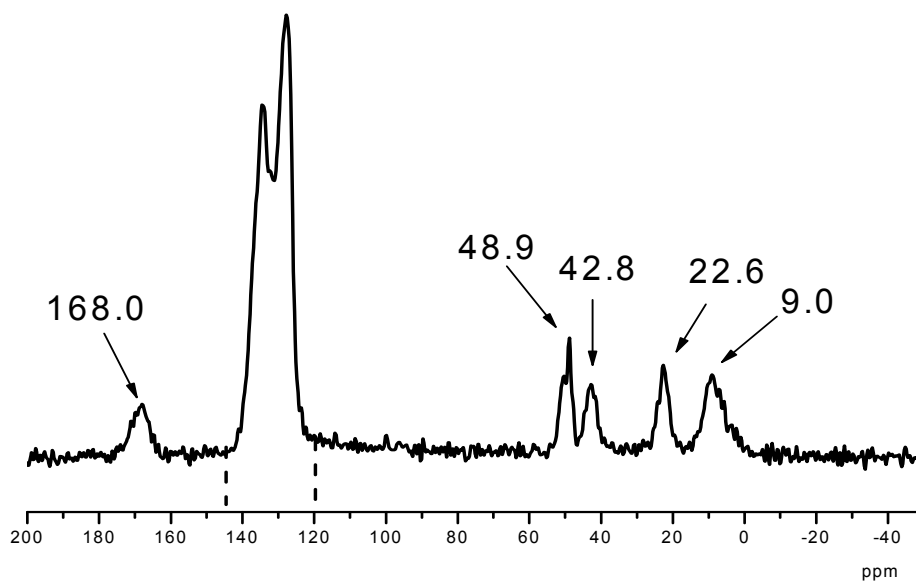


Figure 2. 12 ^{13}C CP-MAS NMR spectrum of the hybrid material **4Pd@SiO₂**.

The structural retention of the palladium (II) complex during the immobilization process is further proved by the ^{31}P CP-MAS NMR of **4Pd@SiO₂**. As shown in Figure 2. 13, the ^{31}P -NMR signal of **4Pd@SiO₂** in the solid state (23.6 ppm) corresponds well with the chemical shift of the palladium complex in solution (24.4 ppm). There is no

signal of uncoordinated phosphine and phosphineoxide, which means the complex can survive in the grafting process under harsh reaction condition. The unsymmetrical phosphorus resonance is probably due to differences in the chemical environment of the phosphine and the palladium sites which are located in close proximity to the surface. The asterisks denote rotational sidebands.

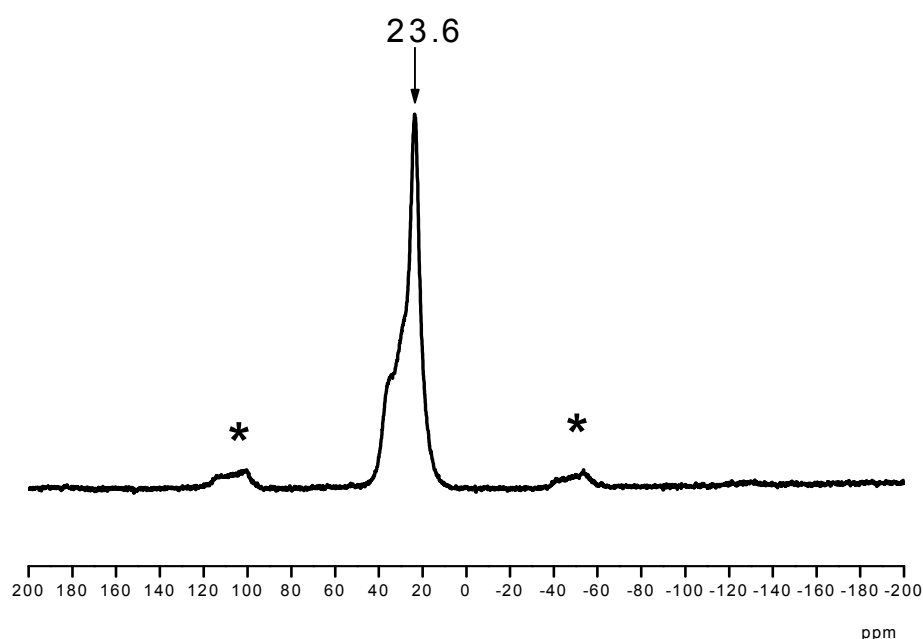


Figure 2. 13 ^{31}P CP-MAS NMR spectrum of the hybrid material **4Pd@SiO₂**.

FT-IR spectroscopy was used to provide further information concerning the organic modification occurring in the silica. Both the silica support **A** and hybrid material **B** show a broad band in the range of $3600\text{--}3200\text{ cm}^{-1}$, which can be assigned to the hydroxyl stretching vibrations of hydrogen bonded internal silanol groups. The asymmetric Si-O-Si vibration appears at around 1100 cm^{-1} , while the peak at 800 cm^{-1} is attributed the symmetric Si-O-Si vibration. The bending vibrations of the surface silanol groups and Si-O are observed at 970 and 460 cm^{-1} , respectively (Figure 2. 14). The presence of the palladium complex on the silica surface is indicated by a weak amide band at 1539 cm^{-1} , which is found at the same wavenumber as for the precursor **3**

(Figure 2. 7). A second amide band at 1645 cm^{-1} , which is observed for **3** overlaps with an absorption of the support at 1636 cm^{-1} .

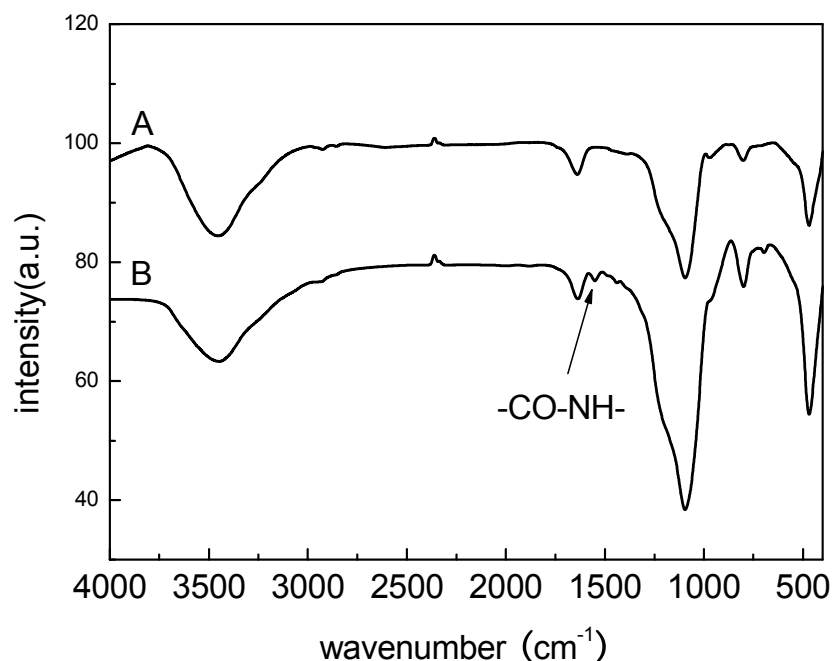
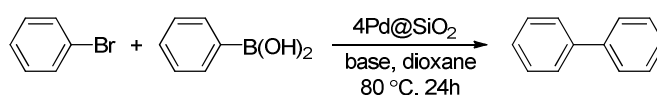


Figure 2. 14 Infrared spectra of neat silica(A) and **4Pd@SiO₂** (B).

Catalysis



Scheme 2. 5 Suzuki coupling of aryl bromobenzene and phenylboronic acid

To evaluate the general activity of catalyst **4Pd@SiO₂**, the Suzuki reaction of phenylboronic acid with bromobenzene was examined (Scheme 2. 5, Table 2. 3). Initially, an optimization of the base was performed using Cs_2CO_3 , K_3PO_4 , K_2CO_3 and KF under identical conditions. These bases have frequently been applied for homogeneously and heterogeneously catalyzed Suzuki coupling reactions.^[75] As shown in Table 2. 2, Cs_2CO_3 and K_3PO_4 turned out to be highly efficient. The solvent effect is probably determined by the solubility of the base. Based upon these results, a series of different substrates were tested in the presence of catalyst **4Pd@SiO₂** (Table 2. 3). The

2. Covalent Immobilization of Triphenylphosphine Complexes

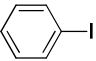
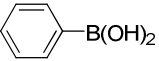
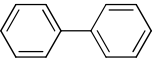
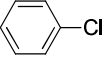
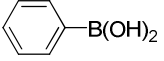
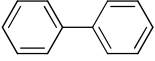
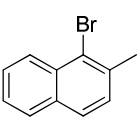
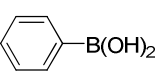
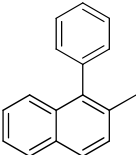
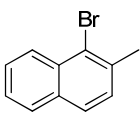
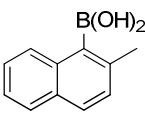
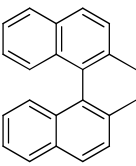
couplings of iodobenzene and phenylboronic acids afforded the expected biaryl in very good yield (entry 1). However, for the less reactive substrate chlorobenzene, a pronounced reduction in activity was observed (entry 2). Rising the reaction temperature up to 120 °C did not increase the conversion but resulted in a yield of only 8% after 24 h, probably due to a rapid catalyst deactivation. Additionally sterically hindered substrates were investigated: The coupling of 1-bromo-2-methylnaphthalene and boronic acid almost reached completion. In contrast, the reaction between 1-bromo-2-methylnaphthalene and 2-methyl-naphthylboronic acid, which would be interesting for the synthesis of 1,1'-dimethyl-2,2'-binaphthyl, afforded only traces of the product due to inherent difficulties in coupling two sterically hindered arenes.

Table 2. 2 Suzuki reaction of bromobenzene and phenylboronic acid with different bases.^a

base	Cs ₂ CO ₃	K ₃ PO ₄	K ₂ CO ₃	KF
yield(%) ^b	90	92	76	71

^aReaction conditions: PhBr (1 mmol); PhB(OH)₂ (1.5 mmol); base (1.2 mmol); Pd (1 mol % relative to aryl halide); dioxane (5 mL), 80 °C; ^bdetermined by GC-MS with n-decane as the internal standard.

Table 2. 3 Suzuki reactions between aryl halides and arylboronic acids.^a

halide	arylboronic acids	product	yield [%] ^b
			99
			24
			98 ^c
			trace

^aReaction conditions: as Table 2. 2 ^bdetermined by GC-MS with n-decane as the internal standard;

^cGC-MS and ¹H NMR.

Reusability is an important feature that determines the applicability of heterogeneous catalysts. We examined the reusability of **4Pd@SiO₂** with Cs₂CO₃ as the external base. After the first use of the catalyst in the Suzuki reaction, the reaction mixture was treated as described in experimental part. The recovered catalyst was used successfully for four subsequent reactions and exhibited consistent catalytic activity, indicating the excellent reusability of this heterogeneous catalyst (Table 2. 4).

Table 2. 4 Study on the reusability of **4Pd@SiO₂** in the Suzuki reaction.^a

recycle	1 st run	2 nd run	3 rd run	4 th run
yield(%)	90	88	89	82

^aReaction conditions: PhBr (1 mmol); PhB(OH)₂ (1.5 mmol); Cs₂CO₃ (1.2 mmol); Pd (1 mol % relative to aryl halide); dioxane (5 mL), 80 °C; ^bdetermined by GC-MS with n-decane as the internal standard.

It should be mentioned here that the initial pale yellow hybrid material **4Pd@SiO₂** turned grey after the first run and gradually got darker after several runs which is possibly due to the formation of palladium nanoparticles. In order to confirm this, we measured the catalyst after the third recovery from the Suzuki reaction by means of TEM. The TEM image clearly shows the presence of palladium nanoparticles with an irregular shape and a narrow-size distribution (4-8 nm) confined inside the irregular pores of the amorphous SiO₂ Figure 2. 15 and Figure 2. 16. All these results indicate the real active center of the Suzuki reaction should not be the precatalyst palladium triphenylphosphine complex, but the palladium nanoparticles formed in the reaction process. Palladium nanoparticles are widely used in coupling reactions, which provides a powerful means for the development of recyclable catalysts.^[39, 92-93] The major challenge of this topic is to prevent the aggregation of the palladium nanoparticles which leads to a loss of catalytic activity. We suppose that both the silica matrix and the organic ligand contribute to a stabilization of small palladium nanoparticles.

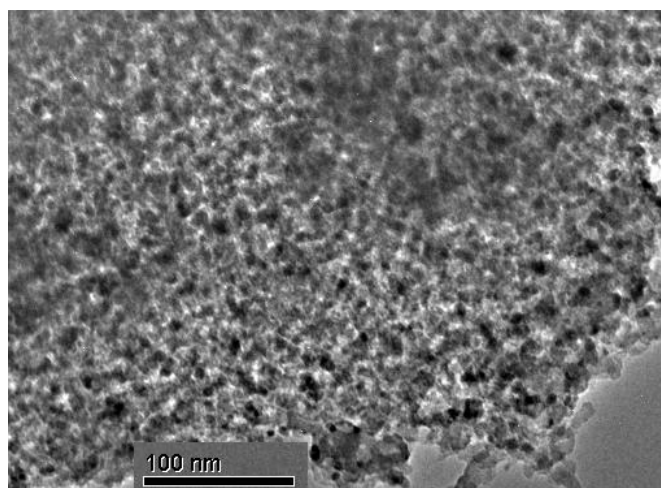


Figure 2. 15 The TEM image of the used catalyst **4Pd@SiO₂**.

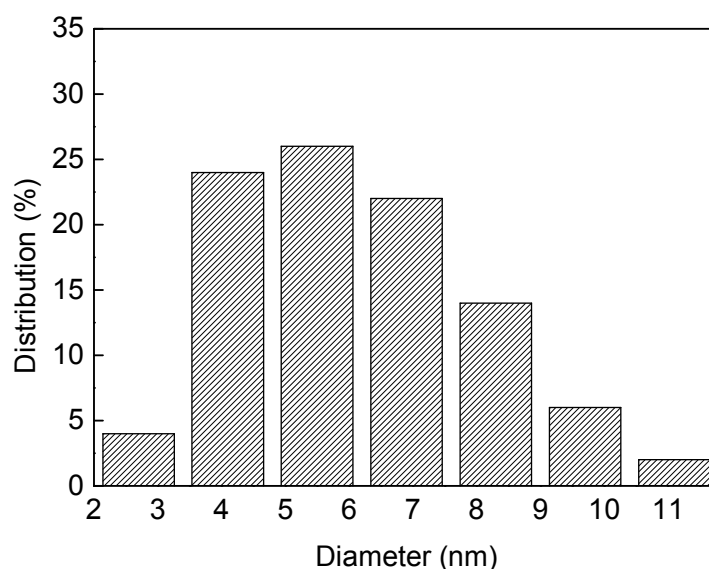


Figure 2. 16 Particle size distribution (50 particles).

To clarify the role of the phosphine ligand, we set up a control experiment, wherein the catalyst was prepared by directly loading $\text{PdCl}_2(\text{CNPh})_2$ on silica. The overall palladium loading was similar to that of **4Pd@SiO₂**. Running a Suzuki reaction between phenylboronic acid and bromobenzene with this catalyst under identical reaction conditions as before gave less than 50% of conversion after 24 h in the first run. The activity of this catalyst was completely lost after the first run. This suggests that the grafted ligands play an important role for the activity and stability of the catalyst.

It is important to find out the state of the triphenylphosphine ligand which can stabilize the palladium nanoparticles after the reaction. The used heterogeneous catalyst (after first run) was therefore further characterized by solid state NMR spectroscopy. Figure 2. 17 shows the ^{13}C CP-MAS NMR spectrum: propylene linker in the precursor **3**. However, the signal at 49 ppm which is matching unreacted methoxy group was disappeared. A signal at 168.5 ppm is assigned to the C=O group of the linker which was obtained by aminolysis reaction between the trimethoxysilane linker and the triphenylphosphine ligand. The signals in the range from 123 to 140 ppm are corresponding to the aryl groups. All these peaks are maintained after the reaction, which means the ligand is still grafted on the surface of the support.

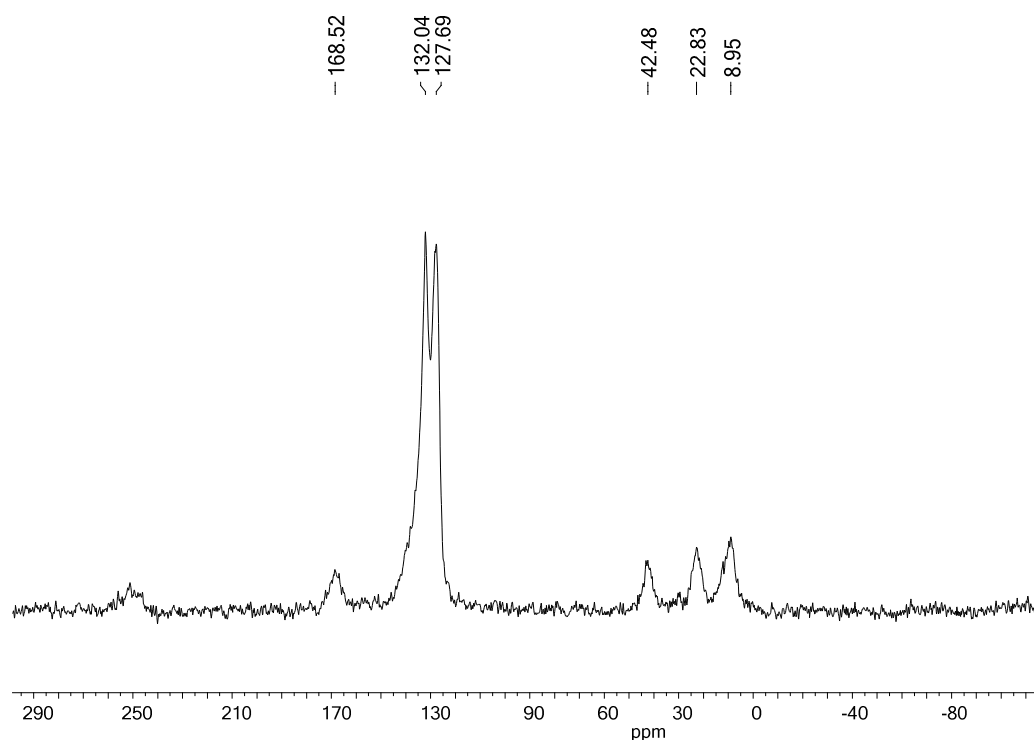


Figure 2. 17 ^{13}C CP-MAS NMR spectrum of the hybrid material **4Pd@SiO₂** after first recycle.

Three resonances at 42.5, 22.8, 9.0 ppm are correlated with the resonances of the The ^{31}P MAS NMR spectrum shows sharp signals at 33.5 ppm and 3.9 ppm with a weak shoulder at -3.1 ppm (Figure 2. 18).

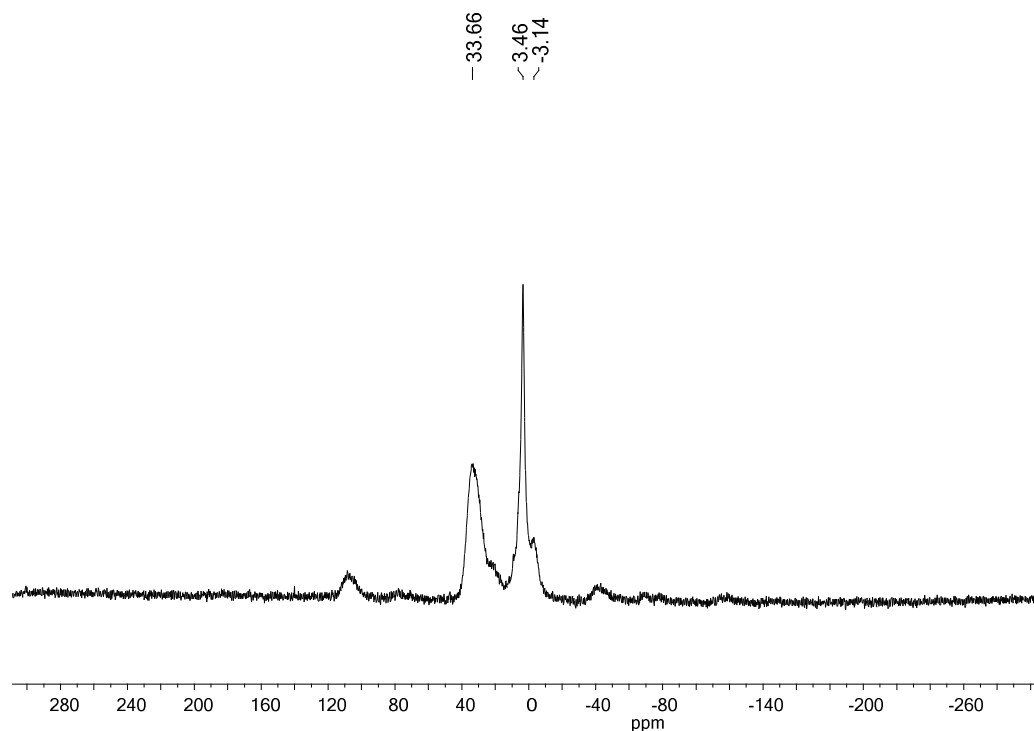


Figure 2. $^{18}\text{ }^{31}\text{P}$ CP-MAS NMR spectrum of the hybrid material **4Pd@SiO₂** after first recycle.

These results prove that the ligand of the decomposed palladium complex gets oxidized partially to phosphine oxide (peak at 33.7 ppm) whereas the weak shoulder at -3.1 ppm arises from the palladium free mono silylated phosphine ligand. Thus we envision that the triphenyl phosphine ligand as well as phosphine oxides derived by oxidation during the reaction assist the stabilization of the palladium nanoparticles - which in turn explains the excellent reusability of this catalyst system. The fact that phosphine oxides can serve as stabilizers for preventing the the nanoparticles from aggregation was already reported by Fan et al.^[94] In our case, both free ligand and phosphine oxides should be responsible for the stability of the palladium nanoparticles.

A further objective of our studies was to determine whether **4Pd@SiO₂** acts as a truly heterogeneous catalyst. To test this, the coupling reaction was carried out for 1 h until a conversion of about 30% was reached. Then the catalyst was removed by filtration at the reaction temperature. The filtrate was treated with another 1.2 equiv. of Cs_2CO_3 and heated for additional 23 h to 80°C. The reaction continued although the conversion did not reach the level obtained with **4Pd@SiO₂**, which means that at least a part of the

catalytic activity of **4Pd@SiO₂** must be assigned to a homogeneous reaction. To determine the degree of leaching of the metal from the heterogeneous catalyst, the catalyst was removed by filtration at 80°C after the reaction was completed (24 h) and the palladium content of the filtrate was determined by atomic absorption spectrometry (AAS). We found a palladium contamination of about 0.4 % relative to the original Pd loading of **4Pd@SiO₂**, which implies that leaching is not a serious problem for this catalyst. This is also confirmed by the excellent reusability of this catalytically active material.

Further research

Although the heterogeneous catalyst **4Pd@SiO₂** with silica as the support shows excellent reusability, we do observe a drop in activity of **4Pd@SiO₂** after the 4th run, which is probably caused by the induced water required for dissolving the base in the recycling process. In cooperation of S. Shylesh the functionalized triphenylphosphine palladium complex was covalently grafted on silica coated magnetic nanoparticles (**SMNP**).^[95] The **SMNP** supported catalyst can be easily separated from the reaction mixture by applying an external magnetic field and can be recycled many times without any loss of activity (Table 2. 5).

Table 2. 5 Study on the reusability of the SMNP supported catalyst in the Suzuki reaction.^a

recycle	1 st run	2 nd run	3 rd run	4 th run	5 th run	6 th run	7 th run
yield(%)	99	94	94	94	93	93	92

^aReaction conditions: PhBr (1 mmol); PhB(OH)₂ (1.5 mmol); Cs₂CO₃ (1.2 mmol); Pd (1 mol %); dioxane (5 mL), 80 °C; ^bdetermined by GC-MS with n-decane as the internal standard.

2.2 Immobilization of a Rhodium Complex by the Post Grafting Method

2.2.1 Introduction

Olefin hydrogenation is one of the most important catalytic methods in synthetic organic chemistry, both on the laboratory and industry scale.^[96-98] Moreover, hydrogen is the cleanest reducing agent, which allows an easy purification of the products with a minimum amount of waste. Homogeneous hydrogenation catalysis developed in the 1960 and is reviewed frequently.^[99-102] Experience has shown that various phosphorus ligands based Rh, Ru and Ir complexes are the most active and the most versatile catalysts for hydrogenation reactions.^[97] Among these non-enantioselective catalysts, Wilkinson's catalyst ($\text{RhCl}(\text{PPh}_3)_3$) was the first homogeneous catalyst that could efficiently catalyze the hydrogenation of alkenes and indeed it is still the most widely applied complex in synthetic chemistry nowadays.^[48]

For more than 100 years chemists have used heterogeneous catalyst based on noble metals on various supports.^[103-104] However, only a few examples have been published in the literature, wherein phosphines have been bound covalently to a silica surface and applied in hydrogenation. Shyu et al. prepared $(\text{EtO})_3\text{Si}-(\text{CH}_2)_3-\text{PPh}_2$ functionalized MCM-41 and treated this hybrid material with $\text{RhCl}(\text{PPh}_3)_3$. The resulting heterogenized catalyst exhibited a higher activity in the hydrogenation of olefins than its homogeneous analogue.^[54] Crudden et al. grafted a functionalized cationic rhodium complex onto mesoporous molecular sieves involving a bidentate phosphine to minimize leaching, and found this material being highly active for olefin hydrogenation.^[58] However, the resulting hybrid catalyst is extremely sensitive to traces of oxygen. Blümel et al. immobilized homogeneous rhodium catalysts onto silica *via* a series of bifunctional diphenylphosphine linkers and used them in hydrogenation reactions. The catalysts display excellent TOFs and can be reused many times without any loss of activity.^[55-57, 105] However, these diphenylphosphine ligands are more

sensitive towards oxidation than triphenylphosphines and it is obligatory to extend the reaction time after recycling to obtain the same yield as in the first run.

In chapter 2.2, by applying a covalent grafting method, a functionalized triphenylphosphine ligand could successfully be immobilized onto the surface of silica gels or magnetic nanoparticles (MNPs).^[95, 106] Efficient (triphenylphosphine)palladium catalysts for the Suzuki reaction could be obtained following the same procedure. As a continuation of this work, keeping in view the extension of this effective and simple grafting of triphenylphosphine based catalysts, immobilization of $\text{RhCl}(\text{CO})(\text{PPh}_3)_2$ on various supports and the application of these materials in olefin hydrogenation were carried out.

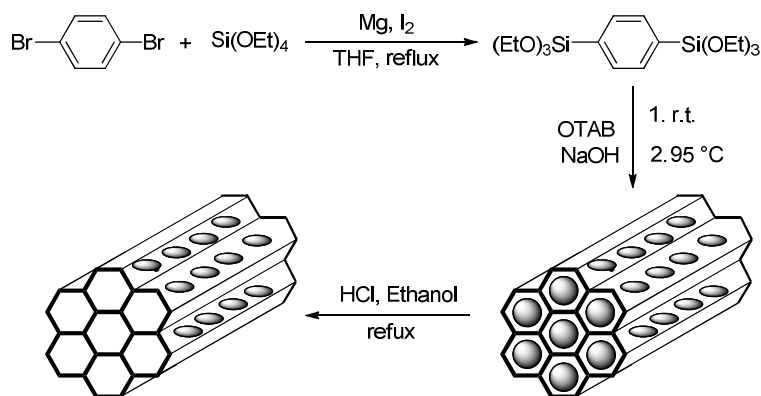
2.2.2 Results and discussion

Synthesis

After immobilization of a homogeneous catalyst on a solid support, the corresponding heterogeneous catalyst often shows better activity in hydrogenation which suggests the support has a certain effect on the activity. It is interesting to find out whether heterogeneous catalysts show different activities in hydrogenation towards the supports with different properties. Therefore, I used the highly ordered mesoporous silicate SBA-15, amorphous silica and periodic mesoporous organosilicas (PMO) which has an enhanced surface hydrophobicity as a support. The PMO as synthesized by following procedure (Scheme 2.2. 1). The first step was the preparation of the precursor 1,4-bis(triethoxysilyl)benzene, which was synthesized by a one step Grignard reaction and distillation according to reported publication.^[107] The obtained colourless liquid was characterized by NMR spectroscopy. Two sets of resonances (1.3 and 3.9 ppm) are observed at low field in the ^1H NMR spectrum, which correspond to the ethoxyl groups. A singlet at 7.7 ppm can be assigned to the aromatic ring. The ^{13}C NMR spectrum shows two resonances at 133.2 and 133.8 ppm, which are attributed to aromatic ring. Two sets of resonances at 58.5 and 18.0 ppm can be correlated with the ethoxyl groups.

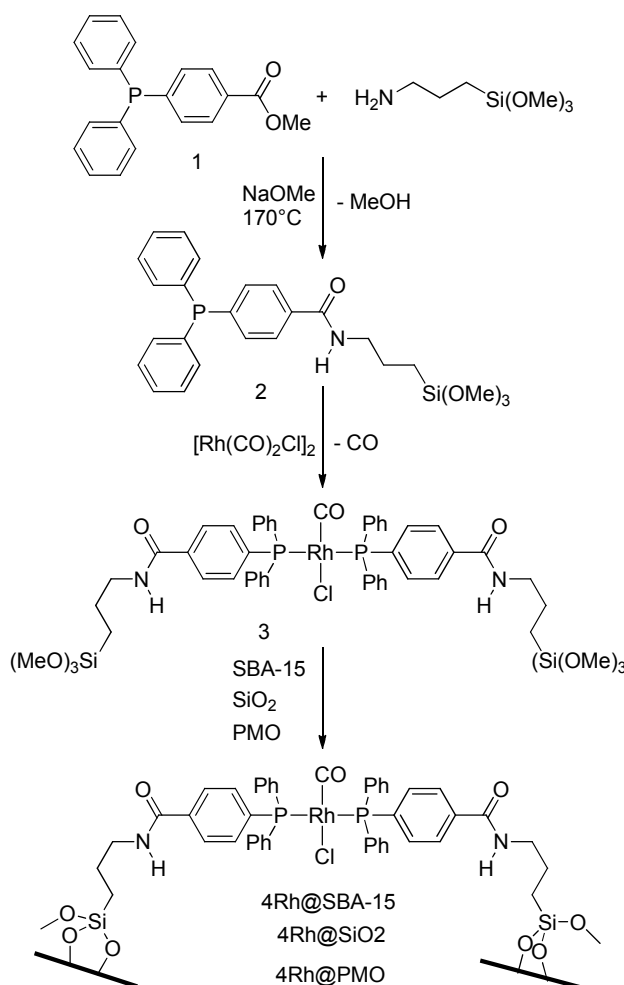
2. Covalent Immobilization of Triphenylphosphine Complexes

Mesoporous phenylene-silica hybrid materials (PMOs) were obtained via a surfactant mediated reaction with octadecyltrimethyl ammonium bromide (OTAB), under hydrothermal conditions with NaOH as the hydrolyzing catalyst (Scheme 2.2. 1). The mesoporous SBA-15 material was synthesized according to a reported procedure using tri-block P123 as a template under acidic conditions.^[20]



Scheme 2.2. 1 Synthesis of de phenylene derived **PMO**.

The hybrid mesoporous products **4Rh@SBA-15**, **4Rh@SiO₂**, and **4Rh@PMO** were obtained by the procedure outlined in Scheme 2.2. 2. The methoxysilylated triphenylphosphine **2** was synthesized as described in chapter 2.1. The *trans* configured rhodium complex **3** was accessible in quantitative yield by reacting [Rh(CO)₂Cl]₂ with four equivalents of the functionalized ligand **2**. In the last step, the synthesized Rh complex was covalently anchored on SBA-15, silica gel or PMO supports. We decided to take the rhodium complex **3** and not the phosphine ligand **2** for the grafting to be sure to have a molecularly well defined catalyst precursor on the support. Grafting the ligand first would generate phosphine centers distributed statistically on the surface, which might not all be in an ideal position to coordinate to the rhodium(I) center. This results in the formation of a multiple site system. The approach we chose finally leads to a chelating phosphine with the support as the ligand backbone.



Scheme 2.2. 2 Synthesis of heterogeneous Rh catalysts with different supports.

Characterization

The ^1H NMR, ^{13}C NMR and ^{31}P NMR spectra of the rhodium complex **3** are shown in Figure 2.2. 1, Figure 2.2. 2 and Figure 2.2. 3. The ^1H NMR, ^{13}C NMR data are in complete agreement with the spectroscopic features of the precursor ligand **2** except the additional weak resonances of the CO group in ^{13}C NMR spectrum (CO resonance: 187.0 ppm, dt, $^1J_{\text{Rh,C}} = 73.5$ Hz, $^2J_{\text{P,C}} = 15.8$ Hz). The ^{31}P NMR spectrum of complex **3** exhibits a doublet due to Rh-P coupling ($\delta = 30.5$ ppm, d, $^1J_{\text{RhP}} = 126.8$ Hz). Compared with free ligand, the phosphorous resonance shifts about 34 ppm downfield, indicating coordination through the phosphorous atom.

2. Covalent Immobilization of Triphenylphosphine Complexes

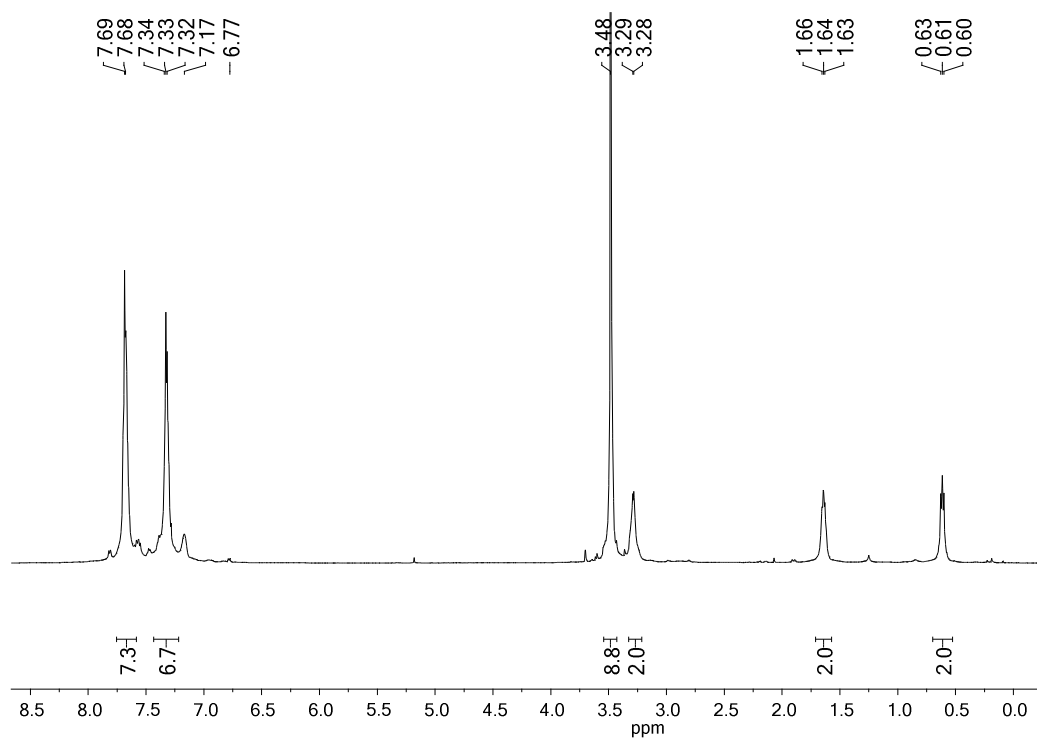


Figure 2.2. 1 ¹H NMR spectrum of rhodium complex **3** (400.13 MHz, 25 °C, CDCl₃).

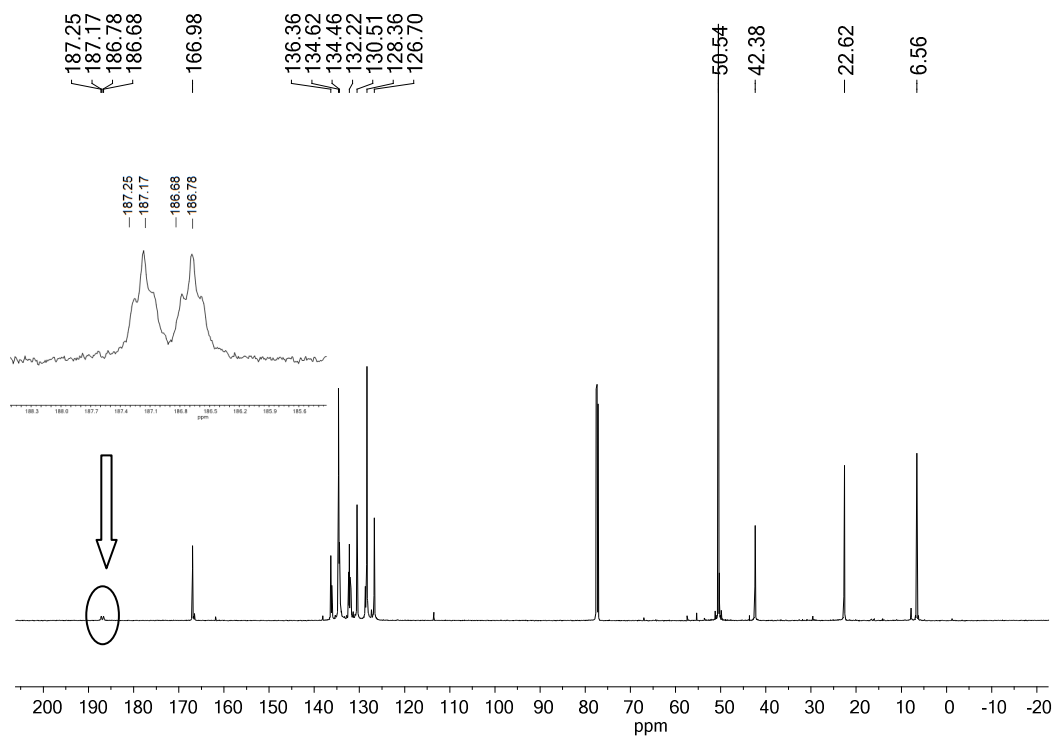


Figure 2.2. 2 ¹³C NMR spectrum of rhodium complex **3** (100.62 MHz, 25 °C, CDCl₃).

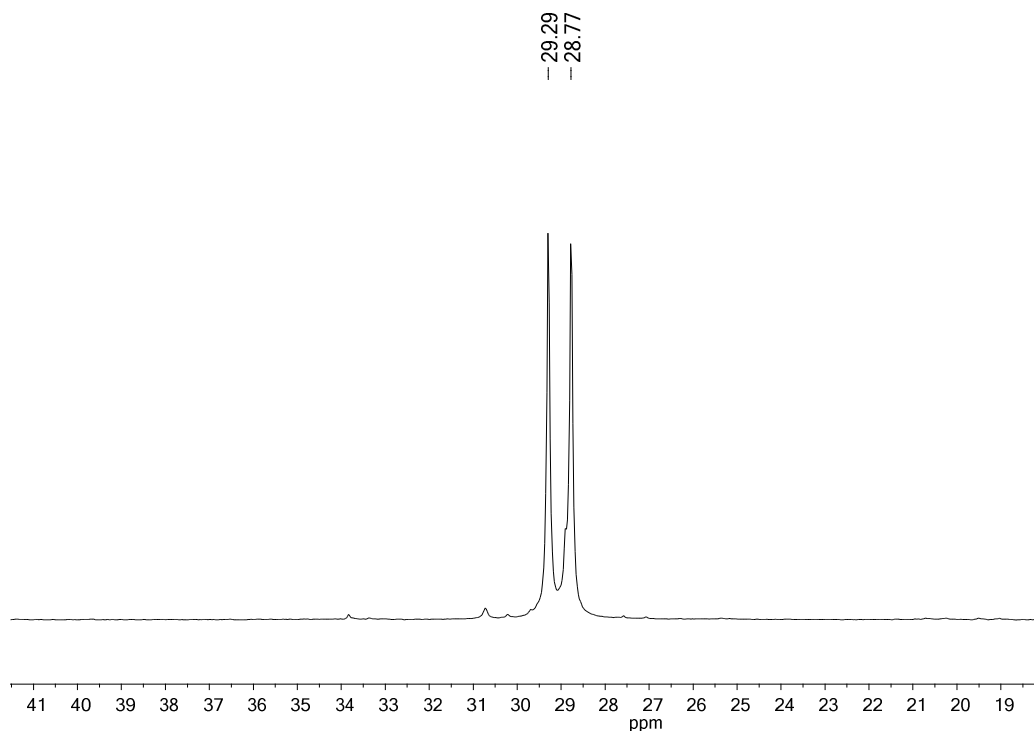


Figure 2.2. ^{31}P NMR spectrum of rhodium complex **3**.

The IR spectrum also shows an intense band at 1978 cm^{-1} , which is the characteristic CO absorption (Figure 2.2. 4) for complexes of the type $(\text{P})_2\text{Ph}(\text{CO})\text{Cl}$ (P = phosphine ligand). The data of ^{13}C NMR, ^{31}P NMR and Infrared spectra are in complete agreement with the spectroscopic features of similar *trans* configured complexes of the type $(\text{P})_2\text{Ph}(\text{CO})\text{Cl}$ (P = phosphine ligand) reported in literature.^[108]

Figure 2.2. 5 presents the XRD patterns of neat SBA-15 and **4Rh@SBA-15**, which exhibit three clear peaks in the low-angle region: one intense signal corresponding to the d_{100} diffraction peak accompanied by two weaker peaks (d_{110} , d_{200}), suggesting that the two-dimensional hexagonal pore structure is preserved after the introduction of the rhodium complex. The XRD pattern of the phenylene bridged hybrid PMO material shows three lower-angles Bragg diffraction peaks indexed as (100), (110) and (200) (Figure 2.2. 6), which can be assigned to the reflections of the hexagonal (P6mm) symmetry of the mesoporous structure, indicating the successful synthesis of the highly ordered PMOs. In addition to these lower angle diffractions, the pattern in the range of

$10^\circ < 2\theta < 40^\circ$ displays three additional sharp diffraction peaks at 2θ values of 12, 23 and 35° (with d spacings of 7.6, 3.8, and 2.5 Å), which can be assigned to a molecular scale periodicity in the walls along the channel directions (inset). The above XRD results demonstrate that besides a well formed hexagonal array of mesostructural pores, this material also contains crystal-like pore walls. After immobilization of the complex **3**, the obtained material showed the same patterns, indicating that the long-range and molecular scale order of the PMO framework was well retained. A slight decrease in intensity of the d_{100} reflection in lower angle region compared to the parent substrate PMO indicates a degradation of the mesostructure due to the incorporation of bulky rhodium complex.

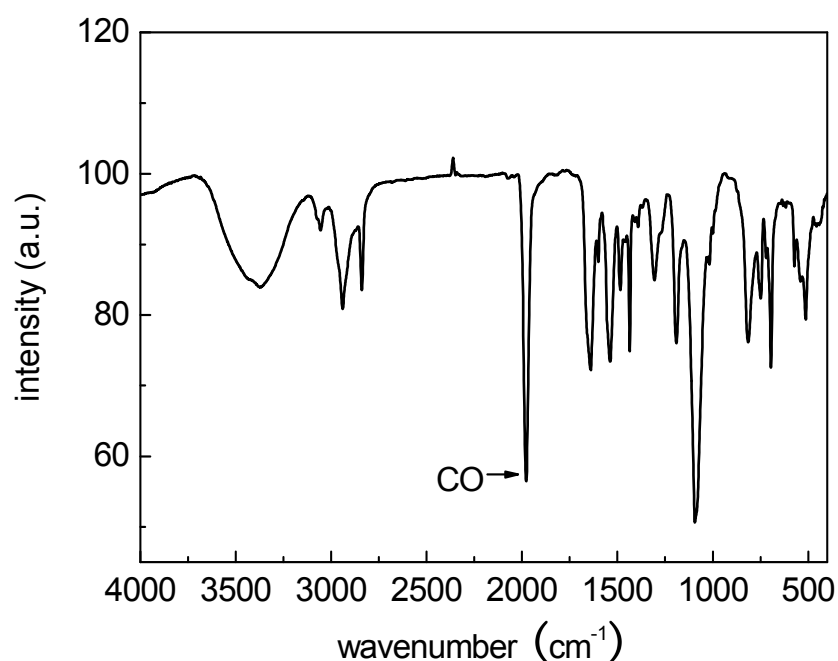


Figure 2.2. 4 Infrared spectrum of rhodium complex **3**.

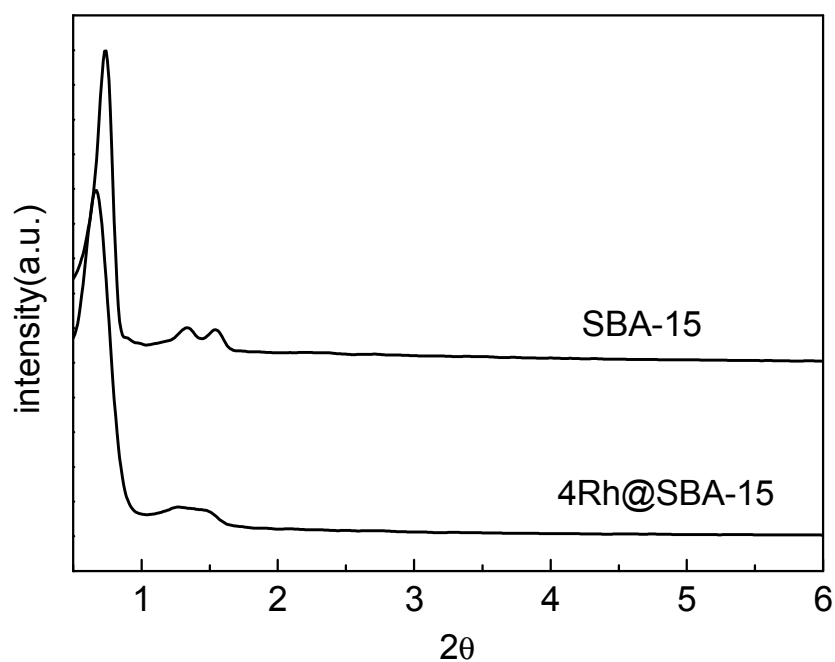


Figure 2.2. 5 XRD patterns of SBA-15 and **4Rh@SBA-15**.

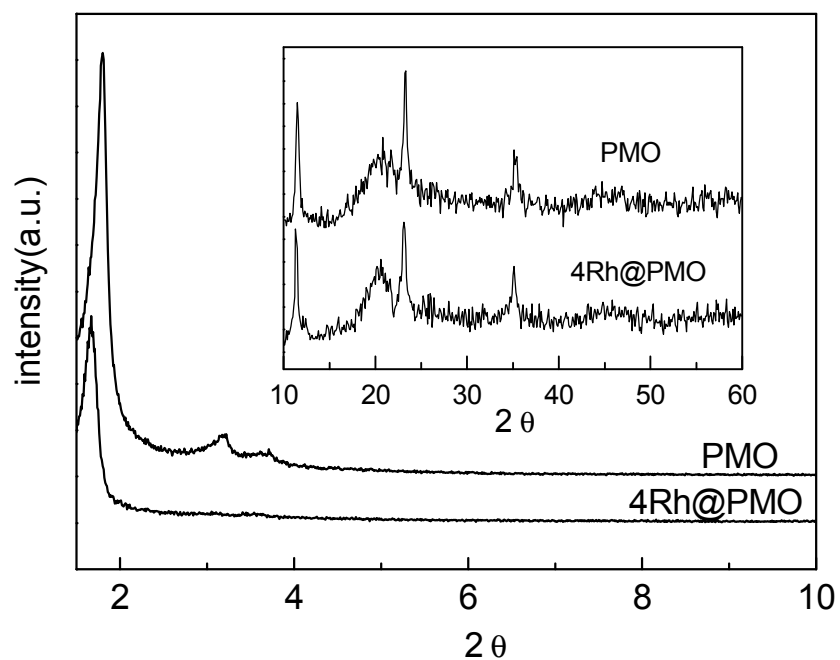


Figure 2.2. 6 Low- and medium-angle (inset) XRD patterns of **PMO** and **4Rh@PMO**.

The nitrogen sorption isotherms of hybrid materials **4Rh@SBA-14**, **4Rh@SiO₂** and **4Rh@PMO** exhibited type IV isotherms with a typical capillary condensation (Figure

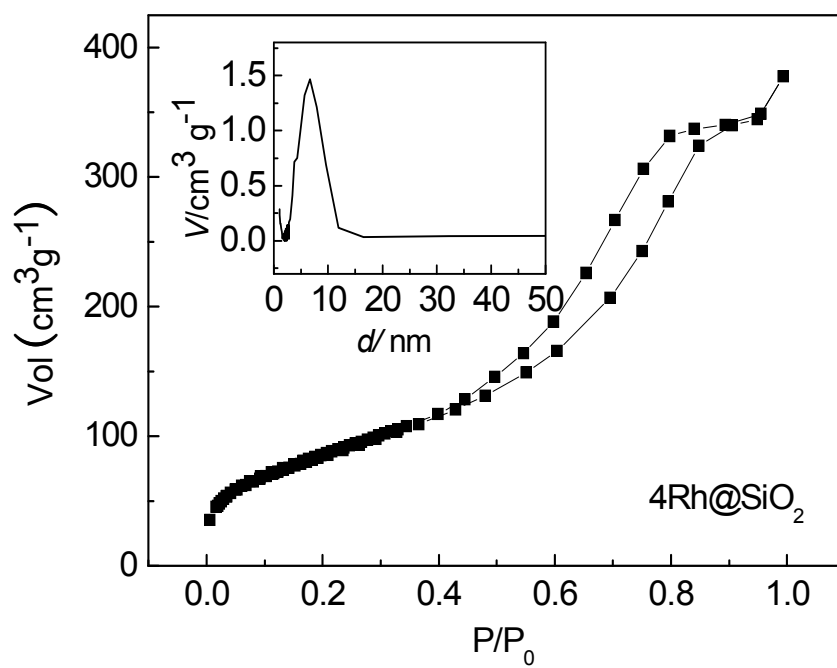
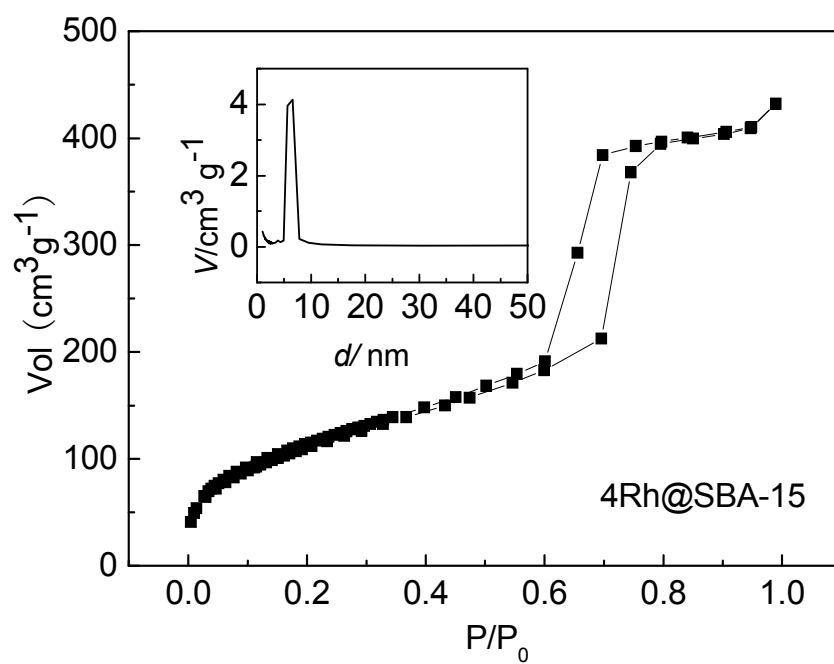
2.2. 7), indicating all samples consisted with well-defined mesoporous structures. The materials also possess a narrow pore size distribution as shown in Figure 2.2. 7 (inset). Table 2.2. 1 shows the structural and compositional data of the hybrid materials, including BET surface area, total pore volume, pore size and calculated content of grafted rhodium complex. Catalyst **4Rh@PMO** possesses much larger specific surface area ($776 \text{ m}^2 \text{ g}^{-1}$) and smaller pore size (2.6 nm) than **4Rh@SBA-15** ($404 \text{ m}^2 \text{ g}^{-1}$, 6.5 nm) and **4Rh@SiO₂** ($314 \text{ m}^2 \text{ g}^{-1}$, 6.5 nm).

The successful covalent immobilization of complex **3** on SBA-15 is proved by the ^{29}Si CP-MAS NMR spectrum of the hybrid material **4Rh@SBA-15** (Figure 2.2. 8). Signals at -110, -101, and -92 ppm correspond to the siloxane sites $\text{Si}(\text{OSi})_4$ (Q^4), $\text{HOSi}(\text{OSi})_3$ (Q^3), and $(\text{HO})_2\text{Si}(\text{OSi})_2$ (Q^2) of the inorganic silica framework, signals at -49 and -58 ppm can be assigned to the organosiloxane sites $\text{R-Si}(\text{RO})_2(\text{OSi})$ (T^1) and $\text{R-Si}(\text{RO})(\text{OSi})_2$ (T^2).^[89] Grafting **3** on the silica surface makes the Q^2 signal of the neat silica support almost disappear due to the consumption of highly reactive geminal $\text{Si}(\text{OH})_2$ groups during the condensation process.^[90] Since the T^1 peak is more intense than the T^2 peak, the rhodium catalyst is mainly grafted via $\text{R-Si}(\text{RO})_2(\text{OSi})$ sites.

Table 2.2. 1 Pore parameters and compositional information of catalysts.

materials	S_{BET} [$\text{m}^2 \text{ g}^{-1}$]	pore vol [$\text{cm}^3 \text{ g}^{-1}$]	BJH pore diam [nm]	composition (wt %)			Rh ^a [mmol g^{-1}]
				C	H	N	
4Rh@SBA-15	404	0.67	6.5	17.1	2.9	0.5	0.16
4Rh@SiO₂	314	0.59	6.5	7.6	1.3	0.4	0.14
4Rh@PMO	776	0.68	2.6	40.6	3.4	0.4	0.14

^aaccording to the nitrogen content of elemental analysis.



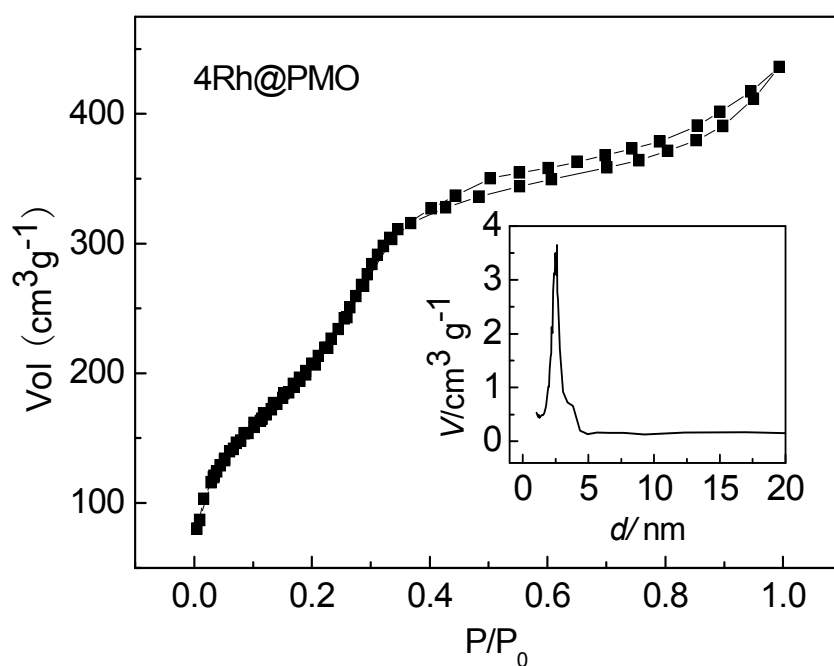


Figure 2.2. 7 N_2 sorption isotherms and BJH pore size distribution (inset) of different catalysts.

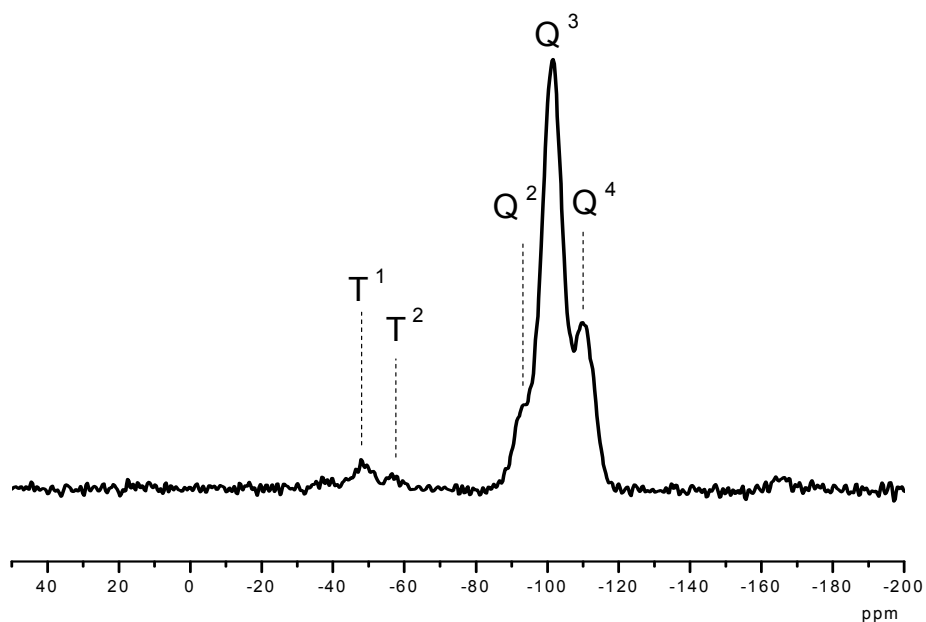


Figure 2.2. 8 ^{29}Si CP-MAS NMR spectrum of **4Rh@SBA-15**.

^{13}C CP-MAS NMR spectroscopy of **4Rh@SBA-15** shows two quite sharp signals at 60 and 16 ppm being assigned to the remaining ethanol from the template extracting

process or from the hydrolysis reaction of TEOS. The resonances around 75 ppm arised from small amounts of residual template P123^[109]. Further weak resonances with chemical shifts are similar to those of the free complex **3** which are assigned by the dashed lines (Figure 2.2. 9). The ¹³C NMR spectrum (Figure 2. 2) shows signals for the aryl groups in the range from 126.8 to 141.8 ppm. Three resonances at 42.3, 22.7, 6.6 ppm can be correlated with the resonances of the propylene linker in the precursor **3** (42.4, 22.7 and 6.6 ppm).

The successful grafting and the integrality of the organic components were additionally verified by ³¹P CP-MAS NMR spectroscopy. The chemical shift of the ³¹P MAS NMR resonance of **4Rh@SBA-15** (Figure 2.2. 10) is in complete agreement with the data of **3** (Figure 2.2. 3). There is no signal for the corresponding phosphine oxide, the expected chemical shift for the latter species is expected at about +23 to +29 ppm. No resonance for free triphenylphosphine in ³¹P CP-MAS NMR spectrum was observed. The asterisks denote rotational sidebands.

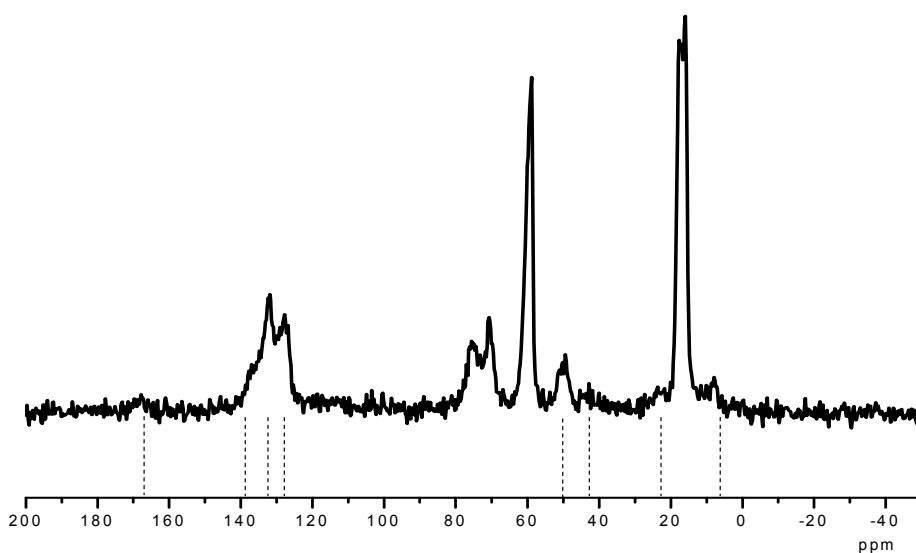


Figure 2.2. 9 ¹³C CP-MAS NMR spectrum of **4Rh@SBA-15**.

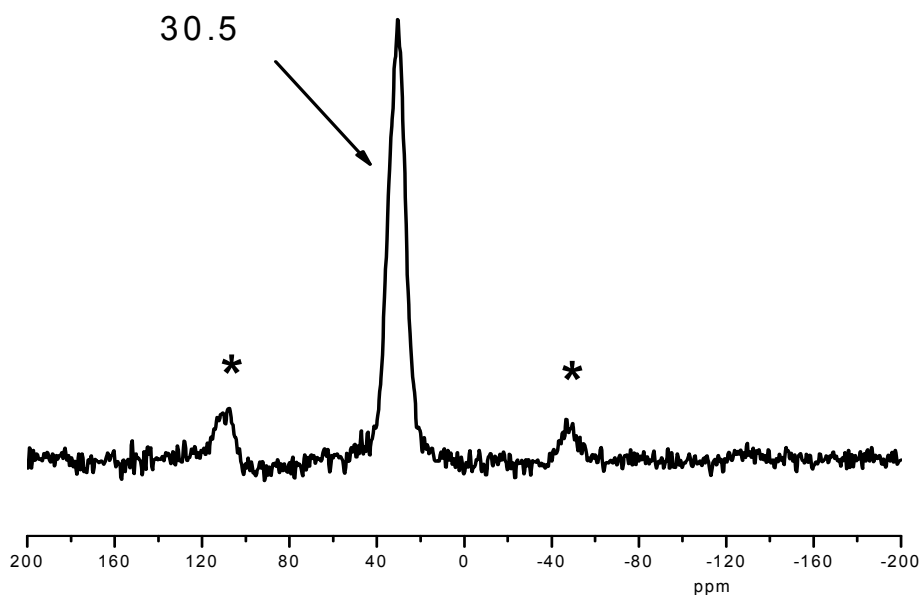


Figure 2.2. $10\ 31\text{P}$ CP-MAS NMR spectrum of **4Rh@SBA-15**.

29Si CP-MAS NMR of **4Rh@PMO** is shown in Figure 2.2. 11. The resonances at -80, -71 and -62 ppm can be assigned to $\text{R-Si}(\text{OH})_2(\text{OSi})$ (T^1), $\text{R-Si}(\text{OH})(\text{OSi})_2$ (T^2) and $\text{R-Si}(\text{OSi})_3$ (T^3) organosiliceous species, respectively. No peak for Q^n [$\text{Q}^n = \text{Si}(\text{OSi})_n(\text{OH})_{4-n}$] species (expected chemical shifts: -110, -101, and -92 ppm) can be observed, which indicates that no carbon-silicon bond cleavage of the organosilica precursor occurred during the synthesis of PMO or the grafting process.

13C CP-MAS NMR spectrum of **4Rh@PMO** is presented in Figure 2.2. 12. The extremely sharp peak around 130 ppm is attributed to the carbon atoms of the aromatic ring of the framework building block (1,4-bis(triethoxysilyl)benzene), which is overlap with the resonances of the aromatic ring of complex **3**. The further resonances with chemical shifts are similar to those of the free complex **3** which are assigned by the dashed lines. The remained ethanol from the extracting process or the free ethanol formed as a side product of grafting reaction gives the resonances at 60 and 16 ppm.

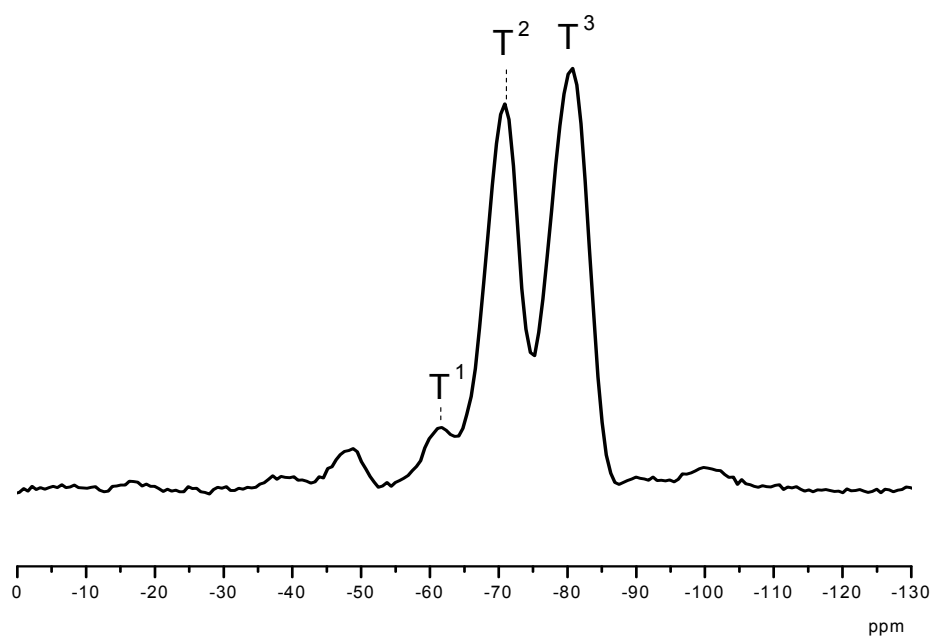


Figure 2.2. 11 ^{29}Si CP-MAS NMR spectrum of **4Rh@PMO**.

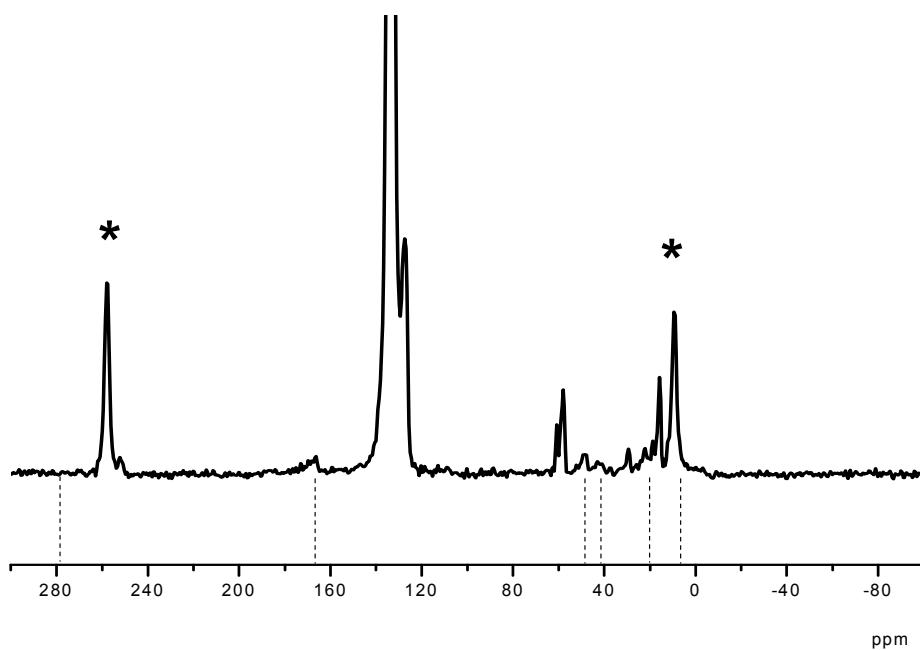


Figure 2.2. 12 ^{13}C CP-MAS NMR spectrum of **4Rh@PMO**.

The ^{31}P CP-MAS NMR resonance (32.6 ppm) of **4Rh@PMO** (Figure 2.2. 13) is slightly shifted towards lower field compared to the solution NMR data of complex **3** (29.0 ppm) (Figure 2.2. 3). This might be explained by some additional weak interactions between the grafted complex center and surface bound silanol sites ($\text{Si-OH}\cdots\text{Cl-Rh}$). A SEM image taken from **4Rh@SBA-15** clearly shows that the particles are joined to form unregular and fibrous aggregates (Figure 2.2. 14)

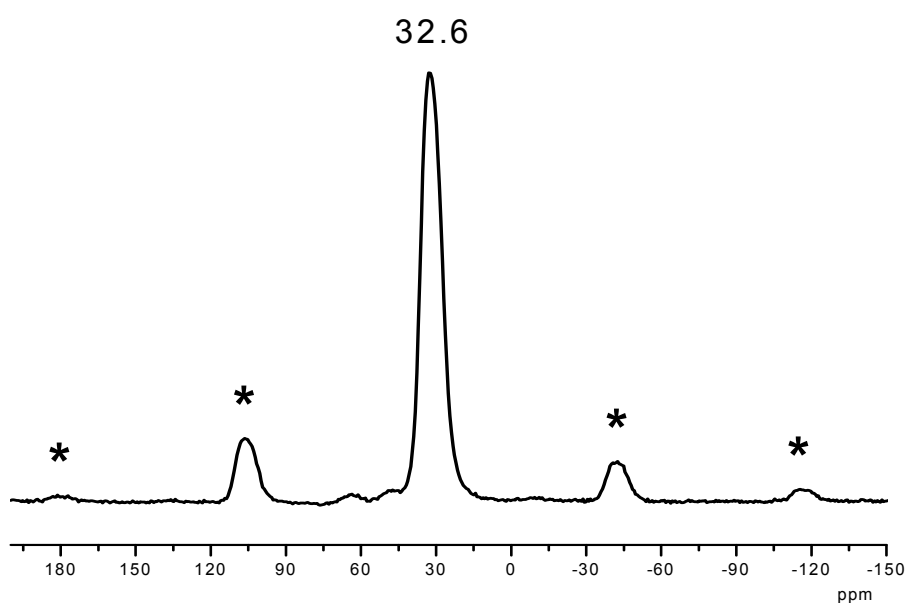


Figure 2.2. 13 ^{31}P CP-MAS NMR spectrum of **4Rh@PMO**.

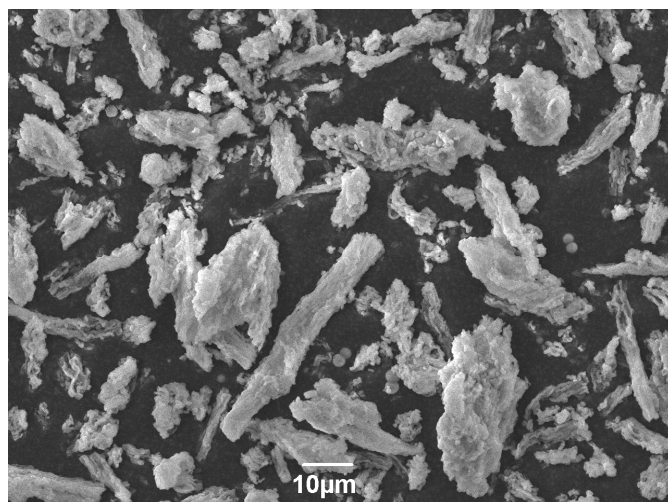
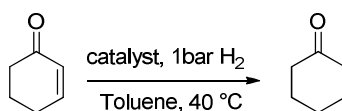


Figure 2.2. 14 SEM image of **4Rh@SBA-15**.

Catalysis

The catalytic performance of the heterogenized catalyst in olefin hydrogenation was initially studied with cyclohex-2-enone as the substrate under mild conditions ($p(\text{H}_2) = 1 \text{ bar}$, $T = 40^\circ\text{C}$, toluene) (Scheme 2.2. 3). The kinetic curves of hydrogenation with the heterogeneous catalysts having different supports are shown in Figure 2.2. 15.



Scheme 2.2. 3 Hydrogenation reaction of 2-cyclohexen-1-one.

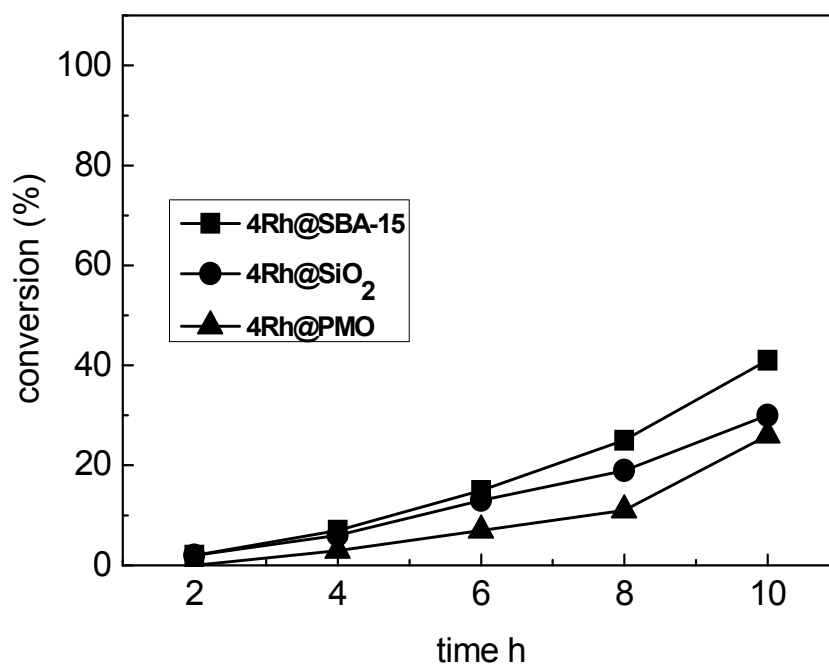


Figure 2.2. 15 Hydrogenation of 2-cyclohexen-1-one with heterogeneous catalysts **4Rh@SBA-15**, **4Rh@SiO₂** and **4Rh@PMO**.

The activities of all the catalysts do not show obvious difference, which confirms the hydrophilic/hydrophobic properties of the support do not play an important role. The same conclusion was also reported by Kralik, M.^[98] However, **4Rh@PMO** with PMO as support shows a slight lower reaction rate compared with **4Rh@SiO₂** and **4Rh@PMO**, which is probably caused by different average pore diameter of the

support. Larger pores should be helpful for the diffusion of substrates to the catalytic centers in the pores. According to the average pore size which was calculated by BJH method in Table 2.2. 1, **4Rh@PMO** has much smaller pore size than **4Rh@SBA-15** and **4Rh@SiO₂**.

The effect of the different solvents on the hydrogenation catalyzed by **4Rh@SiO₂** was studied in six liquids: toluene, dioxane, isopropanol, ethanol, dimethylformamide (DMF) and acetonitrile. The results are shown in Figure 2.2. 16 and demonstrate that the solvent has a significant effect on the reaction rate.

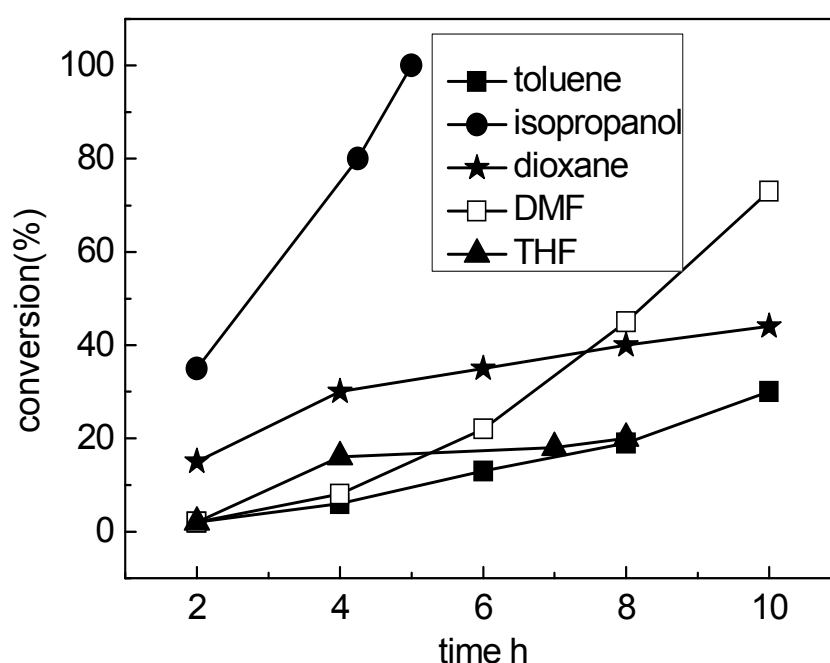


Figure 2.2. 16 Hydrogenation of 2-cyclohexen-1-one with different solvents.

The highest reaction rate was obtained with isopropanol as the solvent. After 5 h the yield can reach 99%. It has to be mentioned here that secondary alcohols can serve as a hydrogen source in a transfer hydrogenation. However, the reaction was carried out under the same condition but without H₂ and there was no conversion after 5 h. When ethanol was used as solvent, the reaction can completely convert the substrate in between 6 h. But ethanol is not good solvent in our reaction condition due to the

formation of traces of the byproduct 3-ethoxy-2-cyclohexan-1-one. The activity of the catalyst in DMF followed the same trend as in toluene, which increased as reaction time increased, but catalyst showed higher conversion (73%) in DMF than in toluene (30%) over 10 h. The more polar solvents may, therefore, favor the activation of catalyst. In dioxane the conversion of hydrogenation reaction did not increase obviously after 4 h. The catalyst was inactivated in the presence of dioxane gradually and conversion only got 48% after 24 h. The similar result was obtained when the THF was used as solvent. This may be caused by the strong interaction between the hydroxyl groups at the surface of the silica and the oxygen atom of solvents, which hinders the access of hydrogen to the active center.

Figure 2.2. 17 shows that aging the catalyst in the air for one week (**c-4Rh@SBA-15**) strongly enhances its activity compared to the freshly synthesized system **a-4Rh@SBA-15**. Storing the catalyst for a long period (>1 month) under N₂ (**b-4Rh@SBA-15**) almost preserves the poor activity of the freshly synthesized system. **c-4Rh@SBA-15** achieves > 99% of conversion to cyclohexanone and > 99 % of selectivity in between 6 h, while **a-4Rh@SBA-15** only gives 10 % of conversion. This is probably due to the replacement of the carbonyl ligand against water by storage in the air. The intensity of the $\nu(\text{CO})$ absorption (1984 cm^{-1}) is strongly reduced during the aging process (Figure 2.2. 18). Gao et al. explained this by replacement of the CO ligand by a water molecule coming from the air, which means that surface Si-OH or Si-O-Si units alone are not capable to cleave the Rh-CO bond.^[110] This agrees with the fact, that it is possible to reach > 99 % with the fresh catalyst when isopropanol and ethanol are used as solvent, which are able to replace the CO ligand. When ethanol was used as solvent, a trace of a byproduct was observed. The further investigation for this side reaction found that the use of methanol gives 1,1-dimethoxycyclohexane in 92% yield after 6 h, which means that **4Rh@SBA-15** is also an efficient catalyst for ketone acetalization. We tested the acetalization of cyclohexanone under identical conditions without catalyst or with the neat SBA-15 support and found only 12 % (resp. 26 %)

yield after 15 h, implying a synergistic effect between the rhodium catalyst and the SBA-15 support. As reported earlier, siliceous mesoporous materials and Rh(III)triphos species can be used as catalysts for acetalization reactions.^[111-112]

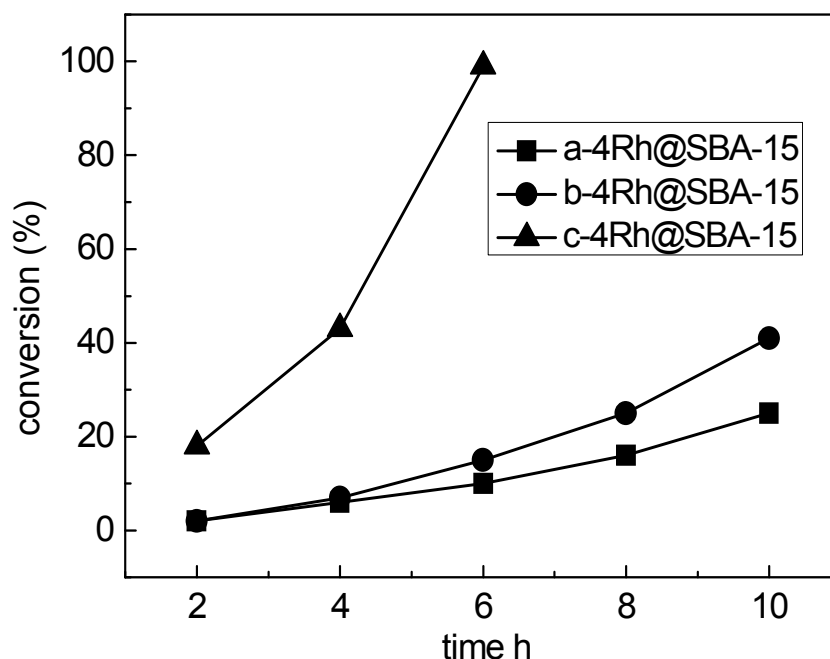


Figure 2.2. 17 Kinetic profiles of differently aged **4Rh@SBA-15** materials: freshly synthesized catalyst (**a-4Rh@SBA-15**), stored under N_2 for more than one month (**b-4Rh@SBA-15**), air-aged for one week (**c-4Rh@SBA-15**).

Reusability is an important feature to be monitored for application of heterogenized catalysts. Before reuse, the catalyst was separated from the reaction mixture by filtration and washed with acetone. It has to be mentioned here that in the first run with catalyst **4Rh@SBA-15** it took more than 20 h to achieve complete conversion (Figure 2.2. 19). However, after the first run the reaction reached >99% after 2 h and this remained steady up to 6th run. The dramatic increase of activity after the first run is quite likely caused by the formation of rhodium nanoparticles which are very efficient catalysts for hydrogenation.^[113] However, TEM images taken from the catalyst after the first run proves the absence of rhodium nanoparticles larger than 1 nm in diameter (Figure 2.2. 20), indicating the high dispersion of rhodium species on the SBA-15.

A solid state NMR investigation on the used catalyst (after the first run) was also carried out to investigate the stability of the catalyst (Figure 2.2. 21, Figure 2.2. 22 and Figure 2.2. 23). The ^{13}C CP-MAS NMR and ^{29}Si CP-MAS NMR exhibit nearly the same resonances compared with the fresh catalyst **4Rh@SBA-15**, proving the high stability of covalent bond between complex and support. However, a slight low field shift was observed in ^{31}P CP-MAS NMR spectrum (34.7 ppm) compared to the fresh catalyst (30.5 ppm, Figure 2.2. 10), suggesting a change of the rhodium species. The asterisks denote to the sidebands.

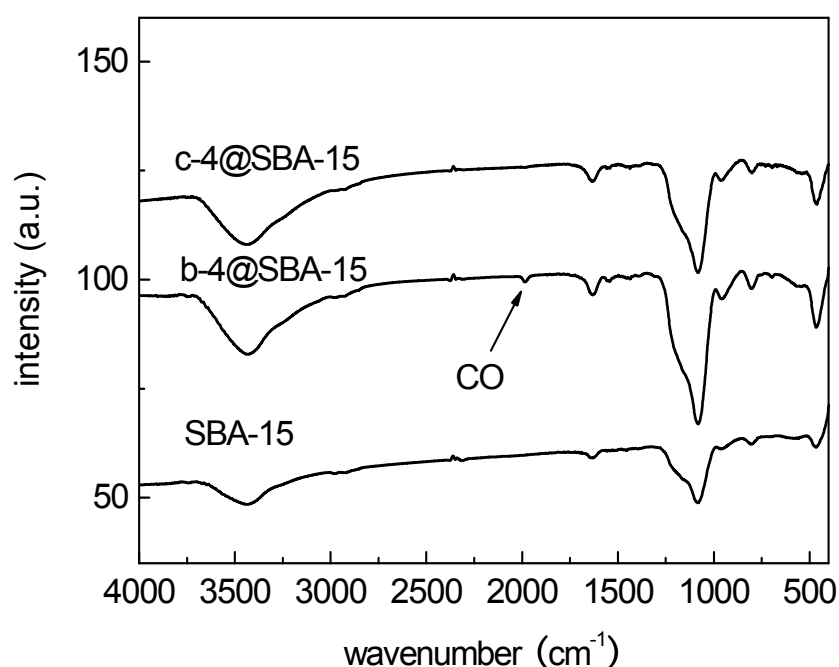


Figure 2.2. 18 Infrared spectroscopy of SBA-15, **4Rh@SBA-15** and air-aged **4Rh@SBA-15**.

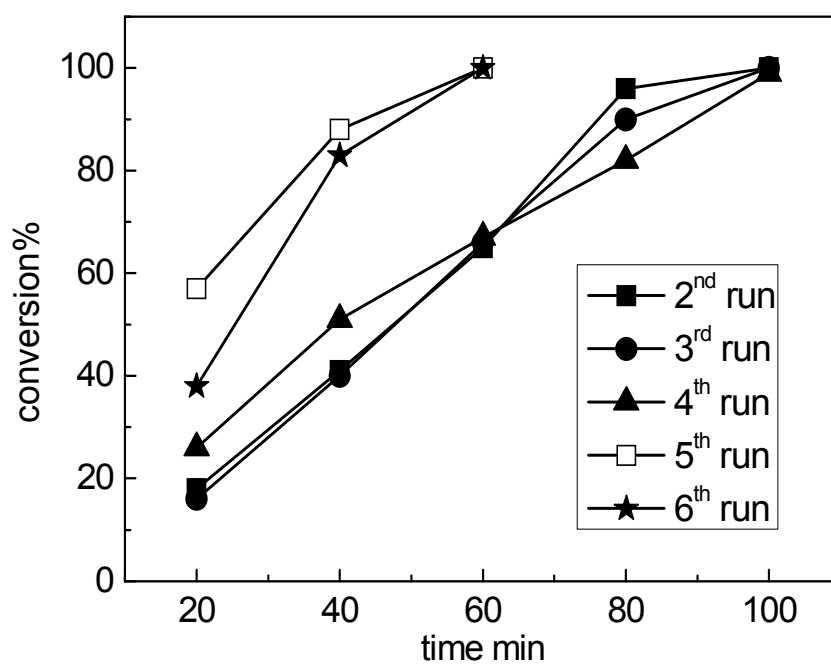


Figure 2.2. 19 Recycling of **4Rh@SBA-15** for the hydrogenation of cyclohex-2-enone.

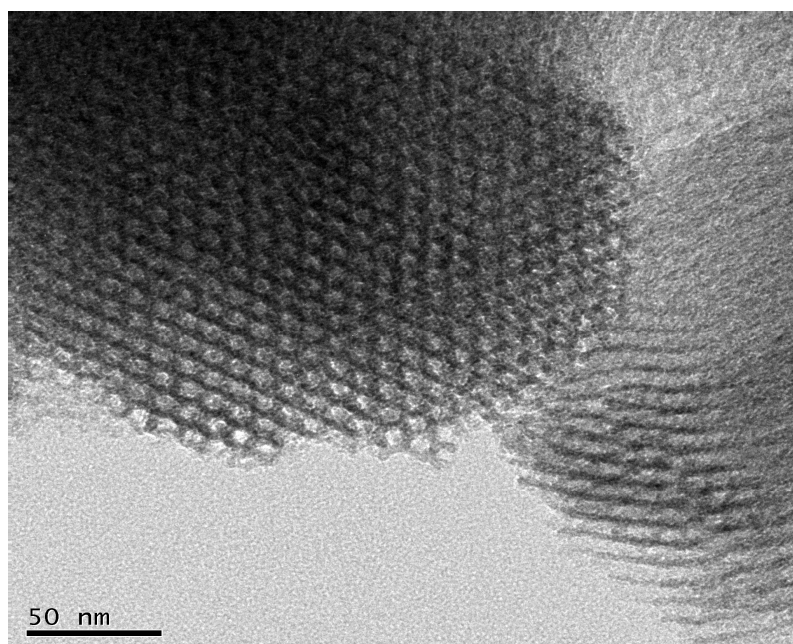


Figure 2.2. 20 TEM images of **4Rh@SBA-15** after being used for one catalytic run.

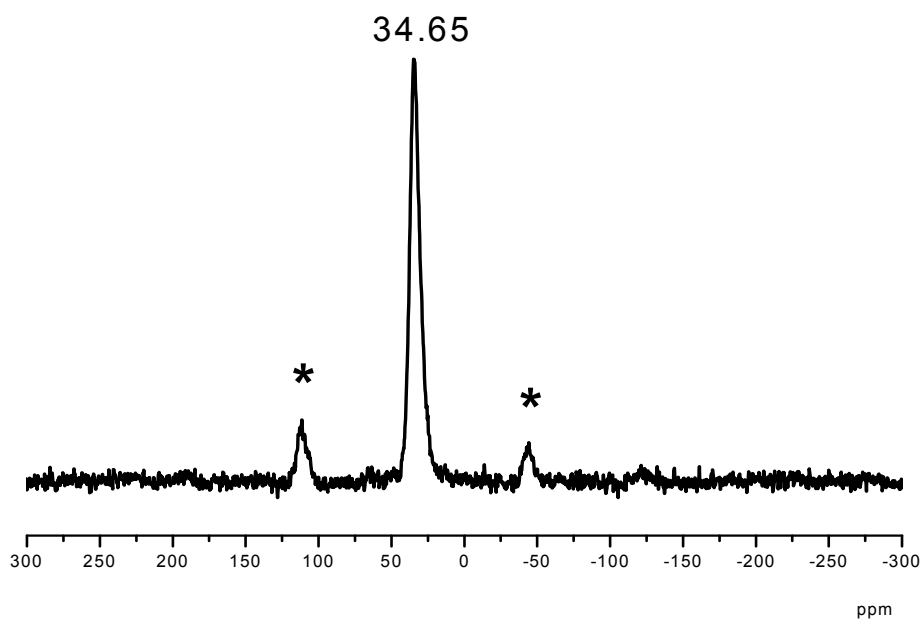


Figure 2.2. 21 ^{31}P CP-MAS NMR of **4Rh@SBA-15** after first run.

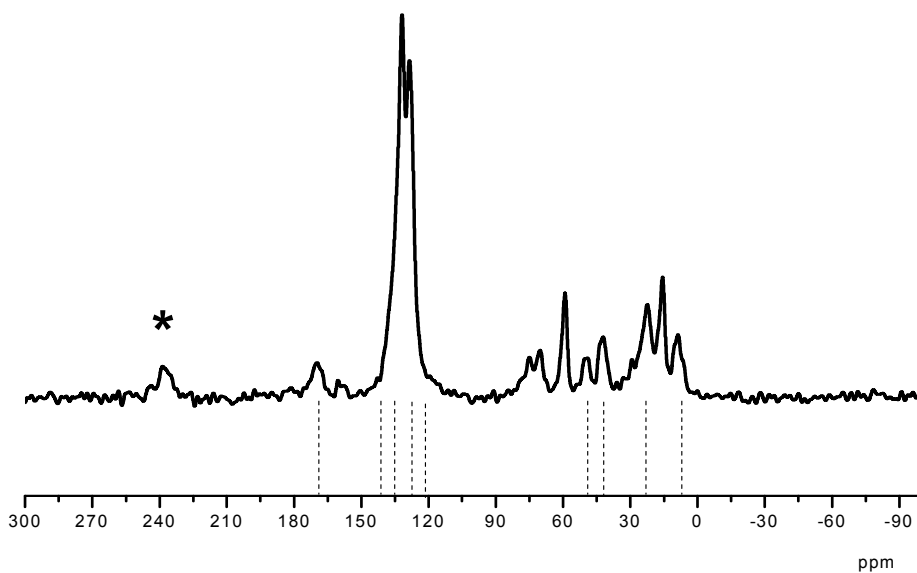


Figure 2.2. 22 ^{13}C CP-MAS NMR of **4Rh@SBA-15** after first run.

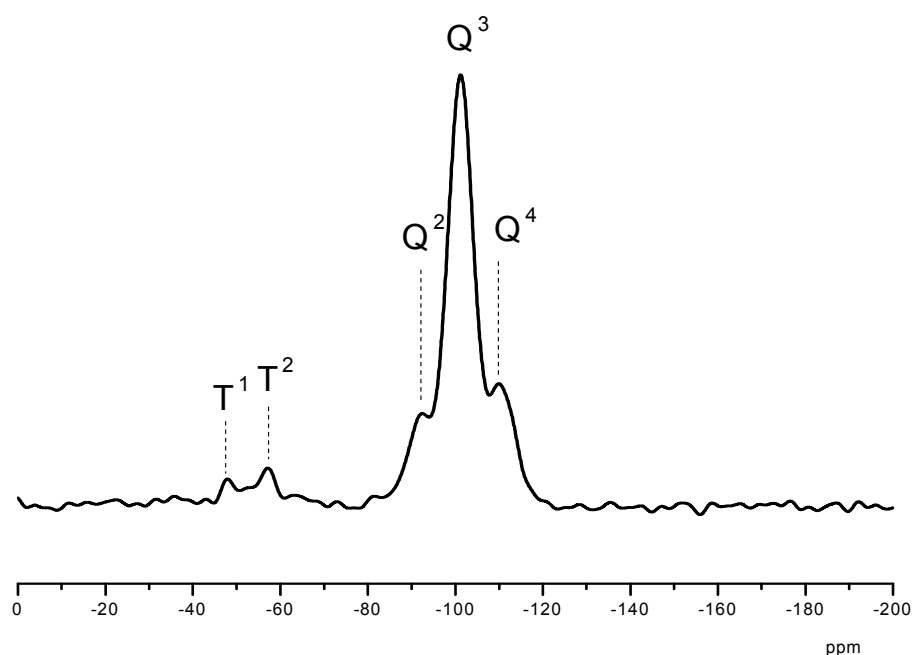


Figure 2.2. ^{29}Si CP-MAS NMR of **4Rh@SBA-15** after first run.

Leaching tests are another important to investigate the stability of heterogeneous catalyst. The leaching of rhodium determined by atomic adsorption showed a significant dependence on the polarity of the solvent and increased with increasing polarity of solvents (Table 2.2. 2, entries 1-3). The non polar solvent toluene showed the lowest amount of leaching with SBA-15 as support (entry 4). In the second run, further decrease of leaching was observed, corresponding to a loss of only 0.1% of the initially added catalyst (entry 5). These results imply that leaching is not a serious problem for this catalyst, which is consistent with the excellent reusability of this catalytically active material. For comparison, leaching of the complex from a hydrophobic PMO support was also tested in the same solvent and a higher Rh leaching was observed (entry 6).

To extend the substrate scope a series of other olefins were examined for the catalytic hydrogenation with **4Rh@SBA-15** (Table 2.2. 3). In our model reaction cyclohex-2-enone was hydrogenated with excellent chemoselectivity to the corresponding alkanone without any attack at the C=O double bond (entry 1). Simple olefins such as

styrene and 1-octene reacted efficiently and without any byproduct under the standard conditions, too (entries 2, 3). However, turning to higher substitution patterns at the C=C double bond strongly reduces the catalytic activity (entries 4-7). Styrenes substituted in the 2-position of their C=C double bonds with functional groups such as hydroxide, aromatic carbonyl and aromatic rings were not at all reduced under the standard conditions (entries 8-10). However, by increasing the reaction temperature up to 60 °C and the H₂ pressure up to 15 bar, cinnamyl alcohol could completely been converted into 3-phenylpropanol (entry 8).

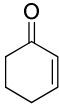
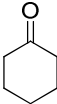
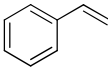
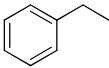
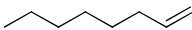
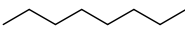
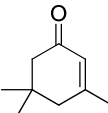
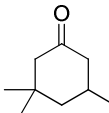
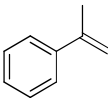
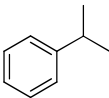
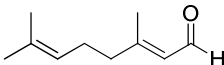
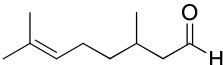
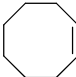
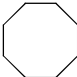
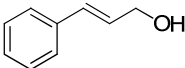
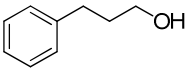
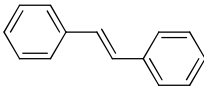
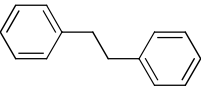
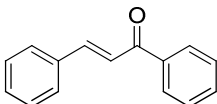
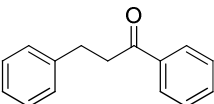
Table 2.2. 2 Leaching of the heterogeneous catalysts.

entry	catalyst	solvent	yield ^a (%)	Rh leaching ^b (%)
1	SiO ₂	DMF	99	6.3
2	SiO ₂	dioxane	48	2.7
3	SiO ₂	isopropanol	99	0.8
4	SBA-15	toluene	99	0.3
5	SBA-15 ^c	toluene	99	0.1
6	PMO	toluene	99	3.5

^aReactions performed at 40 °C, 1 bar H₂ with 1 mmol 2-cyclohexen-1-one as substrate and 1.6% catalyst for 24 h. ^bdetermined by GC-MS. ^cdetermined by atomic absorption.

2. Covalent Immobilization of Triphenylphosphine Complexes

Table 2.2. 3 Hydrogenation of different olefins with **4Rh@SBA-15**.

entry	olefin	product	yield (%) ^b
1			99
2			99
3			99
4			0
5			40
6			< 10
7			< 15
8			0 (99 ^c)
9			0
10			0

^aReaction conditions: 40 °C, 1 bar H₂, 1 mmol of substrate, 1.6 mol% of catalyst **b-4Rh@SBA-15**, toluene, 24 h. ^bdetermined by GC-MS. ^ccarried out at 60 °C and 15 bar H₂.

2.3 Immobilization of a Ruthenium Complex by the Post Grafting Method

2.3.1 Introduction

Ruthenium is relatively inexpensive in comparison with the other group 8 transition metals such as rhodium, and a variety of ruthenium complexes have been prepared and applied in a wide range of organic transformations, such as hydrogenation, oxidations, C-C bond formation and the reactions of CO and CO₂.^[114-115] Among these complexes, those phosphorus-based ligands represent an important class of active catalyst for hydrogenation of ketones^[116] which is a general process for the production of a wide range of alcohols. One of the most successful catalysts, with well-defined air-stable RuCl₂(PR₃)₂(diamine) and RuCl₂(diphosphine)(diamine) complexes as precatalysts, was first reported by Noyori et al.. These homogeneous catalysts are highly chemoselective for C=O bonds in the presence of a base and hydrogen gas, which show the potential application in industry.^[117]

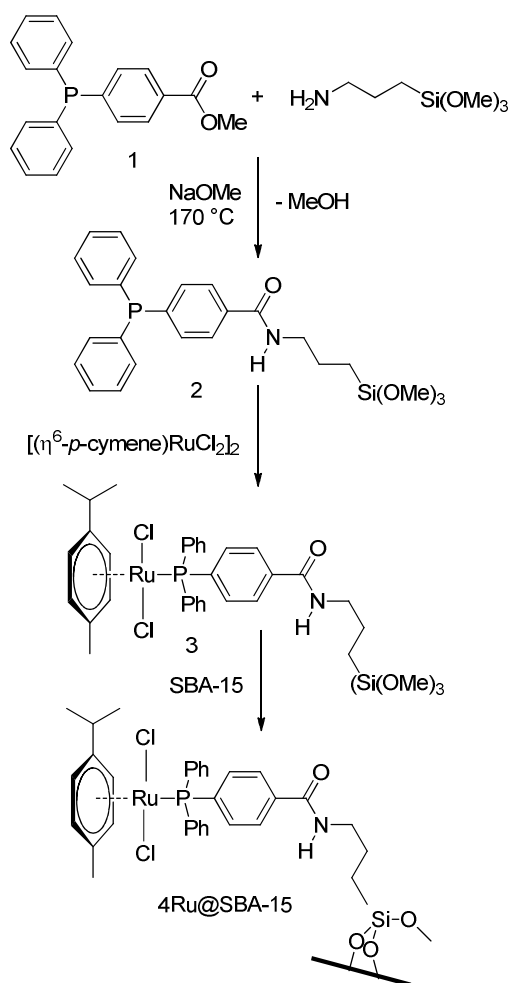
The catalytic transfer hydrogenation has recently emerged as a useful and convenient method beside direct hydrogenation, which is particularly significant and attractive when pressure hydrogenation is not practical. In most cases, 2-propanol is the conventional hydrogen donor solvent, because it is stable, nontoxic and inexpensive and has a moderate boiling point. Many efforts have been made to design highly efficient ruthenium homogeneous catalysts for transfer hydrogenation, however, more attractive heterogeneous catalysts are rarely reported.

In chapter 2.2, the immobilization of a rhodium triphenylphosphine complex on a support and its application in direct hydrogenation were present. As an extension of our previous study, herein the preparation of SBA-15 supported ruthenium triphenylphosphine complex by post grafting method is described. The resulting heterogeneous catalyst was further applied in transfer hydrogenation of ketones.

2.3.2 Results and discussion

Synthesis

The preparation of immobilized mono-triphenylphosphine ruthenium complex **4Ru@SBA-15** is quite similar to the procedure described in chapter 2.1 and chapter 2.2. The procedure is outlined in Scheme 2.3. 1.



Scheme 2.3. 1 Synthesis of the heterogenized ruthenium catalyst **4Ru@SBA-15**.

The dinuclear ruthenium complex $[\text{RuCl}_2(\eta^6\text{-p-cymene})]$ was used as precursor, which reacted with an equimolar amount of methoxysilane functionalized triphenylphosphine ligand **2** and gave the red mono- substituted complex **3** in 90% yield. The complex **3** was completely characterized before immobilization, which guarantees the definition of the active center.

Characterization

Figure 2.3. 1 shows the ^1H NMR spectrum of complex **3**. For the isopropane group of *p*-cymene, the *CH* proton appears at 2.85 ppm as a multiplet and two methyl groups appear at 1.11 ppm as a doublet. One singlet at 1.86 ppm can be assigned to the methyl group of the *p*-cymene and two doublets at 5.21 and 4.98 ppm are attributed to the *CH* proton of *p*-cymene ring. The resonances at 3.43, 1.71, 0.69 ppm are typical for the silicon functionalized propylene chain and a sharp singlet (3.55 ppm) for the $-\text{Si}(\text{OMe})_3$ groups. A weak peak beside this resonance is caused by a little hydrolysis of the $-\text{Si}(\text{OMe})$ group, which also reduces the peak area of the $-\text{Si}(\text{OMe})_3$ resonances. One broad singlet at 6.45 ppm for the NH group and a quite complex pattern of resonances between 7.3 and 8.0 ppm for five magnetically inequivalent protons of the aryl rings, which are all coupling with the phosphorous atom are complexing the spectrum.

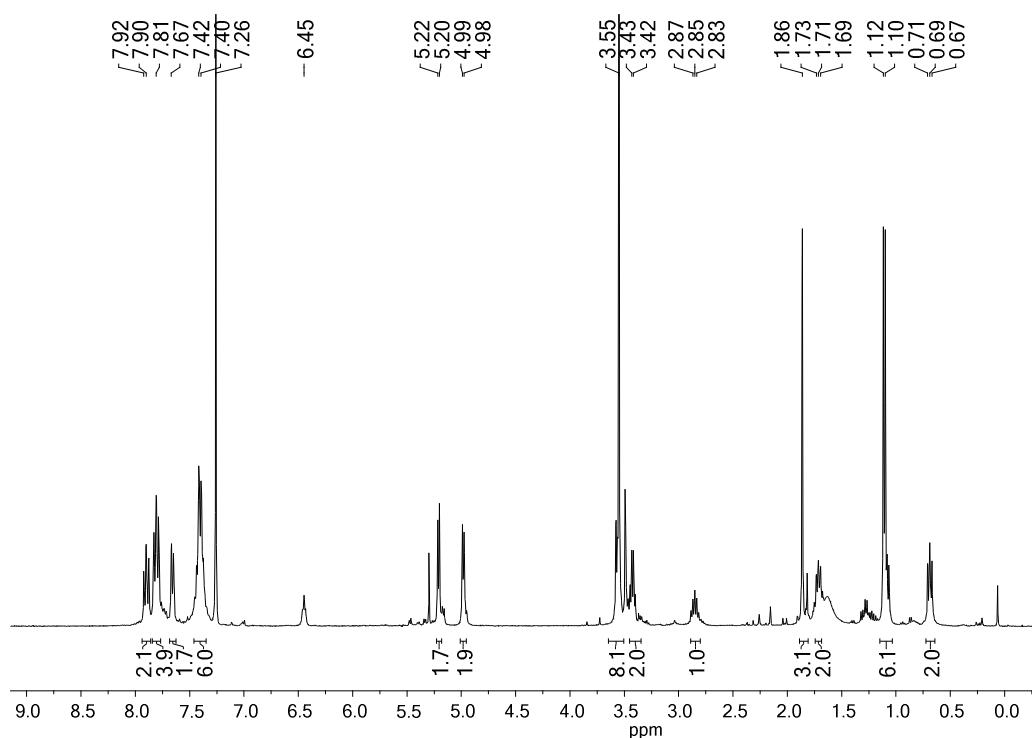


Figure 2.3. 1 ^1H NMR spectrum of complex **3** (400.13 MHz, 25 °C, CDCl_3).

The ^{13}C NMR spectrum (Figure 2.3. 2) shows three singlets at 17.8, 21.9 and 30.3 ppm, which can be attributed to the isopropyl group of the *p*-cymene. The resonances at 87.3, 89.0, 96.2 and 111.3 ppm are assigned to the carbon atoms of the *p*-cymene ring. Other peaks correspond well with the chemical shift of ligand **2**: The resonances for the aryl groups in the range from 126.0 to 137.2 ppm. Three resonances at 42.3, 22.7, 6.6 ppm can be correlated with the resonances of the propylene linker. The resonance at 50.7 ppm can be assigned to the organosilica $-\text{Si}(\text{OCH}_3)_3$ group and a signal at 167.1 ppm can be assigned to the $\text{C}=\text{O}$ group of the linker.

The ^{31}P NMR spectrum of complex **3** exhibits one peak at 24.6 ppm (Figure 2.3. 3). Compared to the chemical shift of free ligand (-4.1 ppm), this resonance shifts downfield, indicating coordination through the phosphorous atom.

The infrared spectrum data (ATE) of complex **3** is shown in Figure 2.3. 4. The band at 1636 cm^{-1} is assigned to the $\nu\text{ C}=\text{O}$ stretching vibration (amide I). The N-H bending vibration (amide II) is observed at 1541 cm^{-1} .

A SEM image taken from **4Ru@SBA-15**, which was used in catalysis, clearly shows that the particles are joined to form unregular and fibrous aggregates (Figure 2.3. 5). This is the characteristic morphology of SBA-15 material.

The powder X-ray diffraction pattern of **4Ru@SBA-15** exhibits three sharp reflections in the low angle region ($2\theta < 2^\circ$), indicating a high degree of mesostructural order (Figure 2.3. 6). The pattern can be indexed as (100), (110) and (200) reflections, indicating a two-dimensional hexagonal symmetry (p6mm) of the material, which suggests that the two-dimensional hexagonal pore structure of SBA-15 is preserved after the introduction of the ruthenium complex.

2. Covalent Immobilization of Triphenylphosphine Complexes

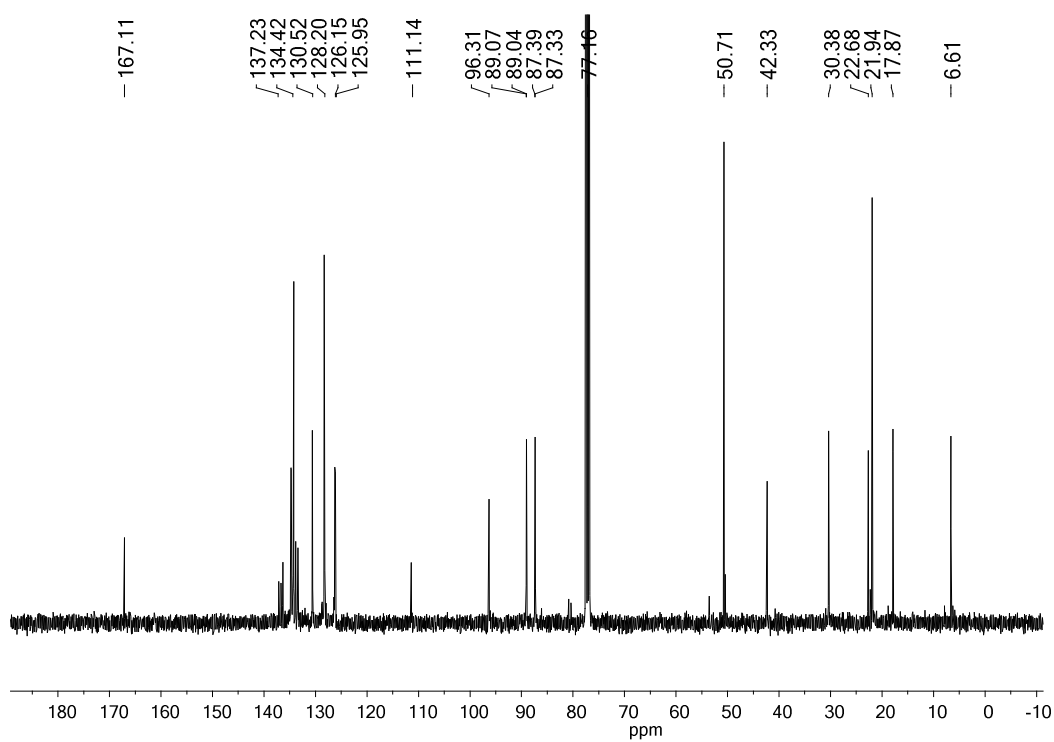


Figure 2.3. 2 ¹³C NMR spectrum of complex 3 (100.62 MHz, 25 °C, CDCl₃).

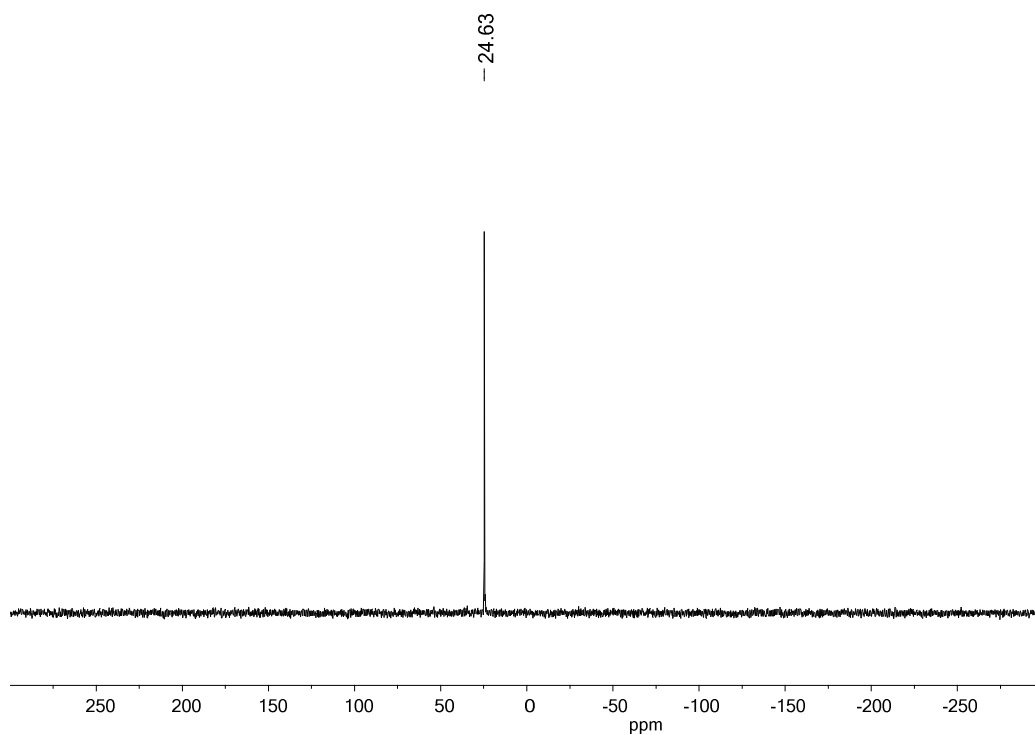


Figure 2.3. 3 ³¹P NMR spectrum of complex 3 (100.62 MHz).

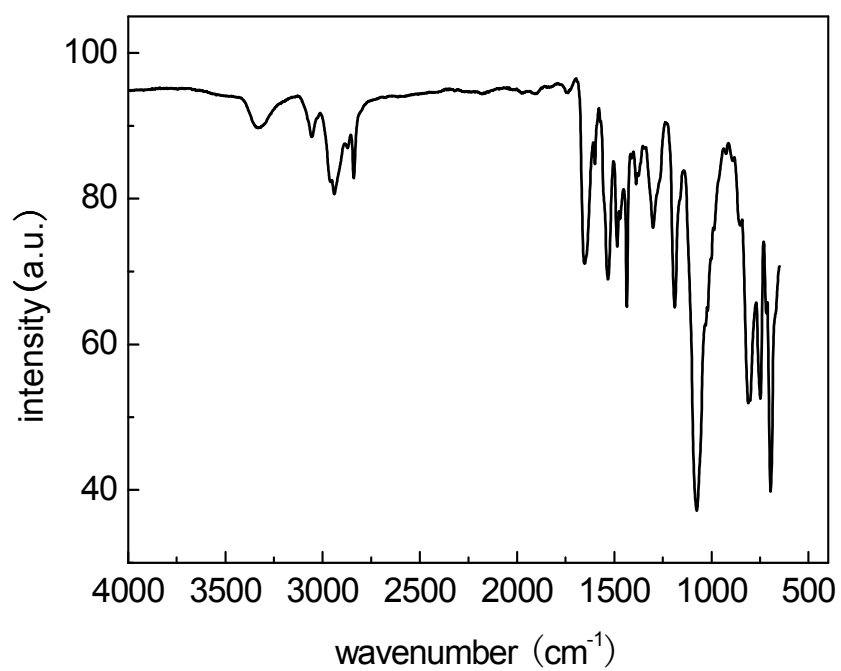


Figure 2.3. 4 FT-IR spectroscopy of complex **3**.

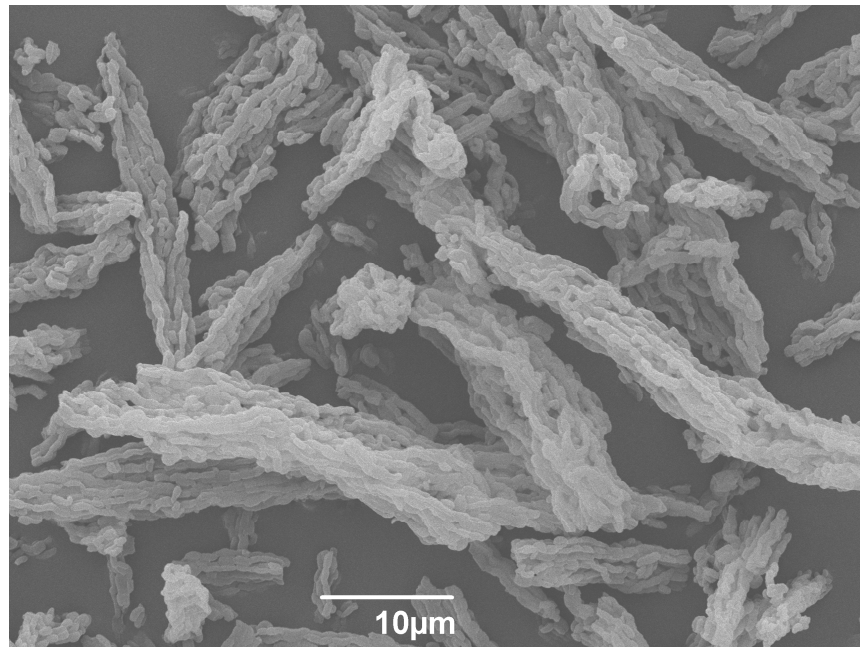


Figure 2.3. 5 SEM image of the catalyst **4Ru@SBA-15**.

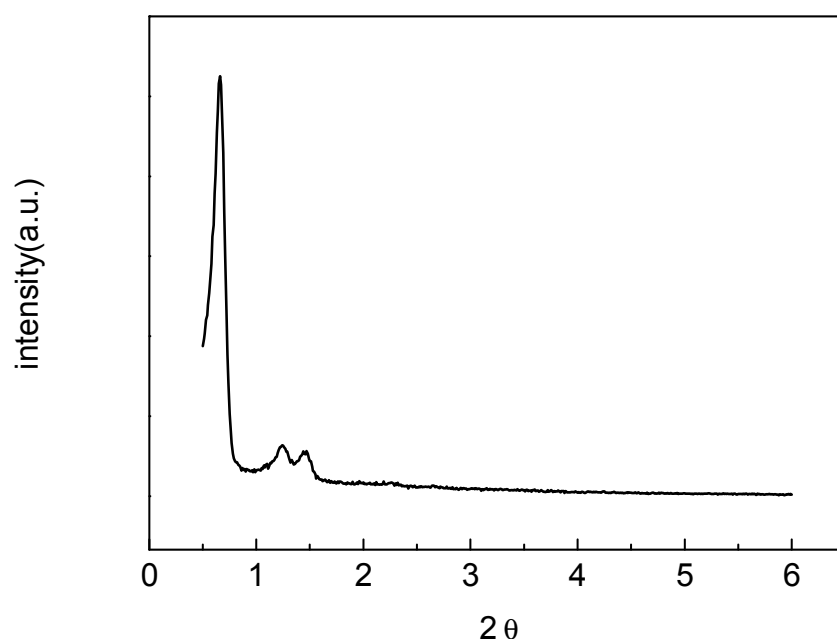


Figure 2.3. 6 XRD pattern of the catalyst **4Ru@SBA-15**.

Nitrogen sorption was used to measure the pore structures of **4Ru@SBA-15**. The specific surface areas and the textural properties of the analysis of the nitrogen adsorption and desorption data exhibited a type IV isotherm with a hysteresis characteristic for mesoporous materials possessing pore diameters between 2 and 50 nm (Figure 2.3. 7).^[88] Besides, a higher uniformity in the pores is reflected by a sharp increase in the capillary condensation with a prominent hysteresis loop. This indicates that the overall mesoporosity is maintained after the introduction of the ruthenium complex. The pore size distribution (PSD) was obtained by applying the BJH pore analysis according to the desorption branch of the nitrogen adsorption–desorption isotherms. The measured data for the BET surface area, the total pore volume and the pore size of **4Ru@SBA-15** are $673 \text{ m}^2\cdot\text{g}^{-1}$, $1.24 \text{ cm}^3\cdot\text{g}^{-1}$ and 6.4 nm respectively. The loading of the ruthenium complex ($0.18 \text{ mmol}\cdot\text{g}^{-1}$) was determined by measuring the nitrogen content of the material.

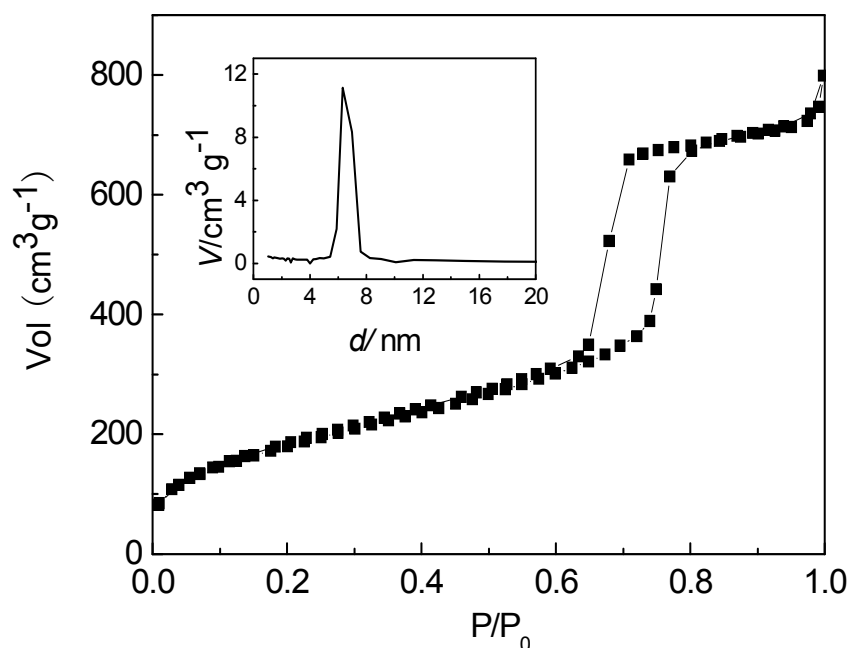


Figure 2.3. 7 N₂ sorption isotherms and BJH pore size distribution (inset) of **4Ru@SBA-15**.

The ³¹P CP-MAS NMR resonance (22.6 ppm) of **4Ru@SBA-15** matches well with the solution NMR data of complex **3** (24.6 ppm) (Figure 2.3. 8), proving the successful immobilization of complex **3** on the SBA-15. No signal of a phosphine oxide (expected at about 29 ppm) and other undesired phosphorus containing by-products can be observed. The successful grafting of the complex **3** was additionally verified by solid-state ¹³C CP-MAS NMR spectroscopy (Figure 2.3. 9). **4Ru@SBA-15** gives a spectrum similar to that of complex **3**, the resonances of which are assigned by the dashed lines, suggesting that the structure of the complex **3** is not affected during the grafting process.

The thermal stability of **Ru@SBA-15** was evaluated with thermogravimetric and differential thermogravimetric (TG-DTG) analysis (Figure 2.3. 10). A small weight loss was observed below 100 °C due to desorption of physisorbed water from the pore channels. A further distinct weight loss between 130 °C and 400 °C combined, with three peaks in the DTG curve (two sharp peaks at 230 °C and 320 °C and one weak peak at about 350 °C) can be observed. It is supported by three exothermic peaks at 230,

315 and 355 °C in the heat flow curve, which implies a three steps decomposition of the phosphine ligand. This result indicates that **Ru@SBA-15** has a thermal stability up to 130 °C.

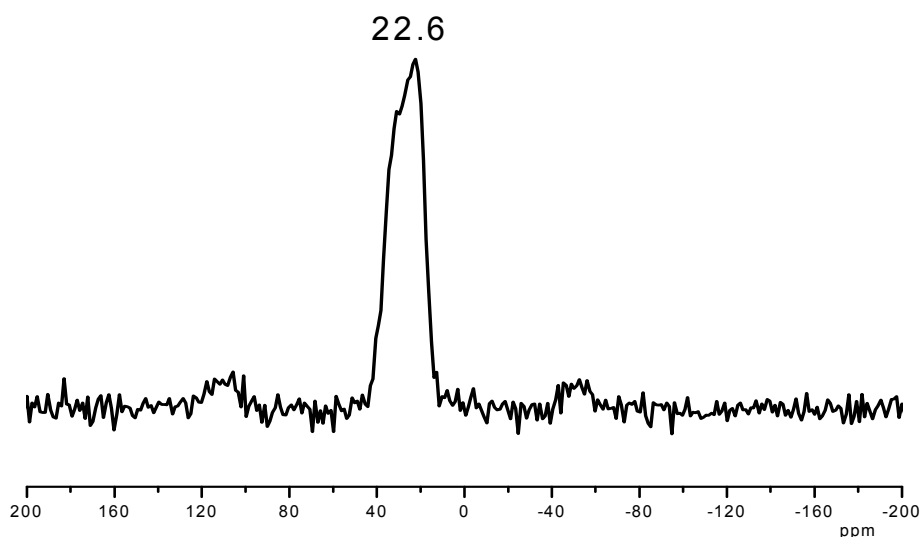


Figure 2.3. ^{81}P CP-MAS NMR spectrum of **4Ru@SBA-15**.

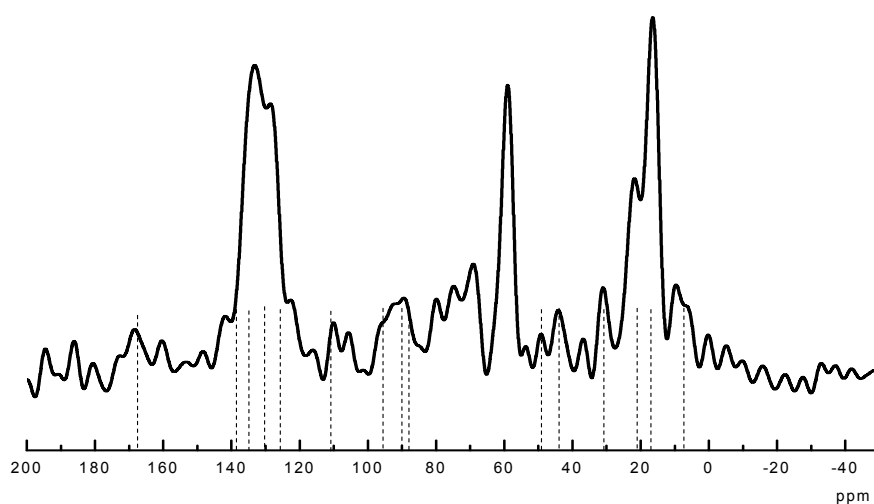


Figure 2.3. ^{13}C CP-MAS NMR spectrum of **4Ru@SBA-15**.

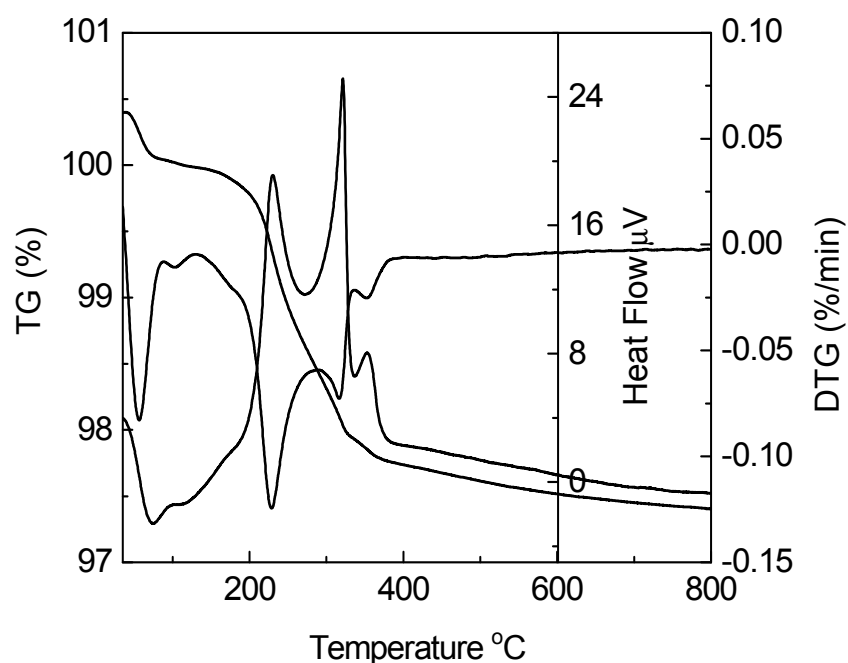
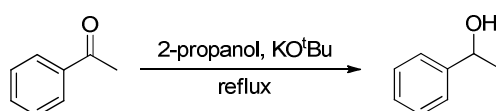


Figure 2.3. 10 Thermogravimetric and differential thermogravimetric analyses of **Ru@SBA-15**.

Catalysis

The obtained catalyst **4Ru@SBA-15** was first used in hydrogenation of cyclohex-2-enone under the same conditions with **4Rh@SBA-15** as catalyst in chapter 2.2. However, there is no activity. Furthermore, the transfer hydrogenation of acetophenone (Scheme 2.3. 2) was carried out under optimized reaction conditions: 2-propanol as hydrogen donor, 0.05 mmol of potassium tert-butoxide (KO^tBu) and 1.8 mol% Ru to 1 mmol substrate acetophenone, at 82 °C. The catalyst **4Ru@SBA-15** showed complete conversion within 24 h, in addition, the catalyst can be further reused 3 times without obvious loss of activity as shown in Table 2.3. 1.



Scheme 2.3. 2 Transfer hydrogenation of acetophenone with catalyst **4Ru@SBA-15**.

2. Covalent Immobilization of Triphenylphosphine Complexes

Table 2.3. 1 Recyclability of **4Ru@SBA-15** used for the hydrogenation of acetophenone.^a

recycle	3h	5h	24h
1 st run	50	90	100
2 nd run	78	99	100
3 rd run	42	56	88

^aReaction conditions: acetophenone (1 mmol), 2-propanol (10 mL), KO^tBu in 2-propanol (0.05 mmol), catalyst (0.017 mmol of Ru), refluxed.

The reusability test shows the catalyst has induction time in the first run and slightly lost activity in the third run. The color of catalyst gradually turns to grey, which suggests the ruthenium nanoparticles were formed during the reaction. The induction time may be partially caused by formation of ruthenium nanoparticles, which are the real active centers for transfer hydrogenation. In addition, the reaction solution turned yellow, which indicates the catalyst has a leaching problem. The used catalyst (after the first run) was also investigated by the solid state NMR (Figure 2.3. 11). The asterisks donate to the sidebands.

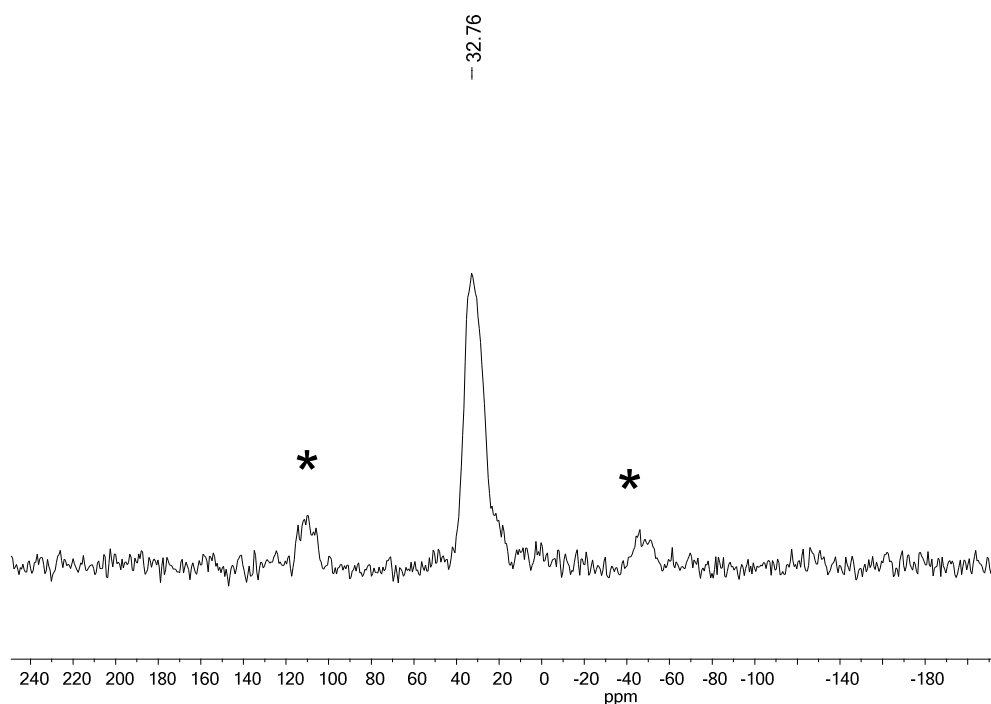


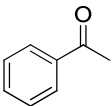
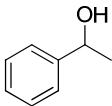
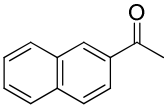
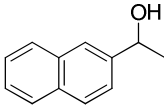
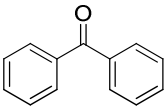
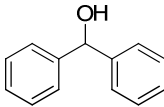
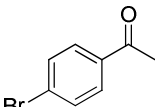
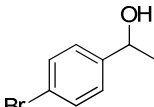
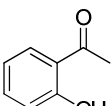
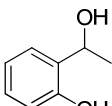
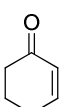
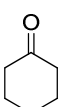
Figure 2.3. 11 ³¹P CP-MAS NMR of **4Ru@SBA-15** after first run.

2. Covalent Immobilization of Triphenylphosphine Complexes

The ^{31}P CP-MAS NMR spectrum exhibits a peak around 32.8 ppm. Compared to the fresh catalyst (22.6 ppm, Figure 2.3. 8), this resonance shifts 10 ppm downfield, indicating the decomposition of the ruthenium complex. It is possible that the phosphorus donor was oxidized.

Finally, **4Ru@SBA-15** catalyzed transfer hydrogenation was applied to other ketones (Table 2.3. 2).

Table 2.3. 2 Transfer hydrogenation of different Ketones with **4Ru@SBA-15**.^a

entry	ketone	product	yield (%) ^b
1			99
2			99
3			61
4			10
5			trace
6			43

^aReaction conditions: **4Ru@SBA-15** (50 mg, 0.018 mmol), KO^tBu (0.05mmol) and ketone (1 mmol) in dry 2-propanol (10mL), reflux for 24 h. ^bYields were determined by GC-MS and related to the unreacted ketone.

Acetophenone and 2'-acetonaphthone can be reduced efficiently and without any byproduct under the standard conditions (entry 1 and 2). However, with benzophenone as substrate, the yield under the same reaction conditions and reaction time was

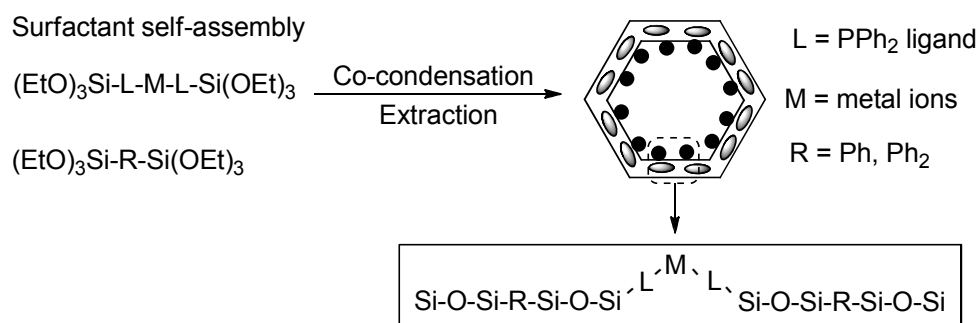
only of 61 % (entry 3). Substituted acetophenones such as 2'-hydroxyacetophenone and 4'-bromoaceto-phenone were also tested. However, strongly reduced catalytic activity was observed (entry 4 and 5). When cyclohex-2-enone was used as substrate, affording the hydrogenation of the alkene C=C bond, without any detectable (GC-MS) amount of the alcohol as hydrogenated product (entry 6).

2.4 Immobilization of a Palladium Complex by Co-condensation Method

2.4.1 Introduction

Periodic mesoporous organosilicas (PMOs) opened a wide range of possibilities for the chemical design of novel nanomaterials due to their highly tunable properties by varying the R group in the bridged organosilicane precursors $(R'O)_3\text{-Si-R-Si-(OR')}_3$. Although remarkable progress has been made in synthesis of various PMOs, most materials are limited to a few types of inert alkane,^[118-120] alkene,^[121] phenyl^[122-123] and aromatic bridging groups^[124].

Organometallic catalysts have been widely used in organic transformations. However, there are still unsolved problems such as product purification and catalyst separation restricting the application of homogeneous catalysts. Therefore, it is desirable to incorporate bridged organometallicsilicas into a silica matrix. This offers an opportunity to obtain materials possessing both highly active centers and a defined periodic mesostructure. However, such large organometallicsilicas are difficult to achieve for a proper assemblage with the surfactant often leading to amorphous materials.^[29, 120, 125] Therefore, the synthesis of PMOs with large and flexible organometallicsilicas groups in the mesoporous wall still remains a significant challenge. Up to now, only a few successes have been achieved in the preparation of PMOs with chemically active bridging groups. Li H. et al. reported an approach for the preparation of ordered mesoporous organometallic catalysts with silylated M-PPh₂ compounds (M refers to Pd²⁺, Au⁺, Ru²⁺, and Rh⁺ ions) embedded in silica walls in the presence of P123 as surfactant (Scheme 2.4. 1). The obtained PMOs materials are active and reusable catalysts in aqueous organic reactions.^[26-27, 126] Dufaud et al. described the synthesis of PMOs with Wilkinson type organometallicsilicas within the pore walls in the presence of cetyltrimethylammonium bromide (CTAB).^[28] An ordered mesostructured PMOs material was obtained and successfully applied for olefin hydrogenation.



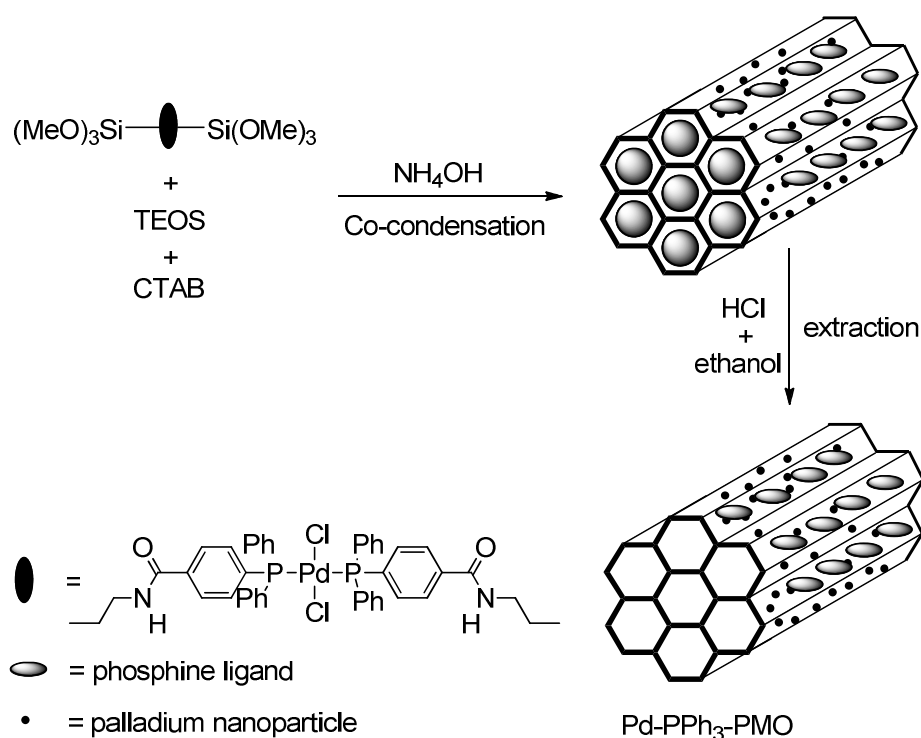
Scheme 2.4. 1 Preparation of M- PPh_2 -PMO materials by surfactant-directed co-condensation.

In chapter 2.1, 2.2 and 2.3, various triphenylphosphine metal complexes were covalently immobilized on the mesoporous silica supports with the post grafting method. However, the presence of organometals terminally bound to the pore surface blocks the pore channels and significantly decreases the specific surface area, pore volume and pore size distribution. Here, a bissilylated triphenylphosphine palladium complex was directly incorporated into the silica framework with the co-condensation method. The obtained hybrid material was further applied for olefin hydrogenation and exhibited excellent activity and stability.

2.4.2 Results and discussion

Synthesis

The bissilylated palladium triphenylphosphine complex was used as precursor for the synthesis of PMOs material and prepared by the same procedure as described in Chapter 2.1. The further synthesis was carried out in cooperation with S. Shylesh and the procedure is outlined in Scheme 2.4. 2. Because the bissilylated palladium complex has a bulky organic group between two trimethoxysilyl groups, it is necessary to use other small silane compound such as TEOS to co-condense with it for constructing an ordered mesostructure. CTAB was used as structure-directing agent under basic conditions. The obtained precipitate was extracted with ethanol-HCl solution to remove the surfactant and further washed and dried.



Scheme 2.4. 2 Preparation of **Pd-PPh₃-PMOs** with co-condensation method.

Characterization

The X-ray powder diffraction pattern of **Pd-PPh₃-PMO** (Figure 2.4. 1) shows a typical pattern of a hexagonally MCM-41-like ordered structure. Three clear peaks in the low-angle region ($2\theta < 10^\circ$) can be assigned to the (100), (110) and (200) diffractions with spacings d of 46, 25 and 22 Å, which can be indexed to two-dimensional hexagonal $p6mm$ symmetry with unit cell $a = 53$ Å ($2d_{100}/\sqrt{3}$), indicating a highly ordered hexagonal structure. The morphology of **Pd-PPh₃-PMO** was studied using SEM (Figure 2.4 2), which shows the formation and aggregation of small particles with diameters less than 1 μm. Further confirmation of the highly ordered mesostructure of the resulting material comes from TEM images, in which a 2D hexagonal arrangement of mesopores is clearly observed (Figure 2.4. 3). Besides, a typical vesicle-like structure with a vesicle size of silica approximately 300 nm was formed. Monodispersed palladium nanoparticles with a narrow size distribution (about 15 nm) are embedded inside the core part of the vesicle-like structure, indicating that a significant decomposition occurred during the co-condensation process.

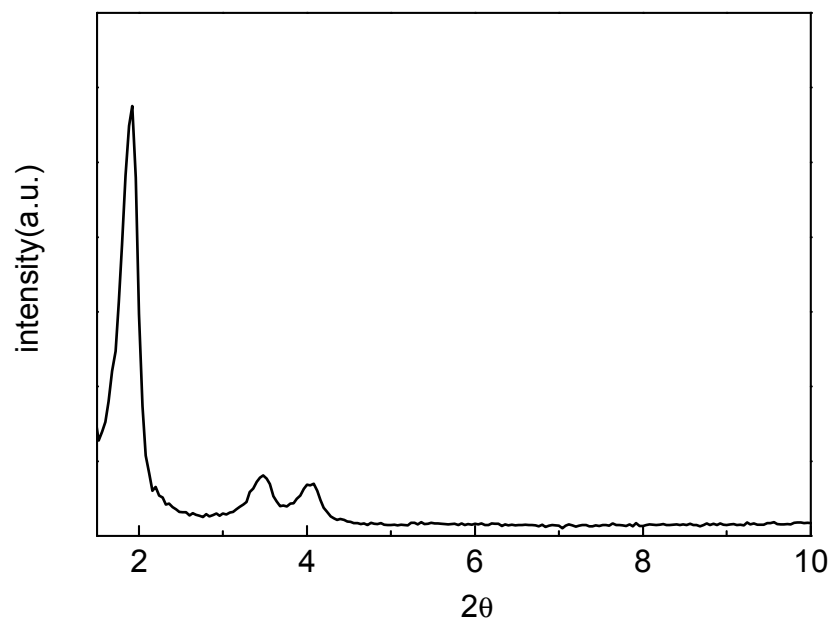


Figure 2.4. 1 XRD pattern of **Pd-PPh₃-PMO**.

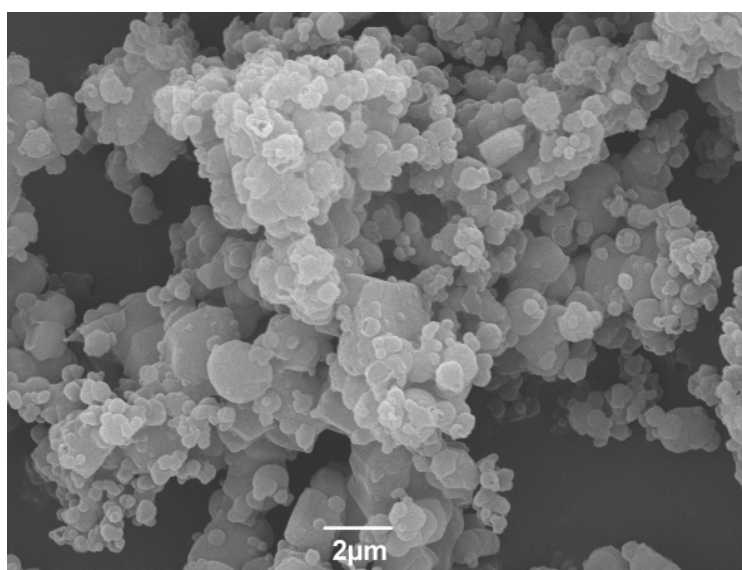


Figure 2.4. 2 SEM image of **Pd-PPh₃-PMO**.

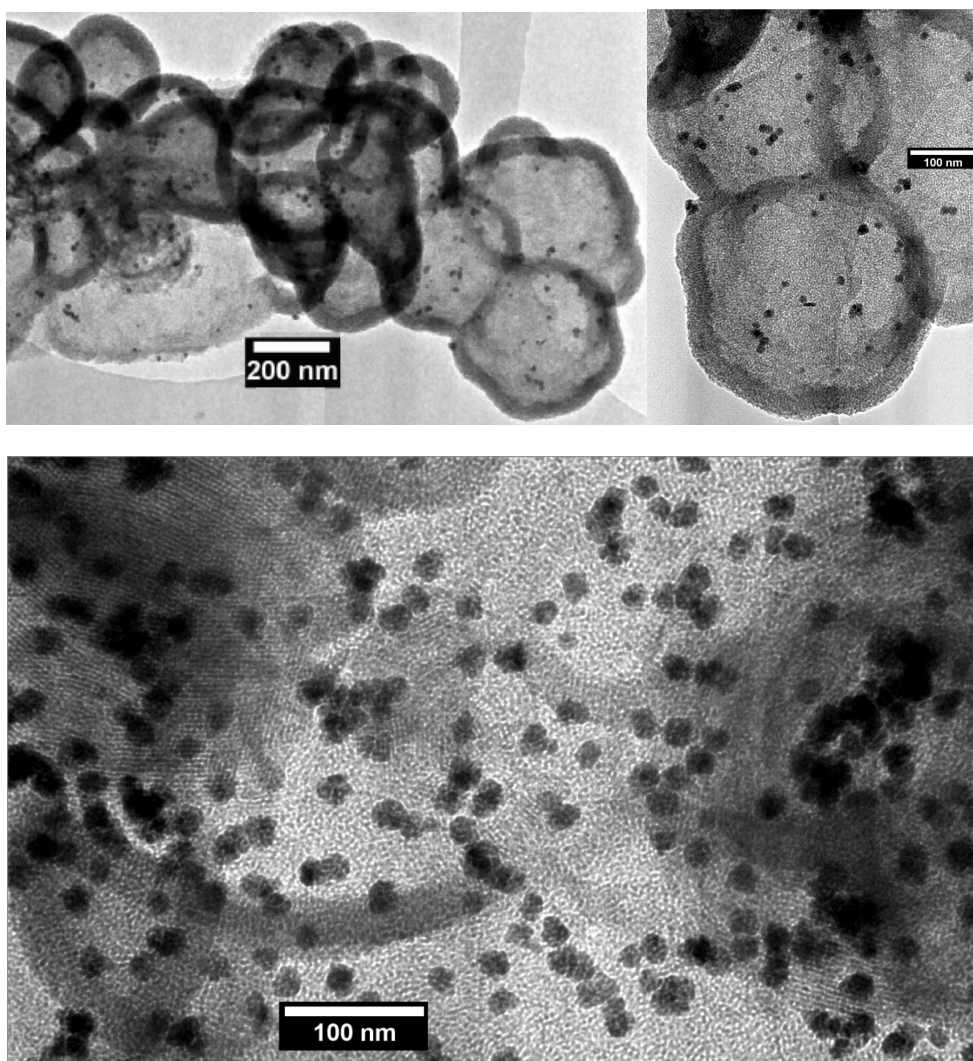


Figure 2.4. 3 TEM images of **Pd-PPh₃-PMO**.

The nitrogen adsorption/desorption isotherms and pore size distribution of **Pd-PPh₃-PMO** are presented in Figure 2.4. 4 and Figure 2.4. 5. **Pd-PPh₃-PMO** exhibits a type IV isotherm with a hysteresis typical for a mesoporous material possessing a pore diameter between 2 and 50 nm.^[88] A narrow pore-size distribution, calculated from desorption branches of the isotherms using the BJH method, confirms the uniformity of the mesopores in the **Pd-PPh₃-PMO** material (Figure 2.4. 5). It further proves that the organic groups are incorporated into the framework of the pores rather than terminally bonded to the pore surface, which effectively diminishes pore channel blockage, leading to higher specific surface area and total pore volume. The measured data for the BET surface area, the total pore volume and the BJH pore size of **Pd-PPh₃-PMO** are

1172 m²·g⁻¹, 0.96 cm³·g⁻¹ and 2.4 nm, respectively. Pore wall thickness is 29 Å, which is estimated by subtracting the pore size from the unit cell *a*.

Reincorporation of organic groups inside the framework can also be confirmed by ²⁹Si CP-MAS NMR. The ²⁹Si CP-MAS NMR spectrum of **Pd-PPh₃-PMO** shows both Tⁿ and Qⁿ sites as expected (Figure 2.4. 6). The resonances at -110.8, -101.1, and -91.9 ppm correspond to the Si(OSi)₄ (Q⁴), HOSi(OSi)₃ (Q³), and (HO)₂Si(OSi)₂ (Q²) sites of the inorganic silica framework, respectively,^[89] implying a high degree of TEOS cross-linking under the employed synthetic condition. According to the literature, the signals that originated from silicon atoms bridged by the organic group appear at -49, -58, and -67 ppm, which can be assigned to R-Si(HO)₂(OSi) (T¹), R-Si(HO)(OSi)₂ (T²), and R-Si(OSi)₃ (T³) organosiloxane sites.^[89] In Figure 2.4. 7, T¹ which represents incomplete hydrolysis/condensation of organosilane cannot be observed. The presence of the resonances T² and T³ confirms that carbon-silicon bond cleavage of phosphine ligand has not occurred during the hydrolysis and condensation process. The intensity of the signal T³ is apparently more pronounced than T², indicating a complete cross-linking reaction between the phosphine ligand and TEOS during the condensation process.

The ¹³C CP-MAS NMR spectrum of **Pd-PPh₃-PMO** (Figure 2.4. 7) shows resonances for the aryl groups in the range from 146 to 124 ppm. Three resonances at 29.6, 22.5, 16.1 ppm can be correlated with the resonances of the propylene linker. A signal at 168.8 ppm can be assigned to the C=O group of the linker, which corresponds well with chemical shift of phosphine ligand in solution (166.7 ppm), indicating that the interaction between the amide group of the linker and the silica framework is only weak.^[91] The dominant resonance at 58.8 ppm can be assigned to organosilica C-SiOCH₃ groups, implying that the hydrolysis/condensation of phosphine ligand is not fully completed, which corresponds with the presence of T² resonance in the ²⁹Si CP-MAS NMR spectrum. The asterisks denote rotational sidebands.

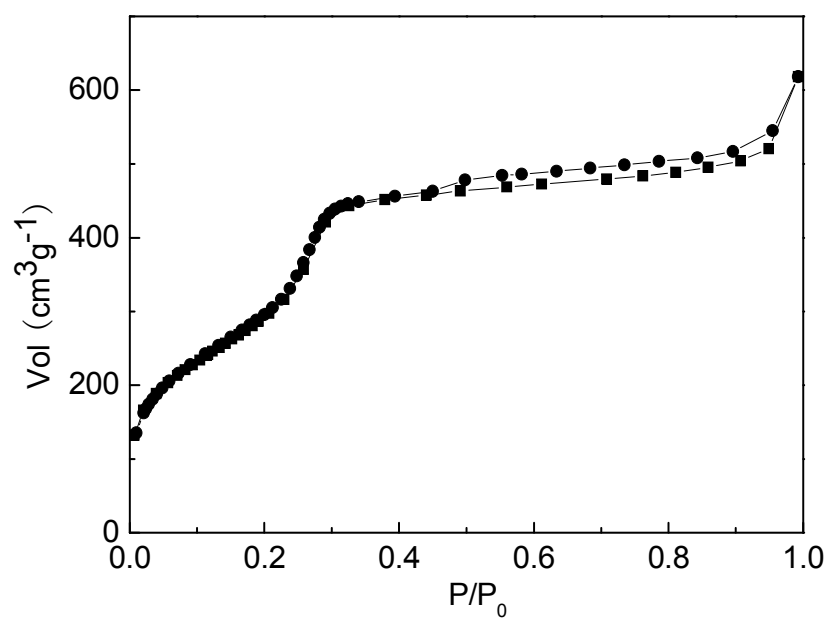


Figure 2.4. 4 N₂ sorption isotherms of **Pd-PPh₃-PMO**.

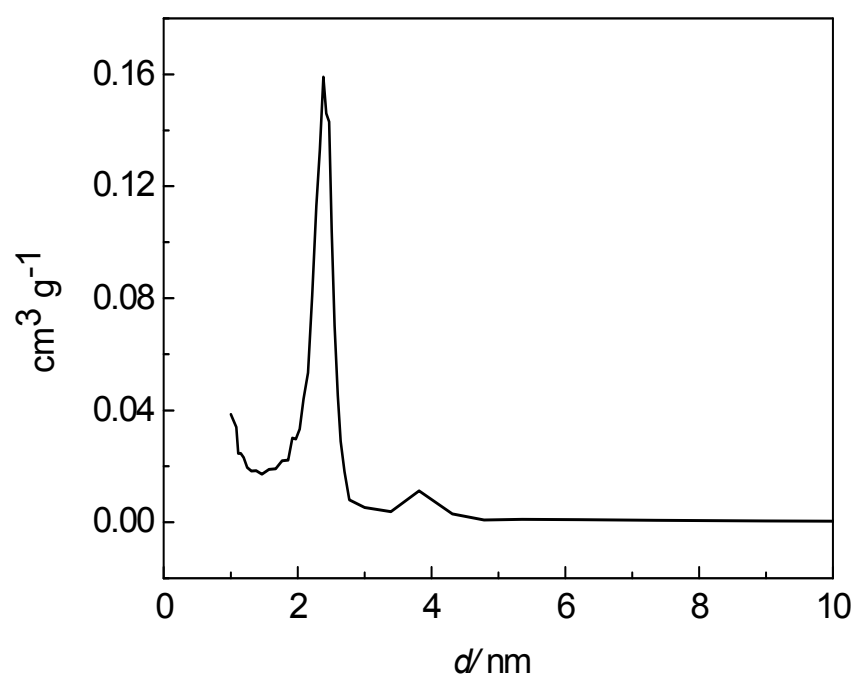


Figure 2.4. 5 Pore-size distribution of **Pd-PPh₃-PMO**.

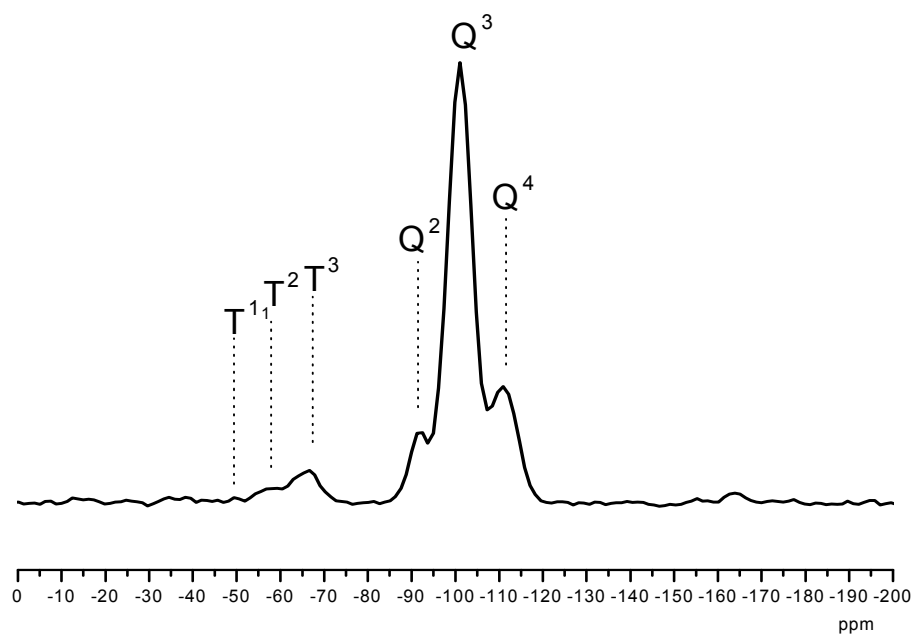


Figure 2.4. 6 ^{29}Si CP-MAS NMR spectrum of **Pd-PPh₃-PMO**.

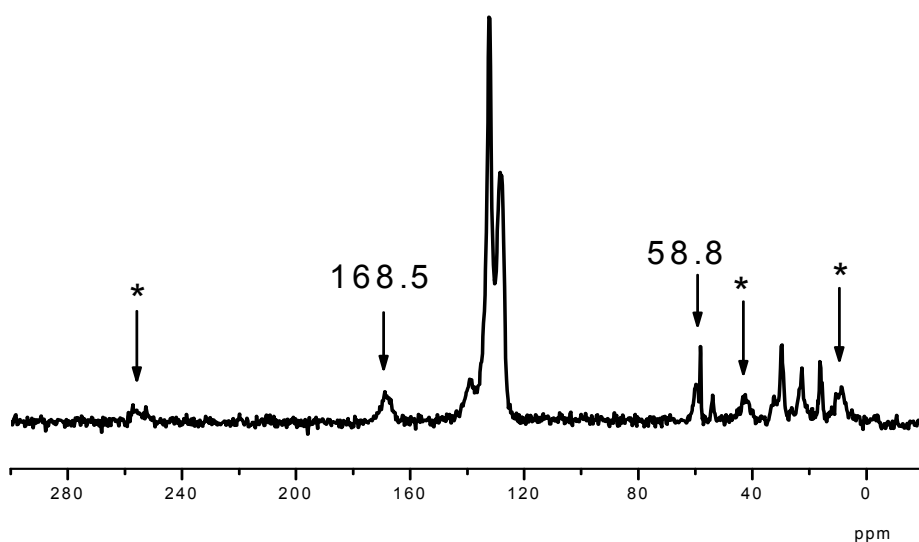


Figure 2.4. 7 ^{13}C CP-MAS NMR spectrum of **Pd-PPh₃-PMO**.

The chemical shift in the ^{31}P CP-MAS NMR spectrum of **Pd-PPh₃-PMO** is shown in Figure 2.4. 8. There is no signal of free triphenylphosphine (about -4.4 ppm) and of the

palladium complex (about 24.3 ppm). Considering the formation of palladium nanoparticles during the condensation process, the triphenylphosphine moiety should be easily oxidized in the air and basic aqueous solution as well as at the high aging temperature. The signal at 35.6 ppm might be attributed to the phosphine oxide (expected chemical shift: 29 ppm). The downfield shift of the ^{31}P CP-MAS NMR resonance (35.6 ppm) is quite likely caused by the environment of framework. The asterisks denote rotational sidebands.

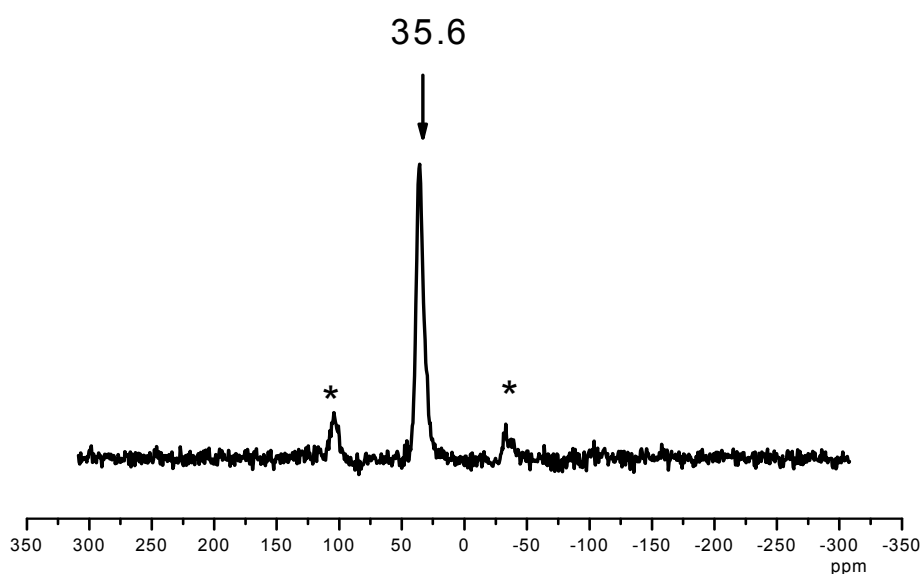


Figure 2.4. $8\ ^{31}\text{P}$ CP-MAS NMR spectrum of **Pd-PPh₃-PMO**.

X-ray photoelectron spectroscopy (XPS) was also used to check the oxidation state of the palladium species (Figure 2.4. 9). According to the literature,^[127-129] the Pd 3d_{5/2} peak binding energy for Pd (0) is 335.1 eV and the Pd 3d_{5/2} peak binding energies for Pd (0) clusters is 334.6 eV. These results agree with the TEM results, proving that the palladium nanoparticles were formed during the synthesis procedure. In addition, the peak at 336.4 eV corresponds to PdO species^[130] and the peak at 337.4 eV can be attributed to Pd coordinating to the phosphine ligand system. These results indicate the

palladium nanoparticle may be incorporated in the lattice of the SiO_2 matrix and part of the palladium atoms are still coordinated to the phosphor species. Both SiO_2 matrix and phosphine ligand should be responsible for the stability of the palladium nanoparticle. Figure 2.4. 10 shows the XPS spectrum of phosphorus. The peak at 132.6 eV can be assigned to P(V) in $\text{Pd}\cdots\text{OPPh}_3$.^[131] The asterisks denote rotational sidebands.

The presence of the phosphine ligand in the silica framework is further indicated by a weak amide bands at 1549 and 1645 cm^{-1} (Figure 2.4. 11). No absorption in 2800-3000 cm^{-1} range is observed in spectrum of **Pd-PPh₃-PMO (B)**, indicating a complete removal of the surfactant from the hybrid material by the acid extraction process.

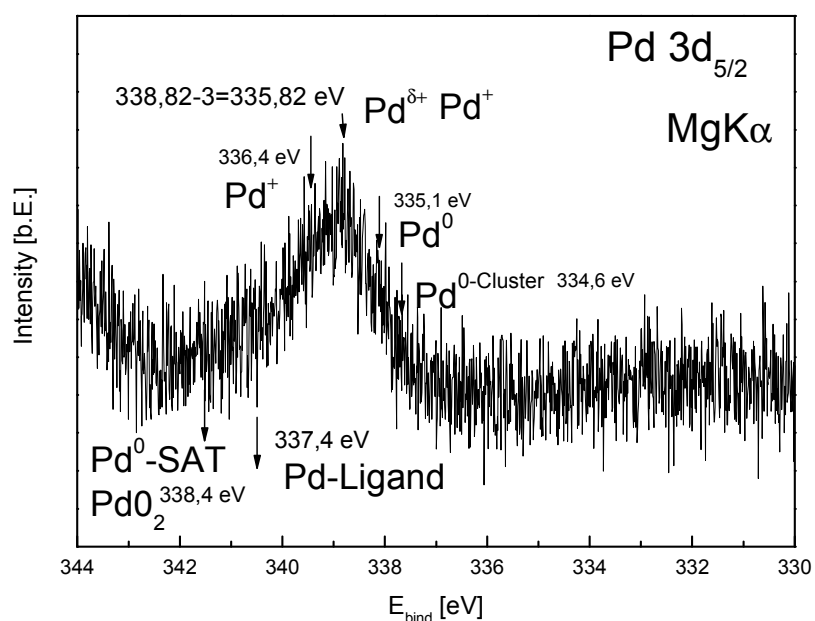


Figure 2.4. 9 XPS spectrum of palladium.

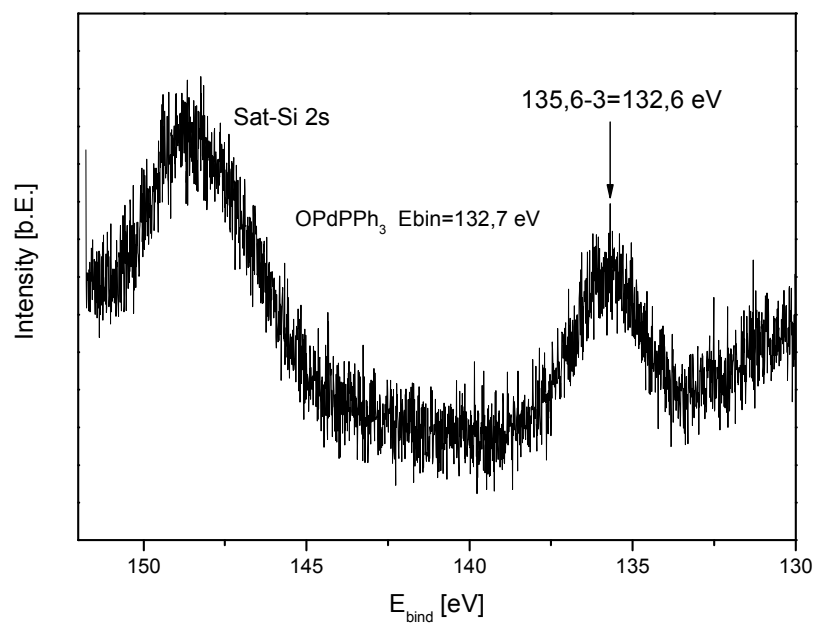


Figure 2.4. 10 XPS spectrum of phosphorus as in **Pd-PMO-E**.

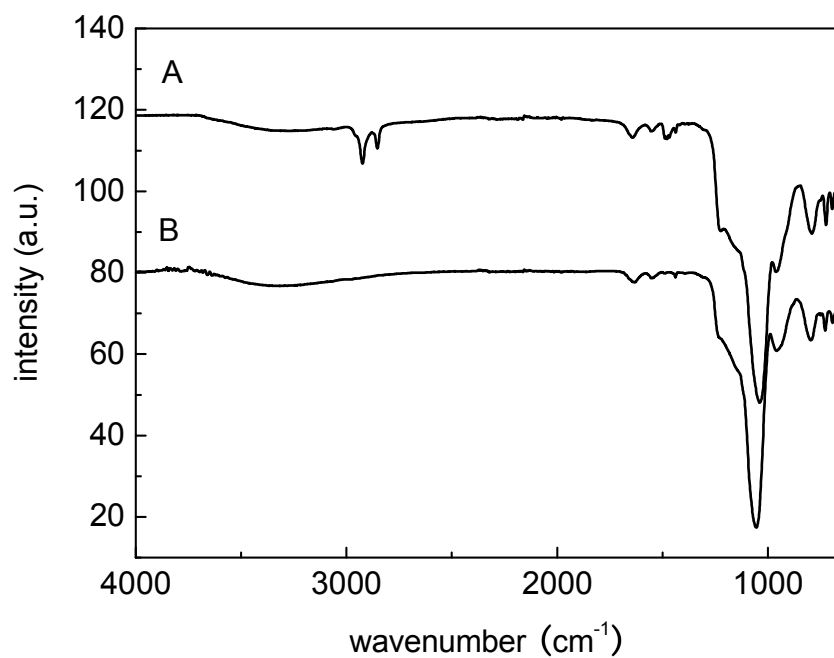


Figure 2.4. 11 IR spectra of **Pd-PPh₃-PMO** with surfactant **A** and **B** without surfactant.

To evaluate the thermal stability of the organosilica material **Pd-PPh₃-PMO**, thermogravimetric and differential thermogravimetric (TG-DTG) analysis experiments were carried out (Figure 2.4.12). A small weight loss was observed below 100 °C due to desorption of physisorbed water from the pore channels. A further distinct weight loss between 300 °C and 600 °C, combined with three peaks in the DTG curve (a weak peak at about 306 °C, a sharp peak at 384 °C and another weak peak at about 464 °C) can be observed. It is supported by three exothermic peaks at 306, 465 and 390 °C in the heat flow curve, which implies a three steps decomposition of the phosphine ligand. This result indicates that **Pd-PPh₃-PMO** has a thermal stability up to 300 °C. No weight loss can be assigned to the decomposition of any surfactant. It usually should appear between 100 and 300 °C. This result further confirms the complete surfactant removal by solvent extraction.

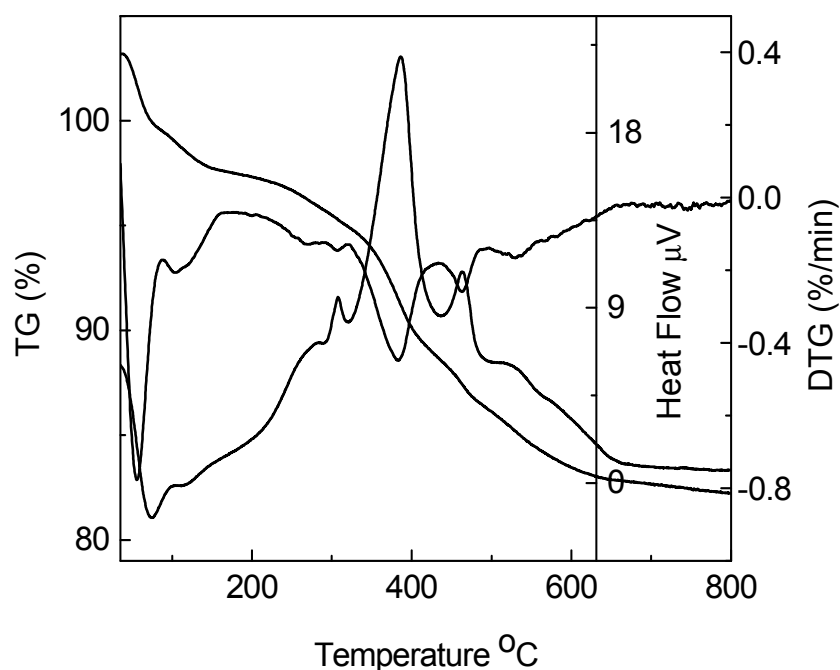


Figure 2.4.12 Thermogravimetric and differential thermogravimetric analyses of **Pd-PPh₃-PMO**.

Catalysis

The catalytic hydrogenation of alkynes, alkenes and aromatics is a very common reaction in heterogeneous catalysis and palladium nanoparticles based catalysts are well established as one of the most efficient catalysts for hydrogenation.^[132-133] The hybrid material **Pd-PPh₃-PMO** was used for the hydrogenation of cyclohex-2-enone. It showed excellent activity, selectivity and stability at room temperature under a pressure of 1 bar H₂ as shown in Figure 2.4. 13. The high stability is mainly because the organosilica matrix prevents the aggregation of the palladium nanoparticles. The TEM image taken from reused catalyst of **Pd-PPh₃-PMO** shows that the 2D hexagonal arrangement of the mesopores is preserved, indicating the high stability of organosilica matrix (Figure 2.4. 14). The size of the palladium nanoparticles is remained at about 15 nm as shown in Figure 2.4. 14, proving the organosilica matrix can effectively stabilize palladium nanoparticles under applied reaction conditions.

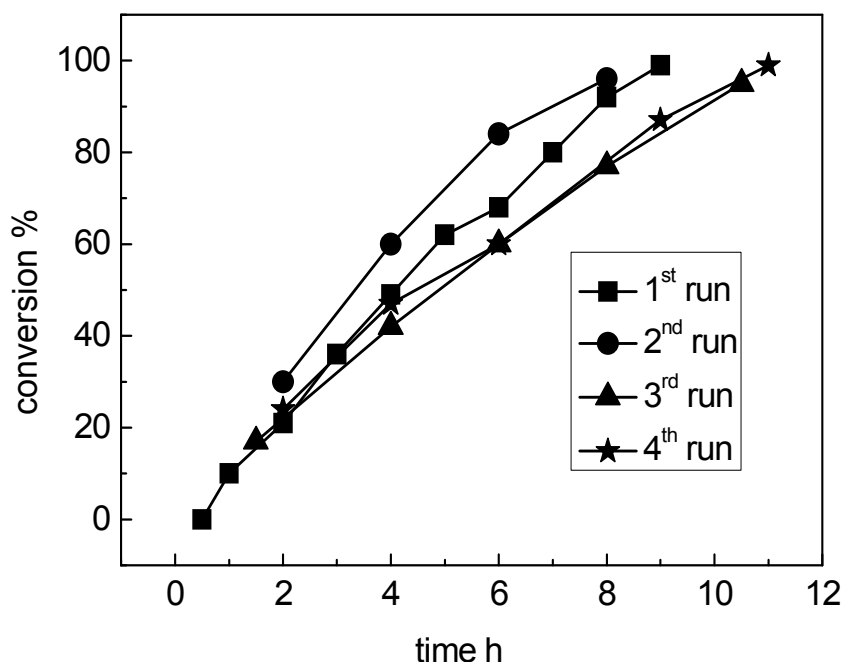


Figure 2.4. 13 Recycling kinetic curves of **Pd-PPh₃-PMO**.

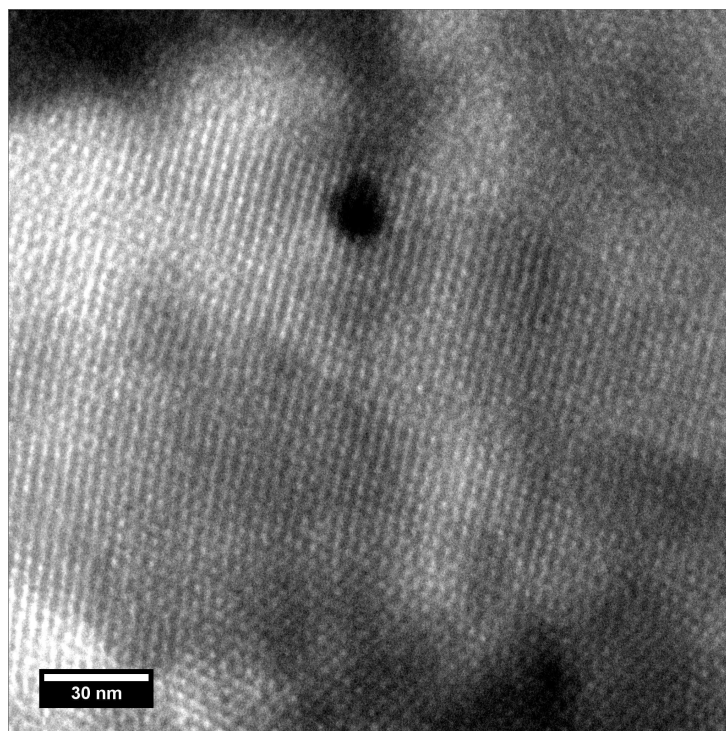


Figure 2.4. 14 TEM image of onefold used catalyst **Pd-PPh₃-PMO**.

The ¹³C and ³¹P CP-MAS NMR spectra of used **Pd-PPh₃-PMO** (Figure 2.4. 15 and Figure 2.4. 16) show unchanged resonances compared with fresh **Pd-PPh₃-PMO** (Figure 2.4. 7 and Figure 2.4. 8). It further proves the high stability of the organosilica matrix. The asterisks denote rotational sidebands.

To make sure whether the heterogeneous palladium nanoparticles incorporated in the silica support or the dissolved homogeneous palladium species is the real active center in the hydrogenation, a filtration experiment was carried out (Figure 2.4. 17). The catalyst was filtrated when a conversion of about 40% was reached. The continued reaction was carried out with the filtrate and there was no further conversion in between 20 h, which clearly demonstrates that it is a truly heterogeneous reaction. By atomic adsorption spectroscopy (AAS) of **Pd-PPh₃-PMO** no palladium contamination down to 0.5×10^{-4} mmol could be detected in the products. The asterisks denote rotational sidebands.

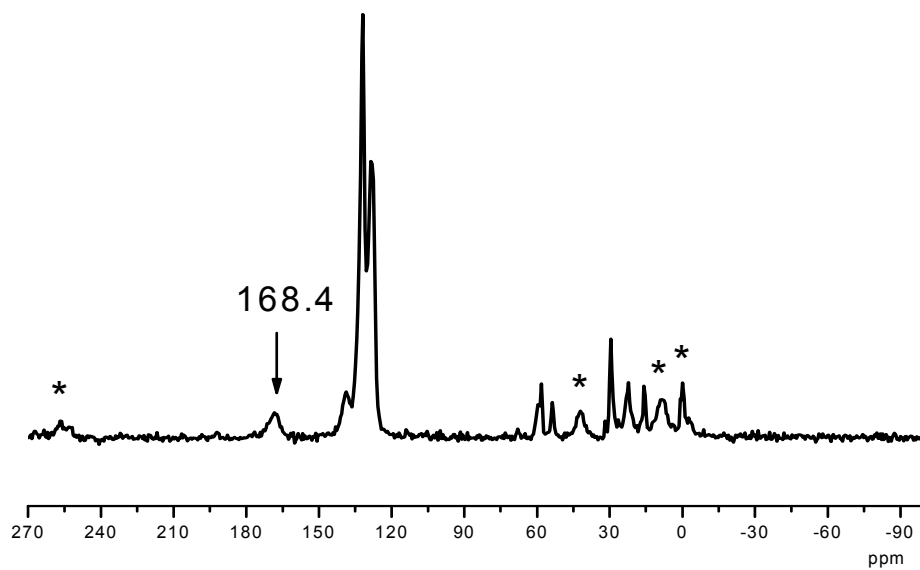


Figure 2.4. ^{15}C CP-MAS NMR of onefold used catalyst **Pd-PPh₃-PMO**.

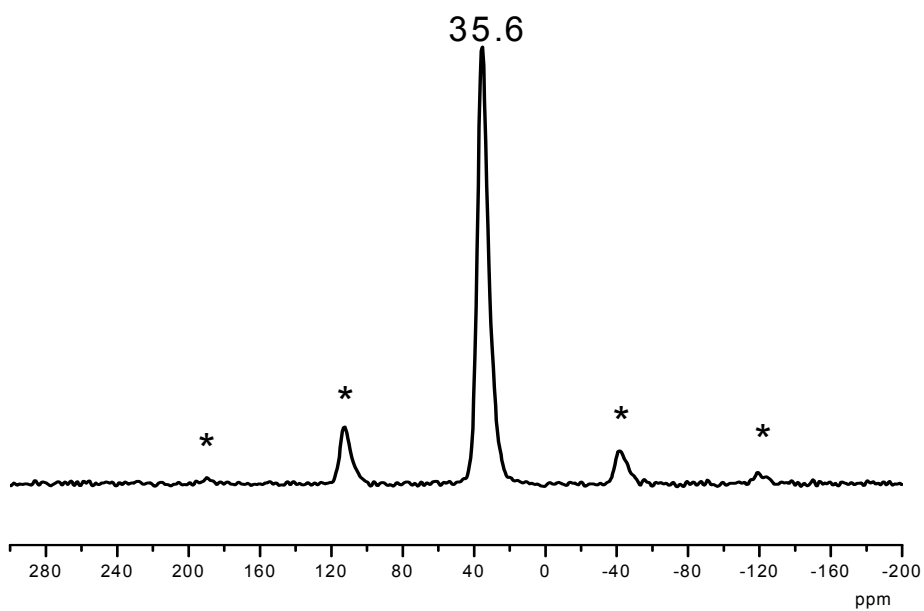


Figure 2.4. ^{31}P CP-MAS NMR of onefold used catalyst **Pd-PPh₃-PMO**.

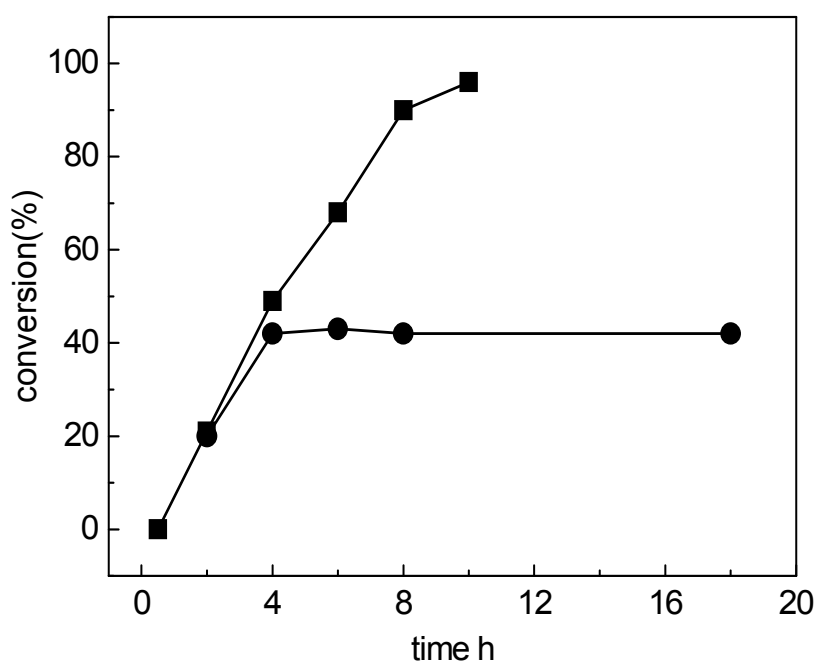
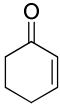
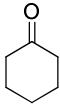
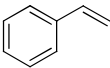
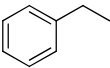
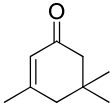
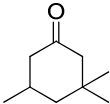
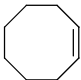
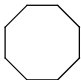
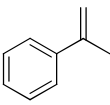
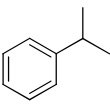
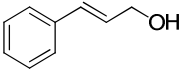
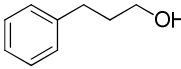
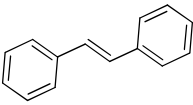
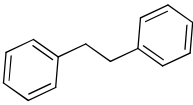
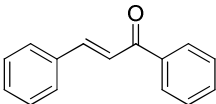
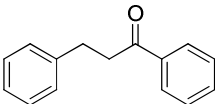


Figure 2.4. 17 Filtration experiment of **Pd-PPh₃-PMO**.

To extend the substrate scope a series of other olefins were examined for the catalytic hydrogenation with **Pd-PPh₃-PMO** (Table 2.4. 1). In the model reaction cyclohex-2-enone was hydrogenated with excellent chemoselectivity to the corresponding alkanone without any attack at the C=O double bond (entry 1). The simple olefin styrene reacted efficiently and without any byproduct under the standard conditions (entries 2). However, turning to higher substitution patterns at the C=C double bond strongly reduces the catalytic activity (entries 3-4). Styrenes substituted in the 1- or 2-position of their C=C double bond with functional groups such as methyl, hydroxide, aromatic carbonyl and aromatic rings can be effectively reduced (entry 5-8).

2. Covalent Immobilization of Triphenylphosphine Complexes

Table 2.4. 1 Hydrogenation of different olefins with **Pd-PPh₃-PMO**.

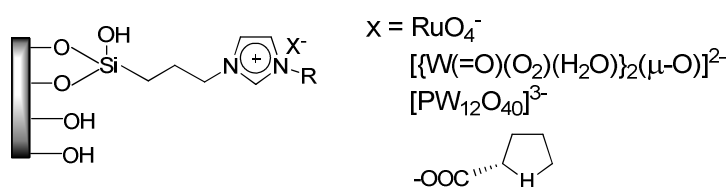
entry	reactants	product	yield ^a (%)
1			99
2			99
3			0
4			15
5			99
6			99
7			80
8			45

^aReaction conditions: room temperature, 1 bar H₂, 1 mmol of substrate, 0.1 mol% of Pd, toluene, 15 -20 h. ^bdetermined by GC-MS.

Chapter 3. Non-covalent Immobilization of a Triphenylphosphine Ligand

3.1 Introduction

As mentioned in chapter 1, various clays and ion exchange resins have widely been used as support materials for synthesis of heterogeneous catalysts by non-covalent electrostatic interactions. Recently, imidazolium cations covalently immobilized on solid supports, used as anion exchangers due to their highly charged nature, are beginning to attract interest.^[134] This concept is different to the so-called SILP catalysis (SILP = supported ionic liquid phase) where the ionic liquid, that contains the dissolved catalyst, is solely adsorbed on a support surface.^[135] Due to a certain solubility of ILs in the organic solvents, the SILP catalysts often suffer significant leaching in liquid phase reactions. Covalent grafting of imidazolium cations onto the surface of solid materials not only heterogenizes the ionic liquid ultimately, but also offers the opportunity to immobilize anionic species by means of replacing the counter anions. This had mainly been done with simple catalytically active anions such as RuO_4^- , $[\{\text{W}(=\text{O})(\text{O}_2)_2(\text{H}_2\text{O})\}_2(\mu\text{-O})]^{2-}$, $[\text{PW}_{12}\text{O}_{40}]^{3-}$ and *L*-proline, which already indicates the proof of concept for the application of imidazolium cation in ion exchange chemistry as shown in Scheme 3. 1.^[136-139]



Scheme 3. 1 Stabilization of anions through covalently grafted cation imidazolium salt.

Since this concept requires a charged catalyst (anion), the immobilization of organic ligands which can be applied to a wide range of catalysts by coordination with different

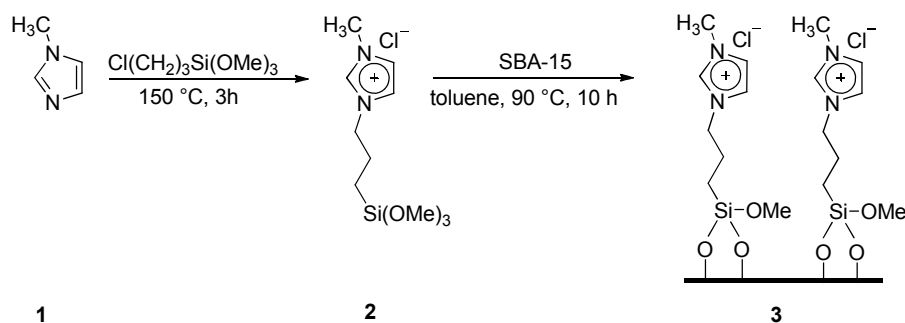
transition metal sites has up to now received less attention.^[136] In Chapter 2, a palladium(II) complex of the type $(L)_2PdCl_2$ and a rhodium(I) complex of the type $(L)_2Rh(CO)Cl$ ($L = Si(OMe)_3$ functionalized PPh_3), grafted on solid supports by formation of covalent Si-O-Si linkers, and their application in heterogeneous single-site catalysis were discussed.^[95, 106, 140] Here, as a novel concept of non-covalent immobilization, a triphenylphosphine derived ligand was immobilized on SBA-15 functionalized with silylated imidazolium cations. The obtained hybrid material was further reacted with palladium(II) and the resulting catalyst was applied for olefin hydrogenation and Suzuki reactions.

3.2 Results and discussion

3.2.1 Synthesis

The functionalization of the mesoporous SBA-15 material with the silylated imidazolium system is shown in Scheme 3. 2. 1-Methyl-3-(trimethoxysilylpropyl)-imidazolium chloride **2** was synthesized by simply heating 1-methylimidazole with one equivalent of (3-chloropropyl)trimethoxysilane to 150 °C. Treatment of degassed SBA-15 with **2** following a published procedure led to the hybrid material **3** which was filtrated and extracted with a Soxhlet apparatus to remove all adsorbents. The grafted amount of compound **2** was calculated according to the nitrogen content determined by elemental analysis, which is $1.16 \text{ mmol} \cdot \text{g}^{-1}$. The BET measurement shows a specific surface area of the SBA-15 of $600 \text{ m}^2 \cdot \text{g}^{-1}$. The grafting concentration is defined as the number of compound **2** per nm^2 of the silica surface, which is revealed as 1.1 ionic liquid fragments per nm^2 . Figure 3. 1 shows the coverage state of imidazolium on the surface of SBA-15. A single molecule takes up 0.9 nm^2 surface area which is represented by a square. In the middle of the square is an immobilized imidazolium cation whose mobility is represented by a circle. The distance between the carbon atoms of the methyl group and of the methylene unit next to the silicon atom in compound **2** was calculated to about 0.7 nm, which is longer than the semidiameter of

the square. That means that the whole surface area is nearly covered by imidazolium cations and they can interact with each other by exchanging their counterions.



Scheme 3. 2 Immobilization of imidazolium chloride **2** on SBA-15.

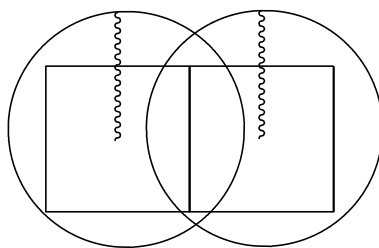
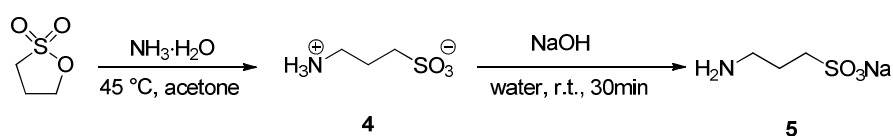


Figure 3. 1 The grafting concentration of compound **3**.

In our previous work,^[106, 140] a methylester group attached at one of the phenyl rings of triphenylphosphine allowed to functionalize the ligand with 3-trimethoxysilylpropylamine, a typical silane coupling agent used for the covalent immobilization of organic compounds on silica surfaces.^[30] For the ionic grafting, sodium(3-amino-1-propanesulfonate) **5** was used to generate an anionic side chain linked to the triphenylphosphine core. The water soluble ligand TPPTS and its transition metal complexes have been immobilized on resins or clays by the ion exchange method.^[141-142] However, the present strategy offers a general method to immobilize organic compounds by electrostatic interaction. Additionally the alkyl chains of the sulfonate and imidazolium linkers will significantly increase the flexibility of the grafted catalyst, which should be beneficial for its activity and selectivity. Compound **5** was obtained as outlined in Scheme 3. 3 according to a reported method by ring opening of 1,3-propane sultone with concentrated ammonium hydroxide in acetone

3. Non-covalent Immobilization of a Triphenylphosphine Ligand

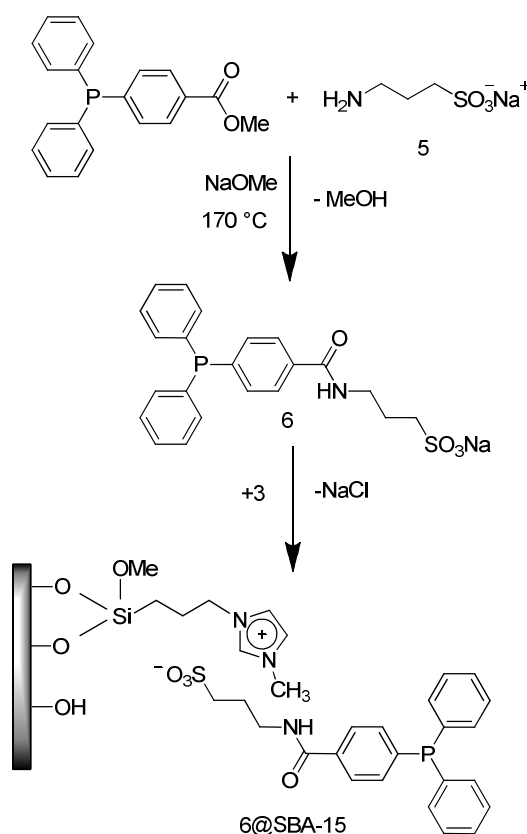
solution,^[143] followed by treatment with NaOH in water. Compound **5** should be coupled with 4-diphenylphosphinylbenzenecarboxylic acid methylester^[144] to give the sulphonate **6** following the procedure previously reported with 3-trimethoxysilylpropylamine as starting material (Scheme 3. 4).^[106, 140] However, because the starting materials as well as the product are solids with quite high melting points, this attempt failed. The reaction was further tested with dimethylformamide (DMF) and dimethyl sulfoxide (DMSO) as solvents at their boiling points, respectively. However, the desired product could not be obtained. In the end, it was found that a mixture of the catalyst NaOMe, of the phosphine ligand and of compound **5** must be carefully mixed with a mortar before starting the reaction and that one equivalent of the catalyst NaOMe is necessary to obtain quantitative conversion. A small part of NaOMe could not directly be removed after the reaction due to the similar solubility of **6** and NaOMe.



Scheme 3. 3 Synthesis of compound **5**.

Finally, compound **6** was added to a degassed suspension of compound **3** in CH₃OH and the mixture was stirred for 48 h at room temperature. The resulting hybrid material **6@SBA-15** was washed with water until pH = 7, extracted with CH₃OH in a Soxhlet apparatus to remove all adsorbed species (water, residual NaOMe, etc.) and dried under vacuum. The amount of grafted compound **6** was calculated according to the sulfur content of the material obtained by elemental analysis: 0.13 mmol g⁻¹ of **6** were finally immobilized, which is much lower than the loading of the imidazolium salt (1.16 mmol g⁻¹). One possible reason for this might be that partially compound **6** got no access to the cationic imidazolium ILs in the pores due to a steric effect of the bulky triphenylphosphine ligand. Another reason could be the competition between the SO₃⁻ group and Cl⁻ for ion exchange with the cationic imidazolium ILs. To obtain the final palladium catalyst, **6@SBA-15** was mixed with half an equivalent of PdCl₂(CNPh)₂ in

dry CH_2Cl_2 and stirred for 2 h at room temperature. After filtration, the CH_2Cl_2 solution was colorless, thus the palladium loading on the hybrid material **Pd@SBA-15** was estimated based on the amount of palladium added.



Scheme 3. 4 Synthesis of the hybrid material **6@SBA-15**.

The synthesis of palladium complex with compound **6** as ligand was also carried out. CH_3OH was chosen as the solvent to dissolve compound **6** and the procedure is quite similar to our previous work,^[106, 140] $\text{PdCl}_2(\text{CNPh})_2$ was dissolved in dry CH_2Cl_2 and slowly added to the CH_3OH solution of compound **6**. However, the solution changed to black color, which is probably caused by the formation of palladium nanoparticles due to the traces of NaOMe.

3.2.2 Characterization

Organic compounds

Compound **2** was characterized by NMR spectroscopy. The most notable feature in the ^1H NMR spectrum of **2** is the characteristic resonance of the hydrogen atom in the 2-position of the 5-membered ring (Figure 3. 2), which is found at 10.4 ppm as a singlet. Triplets ($J_{\text{H,H}} = 1.6$ Hz) are observed for H-4 and H-5.^[145] A resonance at 4.0 ppm is attributed to the *N*-methyl group of the 5-membered ring. Three sets of signals at higher field in the ^1H NMR spectrum (4.2, 1.9, 0.5 ppm) are typical for the silicon functionalized propylene chain and a sharp singlet (3.4 ppm) for the $-\text{Si}(\text{OMe})_3$ group.

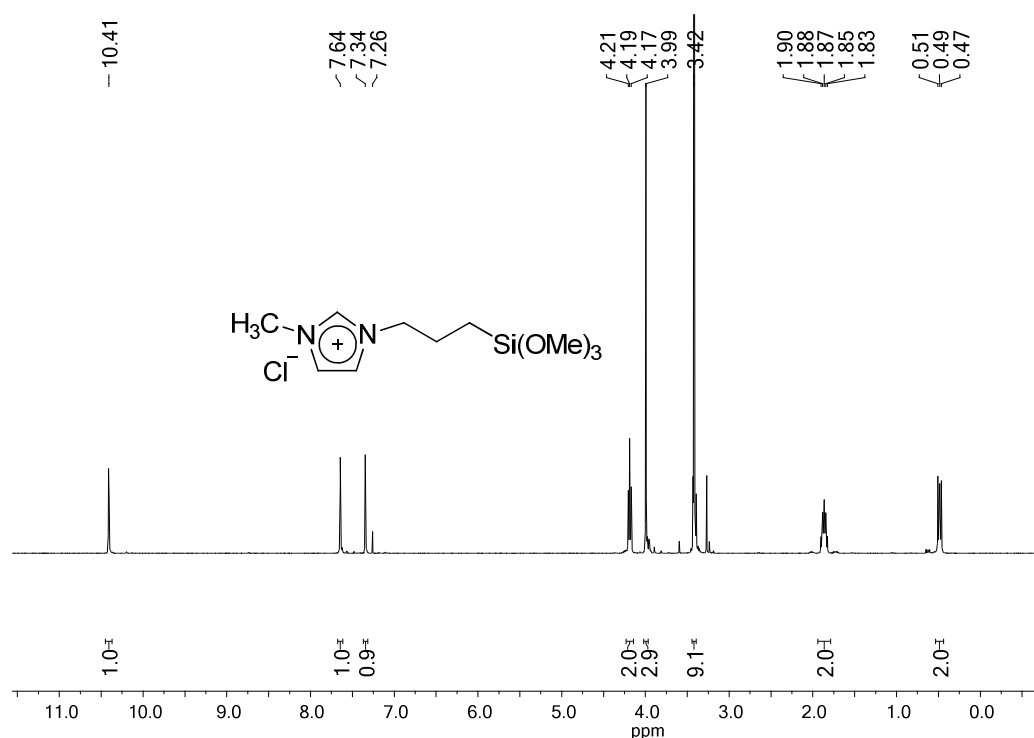


Figure 3. 2 ^1H NMR spectrum of compound **2** (400.13 MHz, 25 °C, CDCl_3).

In the ^{13}C $\{^1\text{H}\}$ NMR spectrum of compound **2**, 137.7, 123.7 and 121.8 ppm are the values for the resonances of the three imidazolium ring carbon atoms (Figure 3. 3). Three resonances at 51.6, 24.0, 5.8 ppm can be correlated with the resonances of the propylene linker. The resonance at 50.6 ppm can be assigned to $-\text{Si}(\text{OCH}_3)_3$ group and a signal at 36.4 ppm can be assigned to the *N*-methyl group of the 5-membered ring.

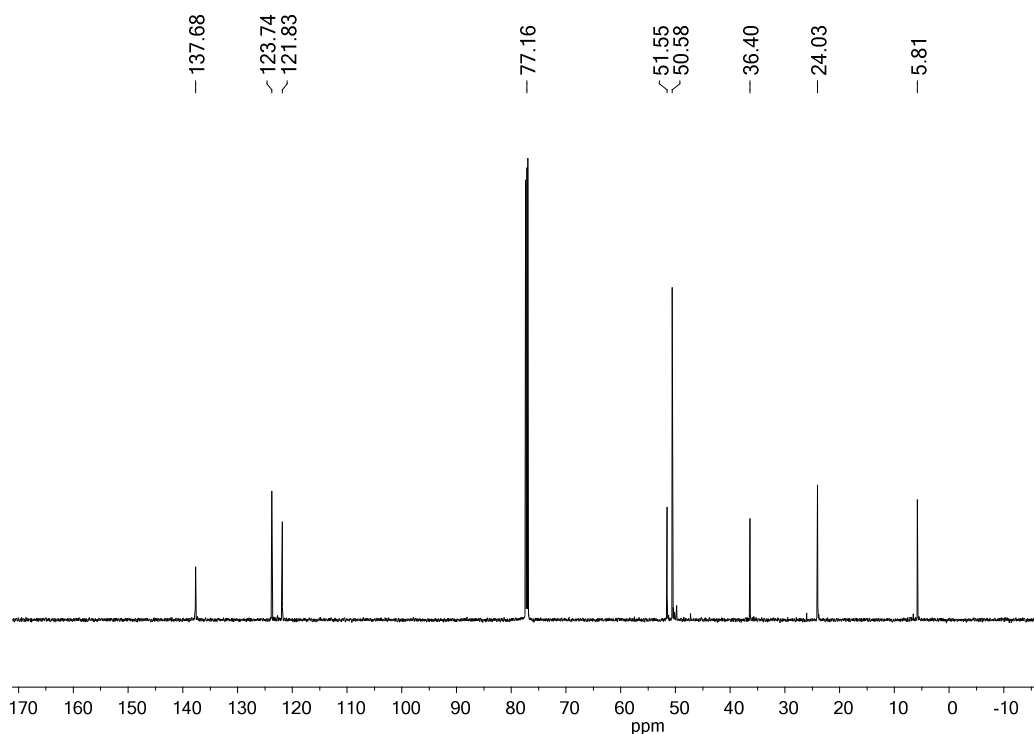


Figure 3. 3 ^{13}C NMR spectrum of compound **2** (100.62 MHz, 25 °C, CDCl_3).

The infrared spectrum (KBr) of the compound **2** is presented in Figure 3. 4 . The unsaturated C-H stretching vibrations of the imidazolium cation appear at 3146 and 3079 cm^{-1} , while the peak at 2947 cm^{-1} can be assigned to aliphatic C-H stretching vibrations. The bands at 1632 and 1576 cm^{-1} are the in-plane C-N and C-C stretching vibrations of the imidazolium ring and the bands at 1460 and 620 cm^{-1} are C-H bending vibrations of imidazolium ring. The bands at 2842, 1088, 821, 776 cm^{-1} could be attributed to the -Si(OMe) group.^[146]

The ^1H NMR spectrum of compound **4** at high field shows two triplets ($J_{\text{H,H}} = 0.8$ Hz) and one quintet, which correspond to the propylene chain H-1 (3.1 ppm), H-2 (2.1 ppm) and H-3 (3.0 ppm), respectively (Figure 3. 5). The carbon resonance at 69.9 ppm which is attributed to the carbon adjacent to the sulfur atom of the sultone is not observed in the ^{13}C NMR spectrum of compound **4** (Figure 3. 6),^[147] indicating complete ring-opening by aqueous $\text{NH}_3 \cdot \text{H}_2\text{O}$. Three resonances at 48.1, 22.6, 38.5 ppm can be assigned to the alkyl carbon atoms C-1, C-2 and C-3 respectively.

The infrared spectrum (KBr) of compound **4** is shown in Figure 3. 7. A broad structured band at 3431 cm^{-1} can be assigned to the O-H and N-H stretching vibrations. A band at 2940 cm^{-1} can be assigned to the CH stretching vibration. The partial protonation of the amine group caused that the N-H stretching band appears at wavenumbers lower than 3200 cm^{-1} . The bending vibrations of N-H at 1627 and 1495 cm^{-1} further prove the generation of a -NH_3^+ group which is expected in the range from 1600 to 1460 cm^{-1} .^[148]

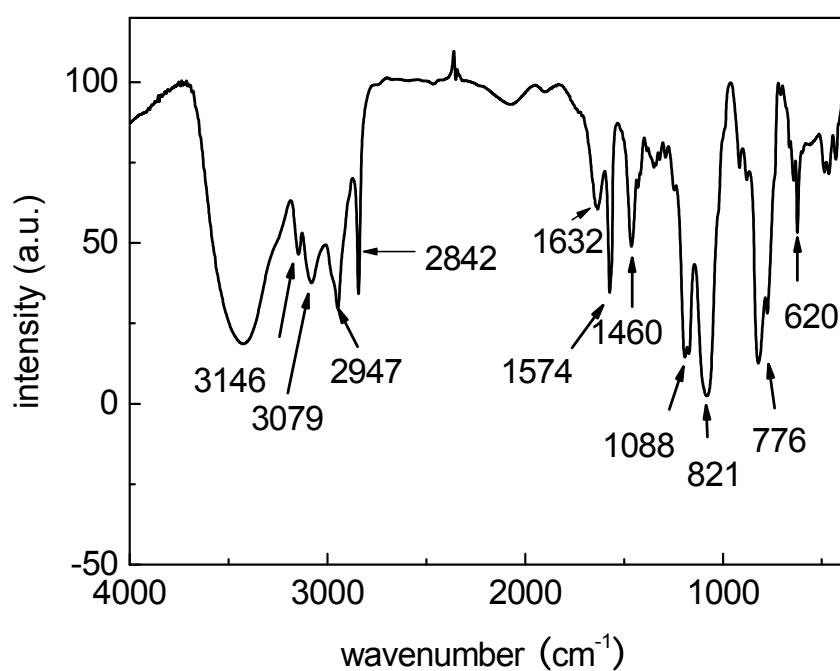


Figure 3. 4 Infrared spectrum of compound **2**.

3. Non-covalent Immobilization of a Triphenylphosphine Ligand

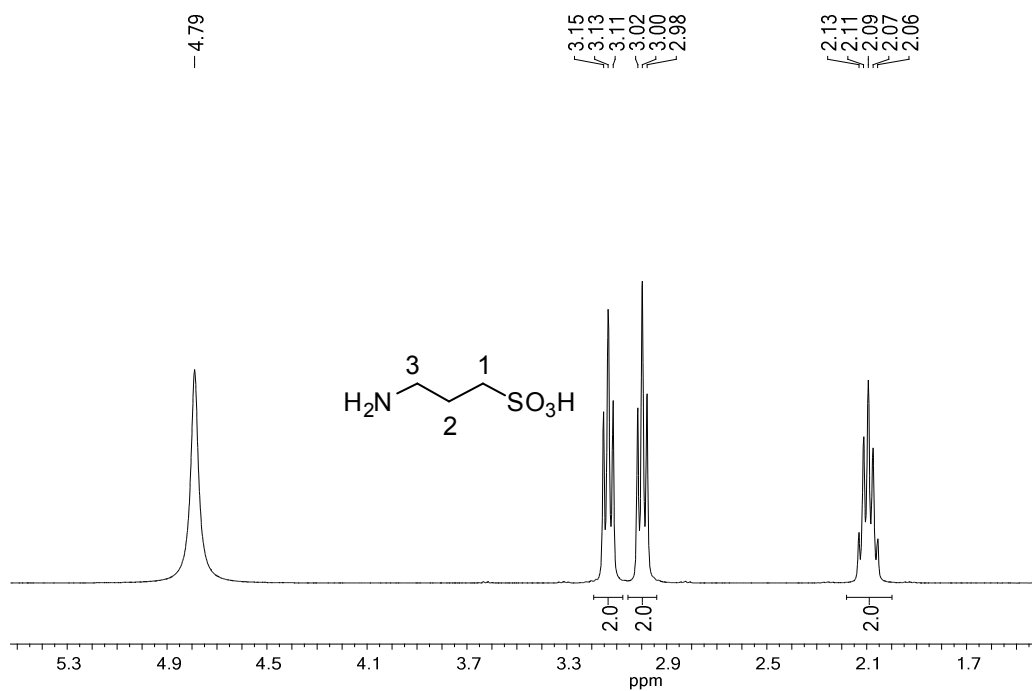


Figure 3. 5 ¹H NMR spectrum of compound **4** (400.13 MHz, 25 °C, D₂O, δ: 4.8 ppm).

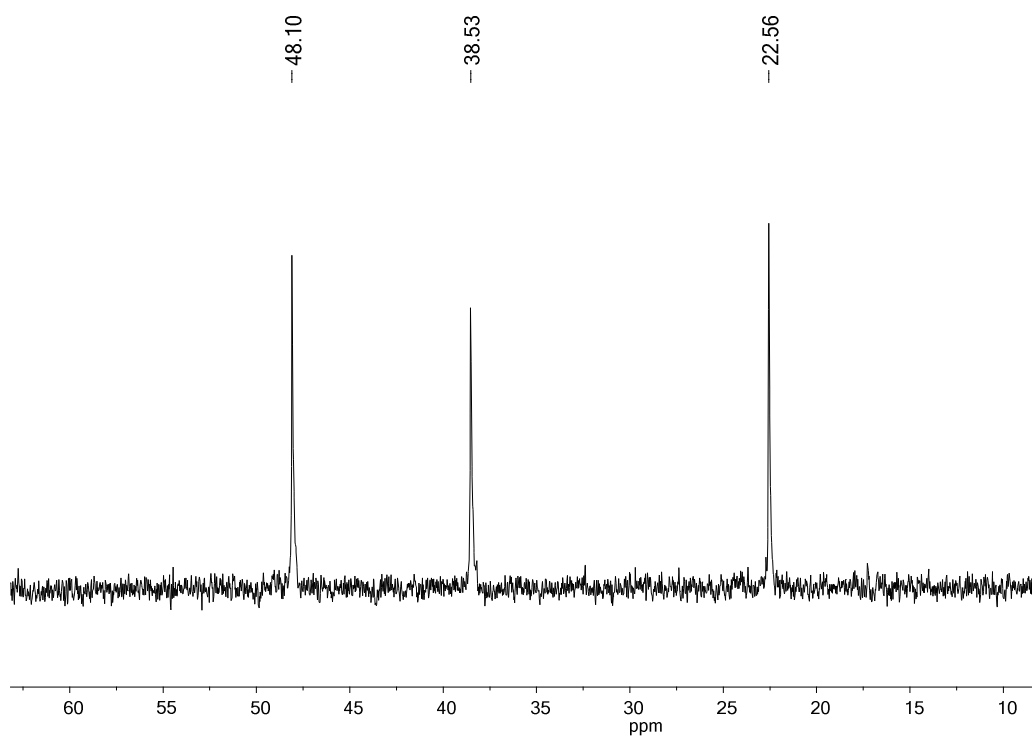


Figure 3. 6 ¹³C NMR spectrum of compound **4** (100.62 MHz, 25 °C, D₂O).

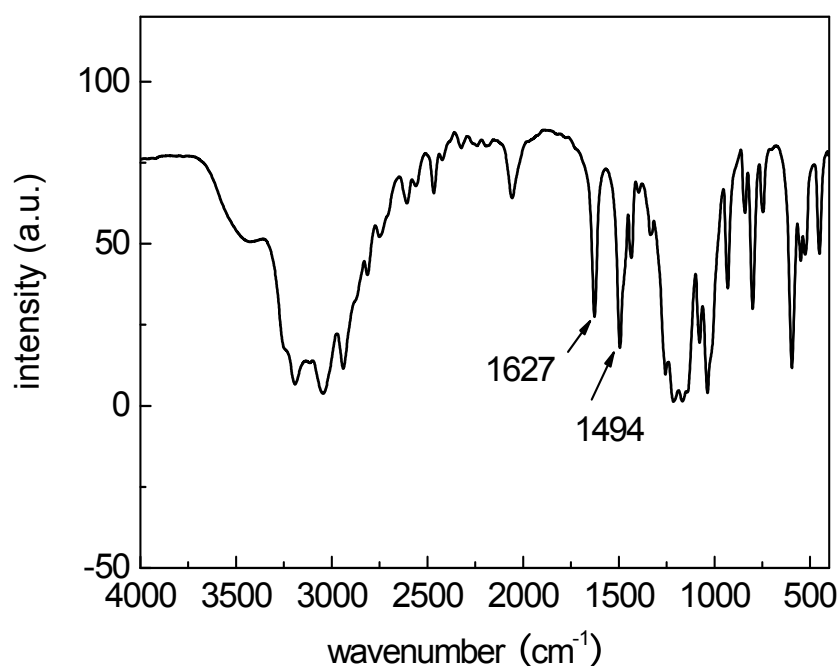


Figure 3. 7 Infrared spectrum of compound **4**.

The chemical shifts in the ^1H NMR and ^{13}C NMR spectra of compound **5** (Figure 3. 8, Figure 3. 9) are similar to the spectra of compound **4** (Figure 3. 5, Figure 3. 6). The protonation of the amine causes a shielding of the carbon atoms in the vicinity of the nitrogen, which leads to 2 ppm highfield shift for the α carbon atom.^[148] Comparing the ^{13}C NMR spectra of compound **5** and **4**, the chemical shift of the carbon atom next to the amine shifts from 40.0 ppm (Figure 3. 9) to 38.5 ppm (Figure 3. 6), which further proves that the amine group of compound **4** is protonated and is consistent with the infrared spectrum of compound **4** (Figure 3. 7).

Compared to the infrared spectrum of compound **4**, the typical aminonium bands in the region 3000-2700 cm^{-1} have now disappeared (Figure 3. 10). The infrared spectrum shows the bending vibration of the $-\text{NH}_2$ group at 1592 cm^{-1} and a strong band at 1193 cm^{-1} , which can be assigned to the $-\text{SO}_3^-$ group.

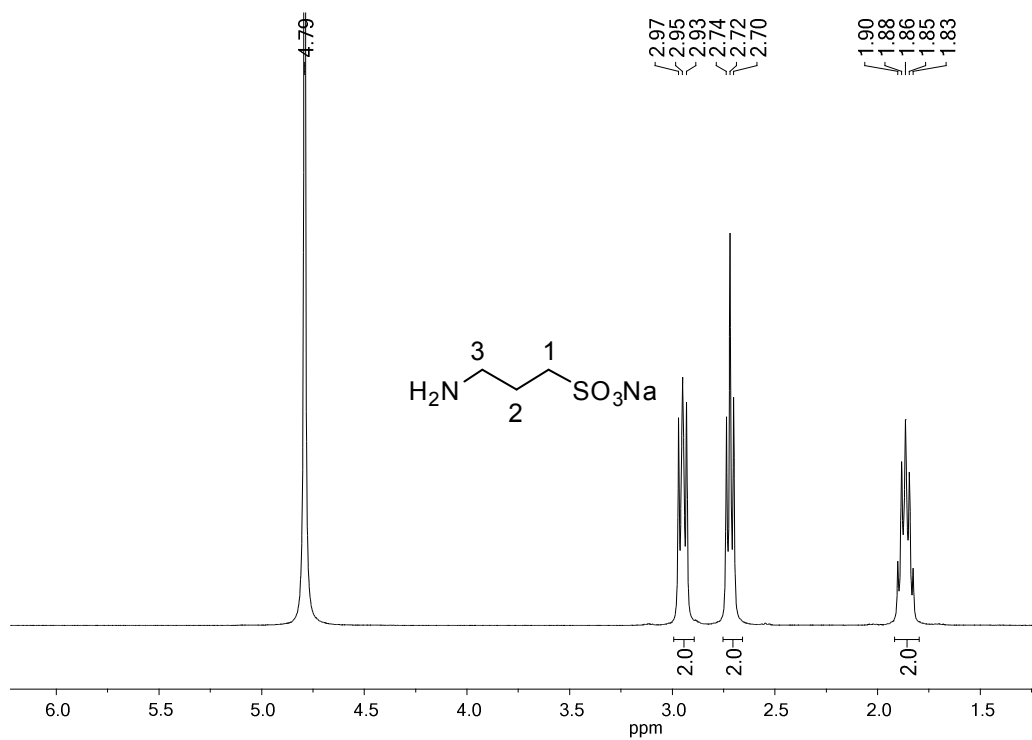


Figure 3. 8 ^1H NMR spectrum of compound 5 (400.13 MHz, 25 °C, D_2O).

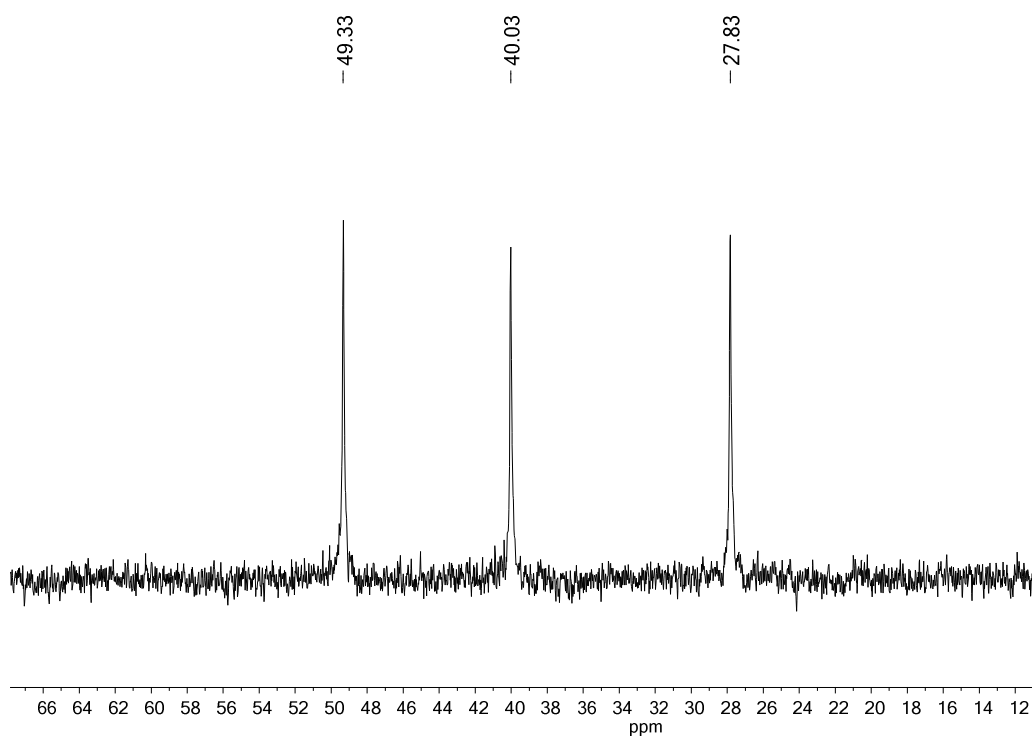


Figure 3. 9 ^{13}C NMR spectrum of compound 5 (100.62 MHz, 25 °C, D_2O).

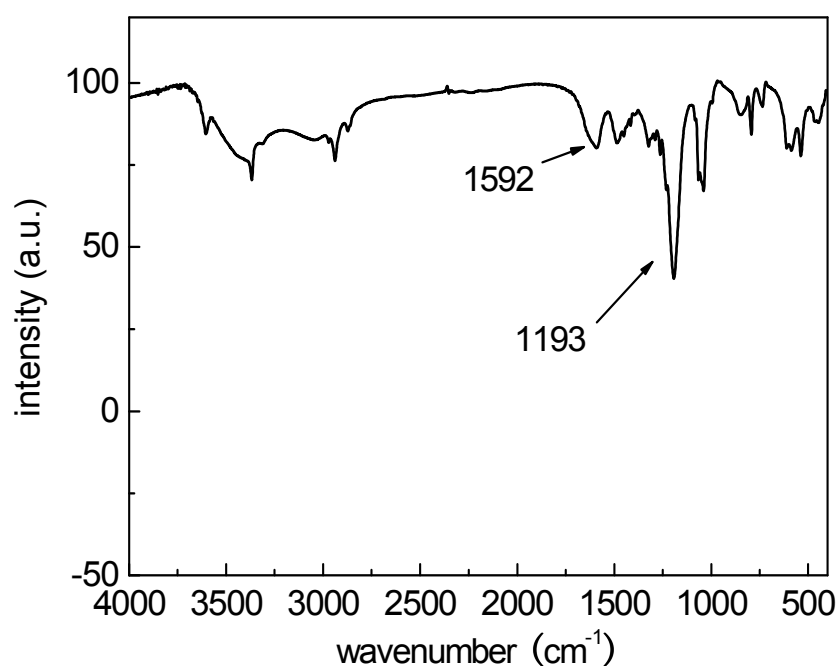


Figure 3. 10 Infrared spectrum of compound **5**.

The ^1H NMR spectrum of compound **6** shows three sets of resonances at high field: 2.9, 2.7 and 1.9 ppm (Figure 3. 11), which correspond to the signals of the propylene chain of the compound **5** in Figure 3. 8. The aromatic resonances are constituted in two multiplets 7.2-7.4 (integrating for 12 protons) and 7.8-8.0 ppm (integrating for 2 protons). In our previous work, a broad singlet at 6.5 ppm (amide group) could be observed in the ^1H NMR spectrum of $(\text{L})_2\text{PdCl}_2$ ($\text{L} = \text{Si}(\text{OMe})_3$ functionalized PPh_3) (Figure 2. 19, in Chapter 2). It cannot be detected for compound **6**, which is due to an immediate exchange of the NH protons with D^+ from CD_3OD .

The ^{13}C $\{^1\text{H}\}$ NMR spectrum of the functionalized triphenylphosphine ligand **6** is presented in Figure 3. 12. Three resonances at high field (29-50 ppm) are assigned to the carbon atoms of the propylene chain, which is in agreement with the data of compound **5**, while the peak in the low field region at 175.0 ppm can be assigned to the carbonyl group, proving the successful aminolysis.

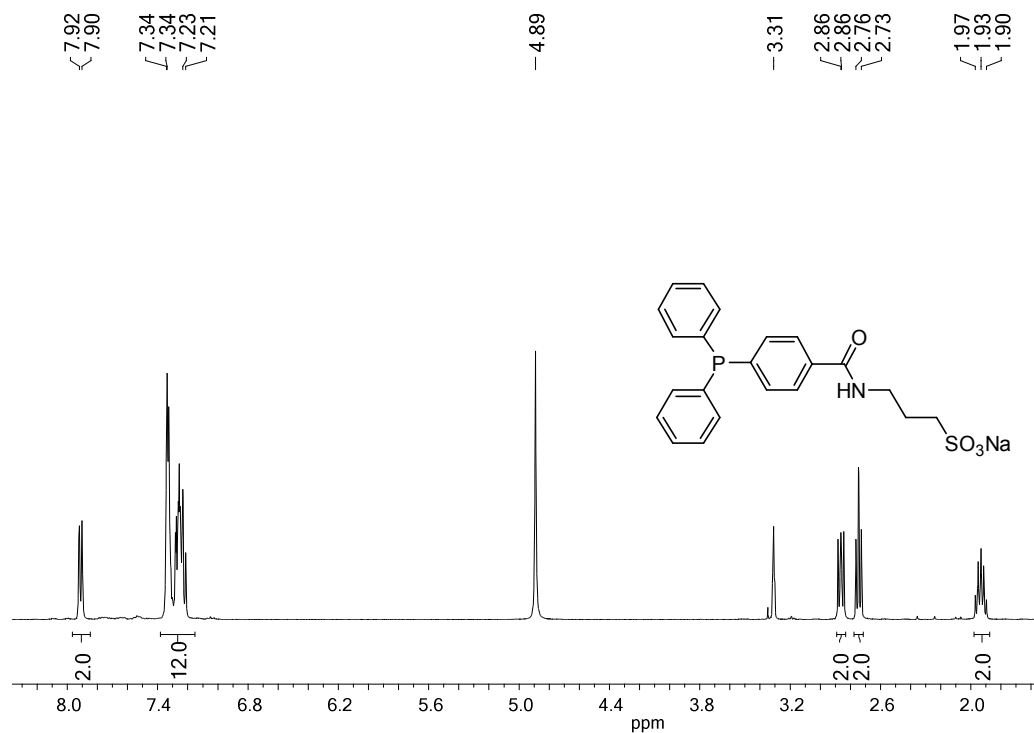


Figure 3. 11 ¹H NMR spectrum of **6** (400.13 MHz, 25 °C, CD₃OD).

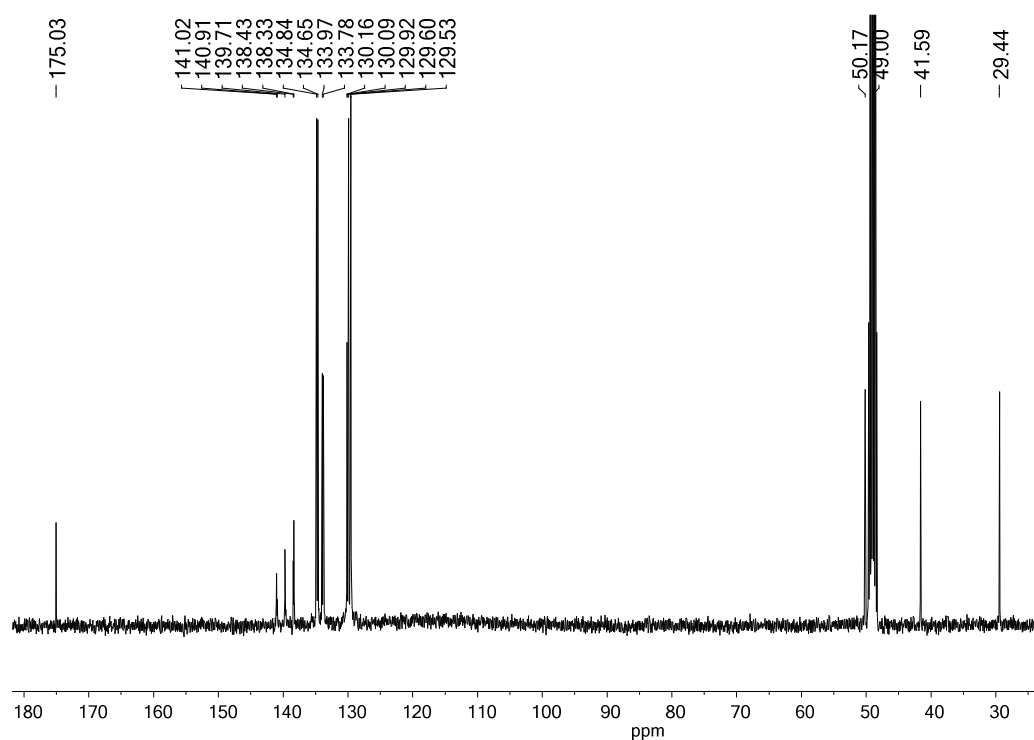


Figure 3. 12 ¹³C NMR spectrum of **6** (100.62 MHz, 25 °C, CD₃OD).

The aryl groups of the functionalized triphenylphosphine ligand **6** give resonances in the range from 142 to 128 ppm. Except C-p and C-d atoms, the resonances of the

3. Non-covalent Immobilization of a Triphenylphosphine Ligand

phenyl groups bound to phosphorus are observed as doublets due to the coupling to ^{31}P as shown in Figure 3. 13.

The ^{31}P { ^1H } NMR resonance of compound **6** is slightly shifted to higher field compared to its precursor 4-diphenylphosphinylbenzenecarboxylicacid methylester (δ : -3.8 ppm) and exhibits only one signal at -4.43 ppm (Figure 3. 14). There is no ^{31}P NMR signal of either unreacted phosphine ligand which is expected at about +2 to -5 ppm or oxidized phosphine species, which indicates the successful synthesis of compound **6**. The expected chemical shift for the latter species is expected at about +23 to +29 ppm.

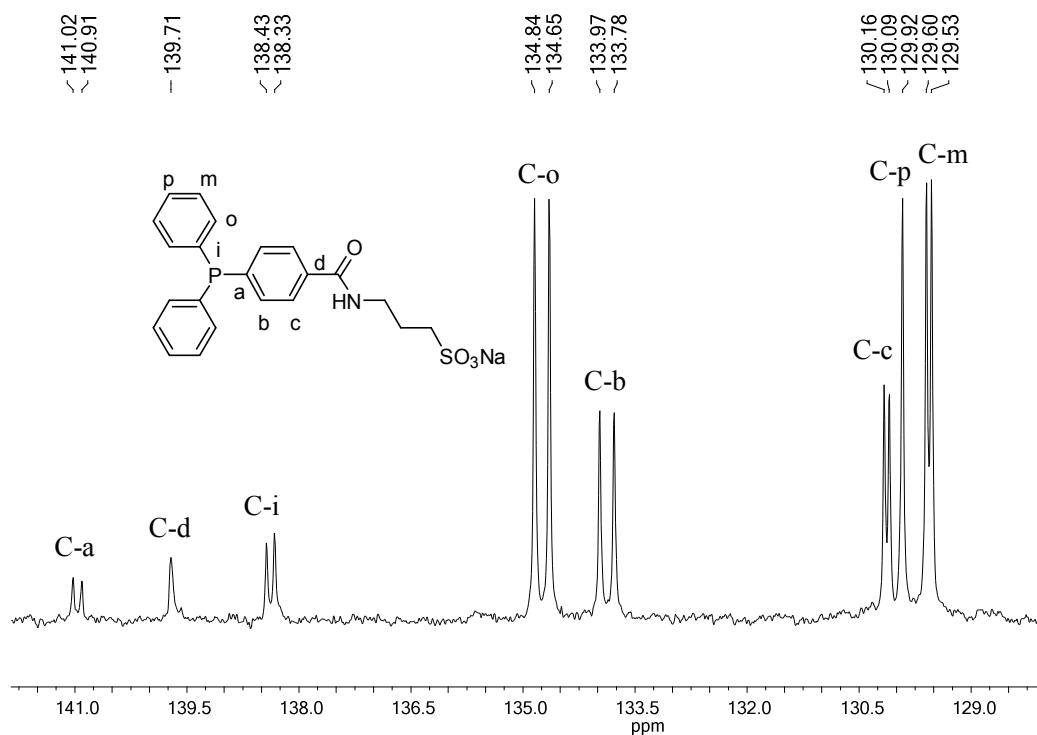


Figure 3. 13 ^{13}C NMR spectrum of **6** (^{13}C and ^{31}P coupling of phenyl groups).

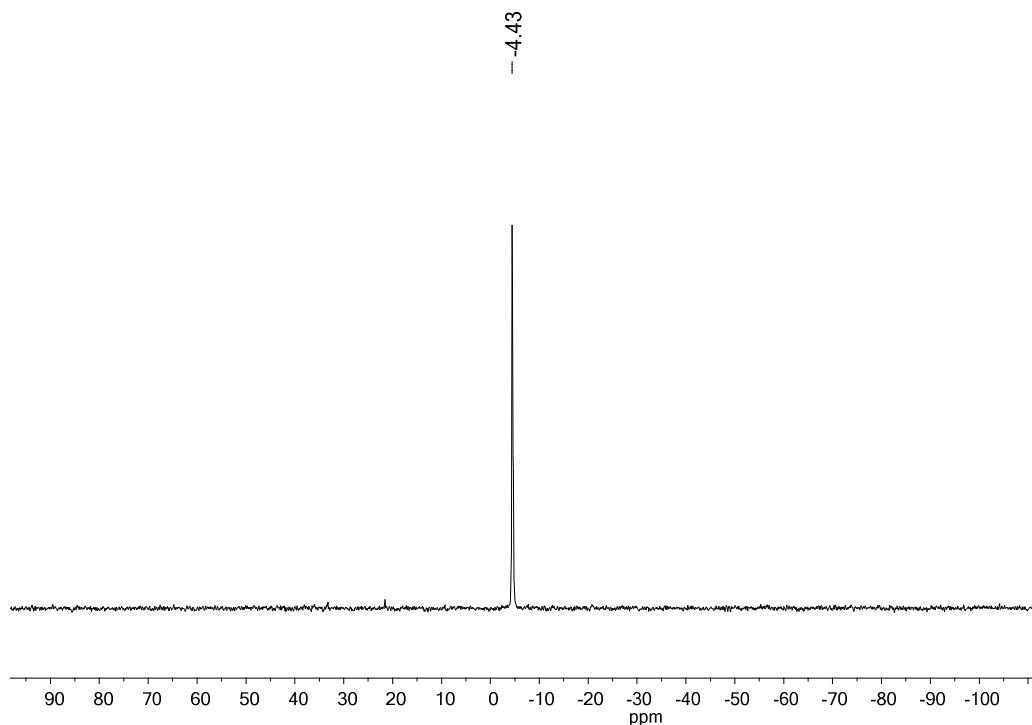


Figure 3. 14 ^{31}P NMR spectrum of **6** (161.98 MHz, 25 °C, CD_3OD).

Material part

Solid state NMR spectroscopy

The resonances in the ^{13}C CP-MAS NMR spectrum of hybrid material **3** (Figure 3. 15) match well with the high resolution spectrum of compound **2** in solution (Figure 3. 2). This indicates that the imidazolium salt **2** is not damaged during the immobilization and extraction process. The resonances in the high field region 51.2, 24.1 and 8.5 ppm can be mainly attributed to the carbon atoms of the propylene chain and a signal at 36.7 ppm is assigned to *N*-methyl group of the 5-membered ring. The resonances at 137.3 and 123.6 are assigned to the carbon atoms of the imidazolium ring. The additional resonances at 17.2 and 60.2 ppm are probably attributed to the residual P123 template in the material.^[109]

Figure 3. 16 shows the ^{29}Si CP-MAS NMR spectrum of hybrid material **3**, which further confirms that compound **2** was successfully grafted on the surface of SBA-15. Three signals in the T region are indicating the presence of organosilica T^3 species

[C-Si(OSi)₃] (-65 ppm) and T² species [C-Si(OSi)₂(OH)] (-57 ppm) and T¹ species [C-Si(OSi)(OH)₂] (-49 ppm). Due to the stronger intensity of the T¹ and T² peaks, the hydrolysis/condensation of compound **2** mainly achieves [C-Si(OSi)(OH)₂] and [C-Si(OSi)₂(OH)] linkages. For the characteristics of the inorganic silica framework, the signals at -110, -101, and -92 ppm correspond to the Si(OSi)₄ (Q⁴), HOSi(OSi)₃ (Q³), and (HO)₂Si(OSi)₂ (Q²), respectively.^[149]

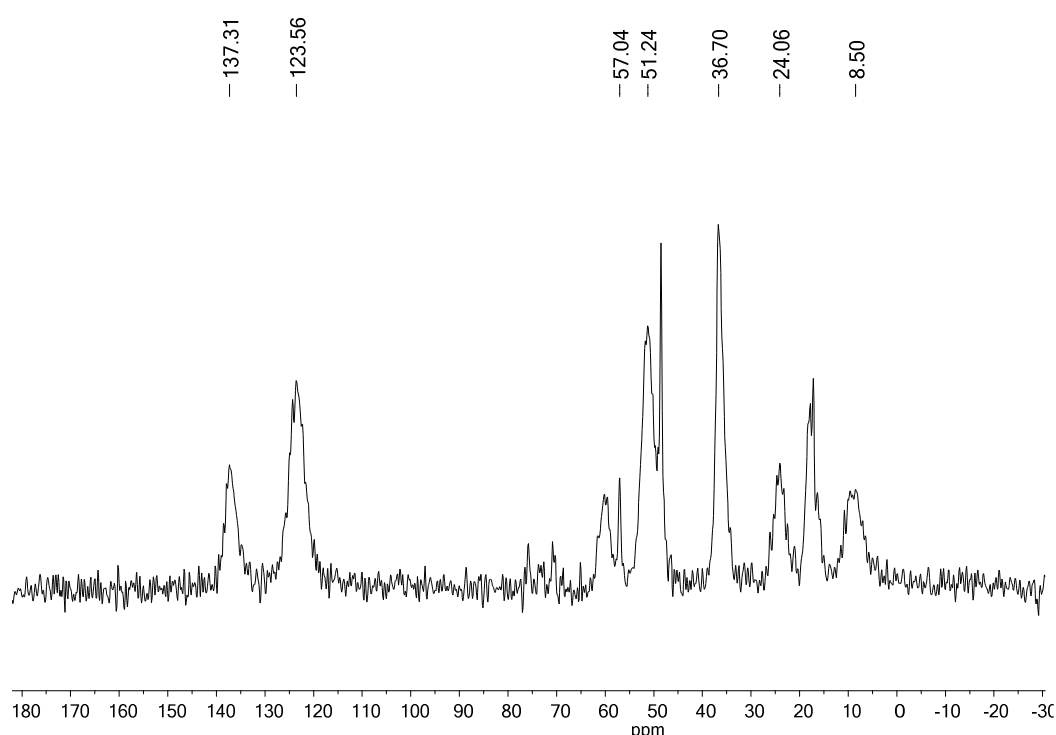


Figure 3. 15 ¹³C CP-MAS NMR spectrum of imidazolium salt functionalized SBA-15 **3**.

The ³¹P CP-MAS NMR resonance (2.6 ppm) of **6@SBA-15** is slightly shifted towards lower field compared to the solution NMR data of **6** (-4.4 ppm) (Figure 3. 17). This might be explained by some additional weak interactions between the phosphorus center and surface bound silanol sites (Si-OH...P).^[91] For sure, there is no signal of a phosphine oxide and other undesired phosphorus containing by-products. Those are often unavoidable in the covalent immobilization process due to the traces of air and the required high reaction temperature.^[105] The hybrid material **6@SBA-15** further was reacted with PdCl₂(CNPh)₂, which mainly changed the ³¹P CP-MAS NMR data. The ¹³C and the ²⁹Si CP-MAS NMR spectra of **6@SBA-15** will not be discussed.

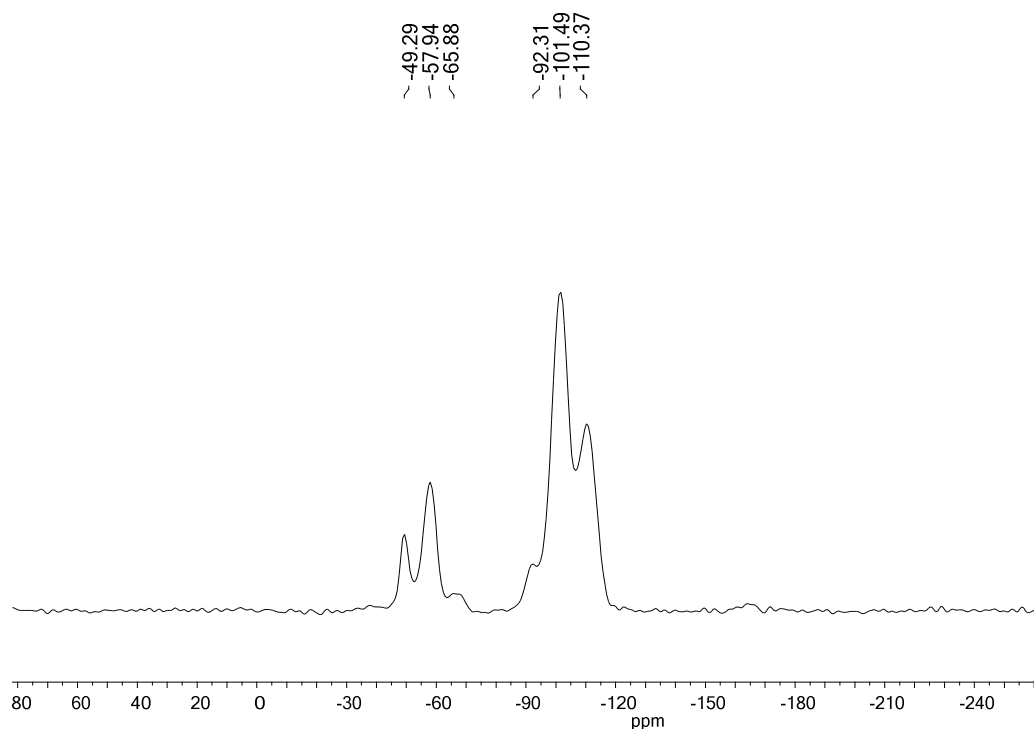


Figure 3. ^{29}Si CP-MAS NMR spectrum of imidazolium salt functionalized SBA-15 **3**.

The ^{13}C CP-MAS NMR spectrum of **Pd@SBA-15** (Figure 3. 18) shows signals for the aryl groups in the range from 148.4 to 115.7 ppm, overlapping with the resonances of the three imidazolium ring carbon atoms (137.7, 123.7, 121.8 ppm). A signal at 36.6 corresponds to the *N*-methyl group of the 5-membered ring. Three resonances at 51.6, 24.0, 9.6 ppm are assigned to the propylene linker (**3**: 51.6, 24.0, 5.8 ppm) of the imidazolium cation. The resonances of the propylene linker of the sulphonate moiety overlap with these signals but one additional resonance at 171.0 ppm can clearly be assigned to the C=O group of the sulphonated amide linker, which further proves the successful grafting of the triphenylphosphine donor. It is found at an almost similar chemical shift as for **6** (175.0 ppm), indicating that the interaction between the amide group of the linker and the silica framework is only weak.^[91] The resonance at 51.6 ppm may also include intensity derived from some unhydrolyzed C-SiOCH₃ groups.^[90] However, the absence of a signal at around 160 ppm indicates that there is no formation of a *N*-heterocyclic carbene palladium(II) complex.^[40]

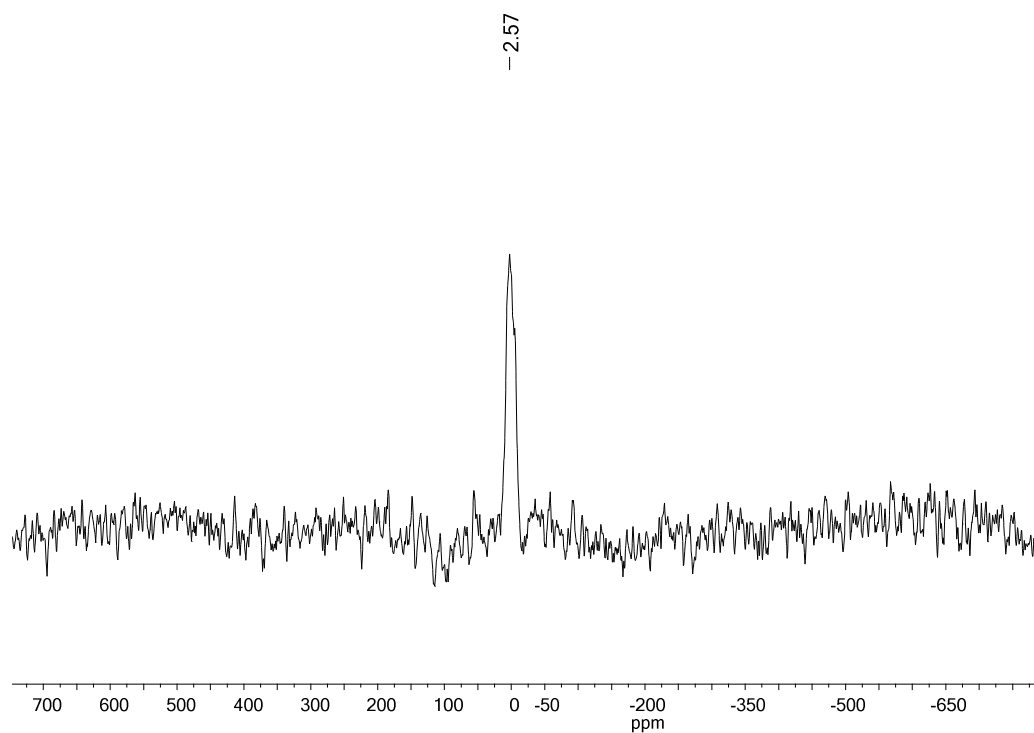


Figure 3.17 ^{31}P CP-MAS NMR spectrum of **6@SBA-15**.

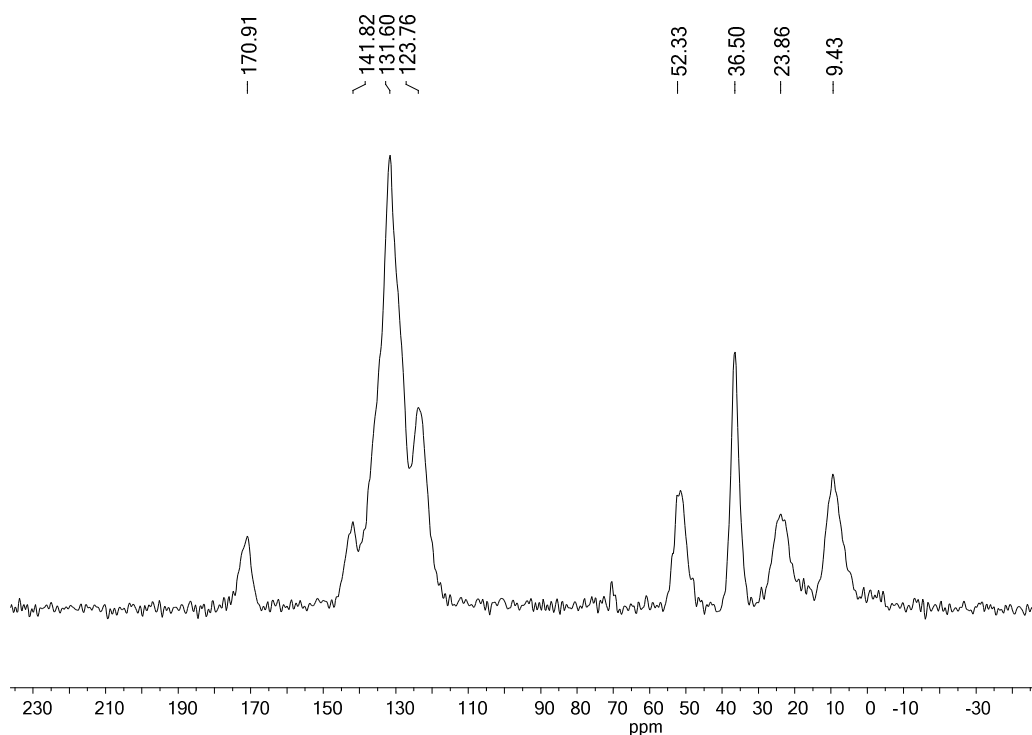


Figure 3.18 ^{13}C CP-MAS NMR spectrum of **Pd@SBA-15**.

The ^{29}Si CP-MAS NMR spectrum of **Pd@SBA-15** shows clearly organosilica signals in the T region, which proves that the covalent bonds between the imidazolium salt and

the support are very stable and retained after the non-covalent immobilization of compound **6** (Figure 3. 19).

As shown in Figure 3. 20, there is no signal for free triphenylphosphine in the solid state ^{31}P CP-MAS NMR spectrum of **Pd@SBA-15**, which is expected at about +2 to -5 ppm. Due to its chemical shift, the signal at 28.6 ppm might either be attributed to triphenylphosphine ligands coordinating to palladium(II) or it might be assigned to the corresponding phosphine oxide. However, triarylphosphines are only slowly oxidized in the air and the synthesis of **Pd@SBA-15** was carried out under an atmosphere of dinitrogen. The formation of palladium(II) triphenylphosphine complexes is therefore strongly supported by the ^{31}P CP-MAS NMR data. In one of our previous publications, a palladium triphenylphosphine complex was covalently grafted on silica gel^[106] and the ^{31}P C-P MAS NMR resonance of the hybrid materials (23.6 ppm) corresponded excellently with the chemical shift of the palladium complex in solution (24.4 ppm). In the present work, the slight downfield shift of the ^{31}P C-P MAS NMR resonance of **Pd@SBA-15** compared to the data of the analogous complex in solution is quite likely caused by the presence of both *cis*- and *trans*-configured complexes of the type $(\text{L})_2\text{PdCl}_2$ on the surface of SBA-15, since ^{31}P resonance of the *cis*-isomer always appears downfield to the *trans*-isomer.^[150-152] This feature was also observed by Chernyshov et al. with palladium(II) complexes bound to a polystyrene-block-poly-m-vinyltriphenylphosphine resin, the presence of the *cis*-isomer was explained by steric restrictions.^[153] Very recently, Mutin also presented this feature with immobilization of palladium complex on bifunctional phosphine-phosphonate ester modified metal oxide system.^[154] Due to the inhomogeneous environment of the palladium site in **Pd@SBA-15**, only one broad and downfield shifted resonance is observed in Figure 3. 20. Terasawa et al. reported the formation of palladiumdichloro complexes with just one phosphine ligand by using a phosphinated polystyrene.^[155] This can be excluded for **Pd@SBA-15** since we do not observe uncoordinated triphenylphosphine moieties.

The neat SBA-15, **6@SBA-15** and **Pd@SBA-15** were structurally investigated by x-ray powder diffraction and nitrogen adsorption/ desorption measurements. The XRD patterns of all the samples shown in Figure 3. 21 exhibit three clear peaks in the low-angle region: one intense signal corresponding to the d_{100} diffraction peak accompanied by two weaker peaks (d_{110} , d_{200}), suggesting that the two-dimensional hexagonal pore structure is preserved after the introduction of the organic species. Surface areas, pore volumes and pore size distribution of **Pd@SBA-15** were determined by N_2 adsorption/desorption measurement. The sample displayed typical type IV isotherms for a mesoporous material^[88], the presence of hysteresis in the N_2 isotherm indicates that its porosity is maintained after modification of the support. The materials possess a narrow pore size distribution as shown in Figure 3. 22 (inset). The measured data for the BET surface area, the total pore volume and the BJH pore size of **Pd@SBA-15** are $548 \text{ m}^2\cdot\text{g}^{-1}$, $0.88 \text{ cm}^3\cdot\text{g}^{-1}$ and 7.0 nm respectively.

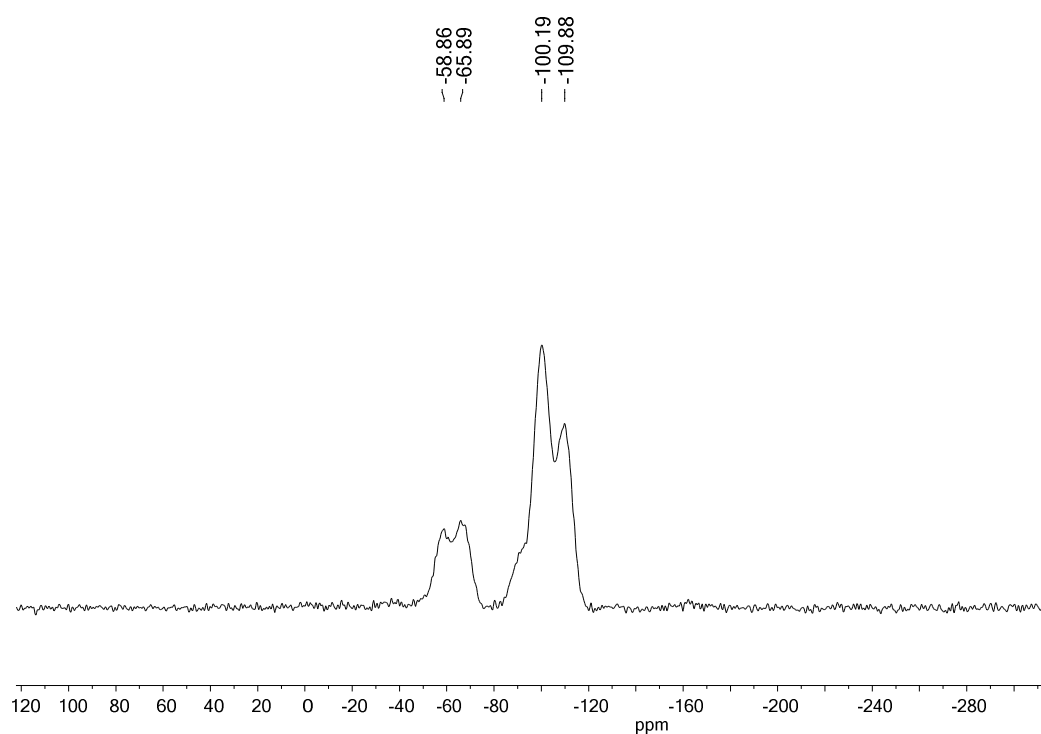


Figure 3. ^{29}Si CP-MAS NMR spectrum of **Pd@SBA-15**.

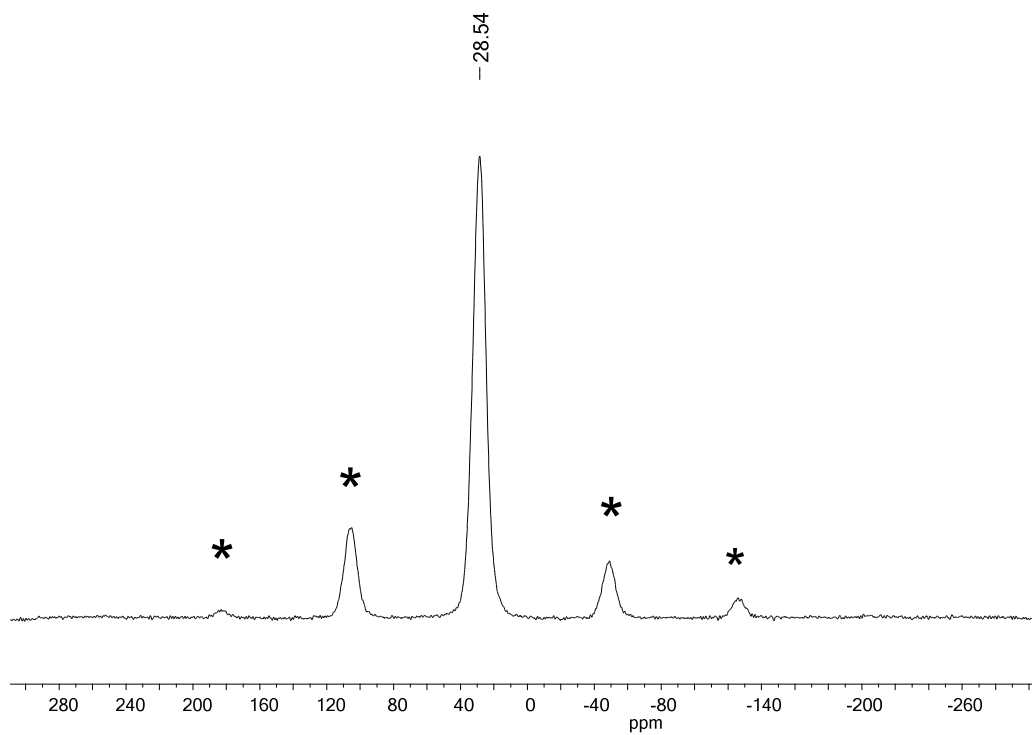


Figure 3. 20 ^{31}P CP-MAS NMR spectrum **Pd@SBA-15**.

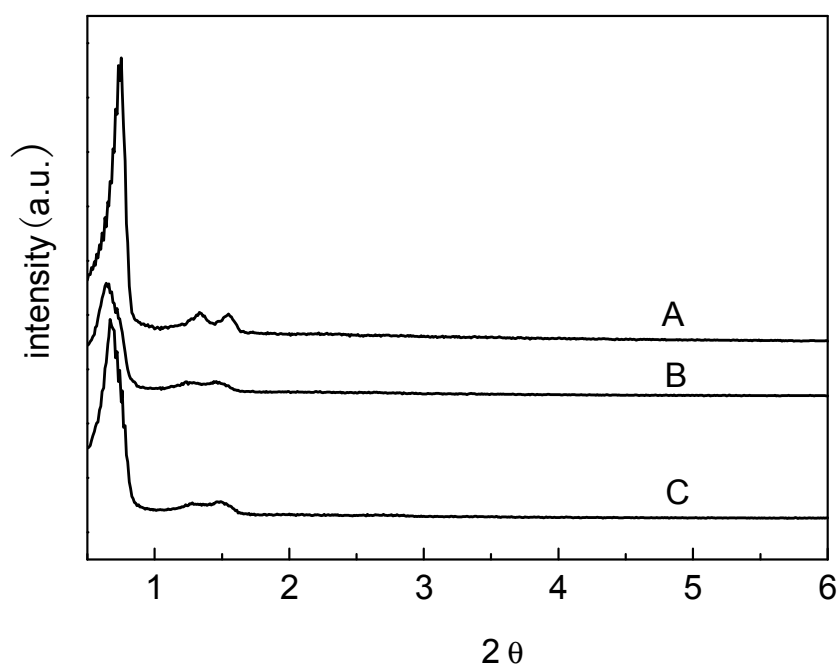


Figure 3. 21 XRD pattern of A, SBA-15, B, **6@SBA-15** and C, **Pd@SBA-15**.

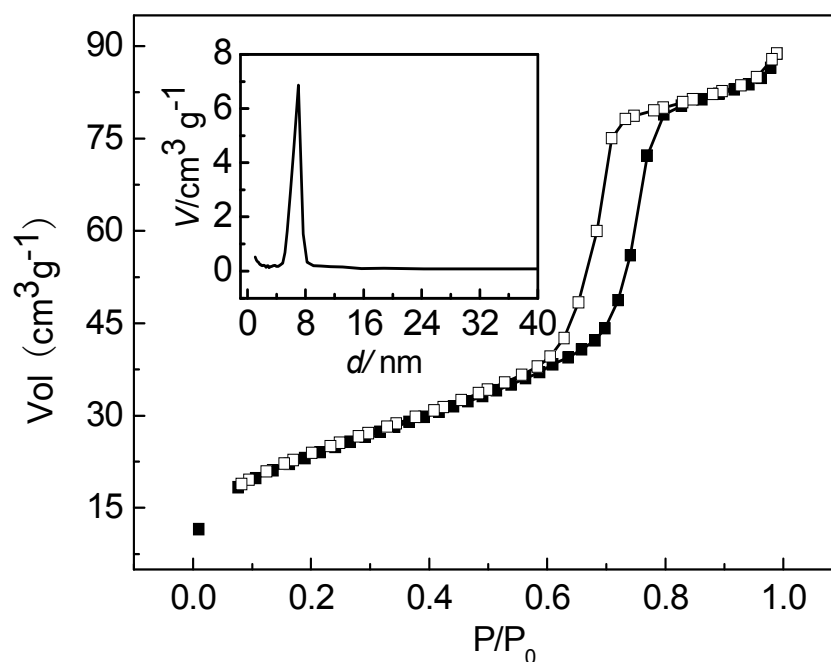


Figure 3. 22 N₂ sorption isotherms and BJH pore size distribution (inset) of **Pd@SBA-15**.

A SEM image taken from the freshly prepared catalyst **Pd@SBA-15** shows the typical morphology of SBA-15 particles being joined to form non-regular aggregates (Figure 3. 23). The TEM images (Figure 3. 24) taken from the same sample clearly proves the preservation of the hexagonally arranged channels and there are no palladium nanoparticles formed during the synthesis.

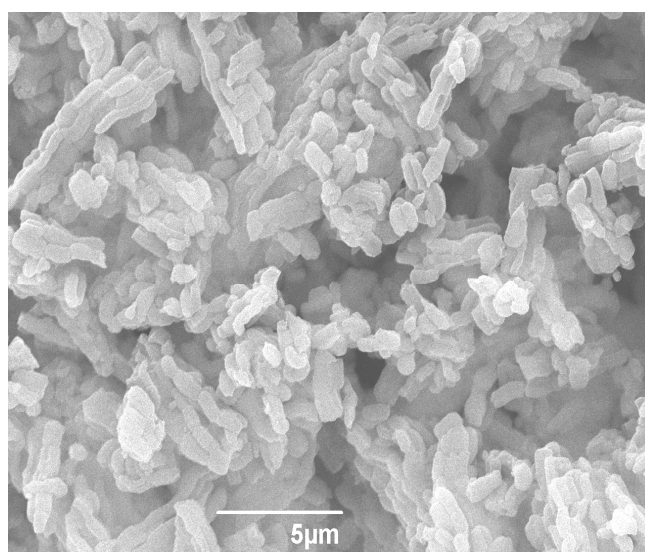
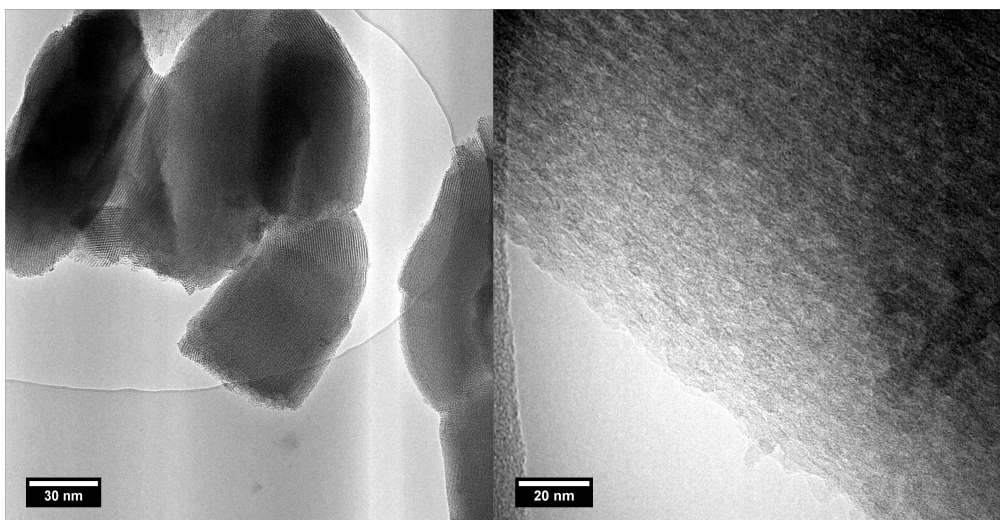
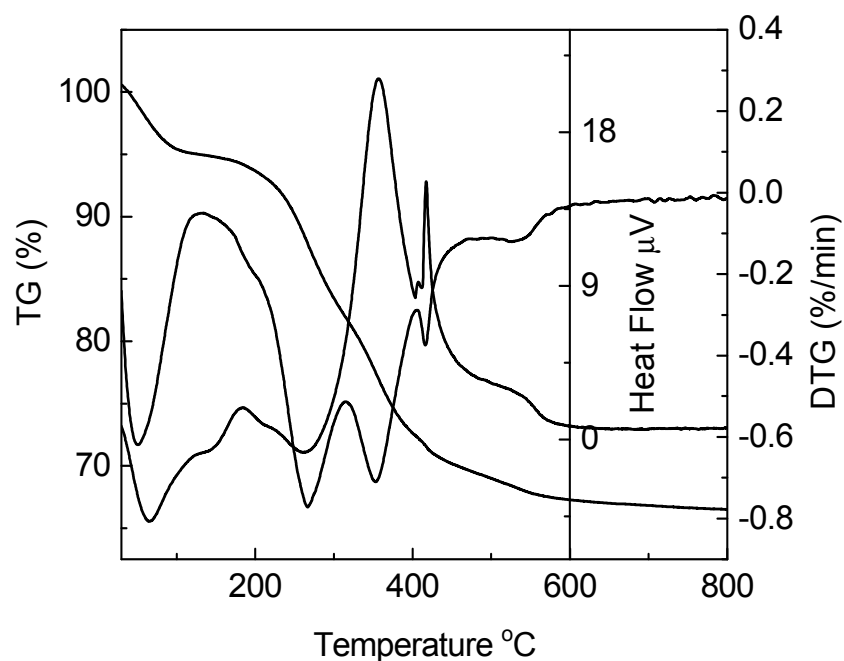


Figure 3. 23 SEM image of **Pd@SBA-15**.

Figure 3. 24 TEM images of **Pd@SBA-15**.

In order to compare the thermal stability of the materials synthesized in different steps (**3** and **6@SBA-15** and **Pd@SBA-15**), thermogravimetric and differential thermogravimetric (TG-DTG) analysis experiments were carried out (Figure 3. 25, Figure 3. 26, Figure 3. 27).

Figure 3. 25 Thermogravimetric and differential thermogravimetric analyses of **3**.

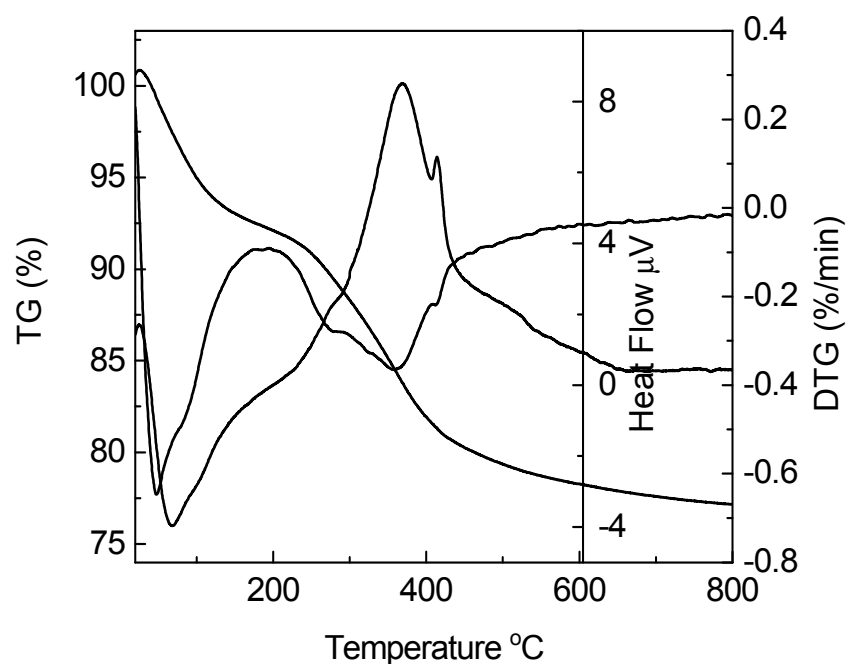


Figure 3. 26 Thermogravimetric and differential thermogravimetric analyses of **6@SBS-15**.

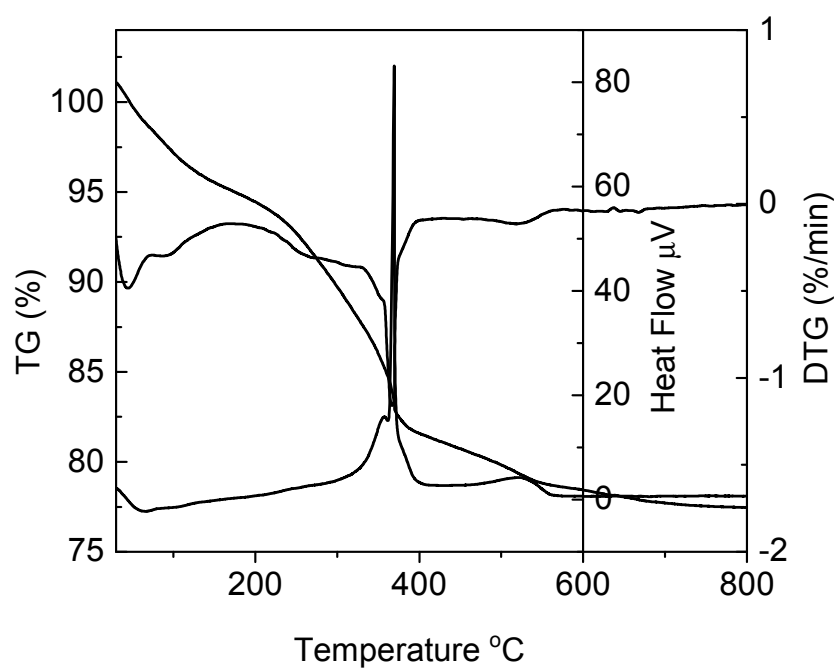


Figure 3. 27 Thermogravimetric and differential thermogravimetric analyses of **Pd@SBS-15**.

A weight loss was observed below 100 °C with all the samples due to desorption of physisorbed water and ethanol from the pore channels. A further distinct weight loss,

between 180 °C and 500 °C supported by a strong exothermic peak centered at 360 °C in the heat flow curve, is attributed to the thermal decomposition of the organic compound. For sample **3** and **6@SBA-16**, the decomposition process was slowly carried out due to the broad exothermic peak, while sample **Pd@SBA-15** has a exothermic peak concentrated at 360 °C, indicating a dramatic decomposition occurring at this temperature.

3.2.3 Catalysis

The hybrid material **Pd@SBA-15** was used for the hydrogenation of cyclohex-2-enone and showed excellent activity and selectivity under mild condition. The conversion reaches 99% after 1.5 h and the total TON (turnover number) exceeds 150 mol·mol⁻¹. After the reaction, the catalyst was separated from the reaction mixture by filtration and washed with acetone. Recyclability tests are summarized in Table 3. 1. Except the first run, where catalyst took 1.5 h to achieve complete conversion, the reaction reached 99% after 1 h in all following runs and this remained steady up to 10th run, proving that the catalyst is highly stable and simple to recycle (Table 3. 1).

Table 3. 1 Recyclability of **Pd@SBA-15** used for the hydrogenation of cyclohex-2-enone.^a

recycle	1 st	2 nd	3 rd	4 th	5 th	6 th	7 th	7 th	9 th	10 th
0.5 h	28	80	99	88	87	58	69	57	54	67
1h	72	99	99	99	99	99	99	99	99	98

^a % of conversion; reaction conditions: 1 bar H₂, 1 mmol of cyclohex-2-enone, 0.65 mol% of **Pd@SBA-15**, r. t., 10 ml of toluene, determined by GC-MS with *n*-decane as the internal standard.

As reported in the literature, palladium nanoparticles are also very active catalysts for hydrogenation reactions.^[132-133, 156-157] To prove the formation of palladium nanoparticles **Pd@SBA-15** was reinvestigated with TEM of after being used in catalysis for 10 runs. The TEM images show clearly that there are no palladium nanoparticles on the support (Figure 3. 28), which again proves the outstanding stability of this material during the hydrogenation reaction.

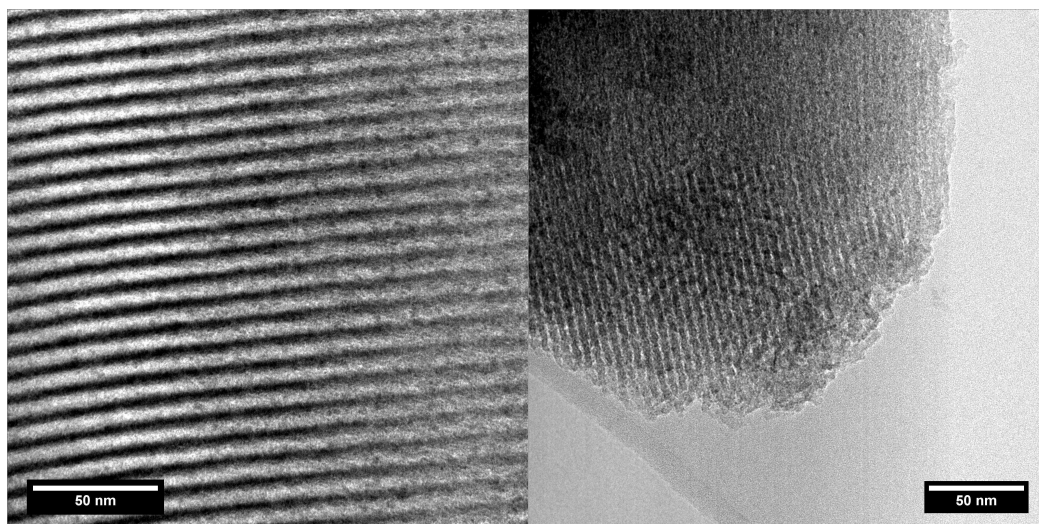


Figure 3. 28 TEM image of **Pd@SBA-15** catalyst after tenfold recycling.

To elucidate the role of the phosphine ligand, a control experiment was carried out, wherein a catalyst prepared by directly loading $\text{PdCl}_2(\text{CNPh})_2$ on the modified SBA-15 support **3** with an overall palladium loading similar to that of **Pd@SBA-15**. The hydrogenation reaction, carried out under identical reaction conditions as before, gave no conversion after 24 h. This proves that the phosphine ligand plays a key role for the activity of the catalyst. Since it is well known that $\text{PdCl}_2(\text{PPh}_3)_2$ is a poor catalyst for homogeneous hydrogenation,^[158] the influence of the support might be responsible for the dramatic difference in activity between **Pd@SBA-15** and $\text{PdCl}_2(\text{PPh}_3)_2$. Therefore a dichloropalladium complex carrying trimethoxysilyl functionalized triphenylphosphine ligands was covalently grafted on the SBA-15 in a control experiment, according to the published method.^[106] This system turned out to be absolutely inactive under the same conditions as shown in Table 3. 1. It therefore can be deduced that the pronounced increase in activity of **Pd@SBA-15** should not be due to the support. According to the ^{31}P CP-MAS NMR result, it is possible that the *cis*-configured complexes are responsible for the high activity. A solid state NMR investigation on the used catalyst (after the first run) was also carried out to investigate the stability of the catalyst (Figure 3. 29, Figure 3. 30, Figure 3. 31). The ^{13}C , ^{29}Si and ^{31}P CP-MAS NMR exhibit nearly the same resonances compared with the fresh catalyst **Pd@SBA-15** (Figure 3. 18, Figure 3. 19, Figure 3. 20), proving the high

stability of covalent bond between complex and support. The asterisk denotes rotational sideband.

For a practical application of a heterogeneous catalyst system, its stability and reusability are important factors. To confirm that the catalytic hydrogenation is indeed heterogeneous, the catalyst was removed after a conversion of about 25% was reached and the filtrate was used for the hydrogenation of cyclohex-2-enone. There is no further conversion in the following 20 h. By AAS no palladium contamination down to 0.5×10^{-4} mmol could be detected, which clearly demonstrates that **Pd@SBA-15** is a truly heterogeneous system.

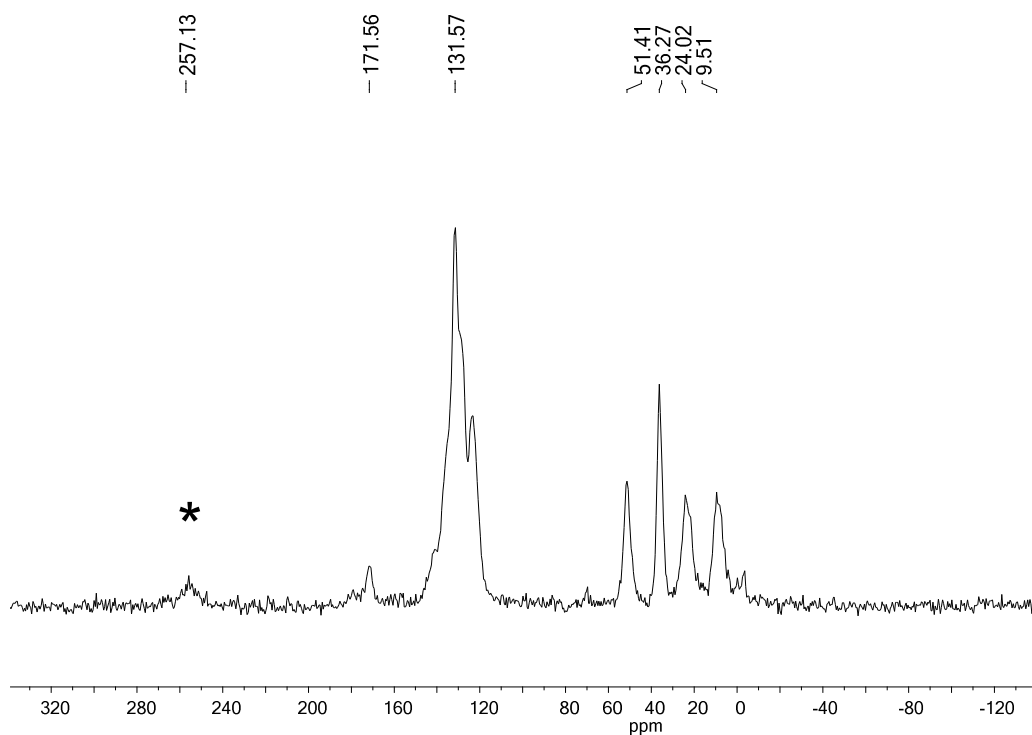


Figure 3. ^{29}Si CP-MAS NMR of **Pd@SBA-15** after first run.

3. Non-covalent Immobilization of a Triphenylphosphine Ligand

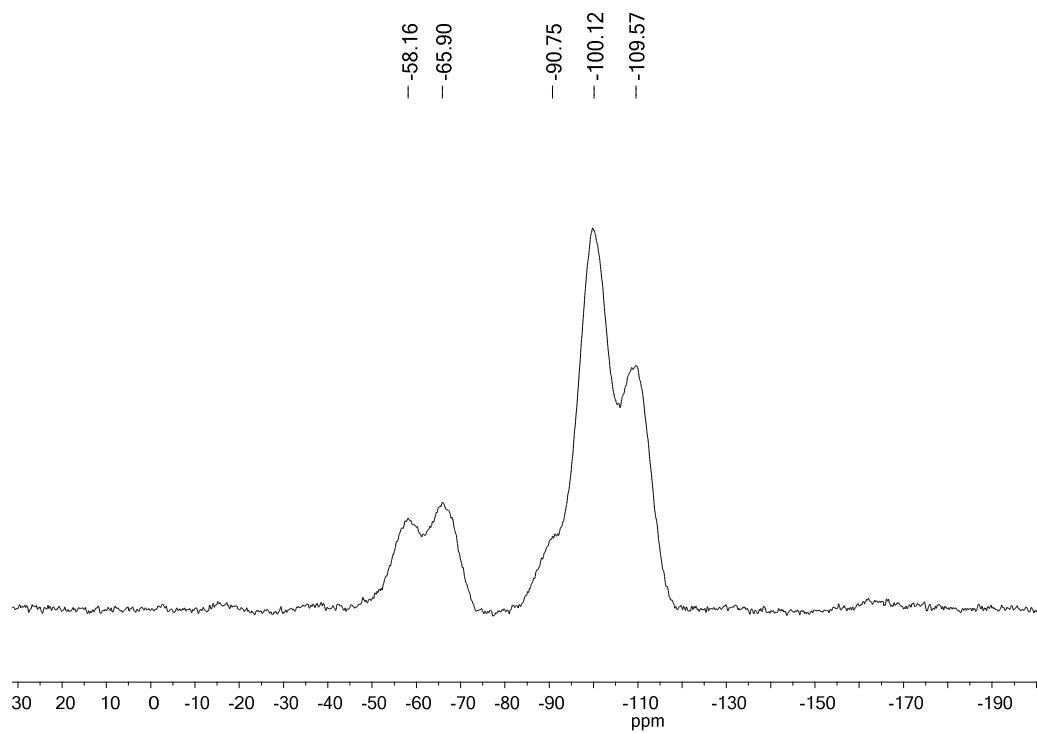


Figure 3. ^{29}Si CP-MAS NMR of **Pd@SBA-15** after first run.

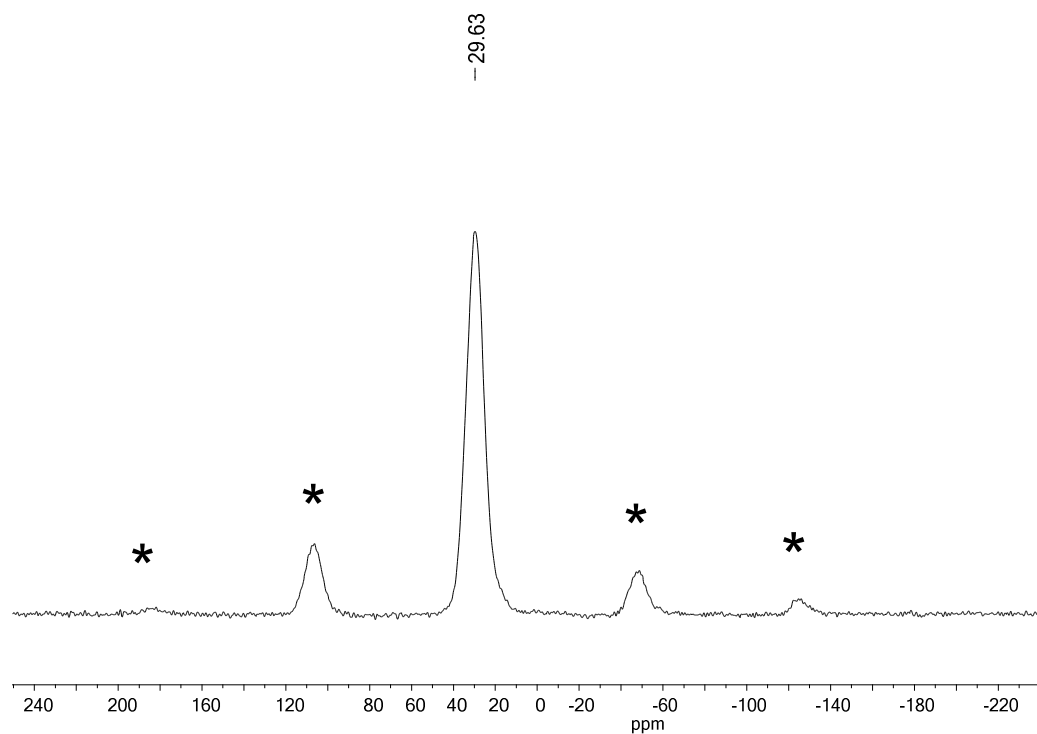
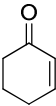
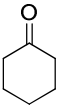
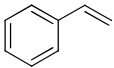
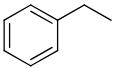
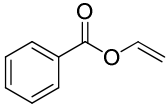
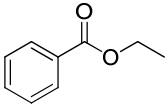
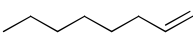
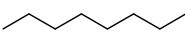
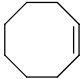

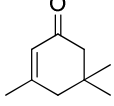
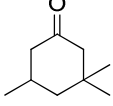
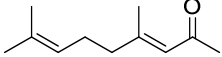
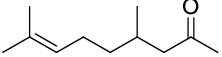
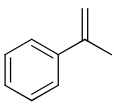
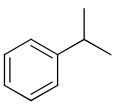
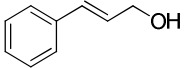
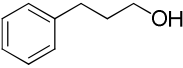
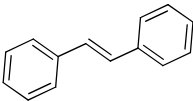
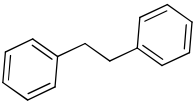
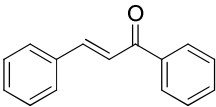
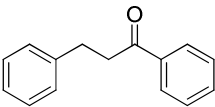


Figure 3. ^{31}P CP-MAS NMR of **Pd@SBA-15** after first run.

3. Non-covalent Immobilization of a Triphenylphosphine Ligand

A series of representative alkenes were employed to investigate the general applicability of **Pd@SBA-15** for hydrogenation reactions (Table 3. 2).

Table 3. 2 Hydrogenation of different olefins with **Pd@SBA-15**^a

entry	olefin	product	yield (%) ^b
1			99
2			99
3			99
4			> 90
5			< 15
6			0
7			70 ^c
8			99
9			99
10			99
11			99 ^b

^aReaction conditions: 1 bar H₂, 1 mmol of substrate, 0.2 mol% of **Pd@SBA-15**, 10 ml of toluene, r. t., 8-12 h. ^b reacted 24 h. ^c determined by GC-MS

3. Non-covalent Immobilization of a Triphenylphosphine Ligand

In our model reaction cyclohex-2-enone was hydrogenated with excellent chemoselectivity to the corresponding alkanone without any attack at the C=O double bond (entry 1). Double bonds which are adjacent to an aromatic ring or a heteroatom can be reduced efficiently and without any byproduct under the standard conditions, too (entry 2 and 3). Generally, substrate isomerization is a common but unwanted side reaction in hydrogenation. In our system, the monofunctional alkene 1-octene only gave less than 10 % of 2- and 3-octene as byproducts. (entry 4). Turning to higher substitution patterns at the C=C double bond strongly reduces the catalytic activity **Pd@SBA-15** (entries 5-7). Nevertheless, **Pd@SBA-15** shows excellent activity and selectivity for styrenes, which can be substituted in the 1- or 2-position of the C=C bond. A series of functional groups are tolerated. (entries 8-11).

In order to extend the application and investigate the stability of **Pd@SBA-15** it was utilized for the Suzuki reaction applying the same harsh reaction conditions as described in ref.^[95, 106]. If the catalyst was removed by filtration after the reaction and 0.1 g Cs₂CO₃ were added as the requested for the next recycle, the catalyst can be reused at least four times without any severe loss of activity (Table 3. 3).

Table 3. 3 The reusability of Pd@SBA-15 in Suzuki reaction of PhBr and PhB(OH)₂.^a

recycle	1 st	2 nd	3 rd	4 th
24h	93	92	90	70

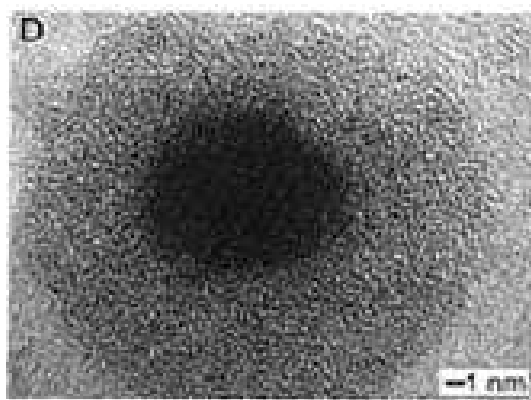
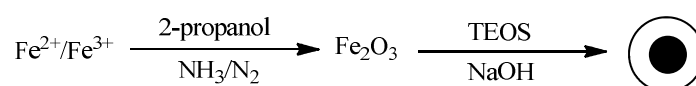
^aReaction conditions: PhBr (1 mmol); PhB(OH)₂ (1.5 mmol); Cs₂CO₃ (1.2 mmol); Pd (0.8 mol% relative to PhBr); dioxane (5 mL), 80 °C, 24 h; yield determined by GC-MS with n-decane as the internal standard.

According to previous work and reports of others in the literature,^[71, 95, 106] palladium(II) complexes can be reduced to palladium nanoparticles during Suzuki reactions. Enders et al. reported the stabilizing effect of supported imidazolium ions on the palladium nanoparticles,^[40] which might also have an influence on the recyclability of **Pd@SBA-15** in the Suzuki reactions. However, as soon as water is used to dissolve and remove cesium salts after the reaction, the electrostatically grafted catalyst loses its

activity completely. This is in contrast to our previous findings with covalently grafted triphenylphosphine palladium complex, which can be reused for the Suzuki coupling up to seven times without losing its activity. We assign this behavior to an ion exchange in basic aqueous solution. Considering all the control experiments, the high catalytic activity and stability of the palladium catalyst relate to the uniformly dispersed triphenylphosphine ligands on the SBA-15 surface. The relatively strong electrostatic interaction between sulfonic anion and imidazolium cation is responsible for the reusability of the catalyst in harsh conditions such as Suzuki reaction.

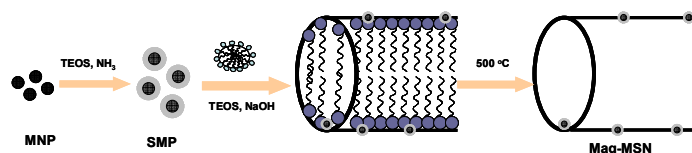
3.2.4 Extended research

Pd@SBA-15 can effectively catalyze the Suzuki reaction in previous experiments. However, once the water is used to dissolve the Cs_2CO_3 for the separation of the catalyst, the activity will completely lose. One possible solution for this drawback is to use magnetic nanoparticles (**MNPs**) as support which can separate the catalyst from the mixture by applying the external magnetic field and avoid utilization of water. The synthesis of silica coated magnetic nanoparticles **SM** was synthesized according to the reported procedure as shown in Scheme 3. 5.^[159]



Scheme 3. 5 Synthesis of **SM**.

The catalyst **Pd@SM** was synthesized by the same procedure as described in **3.2.1 synthesis** part. The amount of grafted ligand **6** was calculated according to the sulfur content of element analysis, which shows that 0.04 mmol g⁻¹ of **6** was finally immobilized on the surface. The loading of palladium was roughly calculated based on the added palladium amount, which is 0.02 mmol g⁻¹. The Suzuki reaction was carried out with 0.1 mmol aryl bromide as starting material and 3 mL dioxane as solvent. The ratio of PhBr, Pd, Cs₂CO₃ and PhB(OH)₂ is 1: 0.01: 1.2: 1.5. The reaction showed 92% yield after 16 h. However, the catalyst did not show any activity in the second run. The low grafting amount of imidazolium salt and ligand **6**, which is caused by low surface area and easy aggregation of magnetic nanoparticles, is mainly responsible for the poor stability of the catalyst. To overcome this drawback, magnetic nanoparticles are typically introduced into mesoporous silicas.^[160] The mesoporous magnetic nanocomposites (**MSM**) support was synthesized by my colleague Shylesh. The process is shown in Scheme 3. 6.



Scheme 3. 6 Formation of mesoporous magnetic nanocomposites **MSM**.

The same procedure as in the 3.2.1 synthesis part was used to immobilize the sulphonate group functionalized triphenylphosphine ligand. It should be mentioned here according to the elemental analysis, the amount of grafted compound **6** (0.3 mmol g⁻¹) with **MSM** as support is much higher than with SBA-15 (0.13 mmol g⁻¹) or **SM** (0.04 mmol) as support. The obtained hybrid material **6@MSM** was characterized by XRD and nitrogen adsorption/desorption (Figure 3. 32 and Figure 3. 33). The XRD patterns of **6@MSM** shows a (100) Bragg reflection, which confirms the preserve of the porous structure during the synthesis. However, there is no secondary reflection in the low-angle region, indicating limited periodicity in the long-range order of the porous system.

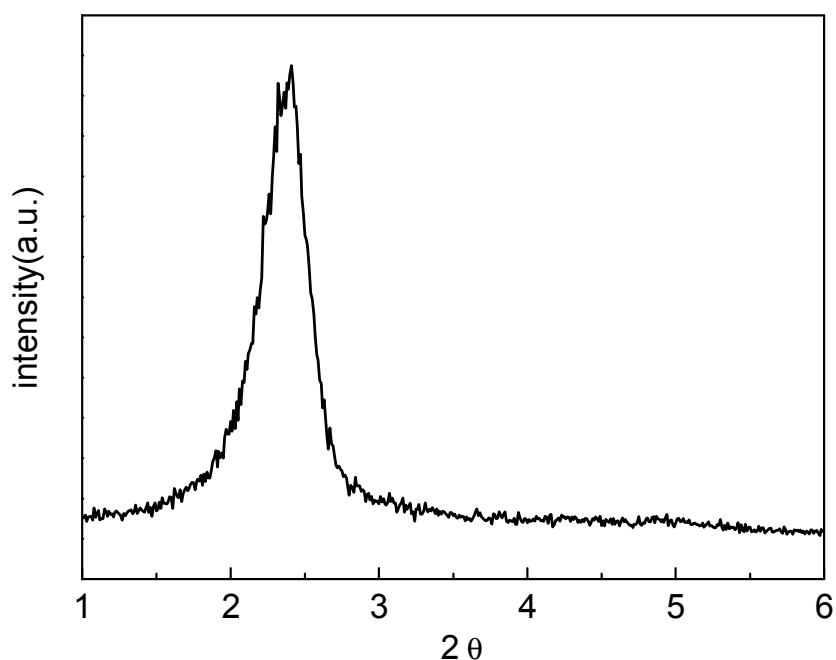


Figure 3. 32 XRD pattern of **6@MSM**.

The N₂ adsorption/desorption isotherm of **6@MSM** shows a type I isotherm (Figure 3. 33), typical of a microporous solid with a pore size distribution centered at 1.5 nm. The measured data for the BET surface area, the total pore volume of **6@MSM** are 771 m²·g⁻¹ and 0.44 cm³·g⁻¹ respectively. In the last step, half an equivalent of PdCl₂(CNPh)₂ was added and the obtained catalyst **Pd@MSM** was measured by SEM (Figure 3. 34). The SEM image of **Pd@MSM** shows the formed particles have different size and a smooth surface.

Pd@MSM was then used as catalyst in the Suzuki reaction with a general condition as Table 3. 3. However, the catalyst showed lower activity than the previous results (92%) with **SM** as support and 66% yield was obtained after 24 h. A possible reason for this result relates to the microporous structure of the hybrid material **Pd@MSM** which has diffusion limitations. Another drawback of this catalyst is that the magnetism of **MSM** is very weak. The catalyst mixed with Cs₂CO₃ cannot be directly separated with external magnetic field and the polar CH₃OH is obligatory for the separation. However, after the recovery with solvent CH₃OH, the catalyst lost the activity completely. Since

compound **6** and Cs_2CO_3 can dissolve in CH_3OH very well, the activity loss of the catalyst can be assigned to supported compound **6** together with coordinated palladium species suffered leaching in basic polar solvent.

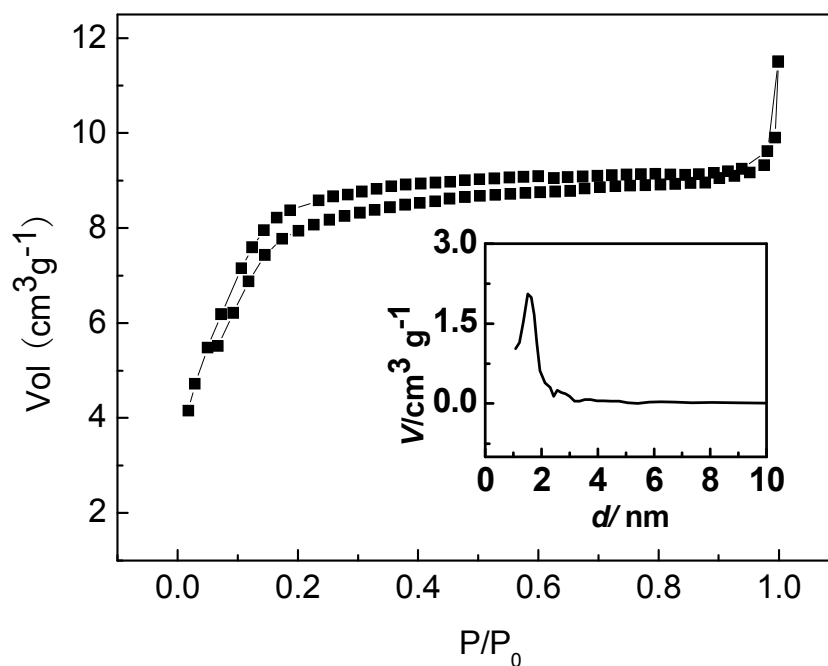


Figure 3.33 N_2 sorption isotherms and BJH pore size distribution (inset) of **6@MSM**.

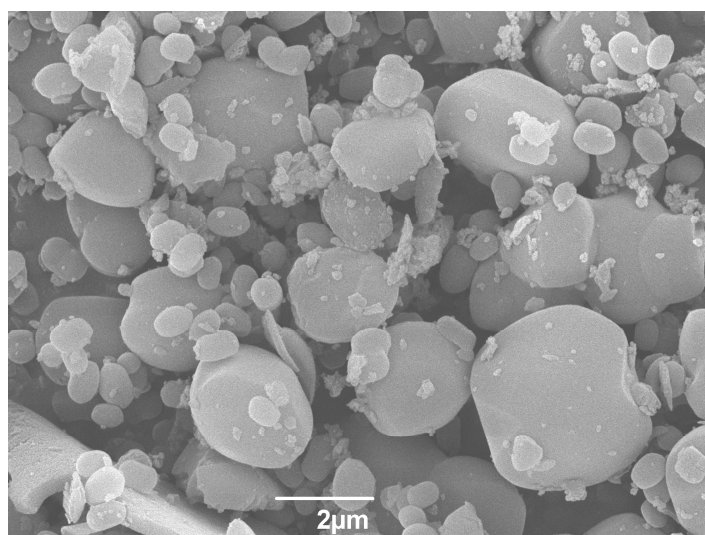


Figure 3.34 SEM image of **Pd@MSM**.

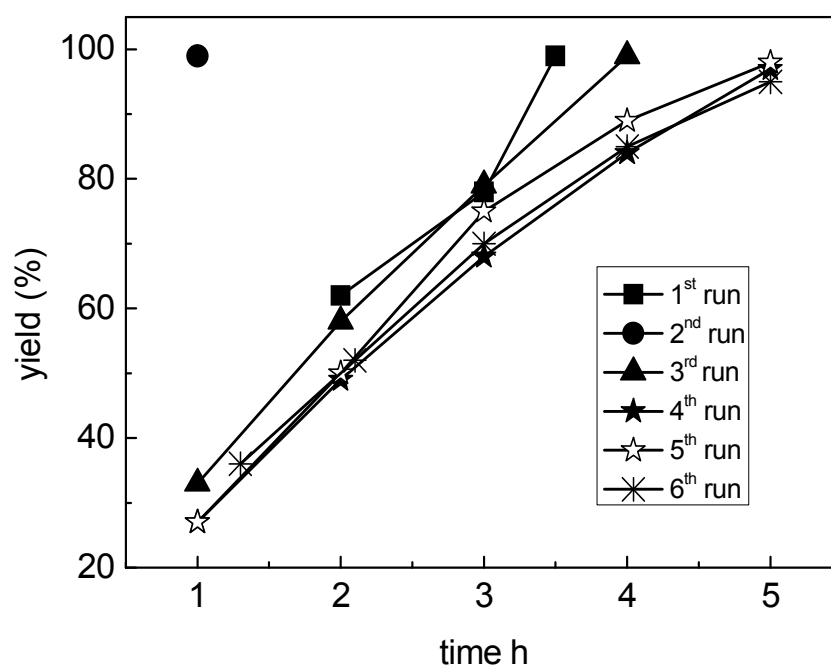
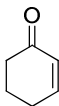
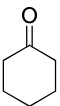
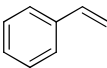
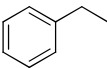


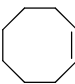
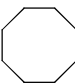
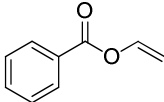
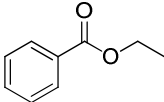
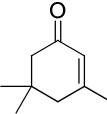
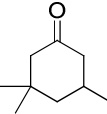
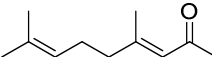
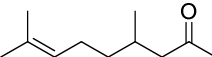
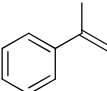
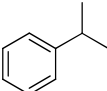
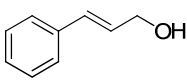
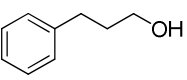
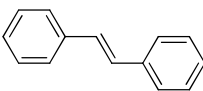
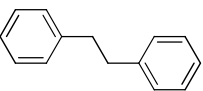
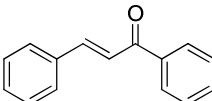
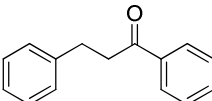


Figure 3. 35 Kinetic curves of recycle reaction of hydrogenation.

Until now the extended research of synthesis of recovery catalyst for Suzuki reaction is not successful. Next the catalyst **Pd@MSM** was applied in olefin hydrogenation reaction (Figure 3. 35). As expected, catalyst **Pd@MSM** showed excellent activity, selectivity and reusability in olefin hydrogenation reaction of cyclohex-2-enone to cyclohexanone. The catalyst also showed comparable yield with the similar catalyst **Pd@SBA-15** for various olefins as shown in Table 3. 4.

3. Non-covalent Immobilization of a Triphenylphosphine Ligand

Table 3. 4 Hydrogenation of different olefins with **Pd@MSM** as catalyst.

entry	olefin	product	yield (%) ^b
1			99
2			99
3			> 75
4			50
5			99
6			0
7			50 ^c
8			99
9			99
10			99
11			99

^aReaction conditions: room temperature, 1 bar H₂, 1 mmol of substrate, 0.45 mol% of catalyst **Pd@MSM**, toluene, 24 h. ^bDetermined by GC-MS. ^cSelectivity is 64%.

Chapter 4. Imidazolium Salt Incorporated in a Mesoporous Framework

4.1 Introduction

The use of transition-metal nanoparticles (NPs) provides an attractive and powerful tool for organic transformations.^[156, 161-165] During the last fifty years, NPs have been frequently used as catalysts in C-C coupling,^[92-93, 166-167] hydrogenation,^[132-133, 168] oxidation,^[169] hydrogenolysis and hydrosilylation and exhibited very high activities.^[156] These unique properties of NPs are mainly because of their high surface-to-volume ratio, which results in a large percentage of atoms remaining at the surface and being available for chemical transformations.^[170] However, having very active surface atoms can also result in aggregation, leading to deactivation of the catalysts. Therefore, the stabilization of NPs is a key point for the application of nanocatalysts.

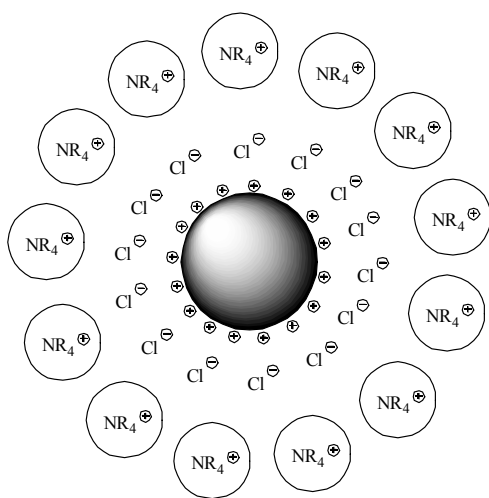


Figure 4. 1 Electrosteric stabilization of NPs.

The general stabilization mechanisms of NPs are usually discussed in terms of two categories: (i) charge stabilization and (ii) steric stabilization. Charge stabilization, also called electrosteric stabilization, is based on the Coulombic repulsion. Because the surface of NPs bears positive charge, it can be stabilized by a first layer of anions and a second layer of bulky cations as shown in Figure 4. 1. Steric

stabilization is achieved by the coordination of sterically demanding organic molecules that act as protective shields on the metallic surface. Due to increasing environmental and economic requirements, catalytic NPs supported on various solids such as metal oxides have recently attracted more and more

attention.^[92, 113, 171-172] The incipient wetness impregnation method is often used, which is convenient but leads to inhomogeneous particles and instable catalytic efficiency.^[173-175] In most cases, the supports are functionalized with organic compounds which play a very important role in the dispersion and stabilization of NPs as well as in the catalytic activity.^[176-179]

Ionic liquids (ILs) are valuable media for stabilizing NPs. Especially various functionalized imidazolium ILs are most frequently used.^[93, 162, 180] For example, 1-butyl-3-methylimidazolium hexafluorophosphate ([BMI][PF₆]) stabilized iridium NPs were used as a highly active and stable catalyst in arene hydrogenation.^[168]

The recent studies have shown that the imidazolium ILs might stabilize NPs not only electrostatically but also by binding to the NPs surface, which play a very important role in the catalytic activity.^[93, 168, 181] The heterogenization of imidazolium based ILs applied to stabilize NPs can lead to catalysts with high activity and stability as well as to simple separation. This method has been successfully applied in C-C coupling, hydrogenation and alcohol oxidation reactions.^[40, 132, 134, 168-169, 182-183] For example, Karimi et al. reported the immobilization of Pd NPs on silica through imidazolium cations, giving a highly active and reusable catalyst for the Heck reaction.^[40] However, immobilization of ligands with the post grafting method often leads to a degradation of the porous structure, which might have disadvantageous effects on the catalysis.

A recent breakthrough in heterogeneous catalysis is the synthesis of periodic mesoporous organosilicas (PMOs) through the surfactant-templated polycondensation of bridged organosilane precursors and silica moieties.^[22, 184-185] Due to the unique chemical properties and heterogeneous requirement of imidazolium salts, PMO type materials synthesized with organosilane bridged imidazolium ILs in the framework are starting to attract interest.^[186-188] Dai et al. described the synthesis of PMOs type materials with dialkylimidazolium groups inside the framework under basic conditions and their application as anion exchange resins.^[186] Hesemann reported the synthesis of

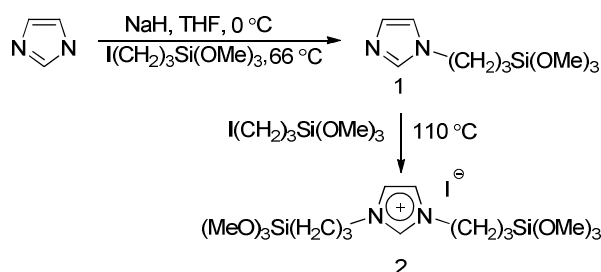
periodic mesoporous organosilica materials under acidic conditions with diarylimidazolium species as precursors having a high degree of rigidity.^[187]

In our previous work (chapter 2.4), the PMOs material composed by a bridged triphenylphosphine palladium complex, which further formed Pd NPs in the framework with co-condensation method showed excellent activity and stability in hydrogenation. In order to get better understanding and extend the application of imidazolium frameworked PMOs materials, here I present the synthesis of mesostructured organosilica with different loading of imidazolium cations in the framework and its application in the stabilization of palladium NPs for olefin hydrogenation.

4.2 Results and discussion

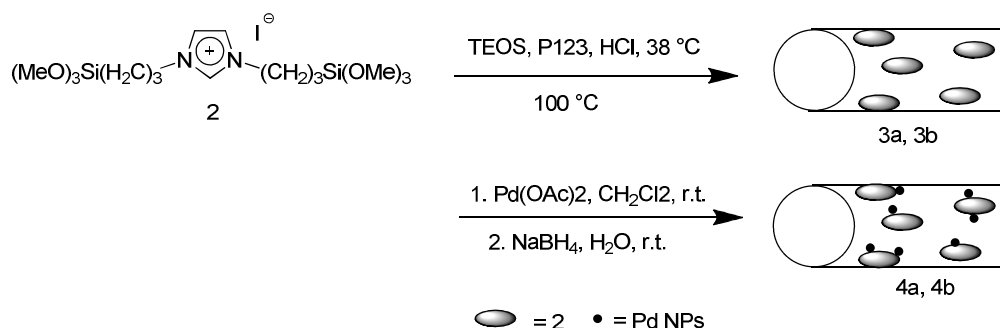
4.2.1 Synthesis

The -Si(OR)₃ bridged imidazolium salt precursor **2** was prepared according to a published procedure as shown in Scheme 4. 1.^[189] In the first step, imidazole was deprotonated by NaH followed by treatment with 3-iodopropyltrimethoxysilane. The obtained compound **1** reacted with 3-iodopropyltrimethoxysilane without solvent, led to quantitative yields of 1,3-d(3-trimethoxysilylpropyl)imidazolium iodide **2** without purification.



Scheme 4. 1 Synthesis of the bis-silylated imidazolium precursor **2**.

2 was further used to synthesize mesoporous organosilica type material possessing imidazolium moieties with different loading in the framework by co-condensation of **2** with tetraethoxysilane (TEOS) in the presence of the structure-directing agent P123 (triblock copolymer $\text{EO}_{20}\text{PO}_{70}\text{EO}_{20}$) in acidic media (Scheme 1) according to the published synthesis procedure of SBA-15 (Scheme 4. 2).^[20] Because the precursor **2** has two bulky propylene chains between the trimethoxysilyl groups, it is necessary to use another small silane compound such as TEOS to co-condense with **2** for constructing the PMOs materials. Ethanol was used to dissolve precursor **2** and TEOS due to the insolubility of **2** in TEOS. The mixtures of **2** and TEOS with various molar ratios (0.10: 0.9, **3a** and 0.25: 0.75, **3b**;) were added to the mixture of P123, H_2O and HCl with the ratio of 0.017: 208: 6, respectively. After the template was removed by extraction with ethanol, the products were dried and characterized systematically by nitrogen absorption isotherms, magic angle spinning (CP-MAS) NMR and infrared spectroscopy, elemental analysis and thermal analysis (TG-DTG) to obtain structural and compositional information of these materials. Finally, the PMOs type materials were treated with a CH_2Cl_2 solution of palladium acetate, followed by reduction with NaBH_4 in aqueous solution to obtain the immobilized palladium nanoparticles. The loading of palladium was roughly calculated based on the added amount of palladium acetate. The catalysts were synthesized and stored in the air, proving that the catalysts are air stable.

Scheme 4. 2 Synthesis of catalysts **4a** and **4b**.

4.2.2 Characterization

The ^1H NMR spectrum of compound **1** gives four sets of resonances in the high field (Figure 4. 2). The signals at 0.6, 1.9 and 3.9 ppm correspond to the propylene chain, while a sharp singlet at 3.5 ppm can be assigned to the $-\text{Si}(\text{OMe})_3$ group. Three singlets at 7.5, 7.0 and 6.9 ppm are attributed to the hydrogen atoms of imidazole. In the ^{13}C $\{^1\text{H}\}$ NMR spectrum of compound **1** (Figure 4. 3), three resonances at 6.3, 24.8 and 49.2 ppm can be attributed to the carbon atoms of the propylene linker. The resonance at 50.6 can be assigned to the organosilica $-\text{Si}(\text{OCH}_3)_3$ group. The chemical shift at 118.8, 129.5 and 137.3 are correlated with the resonances of the three imidazolium ring carbon atoms.

The infrared spectrum (KBr) of compound **1** is shown in Figure 4. 4. The adsorptions around 3000 cm^{-1} can be assigned to the C-H and N-H stretching vibrations. A strong band at 1084 cm^{-1} is attributed to the Si-(OMe) group.

Compound **2** bearing two alkoxyisilyl functions was also characterized by ^1H and ^{13}C NMR spectroscopy. The most notable feature in the ^1H NMR spectrum is the chemical shift (10.0 ppm) of the hydrogen atom in the 2-position of the 5-membered ring (Figure 4. 5). The resonance at 7.5 ppm is attributed to the hydrogen atoms in the 4-,5-position of the imidazolium cation. The resonances of high field correspond well with the chemical shifts of compound **1**. In the ^{13}C NMR spectrum (Figure 4. 6), the characteristic peaks of the imidazolium ring carbon atoms are observed at 135.8 and 121.4 ppm. Three resonances at 5.1, 23.2 and 51.0 ppm can be assigned to the carbon atoms of the propylene linker and the resonance at 49.8 can be assigned to the organosilica $-\text{Si}(\text{OCH}_3)_3$ group, which corresponds well with the ^{13}C NMR data of compound **1**.

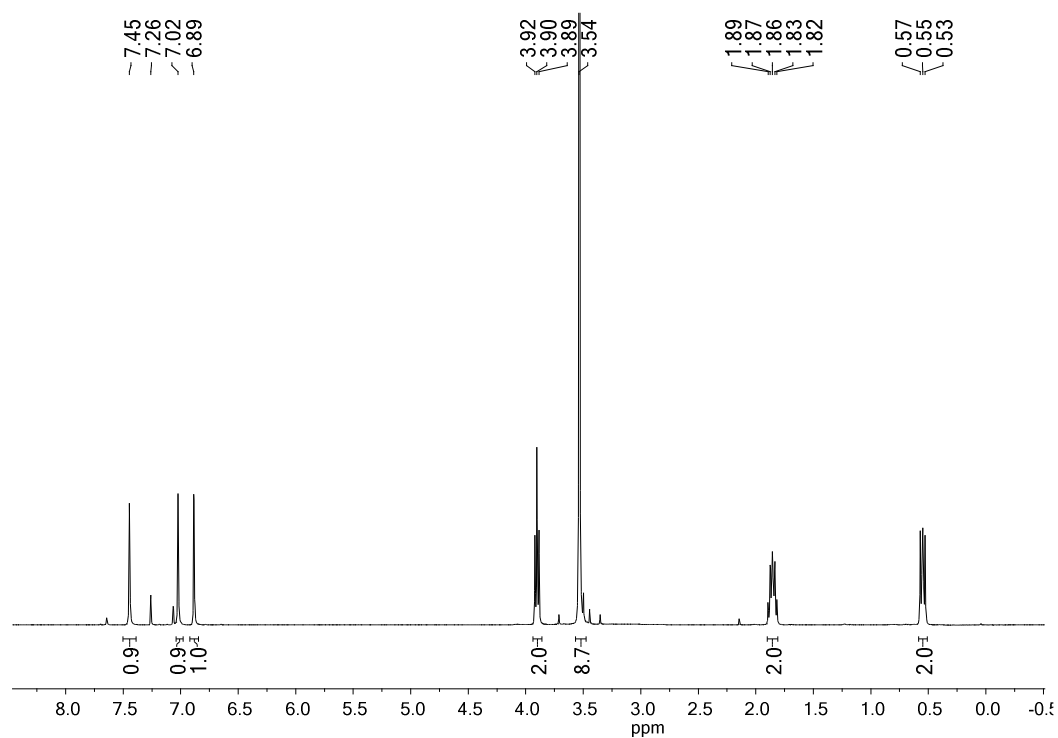


Figure 4. 2 ¹H NMR spectrum of compound **1** (400.13 MHz, 25 °C, CDCl₃).

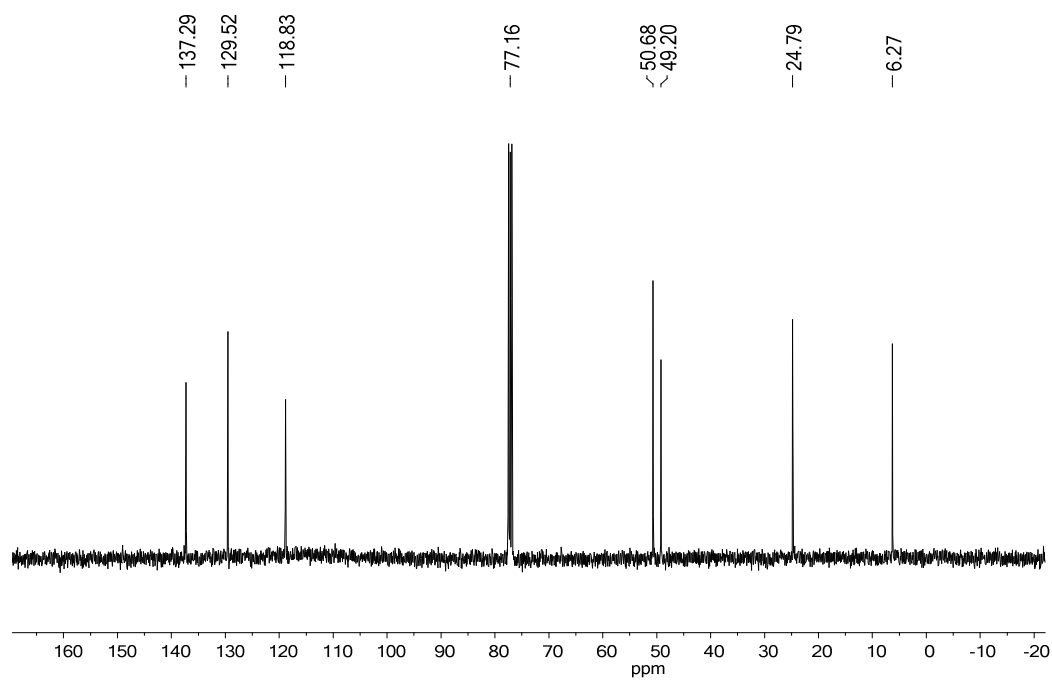


Figure 4. 3 ¹³C NMR spectrum of compound **1** (100.62 MHz, 25 °C, CDCl₃).

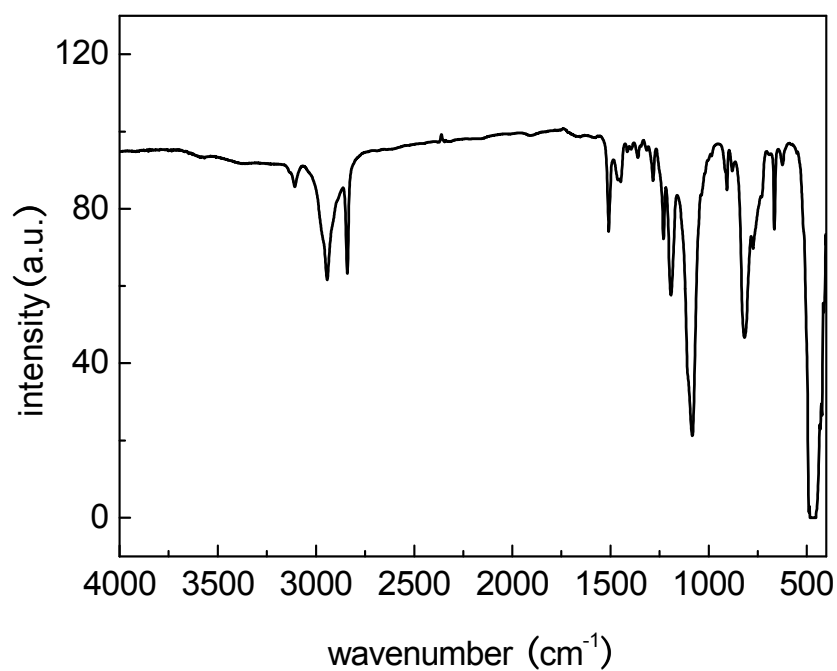


Figure 4. 4 Infrared of compound **1**.

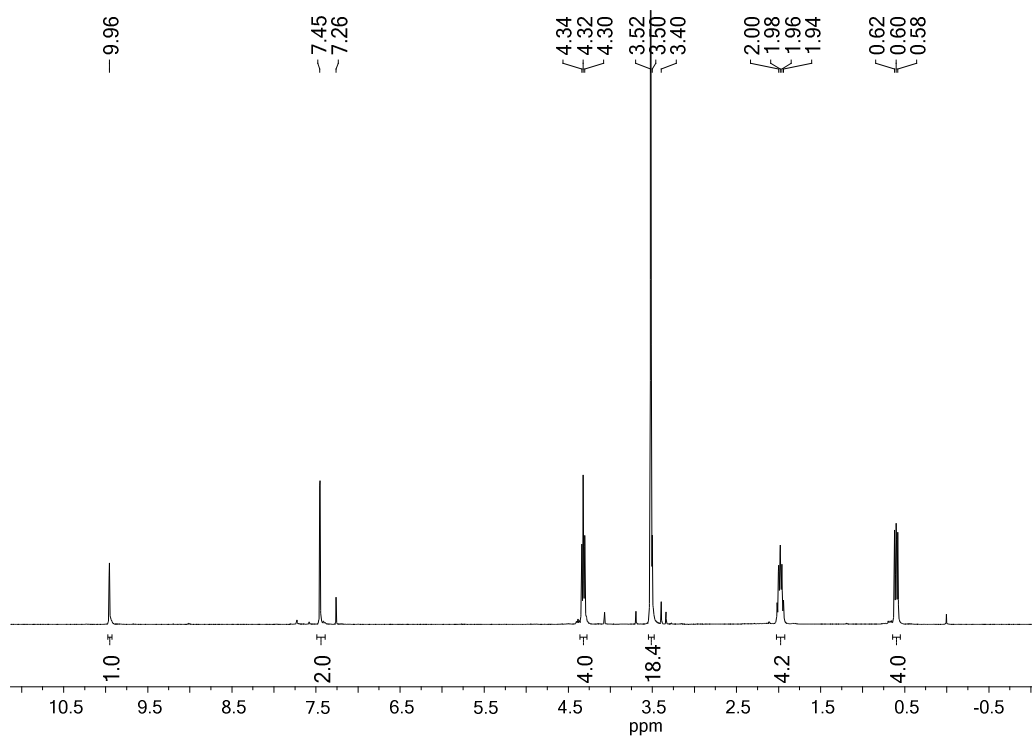


Figure 4. 5 ¹H NMR spectrum of compound **2** (400.13 MHz, 25 °C, CDCl₃).

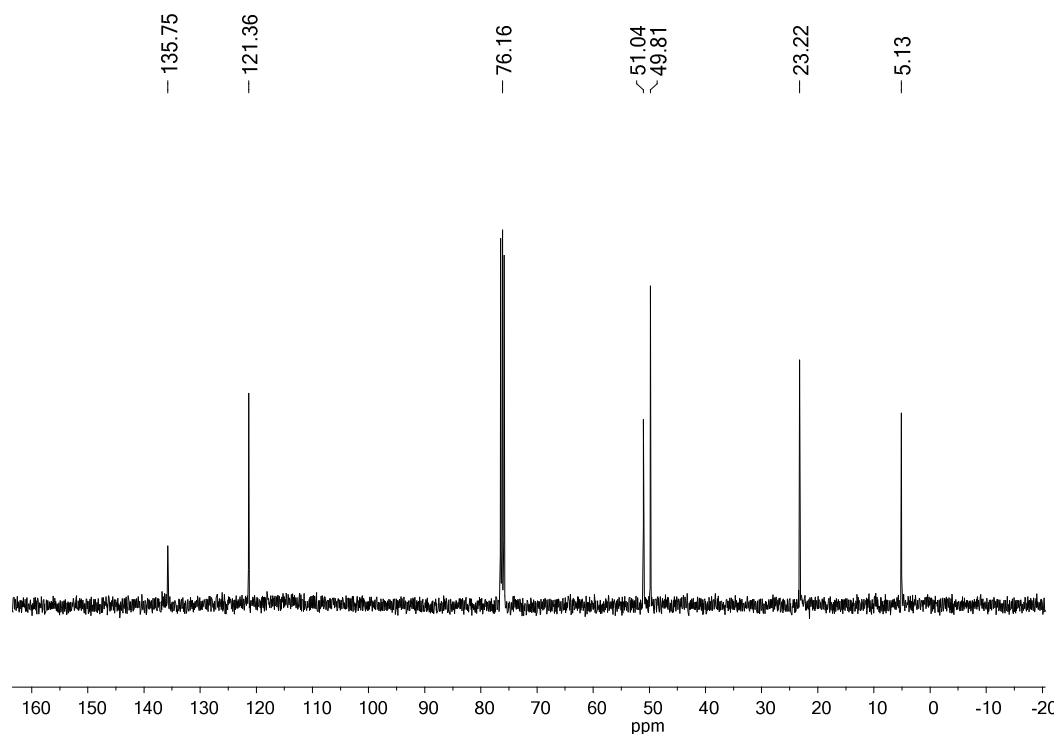


Figure 4. 6 ^{13}C NMR spectrum of compound **2** (100.62 MHz, 25 °C, CDCl_3).

The effect of the differed loadings of imidazolium groups in the mesostructure formation of organosilica was evaluated by means of nitrogen physisorption analysis (Figure 4. 7). The isotherms of **3a** and **3b** could be assigned to type IV, indicating the existence of mesopores. However **3b** exhibits a higher uniformity in the pores reflected by a sharp increase in the capillary condensation with a prominent hysteresis loop. ^[88]

The specific surface area, pore volume and pore diameter of **3a** are $560 \text{ m}^2 \cdot \text{g}^{-1}$, $0.65 \text{ m}^3 \cdot \text{g}^{-1}$ and scaled from 3.5 to 7.5 nm, respectively (Table 4. 1), which is in the range of a typical SBA-15 material. As expected an increased loading (25 mol%) of precursor **2**, exhibits (**3b**) much smaller surface area ($204 \text{ m}^2 \cdot \text{g}^{-1}$), the total volume ($0.19 \text{ m}^3 \cdot \text{g}^{-1}$) and pore size distribution (3.7 nm) due to the presence of bulky bridged organosilane precursors in the framewalls exerting more strain in the mesostructure. ^[190]

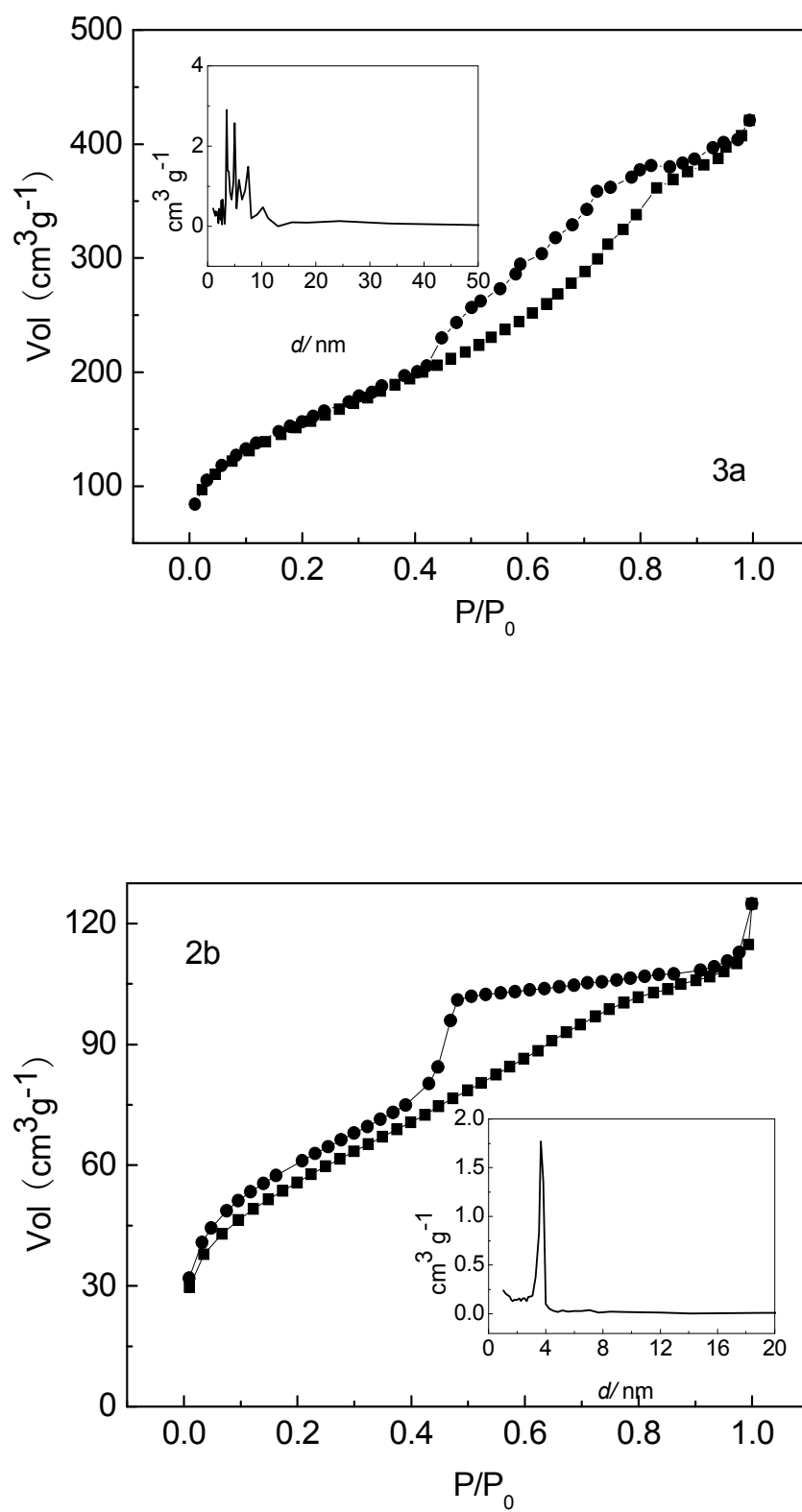
Figure 4. 7 N_2 sorption isotherms and pore size distribution (inset) of the **3a** and **3b**.

Table 4. 1 Characterization of the PMOs **3a** and **3b** as well as the catalysts **4a** and **4b**.

materials	S _{BET} [m ² ·g ⁻¹]	pore vol [cm ³ ·g ⁻¹]	BJH pore diam[nm]	chemical composition			imidazolium ^a [mmol·g ⁻¹]
				C	H	N	
3a	560	0.65	3.5-7.5	11.8	3.3	2.8	1.0
3b	204	0.19	3.7	15.7	4.3	4.8	1.7
4a	353	0.47	3.8	12.4	3.1	2.9	1.0
4b	15	0.05	-	18.2	4.4	4.8	1.7

^aCalculated according to the nitrogen content the elemental analysis.

The ¹³C CP-MAS NMR spectra of **3a** and **3b** match well with the high resolution NMR spectrum of precursor **2** in solution (Figure 4. 8). Three sets of broad peaks (9.5, 24.2 and 52.2 ppm) in the high field, can be assigned to the propylene linker of precursor **1**. The resonances at 136.6 and 123.7 ppm arise from the three imidazolium ring carbon atoms whereas two sharp peaks at 57.5 and 17.8 ppm relate to the retained solvent ethanol. FT-IR spectra of **3a** and **3b** support this conclusion showing bands at 2900 cm⁻¹ for the -CH₂- stretching vibrations of propyl groups and a band at 1635 cm⁻¹ for the C=N stretching vibration of the imidazolium rings in the framework (Figure 4. 9). All these results confirm the presence of organosilane bridged imidazolium ILs in the mesoporous framework without any structural degradation during the synthesis and the following surfactant extraction procedure. The amount of precursor **2** incorporated into the PMOs materials **3a** and **3b** determined by elemental analysis, are 1.0 mmol·g⁻¹ and 1.7 mmol·g⁻¹, respectively (Table 4. 1).

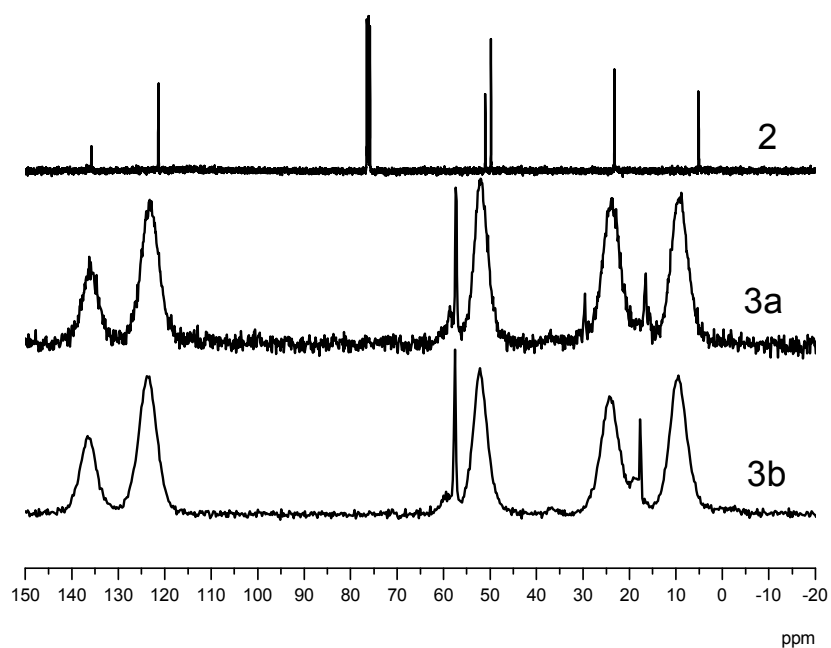


Figure 4. 8 ^{13}C NMR spectra of precursor **2**, **3a** and **3b**.

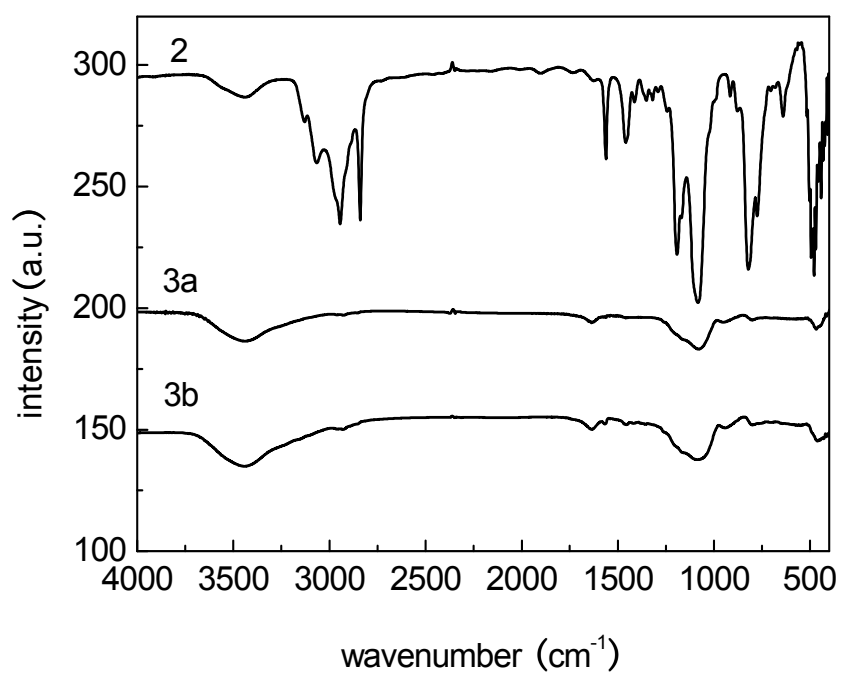


Figure 4. 9 Infrared spectra of **2**, **3a** and **3b**.

The ^{29}Si CP-MAS NMR spectra of **3a** and **3b** show both, the signals of the T^n and of the Q^n series (Figure 4. 10). The signals at -110, -101, and -93 ppm correspond to the framework silica sites $\text{Si}(\text{OSi})_4$ (Q^4), $\text{HOSi}(\text{OSi})_3$ (Q^3), and $(\text{HO})_2\text{Si}(\text{OSi})_2$ (Q^2). The signals that originate from silicon atoms attached to the imidazolium salt appear at -49, -57, and -66 ppm, which can be assigned to $\text{R-Si}(\text{RO})_2(\text{OSi})$ (T^1), $\text{R-Si}(\text{RO})(\text{OSi})_2$ (T^2), and $\text{R-Si}(\text{OSi})_3$ (T^3) organosiloxane sites. The presence of resonances in the T region confirms that carbon-silicon bond cleavage of precursor **2** has not occurred during the hydrolysis and condensation process and indicates that precursor **2** is covalently incorporated in the framework of the organosilica sample. Dominant T^3 and T^2 resonances further indicate a relatively complete cross-linking reaction between the imidazolium precursor **2** and TEOS during the condensation process and thereby ensures the synthesis of a stable organosilica material. It is worthwhile to note that the intensities of T^n peaks gradually increase as the molar fractions of **2** in the initial gel mixture increase. These results reflect that the amount of imidazole precursor incorporated into the solid materials increase.

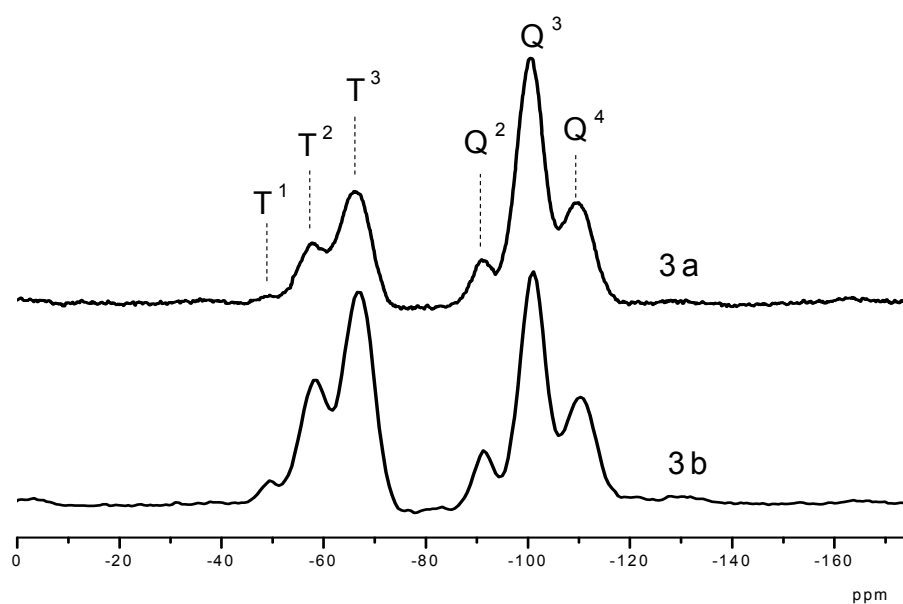
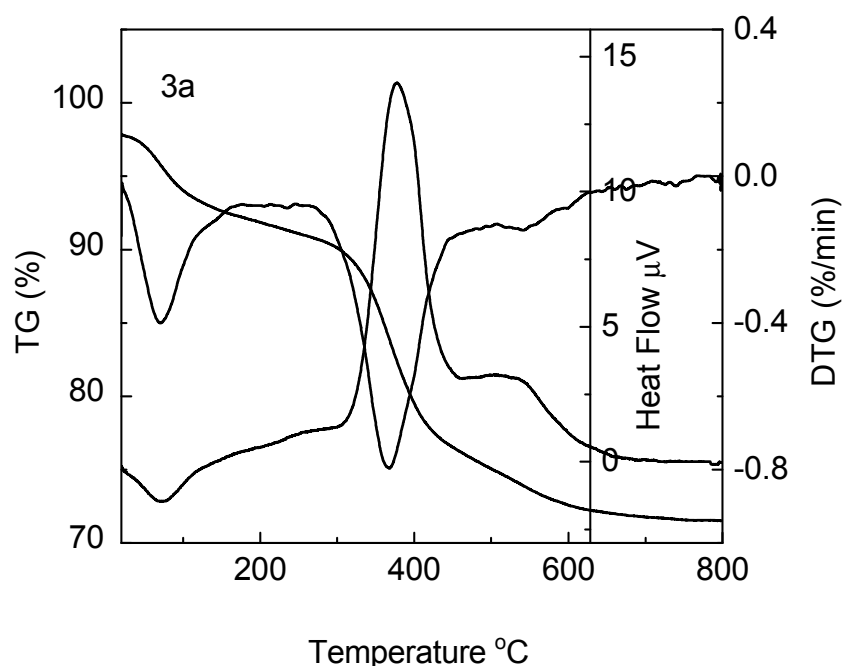


Figure 4. 10 ^{29}Si CP-MAS NMR spectrum of the PMOs **3a** and **3b**.

To evaluate the thermal stability of the organosilicas material (PMOs **3a** and **3b**), thermogravimetric and differential thermogravimetric (TG-DTG) analysis experiment was performed (Figure 4. 11). A weight loss was observed below 100 °C due to desorption of physisorbed water and ethanol from the pore channels. A further distinct weight loss between 300 °C and 500 °C supported by a sharp exothermic peak centered at 350 °C in the heat flow curve, is attributed to thermal dissociation of the imidazolium groups. This result indicates that the PMOs with different loadings of precursor **2** have a thermal stability up to 300 °C.

Noting the stable mesostructure of **3a** and **3b**, the materials were further treated with palladium acetate to develop palladium containing organosilica materials (noted as **4a** and **4b**). After the introduction of Pd NPs, **4a** preserved its mesostructure according to the N₂ adsorption/desorption isotherms (Figure 4. 12).



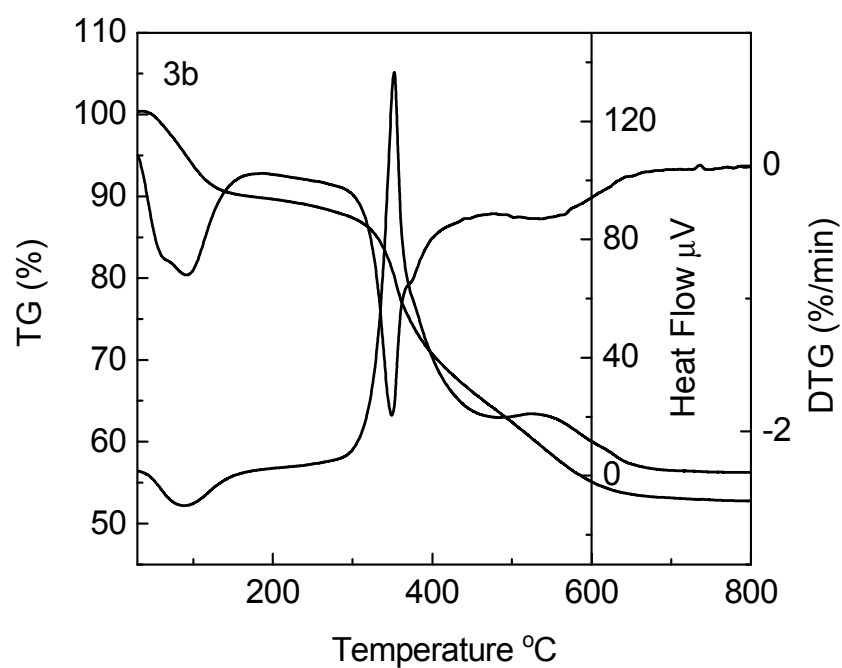


Figure 4. 11 Thermogravimetric and differential thermogravimetric analyses of **3a** and **3b**.

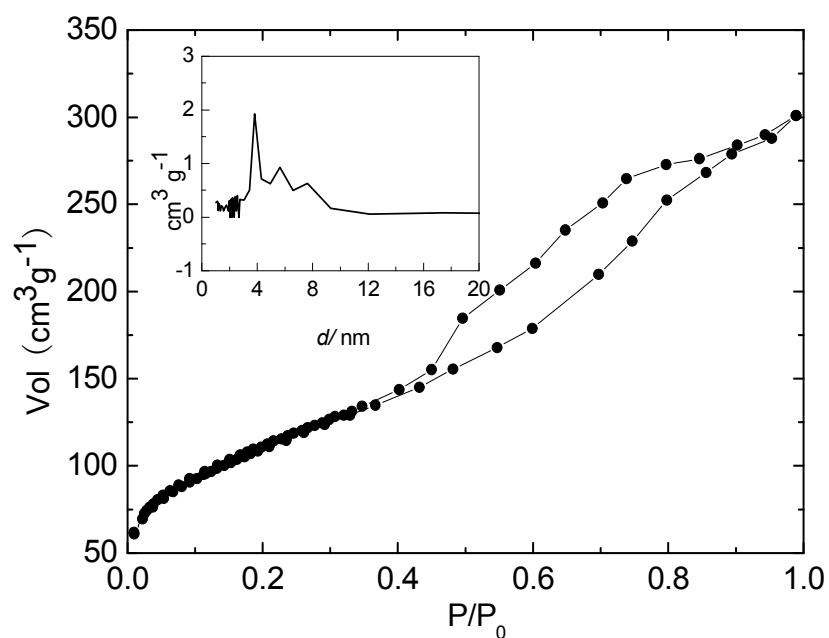


Figure 4. 12 N₂ sorption isotherms and pore size distribution (inset) of **4a**.

Specially, after palladium immobilization **4a** revealed a decrease in specific surface area, total pore volume and the BJH pore size distribution, implying that the Pd NPs

were mainly immobilized in the pore channels (Table 4. 1). In sharp contrast, the specific surface area of **4b** decreased dramatically to $15 \text{ m}^2 \cdot \text{g}^{-1}$, suggesting that sample **4b** nearly lost its porosity. It is possible that partial pores were blocked by the Pd NPs due to the relatively low pore size distribution and specific surface area of the parent support **3b**. These results highlight that a definite percentage of imidazolium sites is necessary for the stabilization of palladium nanoparticles, unless they will clog near the pore mouth disturbing the overall structure of the mesoporous material. Another possible reason might be that the high loading of the precursor **2** leads to an unstable porous material due to intercrossed linking of organosilicas. As a result, most of the pores collapse during the synthesis and purification process of **4b**. The elemental analysis data of **4a** and **4b** in Table 4. 1 show that composition of the hybrid materials did not change after the introduction of the Pd NPs. The ^{13}C and ^{29}Si CP-MAS NMR spectra of catalyst **4a** exhibit the same resonances as **3a**, indicating that the interaction between NPs and imidazolium groups is only weak (Figure 4. 13 and Figure 4. 14).

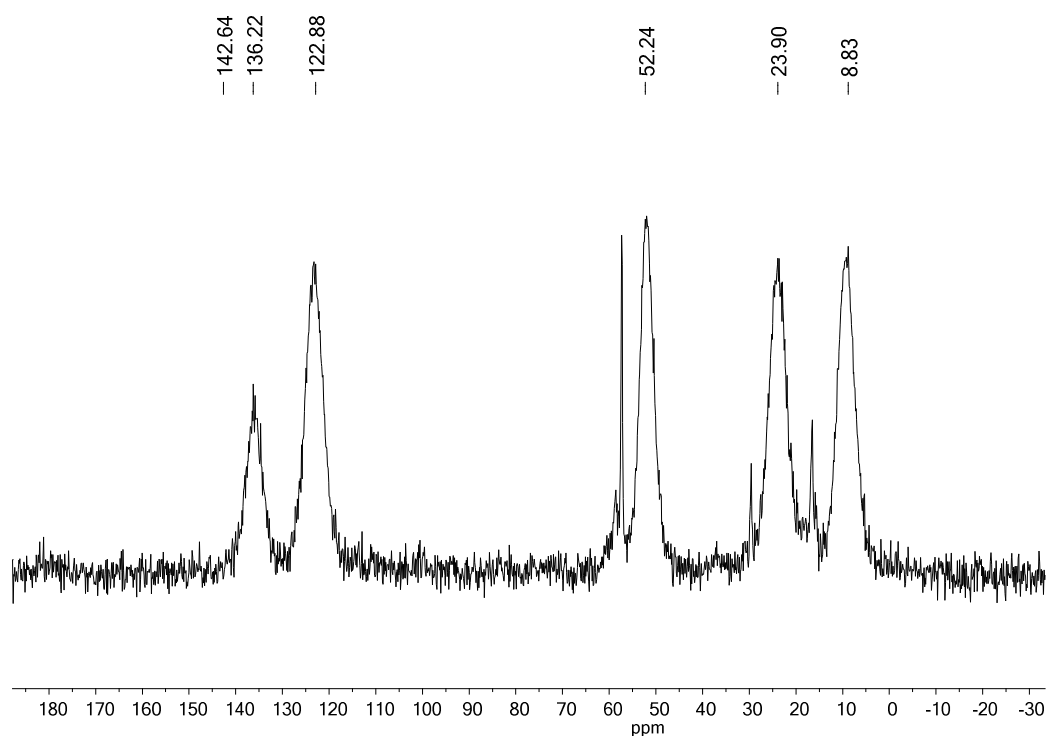


Figure 4. 13 ^{13}C CP-MAS NMR spectrum of catalyst **4a**.

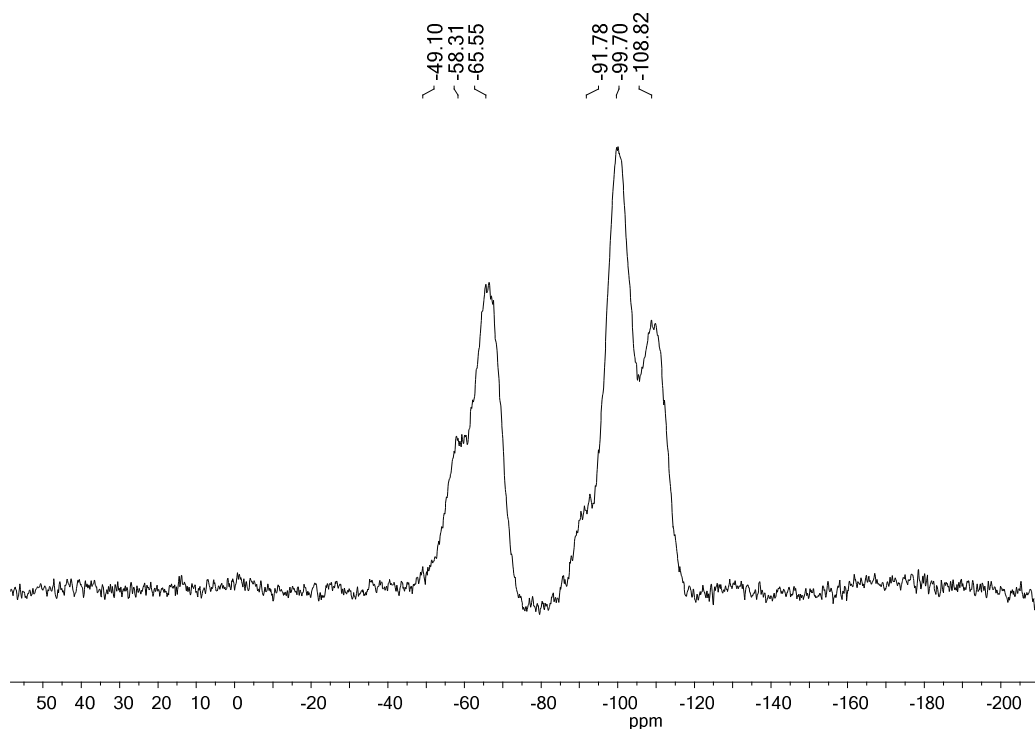


Figure 4. 14 ^{29}Si CP-MAS NMR spectrum of catalyst **4a**.

The SEM image of **4a** reveals that the product displays a sheet shaped morphology (Figure 4. 15 left). Metal particle size and distribution are critical factors for the catalytic activity. No NPs can be observed from the TEM images of **4a** (Figure 4. 15 , right), which proves that extremely small sized NPs were formed and well dispersed in the pores. The SEM image of **4b** shows that it is built up from irregular blocks with different size (Figure 4. 16, left), which indicates that the agglomeration of small fragments happens in the growing process of the material. The TEM image of **4b** demonstrates that the Pd NPs are in a range of 3 to 5 nm and are well distributed on the surface of **4b** (Figure 4. 16, right), indicating that the imidazolium cations are responsible for the fine distribution and stability of the Pd NPs.

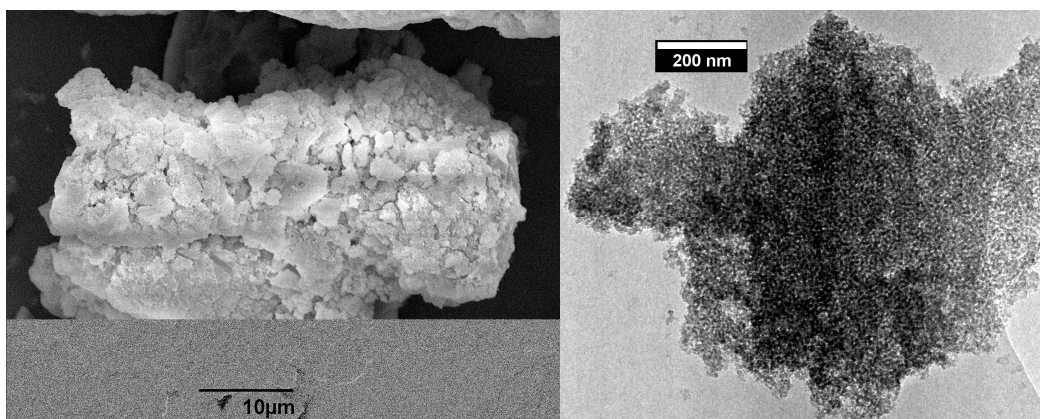


Figure 4. 15 SEM (left) and TEM (right) images of **4a**.

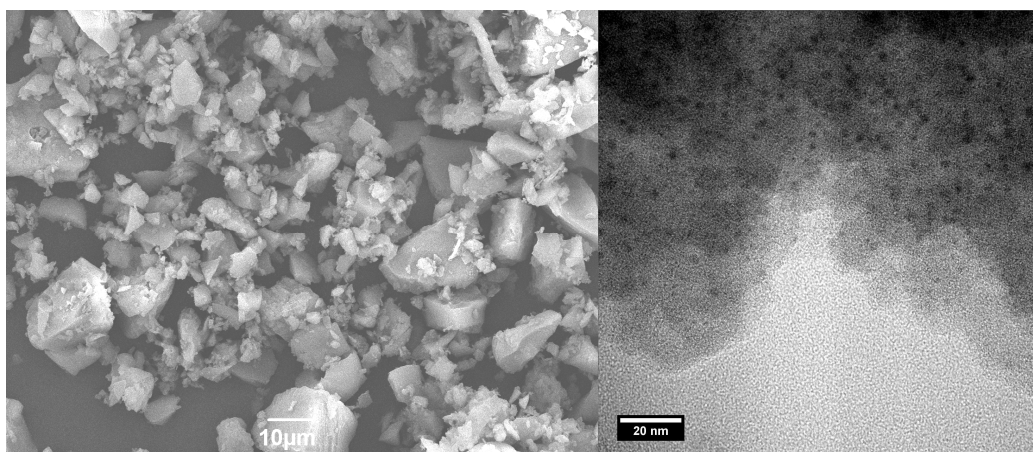


Figure 4. 16 SEM (left) and TEM (right) images of **4b**.

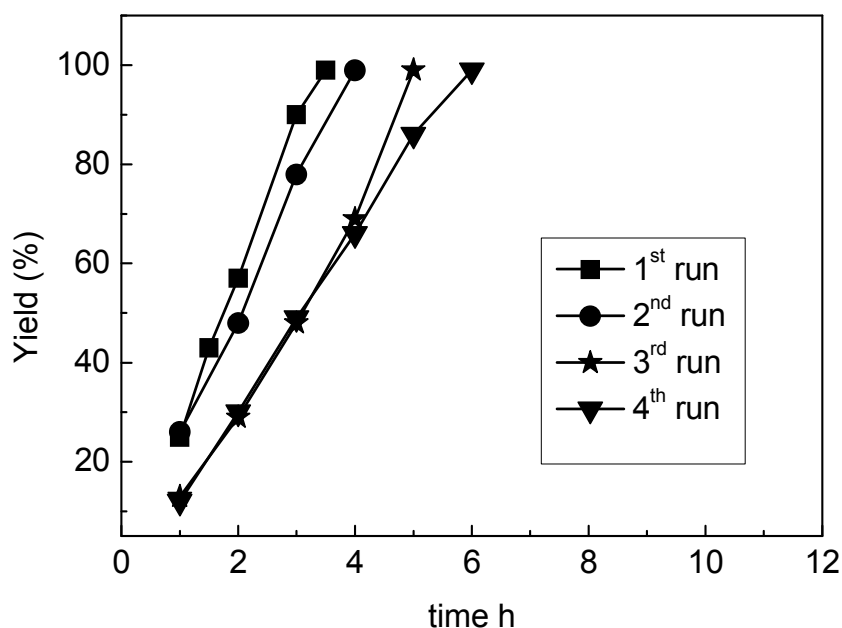
4.2.3 Catalysis

As a model reaction, the hybrid materials **4a** and **4b** were used in the hydrogenation of cyclohex-2-enone to cyclohexanone. Excellent activity and selectivity at room temperature under a pressure of H_2 (1 bar) were obtained with the catalyst **4a**. A complete conversion can be achieved in 40 min, it is recyclable up to 5 runs without any loss in activity (Table 4. 2). While with **4b** as catalyst the reaction needs 3 h to get finished in the first run and a prolonged reaction time is necessary to achieve the same conversion during the consecutive recycling experiments (Figure 4. 17).

Table 4. 2 Reusability of **4a** in hydrogenation.

recycle	1 st	2 nd	3 rd	4 th	5 th
4a	99	99	99	99	99

% of conversion; reaction conditions: 1 bar H₂, 1 mmol of cyclohex-2-enone, 0.65 mol% of catalyst, r. t., 10 mL of toluene, determined by GC-MS with decane as the internal standard, reacted 40 min.

Figure 4. 17 Kinetic curve of recycle reaction of **4b**.

Due to the porous collapse of **4b**, the size distribution and fine dispersion as well as stability of Pd NPs are mainly because of the coordination of a carben ligand to the nanoparticle surface, which was also proposed in the system of imidazolium-based ionic liquids stabilized NPs.^[168, 191] While in the case of **4a**, due to the preserve of organosilica matrix except the imidazolium cation plays an important role in stabilizing palladium nanoparticles, the mesoporous structure could also play a size-restricted role. Beside, the mesostructure with high surface area is favorable for the adsorption of H₂ and further accelerates the reaction speed.^[192] Therefore, **4a** exhibits much higher activity and stability than **4b**. The TEM image taken from the five times recycled **4a** does not show any Pd NPs (Figure 4. 18), indicating the high stability of **4a**.

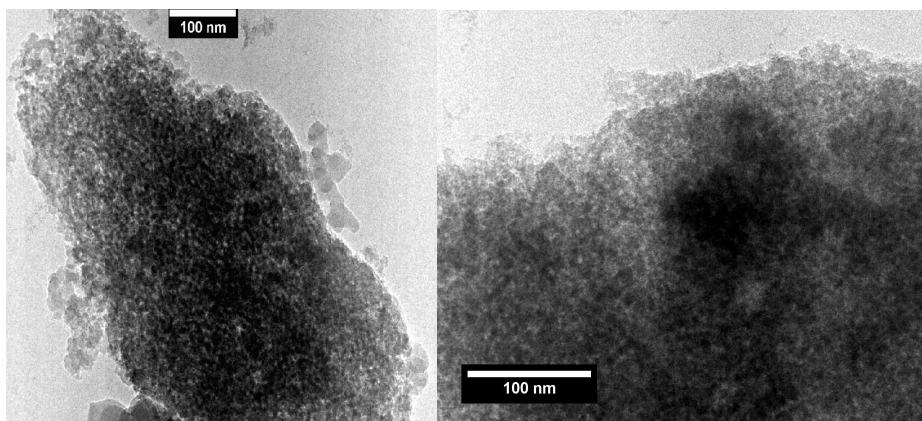


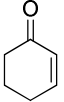
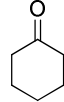
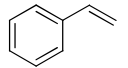
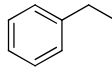
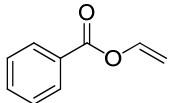
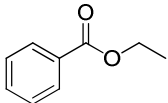
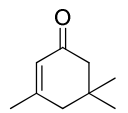
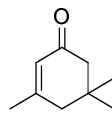
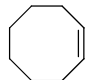
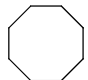
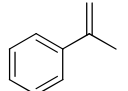
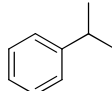
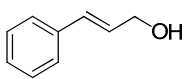
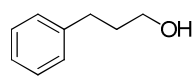
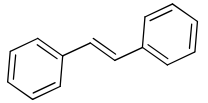
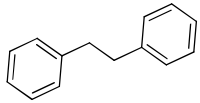
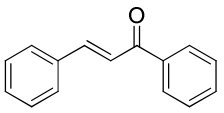
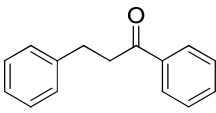
Figure 4. 18 The TEM image of used catalyst **4a**

In order to understand the active center, several control experiments were carried out. The hybrid material **3b** containing $\text{Pd}(\text{OAc})_2$ without reduction with NaBH_4 did not show any activity under the same condition after 24 h, which proves that palladium nanoparticles are the active centers for the hydrogenation reaction and that the supported Pd species cannot be reduced in situ during the reaction. To confirm that the catalytic hydrogenation is indeed heterogeneous, the catalyst was filtrated when a conversion of about 28% was reached. The continued reaction was carried out with the filtrate and there was no further conversion in between 20 h, which clearly demonstrates that it is a truly heterogeneous reaction. By AAS measurement of **4a** no palladium contamination down to 0.5×10^{-4} mmol could be detected in the products.

Concurrently, a series of representative alkenes were employed to investigate the scope of the reaction, the activity and selectivity of **4a** (Table 1). In our model reaction cyclohex-2-enone was hydrogenated with excellent chemoselectivity to the corresponding alkanone without any attack at the $\text{C}=\text{O}$ double bond (entry 1). The double bond adjacent to an aromatic ring or a heteroatom respectively reacted efficiently and without any byproduct under the standard conditions (entry 2 and 3). Turning to higher substitution patterns at the $\text{C}=\text{C}$ double bond strongly reduces the catalytic activity (entries 4-5). Nevertheless, **3a** shows excellent activity and selectivity with styrenes respectively substituted in the 1-position or 2-position with functional groups such as methyl, aromatic rings and aromatic carbonyl (entries 6-9).

4. Imidazoium Salt Incorporated in a Mesoporous Framework

Table 4. 3 Hydrogenation of different olefins with catalyst **4a**.

entry	olefin	product	yield ^b (%)
1			99
2			99
3			99
4			15 ^c
5			64 ^c
6			99
7			99
8			99
9			99

^aReaction conditions: room temperature, 1 bar H₂, 1 mmol of substrate, 0.15 mol% of Pd, toluene, 24 h. ^bdetermined by GC-MS. ^cafter 48 h.

4.2.4 Conclusion

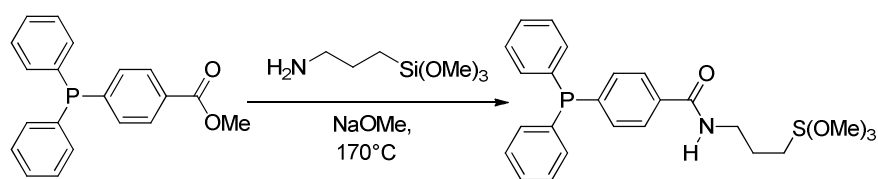
Periodic mesoporous organosilicas (PMOs) materials with bisilylated -Si(OMe)₃ bridged imidazolium ionic liquids in the framework were successfully synthesized. Their properties such as porous structure, surface area, morphologies and stability of PMOs are highly dependent on the amount of the loaded imidazolium cations. The

PMO materials were used for immobilization of Pd NPs and the obtained catalysts showed high activity and reusability for olefin hydrogenation reactions under mild conditions. The combination of palladium nanoparticles, the imidazolium ionic liquid and the mesostructure of the material showed excellent synergistic effects on the enhancement of activity and stability of the catalyst. This approach may find wide potential applications in stabilization of other transition metal nanoparticles and nanocatalysis. In addition to the high activity, the successful recycling of this catalytic system allows a more economic and environmentally friendly process.

Chapter 5. Conclusion

The discovery of ordered mesoporous silicas synthesized by a surfactant template method (following LCT mechanism) has encouraged the development of immobilized catalysts. Based on the LCT mechanism, the mesoporous silica materials further developed into mesoporous organic-inorganic hybrid material containing organic groups as an integral part of the structure (PMOs). This opened a door for the invention of a wide range of hybrid materials, which are very promising for future applications.

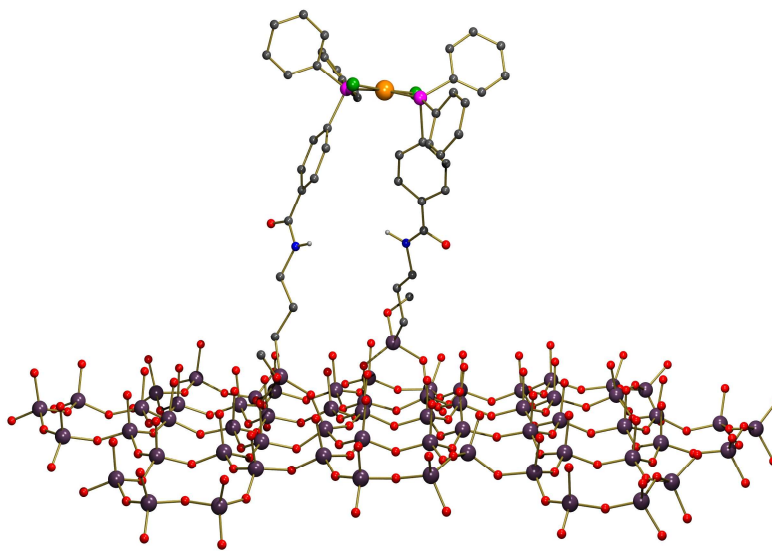
In the first part of my work, a TPP ligand functionalized with a methoxysilane group was synthesized (Scheme 1). The palladium complex based on this ligand was prepared and immobilized on commercial silica (Scheme 2. 4).



Scheme 1 Functionalization of a TPP ligand with 3-methoxysilylpropylamine linker.

The BET measurements demonstrate that the mesostructure of the support was preserved during the grafting and the solid state NMR data proves the palladium complex was covalently bonded to the support. The resulting heterogeneous catalyst was applied in the Suzuki reaction and exhibited excellent activity, selectivity and reusability. To study this reaction in detail, a hot filtration test was carried out. AAS measurements of the filtrate proved that very small amounts of palladium leached during the reaction. The filtration tests further showed that at least part of the reaction was catalyzed by leached palladium species. The TEM images revealed the existence of palladium nanoparticles, which indicates that the complex was not stable under the reaction conditions and that the palladium nanoparticles are the real active center. However, the solid state NMR of the used catalyst proved the retention of the ligand, which means that the covalent bond between the ligand and support is stable under

these conditions. The ^{31}P NMR CP-MAS spectrum showed peaks for phosphine oxide and the free triphenylphosphine ligand. These phosphorus species prevent, together with the mesostructure of the support, the aggregation and leaching of the palladium nanoparticles.

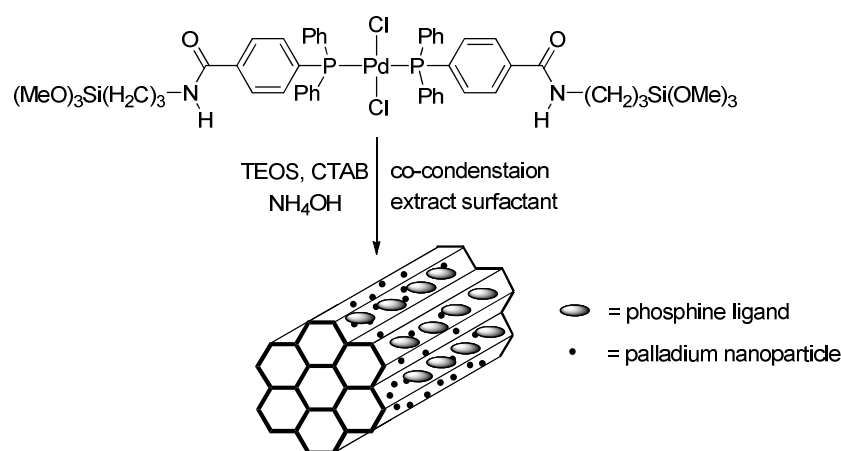


Scheme 2 Simulated model of the $\text{PdCl}_2(\text{PPh}_3)_2$ complex functionalized on a silica surface.

Applying the same strategy a rhodium complex with this ligand was synthesized and immobilized on commercial silica gel, SBA-15 and a PMO material (with $(\text{MeO})_3\text{-Si-C}_6\text{H}_4\text{-Si(OMe)}_3$ as framework). These three materials were applied for the hydrogenation of cyclohex-2-enone in toluene with 1 bar pressure of H_2 at 40°C . The kinetic curves for these reactions show no differences. This confirms that the structure and the hydrophilic/hydrophobic properties of the support do not play an important role. The reusability of the SBA-15 supported catalyst was studied further. After the first run, which needed more than 20 h to achieve 99% yield, the activity dramatically increased (99% yield, 2 h) and it stayed at this level up to the 6th run. The TEM images of the used catalyst proved the absence of rhodium nanoparticles larger than 1 nm and the solid state NMR spectrum proved the preservation of the ligand after the reaction. However,

AAS measurements showed traces of leached rhodium. The catalyst had no activity for alcohol, benzoyl and phenyl groups at the 2-position of styrene. Also a ruthenium complex was synthesized using the same ligand and applied in transfer hydrogenation of acetophenone, which showed excellent activity and reusability.

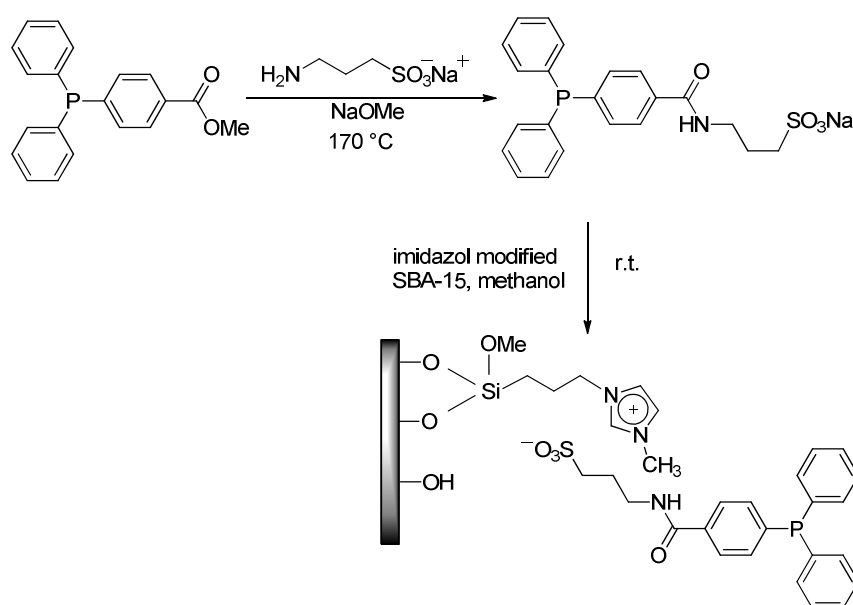
Furthermore a periodic mesoporous organosilica material was synthesized with a functionalized palladium complex (Scheme 3). This hybrid material features a periodic ordered structure with a large specific surface area and a narrow pore size distribution. However, the TEM measurements showed the formation of palladium nanoparticles of about 15 nm size. This means the complex decomposed during the synthesis process. Further catalytic investigations of this material showed no activity in the Suzuki reaction. As we know, palladium nanoparticles present a very effective catalyst for hydrogenation reactions. This material was applied in olefin hydrogenation and showed excellent activity and stability.



Scheme 3 Synthesis of a PMO with a functionalized palladium complex.

In the second part, a sulfonate group functionalized TPP ligand was successfully immobilized via electrostatic interactions on a SBA-15 support modified by a covalently grafted imidazolium salt (Scheme 4). The derived palladium system is a highly active catalyst for olefin hydrogenation under mild conditions and can be reused

at least 10 times without any loss of activity. Beside this, the catalyst also exhibited an outstanding activity for various substituted styrenes. The TEM images of the used catalyst did not show the presence of palladium nanoparticles larger than the size of 1 nm. This indicates the uniform distribution of the palladium species on the surface of the support. The AAS measurement showed no leaching of palladium species down to a concentration of 0.5×10^{-4} mmol. This catalyst was also tested in Suzuki reaction and excellent activity and stability were observed. However, once the catalyst was washed with water, no activity could be observed, which shows the limitation of this immobilization method.



Scheme 4 Immobilization of a sulfonate functionalized TPP.

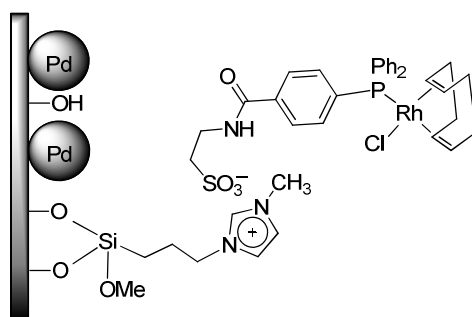
In summary, the work in this thesis investigated the immobilization of functionalized TPP ligands and their complexes on various supports via both covalent and non-covalent bonding. The obtained heterogeneous catalysts combine the benefits of the two fields of catalysis: retaining the high activity and selectivity of the homogeneous catalysts with the ease of separation of heterogeneous catalysts.

Outlook

A number of methods developed from this work, such as the functionalization of the TPP ligand and the modification of the inorganic supports have proved to be very effective and easy to handle. This opens up new possibilities for the usage of various supports other than mesoporous silica and other ligands.

For the methoxysilane functionalized TPP ligand several projects could be interesting: Rhodium complexes with different equivalents of the functionalized phosphine ligand could be synthesized, in order to compare the activity of these catalysts in hydrogenation reactions. Application of these catalysts in hydroformylation reactions could also be possible. It would also be interesting to synthesize mesoporous organosilicas materials with the functionalized complex in acidic conditions, instead of basic conditions, in order to avoid decomposition of the complex. A modification of these approach would be the usage of $(\text{MeO})_3\text{-Si-C}_6\text{H}_4\text{-Si-(OMe)}_3$ instead of TEOS in order to increase the hydrophobic properties of this material.

For the sulfonate functionalized TPP ligand, a very attractive work might be the immobilization of a TPP rhodium complex by charge interaction and the simultaneous stabilization of palladium nanoparticles on the support as shown in Scheme 5.



Scheme 5 Silica-supported catalyst that combines a grafted rhodium complex and palladium nanoparticles

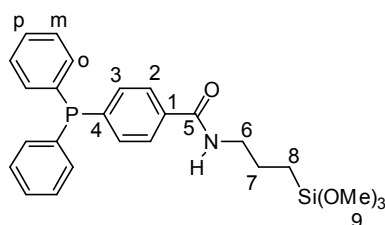
The cooperation of two different active centers could improve the activity significantly for hydrogenation. A hard to achieve but interesting task is utilization of magnetic nanoparticles as support in order to recycle the catalyst without washing with water.

Chapter 6. Experimental Section

Regarding to Chapter 2.1

Synthesis of 4-Diphenylphosphinylbenzenecarboxylicacid-4N-(3-trimethoxysilylpropyl)amide(2).

1.27 g (3.97 mmol) of **1** and 0.021 g (0.397 mmol) of NaOMe were mixed with 0.71 g (3.97 mmol) of 3-trimethoxysilylpropylamine. The mixture was heated to 170 °C and heating was continued for another 4 h. After cooling to room temperature, all volatiles were removed in vacuum. The residue was dissolved in CH₂Cl₂, filtrated over a Whatman filter to remove NaOMe. After removing the solvent, 1.67 g (90 %) of **2** were obtained as a yellow oily residue. ¹H NMR (400.13 MHz, 25 °C, CDCl₃): δ 7.72, 7.74 (2×s, 2H, ratio 1:1, 2×H²), 7.30-7.38 (m, 12H, Har), 6.53 (br, NH), 3.58 (s, 9H, H⁹), 3.45-3.49 (m, 2H, H⁶), 1.78-1.74 (m, 2H, H⁷), 0.71-0.75 (m, 2H, H⁸). ¹³C {¹H} NMR (150.92 MHz, 25 °C, CDCl₃) δ 167.1 (s, C=O), 141.8 (d, ¹J_{PC} = 13.9 Hz, C⁴), 136.5 (d, ¹J_{PC} = 11.1 Hz, Cⁱ), 134.9 (s, C¹), 133.9 (d, ²J_{PC} = 20.3 Hz, C^o), 133.5 (d, ²J_{PC} = 18.5, C³), 129.0, (s, C^p), 128.6 (d, ³J_{PC} = 6.5 Hz, C^m), 126.8 (d, ³J_{PC} = 6.5 Hz, C²), 50.3 (s, C⁹), 42.4 (s, C⁶), 22.7 (s, C⁷), 6.7 (s, C⁸). ³¹P {¹H} NMR (161.98 MHz, 25 °C, CDCl₃) δ -4.10. IR (KBr, cm⁻¹) 3315m, 3052w, 2939m, 2838m, 1636s, 1597m, 1541s, 1481m, 1434m, 1390w, 1305m, 1191m, 1087s, 1018w, 815s, 745s, 697s, 505w.



Synthesis of Dichloridobis[(4-diphenylphosphinylbenzenecarboxylicacid-4N-(3-trimethoxysilylpropyl)amide]-palladium(II) (**3**).

178 mg (0.46 mmol) of di(benzonitrile)dichloropalladium(II) were dissolved in 30 mL of dry CH₂Cl₂. This solution was added to a solution of 430 mg (0.92 mmol) of **2** in 10 mL of CH₂Cl₂. The reaction mixture was stirred for 4 h at room temperature, then filtrated through a Whatman filter and the filtrate was evaporated to dryness under reduced pressure. The residue was washed with ether (3×10 mL) to give a pale yellow solid. Yield: 332 mg (65%). Anal. calcd. for C₅₀H₆₀N₂Cl₂O₈P₂PdSi₂ (1112.5) C, 53.96; H, 5.40; N, 2.52; found (%) C, 53.26; H, 5.38; N, 2.53. ¹H NMR (400.13 MHz, 25 °C, CDCl₃): δ 7.73-7.34 (m, 14H, Har), 6.87 (br, NH), 3.52 (s, 9H, H⁹), 3.35-3.34 (m, 2H, H⁶), 1.69-1.66 (m, 2H, H⁷), 0.65 (t, J_{HH}= 8.3 Hz, 2H, H⁸). ¹³C {¹H} NMR (150.92MHz, 25 °C, CDCl₃) δ 166.7 (s, C=O), 136.7 (s, Ci), 135.0 (m, C^o), 134.8 (m, C³), 133.3 (m, C⁴), 131.5 (s, C^p), 129.0, (m, C¹), 128.3 (m, C^{-m}), 126.5 (m, C²), 50.5 (s, C⁹), 42.4 (s, C⁶), 22.7 (s, C⁷), 6.6 (s, C⁸). ³¹P {¹H} NMR (161.98 MHz, 25 °C, CDCl₃) δ 24.43. IR (KBr, cm⁻¹) 3383m, 3054w, 2939m, 2838w, 1644m, 1538m, 1483w, 1435m, 1304w, 1190m, 1093s, 813w, 747w, 693m, 514m.

Synthesis of hybrid catalyst **4Pd@SiO₂**

3 was immobilized on SiO₂ according to a standard procedure: 150 mg (0.13 mmol) of **3** dissolved in 4 mL of dry CH₂Cl₂ were added to a suspension of 340 mg of silica in 40 mL of dry toluene. The mixture was stirred for 12 h at 100°C. The solid was filtered off and extracted with CH₂Cl₂ in a Soxhlet apparatus for 24 h. Finally, the solid was dried in vacuum at 50 °C to obtain **4Pd@SiO₂**.

General procedure for Suzuki Coupling reaction

A dried Schlenk tube equipped with a magnetic stirring bar was charged under an inert gas atmosphere of nitrogen with the aryl bromide (5.0 mmol), the arylboronic acid (6 mmol), Cs₂CO₃ (6 mmol), **4Pd@SiO₂** (60 mg, 0.01 mmol Pd) and 5 mL of dioxane.

The mixture was heated to 80 °C for 24 h. After cooling to room temperature, the mixture was diluted with Et₂O and filtered. The solid residual catalyst was washed with water (3×10 mL) and Et₂O (3×10 mL) and then dried at 50 °C. After this, it could be used for the next run. The organic phase was separated and dried over MgSO₄ and the GC yield was determined using decane as an internal standard.

Regarding to Chapter 2.2

Synthesis of 1,4-bis(triethoxysilyl)benzene

In a three-necked flask, a mixture of TEOS (88.6 g, 426 mmol), dry THF (65 ml), magnesium turnings (3.1 g 0.129 mol), and a small crystal of iodine was slightly heated under an nitrogen atmosphere, and then a solution of 1,4-dibromobenzene (10.0 g, 42.5 mmol) in THF (22 ml) was added dropwise over two hours. After the mixture had been refluxed overnight, THF was evaporated in vacuum and hexane (150 ml) was added. The precipitated magnesium salts were removed by filtration and the residual TEOS and hexane were evaporated. The remaining crude product was distilled under reduced pressure (3 mbar, 110 °C) giving the product as a colorless liquid (42%). Anal. calc. for C₁₈H₃₄O₆Si₂ (402.65): C 53.70, H 8.51; found: C 53.96, H 8.37. ¹H NMR (CDCl₃, 600 MHz): δ = 1.13 (t, J = 7.2 Hz, 9 H), 3.77 (q, J = 7 Hz, 6 H), 7.58 (4 H). ¹³C NMR (CDCl₃, 75 MHz): δ = 18.0 (CH₃), 58.5 (CH₂), 133.2 (CH), 133.8 (C).

Synthesis of periodical mesoporous organosilicas (PMO)

The synthesis of PMO was performed using a mixture with the following molar ratio: BTEB : surfactant : NaOH : H₂O of 1 : 0.78 : 3.85 : 570. In a typical synthesis, 2.4 g (17 mmol) of octadecyltrimethylammonium bromide (OTAB) were dissolved in a mixture of 80.0 g (4.4 mol) of distilled water and 1.2 g (30 mmol) of sodium hydroxide at room temperature. 3.15 g (7.8 mmol) of 1,4-bis(triethoxysilyl)benzene (BTEB) were added to the above solution and the suspension was kept for 24 h stirring at room temperature. Then aging at 95 °C for 24 h was carried out. The resulting precipitate was recovered

by filtration and dried at 80 °C. The surfactant was removed through solvent extraction: 1.0 g of the as-synthesised sample was stirred in a solution of 1.0 ml 37% HCl and 100 ml ethanol at reflux temperature for 8 hours. The final powder was filtered off, washed with ethanol and dried at 80 °C overnight. Elemental analysis: found C 36.87, H 3.23.

Synthesis of Carbonylchloridobis[(4-diphenylphosphinylbenzenecarboxylic acid-4N-(3-trimethoxysilylpropyl)amide]rhodium(I) (**3**)

A solution of 66 mg (0.17 mmol) of $[\text{Rh}(\text{CO})_2\text{Cl}]_2$ in 10 mL of CH_2Cl_2 was added to a solution of 316 mg (0.68 mmol) of **2** in 10 mL of CH_2Cl_2 . The reaction mixture was stirred for 4 h at room temperature, all volatiles were removed in vacuum and the residue was washed with ether (3×10 mL) to give **3** as a pale yellow solid in 98 % yield. Anal. calcd. for $\text{C}_{51}\text{H}_{60}\text{ClN}_2\text{O}_9\text{P}_2\text{RhSi}_2$ (1101.5): C, 55.56; H, 5.45; N, 2.54, found: C, 55.36; H, 5.54; N, 2.36. ^1H NMR (400.13 MHz, 25 °C, CDCl_3): δ 7.32, 7.69 (2×m, 14H, H_{ar}), 7.17 (br, NH), 3.48 (s, 9H, OCH_3), 3.29 (m, 2H, NCH_2), 1.64 (m, 2H, $\text{CH}_2\text{CH}_2\text{CH}_2$), 0.62 (t, 2H, CH_2Si). ^{13}C NMR (150.92 MHz, 25 °C, CDCl_3) δ 187.0 (dt, CO, $^1J_{\text{Rh,C}} = 73.5$ Hz, $^2J_{\text{P,C}} = 15.8$ Hz), 167.0 (s, C=O), 136.4-126.7 (C_{ar}), 50.5 (s, OCH_3), 42.4 (s, NCH_2), 22.6 (s, $\text{CH}_2\text{CH}_2\text{CH}_2$), 6.6 (s, CH_2Si). ^{31}P NMR (161.98 MHz, 25 °C, CDCl_3) δ 30.5 (d, $^1J_{\text{RhP}}=126.8$ Hz). IR (KBr, cm^{-1}): ν_{CO} 1978.

Synthesis of hybrid catalyst **4Rh@SBA-15**

The same procedure was used for synthesis of hybrid catalyst **4Pd@SiO₂**.

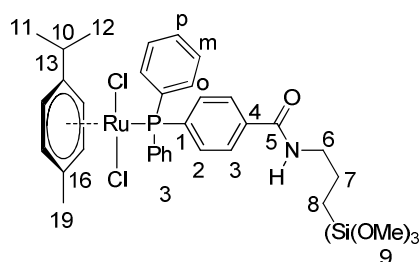
General procedure for the hydrogenation reactions

A dried Schlenk tube equipped with a magnetic stirring bar was charged with the rhodium catalyst **4Rh@SBA-15**, the olefin (1.0 mmol) and 10 mL of toluene under an atmosphere of nitrogen. The mixture was degassed and hydrogen (1 bar) was introduced, which was repeated three times. The reaction mixture was then vigorously stirred at 40 °C for the given reaction time.

Regarding to Chapter 2.3

Synthesis of (η^6 -*p*-cymene)(4-diphenylphosphinylbenzenecarboxylicacid-4*N*-(3-trimethox-silypropyl)amide)dichlororruthenium(II)

To a solution of [$(\eta^6$ -*p*-cymene) RuCl₂]₂ (0.160 g, 0.26 mmol) in 5 mL CH₂Cl₂, 4-diphenylphosphinyl benzenecarboxylicacid-4*N*-(3-trimethoxysilypropyl) amide (0.24 g, 0.52 mmol) dissolved in 5 mL CH₂Cl₂ were added dropwise. After the mixture was stirred at room temperature for 2 h, the solvent was removed in vacuum. The residue was washed with diethylether and dried in vacuum, giving the dark red product. Yield: 90%. Anal. calcd. for C₃₅H₄₄NCl₂O₄PRuSi (773.77) C, 54.33; H, 5.73; N, 1.81; found (%) C, 52.30; H, 5.31; N, 1.81. ¹H NMR (400 MHz, CDCl₃) δ 7.91-7.74 (m, 14H, H_{ar}), 5.21 (d, *J* = 6.1 Hz, 2H, H_{*p*-cym-CH}), 4.98 (d, *J* = 5.5 Hz, 2H, H_{*p*-cym-CH}), 3.55 (s, 9H, H⁹), 3.42 (m, 2H, H⁶), 2.85 (m, 1H, H¹⁰), 1.86 (s, 3H, H¹³), 1.71 (m, 2H, H⁷), 1.11 (d, *J* = 6.9 Hz, 6H, H¹¹, H¹²), 0.69 (m, 2H, H⁸). ¹³C NMR (101 MHz, CDCl₃) δ 167.1 (C⁵), 137.2-126.0 (C^{ar}), 111.1 (C¹³), 96.3 (C¹⁶), 89.1 (d, *J* = 2.9 Hz, C¹⁴ and C¹⁸), 87.4 (d, *J* = 5.5 Hz, C¹⁵ and C¹⁷), 50.7 (C⁹), 42.3 (C⁶), 30.4 (C¹⁰), 22.7 (C⁷), 21.94 (C¹¹ and C¹²), 17.9 (C¹⁹), 6.61 (C⁸). ³¹P NMR (162 MHz, CDCl₃) δ 24.63.

Synthesis of hybrid catalyst **4Ru@SBA-15**

The same procedure was used for synthesis of hybrid catalyst **4Pd@SiO₂**.

General procedure for transfer hydrogenation of ketones

A nitrogen protected schlenk was charged by the catalyst (0.018 mmol Ru), ketones

(1.0 mmol), 2-propanol (9 ml) and KO^tBu (0.05 mmol, dissolved in 1 mL 2-propanol). The mixture was stirred at 90°C (oil bath) for desired time.

Regarding to Chapter 2.4

Synthesis of **Pd-PPh₃-PMO**

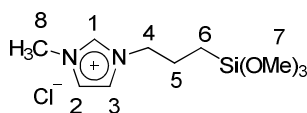
40 g of water and 5 g of NH₄OH are mixed first and to this solution 0.84 g of CTABr were slowly added. The solution was then stirred for another 30 min at room temperature. To this solution, 4 g of TEOS and 0.40 g of the bis-silyated palladium complex were added sequentially. The solution was then stirred for another 4h at room temperature and then aged at 80 °C for 3 d to obtain **Pd-PPh₃-PMO**. The material was washed with copious amount of water and ethanol and vacuum dried to obtain a free flowing powder. Surfactant extraction: 1 g of the **Pd-PPh₃-PMO** sample was mixed with 100 ml ethanol and 0.15 g of con. HCl at 50 °C for 6 h. The sample was then washed with ethanol and dried in vacuum to obtain the surfactant free **Pd-PPh₃-PMO** sample.

This procedure is supplied by Shylesh. S.

Regarding to Chapter 3

Synthesis of 1-(3-Propyltrimethoxysilane)-3-methylimidazolium chlorid (**2**)

(3-Chloropropyl)trimethoxysilane (5.95 mL, 31.7 mmol) was added to *N*-methylimidazole (2.50 mL, 31.7 mmol) and the mixture was heated to 150 °C and kept for 3 h. The product **2** was obtained as yellow oil in nearly quantitative yield. Anal. calcd. for C₁₀H₂₁N₂O₃SiCl (280.8) C, 42.7; H, 7.48; N, 10.0; found (%) C, 42.6; H, 7.49; N, 9.6 ¹H NMR (400.13 MHz, 25 °C, CDCl₃): δ 10.41 (s, 1H, H¹), 7.64 and 7.34 (t, *J*=1.6, 1H, H² and H³), 4.19 (t, *J*=7.2, 2H, H⁴), 3.99 (s, 3H, H⁸), 3.42 (s, 9H, H⁷), 1.90-1.83 (m, 2H, H⁵), 0.49 (t, *J*=8, 2H, H⁶). ¹³C{¹H} NMR (150.92 MHz, 25 °C, CDCl₃) δ 137.7 (C¹), 123.7, 121.8 (C², C³), 51.6 (C⁸), 50.6 (C⁷), 36.4 (C⁴), 24.0 (C⁵), 5.8 (C⁶).

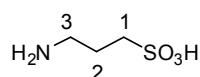


Immobilization of imidazolium salt (**2**)

0.42 g (1.5 mmol) of **2** dissolved in 5 mL of CH_2Cl_2 were added to a suspension of 1.0 g of SBA-15 in 40 mL dry toluene. After the mixture was stirred for 12 h at 90°C , the solid material **3** was filtrated, extracted with CH_2Cl_2 in a Soxhlet apparatus for 24 h and finally dried in vacuum at 50°C . Found (%) C, 13.6; H, 3.0; N, 3.2; corresponding to $(\text{C}_{10}\text{H}_{21}\text{ClN}_2\text{O}_3\text{Si})_1(\text{SiO}_2)_{9.8}(\text{H}_2\text{O})_{2.5}$

Synthesis of 3-Amino-1-propanesulfonic acid (**4**)

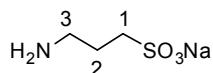
3-Amino-1-propanesulfonic acid was synthesized by followed procedure: To a stirred mixture of ammonium hydroxide (25 % aqueous solution, 20 mL) and acetone (240 mL) was added a solution of 1,3-propane sultone (12.11 g, 100 mmol) at room temperature. The mixture was heated at 40°C for 4 h. After that, it was cooled to room temperature and filtrated. The obtained solid was refluxed with mixture of ethanol (25 mL) and water (5mL) 3 times. The resulting white solid was filtrated and dried at 50°C in vacuum for 4 h to afford a desired product in 85 % yield. Anal. calcd. for $\text{C}_3\text{H}_9\text{NO}_3\text{S}$ (139.2) C, 25.9; H, 6.5; N, 10.1; found (%) C, 25.9; H, 6.6; N, 9.9. ^1H NMR (400.13 MHz, 25°C D_2O) δ = 3.13 (t, J =7.6, 2H, H^1), 3.00 (t, J =7.5, 2H, H^3), 2.16–2.01 (m, 2H, H^2). ^{13}C NMR (100.61 MHz, 25°C , D_2O) δ 48.10 (s, C^1), 38.53 (s, C^3), 22.56 (m, C^2).



Synthesis of compound (**5**)

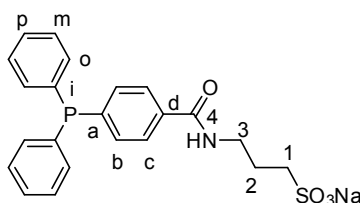
0.5 g (3.6 mmol) of **4** were dissolved in 2 mL water and 0.16 g (0.4 mmol) of NaOH were added. After the mixture was stirred at room temperature for 30 min, the aqueous solution was filtrated and evaporated to dryness on a rotary evaporator. Anal. calcd. for $\text{C}_3\text{H}_8\text{NO}_3\text{SNa}$ (161.2) C, 22.3; H, 5.0; N, 8.7; found (%) C, 20.2; H, 5.5; N, 7.8. ^1H

NMR (400.13 MHz, D₂O) δ = 2.95 (t, J =7.8, 2H, H³), 2.72 (t, J =7.1, 2H, H¹), 1.9-1.83 (m, 2H, H²). ¹³C NMR (100.62 MHz, 25 °C, D₂O) δ = 49.34 (s, C¹), 40.03 (s, C³), 27.84 (m, C²).



Synthesis of Sodium 4-diphenylphosphinylbenzenecarboxylicacid-4N-(propylene-3-sulfon-ate)amide (**6**)

0.5 g (1.56 mmol) of 4-diphenylphosphinylbenzenecarboxylicacid methylester, 0.28 g (1.56 mmol) of **5** and 0.085 g (1.56 mmol) of NaOMe were mixed and grinded to a fine powder using a mortar and pestle. Then the mixture was heated to 170 °C for 24h. **6** was obtained as a pale yellow solid in 95% yield. ¹H NMR (400.13 MHz, 25 °C, CD₃OD): δ 7.92-7.21 (m, 14H, H^{ar}), 2.86 (m, 2H, H¹), 2.75 (t, 2H, H³), 1.97-1.90 (m, 2H, H²). ¹³C{¹H} NMR (100.62 MHz, 25 °C, CD₃OD) δ 175.0 (C⁴), C-a, d, 141.0, J_{PC} = 11.1; C-d, s, 139.7; C-i, d, 138.4, J_{PC} = 10.1; C-o, d, 134.75, J_{PC} = 19.1; C-b, d, 133.88, J_{PC} = 9.6; C-c, d, 130.13, J_{PC} = 10.1; C-p, s, 129.92; C-m, d, 129.57, J_{PC} = 7.0, 50.1 (C¹), 41.6 (C³), 29.4 (C²). ³¹P{¹H} NMR (161.98 MHz, 25 °C, CD₃OD) δ -4.43.



Immobilization of (**6**) on imidazolium salt modified SBA-15

A mixture of 2 g of **3** and 1.4 g of **6** in CH₃OH was stirred for 2 d at room temperature. The solid was filtrated, washed with water until pH = 7, extracted with CH₃OH in a Soxhlet apparatus for 12 h and finally dried in vacuum at 50 °C to obtain **6@SBA-15**.

Synthesis of hybrid material Pd@SBA-15

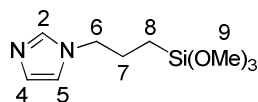
3 mL CH₂Cl₂ solution with 20 mg (0.05 mmol) of PdCl₂(CNPh)₂ was added to a

suspension of 770 mg of **6@SBA-15** in 10 mL of CH₂Cl₂. The mixture was stirred 2 h at room temperature and filtrated. The solid was washed with CH₂Cl₂ and dried in vacuum at 50 °C to obtain **Pd@SBA-15**.

Regarding to Chapter 4

Synthesis of N-(3-propyltrimethoxysilane)imidazole

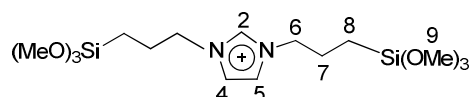
The synthesis was carried out under N₂ protection. A suspension of NaH (2.9 g, 0.12 mol) in a 60 mL THF in a three-neck flask was cooled to 0 °C. A solution of imidazole (8.2 g, 0.12 mol) in 50 mL THF was added dropwise during 2 h. After the addition, the ice bath was removed and the mixture was stirred overnight at room temperature. Then 3-iodopropyltrimethoxysilane (29.0 g, 0.10 mol) was added at 0 °C and the mixture was heated to 66 °C and lasted overnight. The solvent was removed under vacuum and then 150 mL dichloromethane were added. The precipitate was filtered under N₂. The product was then separated by distillation at 125 °C under vacuum. Anal. calcd. for C₉H₁₈N₂O₃Si (230.1) C, 46.93; H, 7.88; N, 12.16; found (%) C, 46.47; H, 7.44; N, 12.61. ¹H NMR (400.13 MHz, 25 °C, CDCl₃): δ 0.55 (t, 2H, H⁸), 1.86 (m, 2H, H⁷), 3.53 (s, 9H, H⁹), 3.90 (t, 2H, H⁶), 6.89 and 7.02 (s, 1H, H⁴ and H⁵), 7.45 (s, 1H, H²). ¹³C{¹H}NMR (100.62 MHz, 25 °C, CDCl₃) δ 6.3 (s, C⁸), 24.8 (s, C⁷), 49.2 (s, C⁶), 50.7 (s, C⁹), 118.8 and 129.5 (s, C⁴ and C⁵), 137.3 (s, C²).



Synthesis of 1,3-di(3-trimethoxysilylpropyl)imidazolium iodide

3-Iodopropyltrimethoxysilane (6.32 mL, 30.69 mmol) was added to *N*-(3-propyltrimethoxysilane) imidazole (7.06g, 30.69 mmol). The reaction mixture was heated to 110 °C overnight with exclusion of light and then cooled to r.t. The crude product was washed with toluene (3×10) and dried in vacuum. The imidazolium salt was obtained

as yellow oil in quantitative yield. Anal. calcd. for $C_{15}H_{33}N_2O_6Si_2I$ (520.1) C, 34.60; H, 6.35; N, 5.38; found (%) C, 34.46; H, 6.34; N, 5.40. 1H NMR (400.13 MHz, 25 °C, $CDCl_3$): δ 0.60 (t, 4H, H^8), 1.98 (m, 4H, H^7), 3.50 (s, 18H, H^9), 4.30 (t, 4H, H^6), 7.45 (s, 2H, H^4 and H^5), 9.96 (s, 1H, H^2) ^{13}C {1H}MR (100.62 MHz, 25 °C, $CDCl_3$) δ 6.1 (s, C^8), 24.2 (s, C^7), 49.8 (s, C^9), 51.0 (s, C^6), 121.4 (s, C^4 and C^5), 135.8 (s, C^2).



Synthesis of the PMO materials

2 g P123 were dissolved in 60 mL of 2 M HCl. After that, additional 15 mL H_2O were added and the solution was stirred at r.t for 3 h. Then a mixture of imidazolium salt **2** and TEOS was dissolved in 4 mL ethanol and added into above solution. The resultant mixture was continuously stirred at r.t for 4h, heated to 38 °C for 24 h and then aged at 100 °C for 48 h. The solid was filtered, washed with water and the surfactant was removed with ethanol in a Soxhlet apparatus for 24 h. Finally, the yellow solid was dried in vacuum at 50 °C.

Synthesis of Pd-PMO materials

1.0 g of PMO was suspended in 10 mL of dry toluene. $Pd(OAc)_2$ (0.05 mmol, 22 mg) was dissolved in 5 mL CH_2Cl_2 and slowly added into the suspension. The mixture was stirred at r.t for 20 min and the color of the material changed from yellow to brown. After that the solid was filtrated and 5 mL $NaBH_4$ 5% solution were added to a suspension of the obtained brown product in 10 mL ethanol. The mixture was stirred at r.t for 4 h, filtrated, washed with water and ethanol and dried at 50 °C.

References

- [1] A. Wight, M. Davis, *Chem. Rev.* 2002, 102, 3589-3614.
- [2] F. Hoffmann, M. Cornelius, J. Morell, *Angew. Chem. Int. Ed.* 2006, 45, 3216-3251.
- [3] A. Corma, H. Garcia, *Adv. Synth. Catal.* 2006, 348, 1391-1412.
- [4] A. Corma, *Chem. Rev.* 1997, 97, 2373-2420.
- [5] D. De Vos, M. Dams, B. Sels, P. Jacobs, *Chem. Rev.* 2002, 102, 3615-3640.
- [6] Z. I. Lu, E. Lindner, H. A. Mayer, *Chem. Rev.* 2002, 102, 3543-3578.
- [7] C. Copéret, M. Chabanas, R. Saint-Arroman, J. Basset, *Angewandte Chemie International Edition* 2003, 42, 156-181.
- [8] Z. Lu, E. Lindner, H. Mayer, *Chem. Rev.* 2002, 102, 3543-3578.
- [9] E. Lindner, T. Schneller, F. Auer, H. Mayer, *Angew. Chem. Int. Ed.* 1999, 38, 2154-2174.
- [10] A. Taguchi, F. Schüth, *Microporous and mesoporous materials* 2005, 77, 1-45.
- [11] J. S. Beck, J. C. Vartuli, W. J. Roth, M. E. Leonowicz, C. T. Kresge, K. D. Schmitt, C. T. W. Chu, D. H. Olson, E. W. Sheppard, *J. Am. Chem. Soc.* 1992, 114, 10834-10843.
- [12] C. Kresge, M. Leonowicz, W. Roth, J. Vartuli, J. Beck, *Nature* 1992, 359, 710-712.

- [13] J. Ying, C. Mehnert, M. Wong, *Angew. Chem. Int. Ed.* 1999, 38, 56-77.
- [14] A. Berggren, A. Palmqvist, K. Holmberg, *Soft Matter* 2005, 1, 219-226.
- [15] N. K. Raman, M. T. Anderson, C. J. Brinker, *Chem. Mater.* 1996, 8, 1682-1701.
- [16] J. Beck, J. Vartuli, W. Roth, M. Leonowicz, C. Kresge, K. Schmitt, C. Chu, D. Olson, E. Sheppard, *J. Am. Chem. Soc.* 1992, 114, 10834-10843.
- [17] J. C. Vartuli, C. T. Kresge, M. E. Leonowicz, A. S. Chu, S. B. McCullen, I. D. Johnson, E. W. Sheppard, *Chem. Mater.* 1994, 6, 2070-2077.
- [18] Q. Huo, D. I. Margolese, U. Ciesla, P. Feng, T. E. Gier, P. Sieger, R. Leon, P. M. Petroff, F. Schüth, G. D. Stucky, *Nature* 1994, 368, 317-321.
- [19] Q. Huo, D. Margolese, U. Ciesla, D. Demuth, P. Feng, T. Gier, P. Sieger, A. Firouzi, B. Chmelka, *Chem. Mater.* 1994, 6, 1176-1191.
- [20] D. Zhao, J. Feng, Q. Huo, N. Melosh, G. Fredrickson, B. Chmelka, G. Stucky, *Science* 1998, 279, 548-552.
- [21] P. Price, J. Clark, D. Macquarrie, *J. Chem. Soc., Dalton Trans.* 2000, 101-110.
- [22] S. Inagaki, S. Guan, Y. Fukushima, T. Ohsuna, O. Terasaki, *J. Am. Chem. Soc.* 1999, 121, 9611-9614.
- [23] W. Hunkeler, G. Ozin, *J. Mater. Chem.* 2005, 15, 3716-3724.
- [24] S. Fujita, S. Inagaki, *Chem. Mater* 2008, 20, 891-908.
- [25] S. Shylesh, J. MINGJUN, A. Seifert, S. Adappa, S. Ernst, W. Thiel, *New J. Chem.* 2009, 33, 717-719.

- [26] X. Yang, F. Zhu, J. Huang, F. Zhang, H. Li, *Chem. Mater.* 2009, 21, 4925-4933.
- [27] J. Huang, F. Zhu, W. He, F. Zhang, W. Wang, H. Li, *J. Am. Chem. Soc.* 2010, 132, 1492-1493.
- [28] V. Dufaud, F. Beauchesne, L. Bonneviot, *Angew. Chem.* 2005, 117, 3541-3543.
- [29] C. Baleizão, B. Gigante, D. Das, M. Alvaro, H. Garcia, A. Corma, *Chem. Commun.* 2003, 1860-1861.
- [30] H. Zou, S. Wu, J. Shen, *Chem. Rev.* 2008, 108, 3893-3957.
- [31] S. Shylesh, V. Schünemann, W. Thiel, *Angew. Chem. Int. Ed.* 2010, 49, 3428-3459.
- [32] D. Yi, S. Lee, J. Ying, *Chem. Mater.* 2006, 18, 2459-2461.
- [33] D. Yi, S. Selvan, S. Lee, G. Papaefthymiou, D. Kundaliya, J. Ying, *J. Am. Chem. Soc.* 2005, 127, 4990-4991.
- [34] A. Lu, E. Salabas, F. Schüth, *Angew. Chem. Int. Ed.* 2007, 46, 1222-1244.
- [35] N. Phan, C. Jones, *J. Mol. Catal. A: Chem.* 2006, 253, 123-131.
- [36] Y. Deng, C. Wang, J. Hu, W. Yang, S. Fu, *Colloids Surf., A* 2005, 262, 87-93.
- [37] D. Cauzzi, M. Lanfranchi, G. Marzolini, G. Predieri, A. Tiripicchio, M. Costa, R. Zaroni, *J. Organomet. Chem.* 1995, 488, 115-125.
- [38] Q. Xu, W. Hao, M. Cai, *Catal. Lett.* 2007, 118, 98-102.

- [39] M. Trilla, R. Pleixats, M. Man, C. Bied, J. Moreau, *Adv. Synth. Catal.* 2008, 350, 577-590.
- [40] B. Karimi, D. Enders, *Org. Lett.* 2006, 8, 1237-1240.
- [41] M. Lim, A. Stein, *Chem. Mater.* 1999, 11, 3285-3295.
- [42] A. Walcarius, C. Delac te, *Chem. Mater.* 2003, 15, 4181-4192.
- [43] R. Richer, *Chem. Commun.* 1998, 1775-1777.
- [44] J. Fraile, J. Garci a, J. Mayoral, *Chem. Rev.* 2009, 109, 360-417.
- [45] J. Horn, F. Michalek, C. Tzschucke, W. Bannwarth, *Non-covalently solid-phase bound catalysts for organic synthesis* 2004, *Topics in Organometallic Chemistry Vol. 242; Springer: Berlin/Heidelberg*, 43-75.
- [46] K. Müller-Dethlefs, P. Hobza, *Chem. Rev.* 2000, 100, 143-168.
- [47] C. Barnard, *Platinum Met. Rev.* 2008, 52, 38-45.
- [48] D. Evans, J. Osborn, G. Wilkinson, *Nature* 1965, 208, 1203-1204.
- [49] J. Blümel, *Coord. Chem. Rev.* 2008, 252, 2410-2423.
- [50] Y. Uozumi, Y. Nakai, *Org. Lett.* 2002, 4, 2997-3000.
- [51] K. Inada, N. Miyaura, *Tetrahedron* 2000, 56, 8661-8664.
- [52] Y. Uozumi, H. Danjo, T. Hayashi, *J. Org. Chem.* 1999, 64, 3384-3388.
- [53] M. Cai, J. Sha, Q. Xu, *J. Mol. Catal. A: Chem.* 2007, 268, 82-86.
- [54] S. Shyu, S. Cheng, D. Tzou, *Chem. Commun.* 1999, 2337-2338.

- [55] C. Merckle, S. Haubrich, J. Blümel, *J. Organomet. Chem.* 2001, 627, 44-54.
- [56] C. Merckle, J. Blümel, *Top. Catal.* 2005, 34, 5-15.
- [57] C. Merckle, J. Blümel, *Adv. Synth. Catal.* 2003, 345, 584-588.
- [58] C. Crudden, D. Allen, M. Mikoluk, J. Sun, *Chem. Commun.* 2001, 1154-1155.
- [59] W. Zhou, D. He, *Catalysis Letters* 2009, 127, 437-443.
- [60] W. Zhou, D. He, *Chem. Commun.* 2008, 5839-5841.
- [61] W. Zhou, D. He, *Green Chem.* 2009, 11, 1146-1154.
- [62] A. Liu, K. Hidajat, S. Kawi, *J. Mol. Catal. A: Chem.* 2001, 168, 303-306.
- [63] U. Schubert, C. Egger, K. Rose, C. Alt, *J. Mol. Catal.* 1989, 55, 330-339.
- [64] O. Kröcher, R. Köppel, M. Fröba, A. Baiker, *J. Catal.* 1998, 178, 284-298.
- [65] O. Kröcher, R. Köppel, A. Baiker, *J. Mol. Catal. A: Chem.* 1999, 140, 185-193.
- [66] N. Miyaoura, A. Suzuki, *Chem. Rev.* 1995, 95, 2457-2483.
- [67] A. Suzuki, *Chem. Commun.* 2005, 4759-4763.
- [68] U. Christmann, R. Vilar, *Angew. Chem. Int. Ed.* 2005, 44, 366-374.
- [69] A. Braga, N. Morgon, G. Ujaque, F. Maseras, *J. Am. Chem. Soc.* 2005, 127, 9298-9307.

- [70] K. Matos, J. Soderquist, *J. Org. Chem.* 1998, 63, 461-470.
- [71] N. Phan, M. Van Der Sluys, C. Jones, *Adv. Synth. Catal.* 2006, 348, 609-679.
- [72] N. Miyaaura, T. Yanagi, A. Suzuki, *Synth. Commun.* 1981, 11, 513-519.
- [73] A. Suzuki, *J. Organomet. Chem.* 1999, 576, 147-168.
- [74] A. Zapf, A. Ehrentraut, M. Beller, *Angew. Chem. Int. Ed.* 2000, 39, 4153-4156.
- [75] A. Littke, C. Dai, G. Fu, *J. Am. Chem. Soc.* 2000, 122, 4020-4028.
- [76] N. Leadbeater, M. Marco, *Chem. Rev.* 2002, 102, 3217-3274.
- [77] G. Stork, Y. Nakahara, Y. Nakahara, W. J. Greenlee, *J. Am. Chem. Soc.* 1978, 100, 7775-7777.
- [78] C. Andersson, K. Karabelas, A. Hallberg, C. Andersson, *J. Org. Chem.* 1985, 50, 3891-3895.
- [79] S. Jang, *Tetrahedron Lett.* 1997, 38, 1793-1796.
- [80] H. Qiu, S. Sarkar, D. Lee, M. Jin, *Green Chem.* 2008, 10, 37-40.
- [81] D. Choudhary, S. Paul, R. Gupta, J. Clark, *Green Chem.* 2006, 8, 479-482.
- [82] B. Nohair, S. MacQuarrie, C. Crudden, S. Kaliaguine, *J. Phys. Chem. C* 2008, 112, 6065-6072.
- [83] S. Paul, J. Clark, *J. Mol. Catal. A: Chem.* 2004, 215, 107-111.
- [84] C. Crudden, M. Sateesh, R. Lewis, *J. Am. Chem. Soc.* 2005, 127, 10045-10050.

- [85] C. Baleiz o, A. Corma, H. García, A. Leyva, *Chem. Commun.* 2003, 606-607.
- [86] J. Bliimel, *Inorg. Chem.* 1994, 33, 5050-5056.
- [87] C. Merckle, J. Blümel, *Chem. Mater.* 2001, 13, 3617-3623.
- [88] S. J. Gregg, K. S. W. Sing, *Adsorption, Surface Area, and Porosity* 1982, *Academic Press: San Diego*, 2nd ed.
- [89] K. Albert, E. Bayer, *J. Chromatogr. A* 1991, 544, 345-370.
- [90] M. Jia, A. Seifert, M. Berger, H. Giegengack, S. Schulze, W. Thiel, *Chem. Mater.* 2004, 16, 877-882.
- [91] Z. Zhou, A. Franz, M. Hartmann, A. Seifert, T. Müller, W. Thiel, *Chem. Mater.* 2008, 20, 4986-4992.
- [92] R. Bedford, U. Singh, R. Walton, R. Williams, S. Daviss, *Chem. Mater.* 2005, 17, 701-707.
- [93] D. Astruc, *Inorg. Chem.* 2007, 46, 1884-1894.
- [94] L. Wu, Z. Li, F. Zhang, Y. He, Q. Fan, *Adv. Synth. Catal.* 2008, 350, 846-862.
- [95] S. Shylesh, L. Wang, W. Thiel, *Adv. Synth. Catal.* 2010, 352, 425-432.
- [96] B. Chen, U. Dingerdissen, J. Krauter, H. Lansink Rotgerink, K. Möbus, D. Ostgard, P. Panster, T. Riermeier, S. Seebald, T. Tacke, *Appl. Catal., A* 2005, 280, 17-46.
- [97] H. Blaser, C. Malan, B. Pugin, F. Spindler, H. Steiner, M. Studer, *Adv. Synth. Catal.* 2003, 345, 103-151.

- [98] M. Zecca, R. Fisera, G. Palma, S. Lora, M. Hronec, M. Kralik, *Chem. Eur. J.* 2000, 6, 1980-1986.
- [99] J. G. de Vries, C. J. Elsevier, *The Handbook of Homogeneous Hydrogenation*, 2007, Wiley-VCH, Weinheim.
- [100] P. W. N. M. v. Leeuwen, *Homogeneous Catalysis – Understanding the Art*, chapt. 4, 2004, Kluwer Academic Publ.
- [101] S. Bhaduri, D. Mukesh, *Hydrogenation of Alkenes*, 2000, Wiley-Interscience, New York,.
- [102] A. Börner, J. Holz, *Homogeneous Hydrogenations, in Transition Metals for Organic Synthesis* (eds.: M. Beller, C. Bolm), vol. 2, 2nd ed., 2004, Wiley-VCH, Weinheim, .
- [103] O. Schmidt, *Chem. Rev.*, 12, 363–417.
- [104] R. A. W. Johnstone, A. H. Wilby, I. D. Entwistle, *Chem. Rev.* 1985, 85, 129-170.
- [105] J. Blümel, *Inorg. Chem.* 1994, 33, 5050-5056.
- [106] L. Wang, A. Reis, A. Seifert, T. Philippi, S. Ernst, M. Jia, W. Thiel, *Dalton Trans.* 2009, 3315-3320.
- [107] K. Shea, D. Loy, O. Webster, *J. Am. Chem. Soc.* 1992, 114, 6700-6710.
- [108] K.S. Joo, S. Y. Kim, C. S. Chin, *Bull.Korean Chem. Soc.* 1997, 18, 1296-1301.
- [109] C. Yang, B. Zibrowius, W. Schmidt, F. Schüth, *Chem. Mater.* 2004, 16, 2918-2925.
- [110] H. Gao, R. Angelici, *J. Mol. Catal. A: Chem.* 1999, 149, 63-74.

- [111] Y. Tanaka, N. Sawamura, M. Iwamoto, *Tetrahedron Lett.* 1998, 39, 9457-9460.
- [112] J. Ott, G. Ramos Tombo, B. Schmid, L. Venanzi, G. Wang, T. Ward, *Tetrahedron Lett.* 1989, 30, 6151-6154.
- [113] D. Astruc, F. Lu, J. R. Aranzaes, *Angew. Chem. Int. Ed.* 2005, 44, 7852-7872.
- [114] P. Mäki-Arvela, J. Hájek, T. Salmi, D. Murzin, *Applied Catalysis A: General* 2005, 292, 1-49.
- [115] T. Naota, H. Takaya, S. Murahashi, *Chem. Rev* 1998, 98, 2599-2660.
- [116] R. Noyori, T. Ohkuma, *Angewandte Chemie International Edition* 2001, 40, 40-73.
- [117] H. Doucet, T. Ohkuma, K. Murata, T. Yokozawa, M. Kozawa, E. Katayama, A. England, T. Ikariya, R. Noyori, *Angewandte Chemie International Edition* 1998, 37, 1703-1707.
- [118] T. Asefa, M. MacLachlan, H. Grondey, N. Coombs, G. Ozin, *Angew. Chem.* 2000, 112, 1878-1881.
- [119] S. Guan, S. Inagaki, T. Ohsuna, O. Terasaki, *J. Am. Chem. Soc.* 2000, 122, 5660-5661.
- [120] O. Olkhoviyk, M. Jaroniec, *J. Am. Chem. Soc.* 2005, 127, 60-61.
- [121] S. Polarz, A. Kuschel, *Adv. Mater.* 2006, 18, 1206-1209.
- [122] S. Inagaki, S. Guan, T. Ohsuna, O. Terasaki, *Nature* 2002, 416, 304-307.
- [123] M. Burleigh, M. Markowitz, E. Wong, J. Lin, B. Gaber, *Chem. Mater.* 2001, 13, 4411-4412.

- [124] M. Kapoor, Q. Yang, S. Inagaki, *Chem. Mater.* 2004, 16, 1209-1213.
- [125] R. Corriu, A. Mehdi, C. Rey  , C. Thieuleux, *Chem. Commun.* 2002, 1382-1383.
- [126] H. Li, H. Yin, F. Zhang, Y. Huo, Y. Lu, *Environ. Sci. Technol.* 2009, 43, 188-194.
- [127] L. Rossi, F. Silva, L. Vono, P. Kiyohara, E. Duarte, R. Itri, R. Landers, G. Machado, *Green Chem.* 2007, 9, 379-385.
- [128] D. Briggs, M. Seah, Eds., 1983, *Practical Surface Analysis by Auger and X-ray Photoelectron Spectroscopy*, Wiley.
- [129] J. F. Moulder, W. F. Stickle, P. E. Sobol, K. D. Bomben, 1992, *Handbook of X-ray Photoelectron Spectroscopy*, Perkin-Elmer
- [130] F. Leisenberger, G. Koller, M. Sock, S. Surnev, M. Ramsey, F. Netzer, B. Kl  tzer, K. Hayek, *Surf. Sci.* 2000, 445, 380-393.
- [131] M. Pelavin, D. Hendrickson, J. Hollander, W. Jolly, *J. Phys. Chem.* 1970, 74, 1116-1121.
- [132] J. Huang, T. Jiang, H. Gao, B. Han, Z. Liu, W. Wu, Y. Chang, G. Zhao, *Angew. Chem.* 2004, 116, 1421-1423.
- [133] M. Zhao, R. Crooks, *Angew. Chem. Int. Ed.* 1999, 38, 364-366.
- [134] Y. Gu, G. Li, *Adv. Synth. Catal.* 2009, 351, 817-847.
- [135] A. Riisager, R. Fehrmann, M. Haumann, P. Wasserscheid, *Eur. J. Inorg. Chem.* 2006, 2006, 695-706.
- [136] W. Chen, Y. Zhang, L. Zhu, J. Lan, R. Xie, J. You, *J. Am. Chem. Soc.* 2007, 129, 13879-13886.

- [137] R. Ciriminna, P. Hesemann, J. Moreau, M. Carraro, S. Campestrini, M. Pagliaro, *Chem. Eur.J.* 2006, 12, 5220-5224.
- [138] K. Yamaguchi, C. Yoshida, S. Uchida, N. Mizuno, *J. Am. Chem. Soc.* 2005, 127, 530-531.
- [139] Y. Zhang, Y. Shen, J. Yuan, D. Han, Z. Wang, Q. Zhang, L. Niu, *Angew. Chem. Int. Ed.* 2006, 45, 5867-5870.
- [140] L. Wang, M. Jia, S. Shylesh, T. Philippi, A. Seifert, S. Ernst, A. Singh, W. Thiel, *ChemCatChem*, accepted.
- [141] P. Barbaro, F. Liguori, *Chem. Rev.* 2009, 109, 515-529.
- [142] B. Choudary, M. Lakshmi Kantam, N. Mahender Reddy, N. Gupta, *Catal. Lett.* 2002, 82, 79-83.
- [143] X. Q. Kong, 2004, WO2004113391.
- [144] A. Reis, W. R. Thiel, DE102008039167.
- [145] C. S. J. Cazin, M. Veith, P. Braunstein, R. B. Bedford, *Synthesis* 2005, 622-626.
- [146] V. Jovanovski, B. Orel, R. Ješe, A. Šurca Vuk, G. Mali, S. B. Hocēvar, J. Grdadolnik, E. Stathatos, P. Lianos, *J. Phys. Chem. B* 2005, 109, 14387-14395.
- [147] M. Smith, J. Wolinsky, *Organic Magnetic Resonance* 1982, 19, 129-133.
- [148] E. Pretsch, P. Bühlmann, C. Affolter, *Structure determination of organic compounds: tables of spectral data* 2000, Springer Verlag.
- [149] K. Albert, E. Bayer, *J. Chromatogr.* 1991, 544, 345-370.

- [150] S. Grim, R. Keiter, *Inorg. Chim. Acta* 1970, 4, 56-60.
- [151] J. Rahn, J. Nelson, D. O'Donnell, A. Pamer, *Inorg. Chem.* 1989, 28, 2631-2635.
- [152] J. A. Davies, S. Dutremez, *Coord. Chem. Rev.* 1992, 114, 61-103.
- [153] D. Chernyshov, L. Bronstein, H. Borner, B. Berton, M. Antonietti, *Chem. Mater.* 2000, 12, 114-121.
- [154] G. Guerrero, P. Mutin, E. Framery, A. Vioux, *New J. Chem.* 2008, 32, 1519-1525.
- [155] M. Terasawa, K. Kaneda, T. Imanaka, S. Teranishi, *J. Catal.* 1978, 51, 406-421.
- [156] J. Aiken III, R. Finke, *J. Mol. Catal. A: Chem.* 1999, 145, 1-44.
- [157] J. Huang, T. Jiang, B. Han, H. Gao, Y. Chang, G. Zhao, W. Wu, *Chem. Commun.* 2003, 1654-1655.
- [158] B. R. James, "*Homogeneous Hydrogenation.*" 1973, Wiley, New York.
- [159] S. Shylesh, J. Schweizer, S. Demeshko, V. Schünemann, S. Ernst, W. Thiel, *Adv. Synth. Catal.* 2009, 351, 1789-1795.
- [160] W. Zhao, J. Gu, L. Zhang, H. Chen, J. Shi, *J. Am. Chem. Soc.* 2005, 127, 8916-8917.
- [161] A. Roucoux, J. Schulz, H. Patin, *Chem. Rev.* 2002, 102, 3757-3778.
- [162] D. Astruc, F. Lu, J. Aranzaes, *Angew. Chem. Int. Ed.* 2005, 44, 7852-7872.
- [163] L. Pachon, G. Rothenberg, *Appl. Organometal. Chem.* 2008, 22, 288-299.

- [164] H. Bönemann, R. Richards, *Eur. J. Inorg. Chem.* 2001, 2455-2480.
- [165] A. Bell, *Science* 2003, 299, 1688-1691.
- [166] R. Narayanan, M. El-Sayed, *J. Am. Chem. Soc.* 2003, 125, 8340-8347.
- [167] I. Beletskaya, A. Cheprakov, *Chem. Rev.* 2000, 100, 3009-3066.
- [168] J. Dupont, G. S. Fonseca, A. P. Umpierre, P. F. P. Fichtner, S. R. Teixeira, *J. Am. Chem. Soc.* 2002, 124, 4228-4229.
- [169] Y. Hou, X. Ji, G. Liu, J. Tang, J. Zheng, Y. Liu, W. Zhang, M. Jia, *Catal. Commun.* 2009, 10, 1459-1462.
- [170] L. Pachón, G. Rothenberg, *Appl. Organometal. Chem.* 2008, 22, 288-299.
- [171] I. Yuranov, L. Kiwi-Minsker, P. Buffat, A. Renken, *Chem. Mater.* 2004, 16, 760-761.
- [172] B. Choudary, S. Madhi, N. Chowdari, M. Kantam, B. Sreedhar, *J. Am. Chem. Soc.* 2002, 124, 14127-14136.
- [173] P. Canton, F. Menegazzo, S. Polizzi, F. Pinna, N. Pernicone, P. Riello, G. Fagherazzi, *Catal. Lett.* 2003, 88, 141-146.
- [174] P. Landon, P. Collier, A. Papworth, C. Kiely, G. Hutchings, *Chem. Commun.* 2002, 2058-2059.
- [175] S. Hu, Y. Chen, *Ind. Eng. Chem. Res.* 2001, 40, 3127-3132.
- [176] A. Barau, V. Budarin, A. Caragheorgheopol, R. Luque, D. Macquarrie, A. Prelu, V. Teodorescu, M. Zaharescu, *Catal. Lett.* 2008, 124, 204-214.

- [177] N. Toshima, Y. Shiraishi, T. Teranishi, M. Miyake, T. Tominaga, H. Watanabe, W. Brijoux, H. Bönemann, G. Schmid, *Appl. Organometal. Chem.* 2001, *15*, 178-196.
- [178] Y. Li, M. El-Sayed, *J. Phys. Chem. B* 2001, *105*, 8938-8943.
- [179] S. Son, Y. Jang, K. Yoon, E. Kang, T. Hyeon, *Nano lett.* 2004, *4*, 1147-1151.
- [180] P. Migowski, J. Dupont, *Chem. Eur. J.* 2007, *13*, 32-39.
- [181] X. Mu, J. Meng, Z. Li, Y. Kou, *J. Am. Chem. Soc.* 2005, *127*, 9694-9695.
- [182] Y. Kume, K. Qiao, D. Tomida, C. Yokoyama, *Catal. Commun.* 2008, *9*, 369-375.
- [183] J. Shin, B. Lee, Y. Jung, S. Kim, S. Lee, *Chem. Commun.* 2007, 5238-5240.
- [184] T. Asefa, M. MacLachlan, N. Coombs, G. Ozin, *Nature* 1999, *402*, 867-871.
- [185] B. Melde, B. Holland, C. Blanford, A. Stein, *Chem. Mater.* 1999, *11*, 3302-3308.
- [186] B. Lee, H. Im, H. Luo, E. Hagaman, C. Dai, *Langmuir* 2005, *21*, 5372-5376.
- [187] T. P. Nguyen, P. Hesemann, P. Gaveau, J. J. E. Moreau, *J. Mater. Chem.* 2009, *19*, 4164-4171.
- [188] B. Karimi, D. Elhamifar, J. Clark, A. Hunt, *Chem. Eur. J.* 2010, *16*, 8047-8053.
- [189] C. Cazin, M. Veith, P. Braunstein, R. Bedford, *Synthesis* 2005, 622-626.

[190] Q. H. Yang, J. Liu, L. Zhang, C. Li, *J. Mater. Chem.* 2009, 19, 1945-1955.

[191] L. S. Ott, M. L. Cline, M. Deetlefs, K. R. Seddon, R. G. Finke, *J. Am. Chem. Soc.* 2005, 127, 5758-5759.

[192] M. Alcon, A. Corma, M. Iglesias, F. Sánchez, *J. Organomet. Chem.* 2002, 655, 134-145.

Eidesstattliche Erklärung

Hiermit bestätige ich, dass ich die vorliegende Arbeit gemäß der Promotionsordnung des Fachbereichs Chemie der Technischen Universität Kaiserslautern selbstständig und nur unter Verwendung der angegebenen Quellen und Hilfsmittel angefertigt habe.

Kaiserslautern, Januar, 2011

Lei Wang

Acknowledgements

First and foremost I would like to thank my supervisor Prof. Werner R. Thiel for giving me this opportunity to study in his group on this highly interesting topic. He has provided me many chances to increase my abilities as a researcher. His constant support, invaluable guidance, timely help and friendly encouragement enable me to dissolve many problems in my research. I am so lucky to work with a professor like him, who is so kind and always eager to help and positively consider my work. I strongly benefit from his abundant knowledge, helpful discussion, positive attitude and effective working style, which will also profoundly affect my work and life in the future. I wish to take this opportunity to express my deepest gratitudes and regards to him.

I would like also to express my sincere gratitude to Prof. Ming J. Jia, who was my supervisor for the master degree and recommended me to Prof. Thiel's group. I am very grateful for his trust in my abilities, persistent support and encouragement as well as valuable help even when I am in Germany. Without his patient guidance for both work and life during my master work, I would not be able to adapt new research topic and environment so rapidly. I will never forget his help and support.

I would like also to thank my another supervisor of master degree in China Prof. Wen X. Zhang for his co-directions with Prof. Jia.

My grateful thanks also go to Dr. Yu Sun. He gave me many scientific advices about organic synthesis and helpful suggestion for personal life.

I would like to thank Dr. Shylesh Sankar, who introduced the concept of magnetic nanoparticle to me. I benefited a lot from our positive cooperation and valuable discussions.

I am very grateful for Andreas Pirro, who gave me many helpful suggestions

regarding organic synthesis. I benefited a lot from our valuable discussions. In the last three years he became one of my closest friends. I will always remember the happy time we had together.

I would like to thank one of my most important friends Zhou Zhou, who helped me adapt to the life in Germany and get familiar with the lab. I really enjoyed the time with her for walking from home to university, having party with other Chinese, cooking and eating delicious food, playing badminton, hiking...She helped me a lot during her PhD study in our group. Even now, she still gives me continuous support.

My deep gratitude also goes to Prof. Ernst and his staff of the Technisch Chemie group for providing me the facilities. Especially I would like to thank Thomas Philippi and Gunder Dörr for all the measurements they made for me as well as the data collection, compilation and valuable discussion ☺.

I am also deeply indebted to Dr. Andreas Seifert (Institut für Chemie, Technische Universität Chemnitz) and Dr. Stefan Lach (Physic TU Kaiserslautern) for their help in solid state NMR and XPS measurements. I also wish to thank Prof. Robin N. Klupp Taylor (Institute of Particle Technology, Erlangen), Prof. Ming J. Jia, Zhou Zhou, Dr. Anand P. Singh (National Chemical Laboratory, India) for their help with TEM characterization.

My deep appreciation also goes to Ms Christiane Müller, Frau Birgit Dusch and Frau Jana Ellmer for their NMR and elemental analysis measurements.

I would like to thank Frau Ruth Bergsträßer and Anke Kaiser for their help in AAS measurements.

My special thanks are given to all current and former members, because of them I really enjoyed the study time in our group. Claudia and Ezgi are always very happy and also bring our group a lot of happiness. Max is very helpful and friendly, I am very happy for attending conferences with him. I thank Anett Schubert for the

preparation of dry NaOMe. I am also very grateful for Andreas Reis's positive cooperation. I would like to thank Christoph for maintaining the anhydrous solvent purify system, Computers and printer. Thanks to Kevin for his effort in cleaning GC-MS together with Dr. Yu, which is very important for my research. Thanks to Katrin for her organization of many activities. She really tried her best to make everything nice and everyone satisfied. Thanks to Thomas for his responsibility for ordering the consumables of our lab. I will never forget the happy time in our group of hiking, parties, BBQ, dinners and football game...

I would like to thank Frau Ina Berwanger-Nicklas, who really did very good job to help us.

I am also very grateful for Prof. Lukas Gooßen and Prof. Sitzmann for allowing me to use the chemicals from their group.

I am very thankful for the help of Jie Chen in the AC lab course.

My thanks and appreciation also go to the China Scholarship Council (CSC) for giving me the scholarship which enabled me to undertake this study.

I cannot find any word to express my great gratitudes to Daniel, who has supported and helped me since the first day I worked in the lab. I will never forget his patient explanations for everything in the lab. I will also never forget his help for computer stuff, experiments, article writing, lab course... all my progress involves his selfless help. I am also very grateful for all the happiness he brings to me.

I wish to take this opportunity to show my deepest appreciation to my parents. Without their support, understanding and encouragement, I cannot even imagine to go so far from a small village.

I would like to thank all my friends, people I known in my study and life. Because of them, my life is so colourful and happy.

Curriculum Vitae

- Name: Lei Wang
- Date of birth: 19.04.1981
- Place of birth: Wudalianchi, HeiLongjiang province, China
- Status of marriage: Single

EDUCATION:

11/2007–05/2011

Technische Universität Kaiserslautern, Kaiserslautern, Germany
Ph.D. study in Inorganic Chemistry.

09/2004–07/2007

Jilin University, Chang Chun, Jilin province, China
Master of Science degree in Physical Chemistry.

09/2000–07/2004

Mudanjiang teacher's college, Mudanjiang, HeiLongjiang Province, China
Bachelor of Science degree in Chemistry Education.

Publications

A simple procedure for the covalent grafting of triphenylphosphine ligandson silica: application in the palladium catalyzed Suzuki reaction.

L. Wang, A. Reis, A. Seifert, T. Philippi, S. Ernst, Ming j. Jia and Werner R. Thiel; *Dalton Trans.*, **2009**, 3315-3320

A Covalently Immobilized Triphenylphosphine Rhodium Complex: Synthesis, Characterization, and Application in Catalytic Olefin Hydrogenation.

L. Wang, Ming j. Jia, S. Shylesh, T. Philippi, A. Seifert, S. Ernst, Anand P. Singh and Werner R. Thiel; *ChemCatChem*, **2010**, 2, 1477 - 1482

Electrostatic grafting of a Triphenylphosphine Sulphonate on SBA-15: Application in Palladium Catalyzed Hydrogenation.

L. Wang, D. Dehe, T. Philippi, A. Seifert, S. Ernst, Z. Zhou, Robin N. Klupp Taylor, Ming j. Jia, Anand P. Singh and Werner R. Thiel; Submitted for publication.

Embedding imidazolium cations inside the walls of a mesostructured silica support: A way to a highly active and selective palladium catalyst for olefin hydrogenation.

L. Wang, S. Shylesh, T. Philippi, G. Dörr, D. Dehe, A. Seifert, S. Ernst, Ming j. Jia, and Werner R. Thiel; to be submitted for publication.

Mesoporous SBA-15 materials modified with oxodiperoxo tungsten complexes as efficient catalysts for the epoxidation of olefins with hydrogen peroxide.

Jian y. Tanga, L. Wang, G. Liu, Y. Liu, Ya z. Hou, Wen x. Zhang, Ming j. Jia and Werner R. Thiel; *Journal of Molecular Catalysis A: Chemical*, 313, **2009**, 31-37.

Palladium(II)-Phosphine Complexes Supported on Magnetic Nanoparticles: Filtration-Free, Recyclable Catalysts for Suzuki–Miyaura Cross-Coupling Reactions

S. Shylesh, L. Wang, Werner R. Thiel; *Adv. Synth. Catal.*, 352, **2010**, 425-432.

Facile Synthesis of Mesoporous Magnetic Nanocomposites and their Catalytic Application in Carbon–Carbon Coupling Reactions

S. Shylesh, L. Wang, S. Demeshko and Werner R. Thiel; *ChemCatChem*, 2, **2010**, 543-1547.